# Source Speciation of Central Valley GHG Emissions using In-Situ Measurements of Volatile Organic Compounds

**Final Report**

**Contract No. 11-315**

**Prepared for the California Air Resources Board**


**Principal Investigator**
Professor Allen H. Goldstein
Department of Environmental Science, Policy and Management
University of California Berkeley
330 Hilgard Hall
University of California
Berkeley, CA 94720-3110
(510) 643-2451
ahg@berkeley.edu

**Subcontractor**
Dr. Marc L. Fischer
Lawrence Berkeley National Laboratory (LBNL)
United States Department of Energy
Berkeley, CA 94720
(510) 486-5539
mlfischer@lbl.gov

**Contributing Researchers**
Dr. Abhinav Guha, UC Berkeley (now at Bay Area Air Quality Management District)
Dr. Pawel Misztal, Post-Doctoral Researcher, UC Berkeley
Dr. Seongeun Jeong, Science and Engineering Associate, LBNL
Dr. Xinguang Cui, Post-Doctoral Researcher, LBNL
Robin Weber, Staff Research Associate, UC Berkeley


April 18, 2016

## DISCLAIMER

The statements and conclusions in this Report are those of the contractor and not necessarily those of the California Air Resources Board. The mention of commercial products, their source, or their use in connection with material reported herein is not to be construed as actual or implied endorsement of such products.

**ACKNOWLEDGEMENTS**

We thank Dave Bush for providing us with logistical support and meteorological data from the Walnut Grove tower. We thank Arlyn Andrews, Jon Kofler and Ed Dlugokencky at the National Oceanic and Atmospheric Administration's Earth Science Research Laboratory (NOAA-ESRL) for maintaining the air sampling and calibration system used for $CH_4$ and CO measurements, and for flask analysis of $CH_4$ and $N_2O$ used to check the continuous in-situ measurements. Work at UC Berkeley and LBNL on this study was funded by the California Air Resources Board (ARB) under contract number 11-315 with work at LBNL conducted under US Department of Energy Contract DE-AC02-05CH11231. The project team expresses their sincere gratitude to ARB and are very thankful for their support.

**TABLE OF CONTENTS**

Disclaimer..... i

Acknowledgments..... ii

Table of Contents..... iii

List of Figures..... vi

List of Tables..... xiv

Abstract..... xv

**1. EXECUTIVE SUMMARY……..... 1**

1.1 Background……... 1

1.2 Methods……. 2

1.3 Result …… 2

1.4 Conclusion …… 5

**2. INTRODUCTION……. 7**

2.1 Background…….. 7

2.2 Literature Review…….. 12

2.2 Rationale and Objectives…….. 16

2.3 References …… 19

**3. MEASUREMENTS …… 27**

3.1 Site, Greenhouse Gas Sources and Meteorology…… 27

3.2 Instrumentation for GHGs and CO ……. 34

3.3 Measurement of VOCs……...….. 36

3.3.1 PTRMS Instrument and Measurement Approach……. 36

3.3.2 VOCs of Interest…… 38

3.3.3 Quality Analysis and Quality Control……..……. 41

3.4 Pilot Measurements ……..… 44

3.5 References …… 51

**4. POSITIVE MATRIX FACTORIZATION (PMF) ANALYSIS……... 58**

4.1 Experiment…… 58

4.1.1 Principles of PMF…….. 58

4.1.2 Choice of Sampling Periods…….. 59

4.1.3 Mathematical Framework of PMF……. 61

4.1.4 Choice of Measurement Height for PMF Analysis ..... 63

4.1.5 Background Concentrations of GHG, CO and VOC Tracers…… 64

4.1.6 Uncertainty Matrix……..…….. 65

4.1.7 PMF Factor Numbers, Rotations and Error Analysis…… 67

4.2 Results and Discussion…… 69

4.2.1 Description of PMF Source Factors ……. 69

4.2.2 Seasonal PMF Results…… 85

4.3 References ……...…… 112

**5. SEASONAL VARIABILITY IN METHANE AND NITROUS OXIDE EMISSIONS USING INVERSE MODELING OF ATMOSPHERIC BACK TRAJECTORIES…...… 124**

5.1 Introduction……...124

5.2 Data and Models……125

5.2.1 Measurements……. 125

5.2.2 Prior $CH_4$ Emission Map…….. 127

5.2.3 Atmospheric Transport Modeling……..... 131

5.2.4 Bayesian Inverse Model……. 133

5.3 Results…….. 135

5.3.1 Methodology and Footprints …….. 135

5.3.2 Estimating $CH_4$ Emissions…….. 137

5.3.3 Estimating $N_2O$ Emissions…… 144

5.4 Discussion…… 150

5.5 References…… 151

**6. PMF BASED $CH_4$ AND $N_2O$ SOURCE APPORTIONMENT AT WALNUT GROVE……. 156**

6.1 Comparison with Inventory Source Distribution……...…….. 156

6.2 Comparison with Inverse Analysis based Source Distribution ……. 162

6.3 References…… 166

**7. SUMMARY AND RECOMMENDATIONS……..167**

7.1 Summary of Source Speciation Work using VOCs……..167

7.2 Recommendations on Future Work……...169

7.3 References……176

Glossary of Symbols and Acronyms..... 181

**LIST OF FIGURES**

Figure 1.1 2013 California emissions inventory for (top) methane ($CH_4$) - 41.1 million ton $CO_2$eq at GWP = 25; and (bottom) nitrous oxide ($N_2O$) - 13.1 million ton $CO_2$eq at GWP = 298. (Source: CARB GHG Inventory Tool, Nov 2015)……..... 11

Figure 3.1 Walnut Grove tower (WGC) site map showing land cover (Homer et al., 2007) and location of local $CH_4$ and $N_2O$ sources, including dairies (solid purple circles) and landfills (solid yellow circles).The increasing size of the purple and yellow circles represent increasing number of cows and amount of waste treated, respectively . The solid blue boundary line represents the extent of the Sacramento-San Joaquin River Delta ……28

Figure 3.2 Daytime distribution of wind speed and direction at WGC during (a) Summer 2012; (b) early Fall 2012 (Sep 1 – Oct 15); (c) late Fall 2012 (Oct 16- Nov 30); (d) Winter (Dec-Jan); (e) Winter/Spring 2013 (Feb- Mar); (f) Spring 2013 (Apr- May); and (g) Summer 2013 (Jun- Aug). The values are measured at 91 m a.g.l, the color scale denotes wind speeds (in m/s) and the concentric circles represent the intensity subdivisions (in percent)..... 31

Figure 3.3 Nighttime distribution of wind speed and direction at WGC during (a) Summer 2012; (b) early Fall 2012 (Sep 1 – Oct 15); (c) late Fall 2012 (Oct 16- Nov 30); (d) Winter (Dec-Jan); (e) Winter/Spring 2013 (Feb- Mar); (f) Spring 2013 (Apr- May); and (g) Summer 2013 (Jun- Aug). The values are measured at 91 m a.g.l, the color scale denotes wind speeds (in m/s) and the concentric circles represent the intensity subdivisions (in percent)…… 32

Figure 3.4 Simplified schematic at Walnut Grove tower showing location of sampling inlets for the GHG and PTR-MS instruments…… 33

Figure 3.5 Diurnal cycles of vertically resolved GHG and VOC profiles measured at Walnut Grove tower during pilot deployment of UCB PTR-MS: (a) $CH_4$, (b) CO (tracer of fuel combustion, biomass burning), and (c) $CO_2$ measured by LBNL and NOAA at the Walnut Grove tower from June 15-August 21, 2011. VOCs shown include (d) acetonitrile (biomass burning), (e) toluene (gasoline, fugitive emissions), (f) benzene (fugitive emissions, gasoline, biomass burning) (h) isoprene (biogenic emission), (i)

acetone (livestock, rice, vegetation, photooxidation), (j) methylvinylketone + methacrolein (isoprene photooxidation products), (k) acetaldehyde (rice, biomass burning, vegetation), (l) mixture of MBO + C5 hydrocarbons + pentanones (livestock, rice, vegetation), and (m) methanol (livestock, manure management, vegetation, biomass burning)……45,46

Figure 3.6 Time series GHG and pilot PTR-MS VOC measurements at the Walnut Grove tower (June 15-August 21, 2011)…….. 48

Figure 3.7 Example events highlight 3 different species specific GHG and VOC enhancements. Specific events include (a) fossil fuel signatures of $CH_4$, $CO_2$, CO, benzene, and xylenes, (b) likely dairy source with enhanced $CH_4$, $CO_2$, and methanol, and (c) a fire event showing a small enhancement in $CH_4$ with a significant of acetaldehyde, CO, methanol, acetonitrile, and benzene signals…… …… 50

Figure 4.1 Mean diurnal distribution (x-axis) of $CH_4$, combustion tracer CO and aromatic VOCs showing interpolated vertical profiles across all measured heights (y-axis) during different seasons at WGC. The color axis represents the mixing ratio of each compound. Species shown include (a-d) $CH_4$, (e-h) CO, (i-l) benzene, and (m-p) toluene. The x-axis of each figure lists the season for which the concentrations have been plotted. The horizontal dotted lines in each plot represent the height (m a.g.l) on WGC at which the measurements are made……..72

Figure 4.2 Mean diurnal distribution (x-axis) of oxygenated VOCs showing interpolated vertical profiles across all measured heights (y-axis) during different seasons at WGC. The color axis represents the mixing ratios of each VOC. Species shown include (a-d) methanol, (e-h) acetaldehyde, (i-l) acetone, and (m-p) methyl ethyl ketone (MEK). The x-axis of each figure lists the season for which the concentrations have been plotted. The horizontal dotted lines in each plot represent the height (m a.g.l) on WGC at which the measurements are made. There were no methanol measurements in the winter season at any height (Figure c)……... 77

Figure 4.3 Mean diurnal distribution (x-axis) of primary and secondary biogenic VOCs along with $N_2O$ showing interpolated vertical profiles across all measured heights (y-axis) during different seasons at WGC. The color axis represents the mixing ratios of each VOC. Species shown include (a-d) isoprene, (e-h) methyl vinyl ketone (MVK) +

methacrolein (MAC), (i-l) $N_2O$, and (m-p) monoterpenes (*m/z* 137). The x-axis of each figure lists the season for which the concentrations have been plotted. The horizontal dotted lines in each plot represent the elevation (m a.g.l) on WGC at which the measurements are made. $N_2O$ was not measured at 30 m a.g.l, hence measurements begin at 91 m a.g.l……... 81

Figure 4.4 Factor profiles of resolved PMF source factors denoting major source categories influencing the chemical composition of each profile during early fall of 2012 (Sep 1 – Oct 16). The sum of the scaled mass fractions of all species adds up to unity for each profile. The VOCs with an asterisk sign may have minor contributions from other VOCs detected at the same *m/z* depending on the season (see text)…… 88

Figure 4.5 Mean diurnal distribution plots apportioned by PMF generated source factors for early Fall 2012 period (Sep 1 – Oct 16). The plots include (a) source-wise distribution of methane enhancements above seasonal minimum, (b) source-wise distribution of methanol enhancements, and (c) source-wise distribution of methane enhancements by percentage. The legend represents the factor source categories of the 6-factor PMF solution for early Fall 2012……... 89

Figure 4.6 Factor profiles of resolved PMF source factors denoting major source categories influencing the chemical composition of each profile during late fall of 2012 (Oct 17 – Nov 30). The sum of the scaled mass fractions of all species adds up to unity for each profile. The VOCs with an asterisk sign may have minor contributions from other VOCs detected at the same *m/z* depending on the season (see text)……91

Figure 4.7 Mean diurnal distribution plots apportioned by PMF generated source factors for late Fall 2012 period (Oct 17 – Nov 30). The plots include source-wise distribution of methane enhancements (a) in ppb above seasonal minimum and (c) by percentage; source-wise distribution of nitrous oxide enhancements (b) in ppb above seasonal minimum and (d) by percentage, and (e) source-wise distribution of methanol enhancements above seasonal minima. The legend represents the factor source categories of the 4-factor PMF solution for late Fall 2012…….....92

Figure 4.8 Factor profiles of resolved PMF source factors denoting major source categories influencing the chemical composition of each profile during winter / wet season (Dec 1 – Jan 29). The sum of the scaled mass fractions of all species adds up to unity

for each profile. The VOCs with an asterisk sign may have minor contributions from other VOCs detected at the same *m/z* depending on the season (see text)……94

Figure 4.9 Mean diurnal distribution plots apportioned by PMF generated source factors for winter (wet season) period (Dec 1 – Jan 29). The plots include source-wise distribution of methane enhancements (a) in ppb above seasonal minimum and (c) by percentage; source-wise distribution of nitrous oxide enhancements (b) in ppb above seasonal minimum and (d) by percentage. The legend represents the factor source categories of the 3-factor PMF solution for this season. ……...95

Figure 4.10 Factor profiles of resolved PMF source factors denoting major source categories influencing the chemical composition of each profile during winter / early spring of 2013 (Feb 16 – Apr 4). The sum of the scaled mass fractions of all species adds up to unity for each profile. The VOCs with an asterisk sign may have minor contributions from other VOCs detected at the same *m/z* depending on the season (see text)……97

Figure 4.11 Mean diurnal distribution plots apportioned by PMF generated source factors for the late winter / early spring season (Feb 16 – Apr 4). The plots include mass distribution of (a) scaled 'dairy and livestock' factor concentrations, (b) scaled 'urban + oil / gas' factor concentrations, (c) scaled 'primary biogenics and secondary organics' factor concentrations, and (d) scaled 'agriculture + soil management + delta' factor concentrations. The solid colored line represents the average concentration for that hour of day while the semi-transparent shaded region represents the 1σ standard deviation. The remaining plots show source-wise distribution of methane enhancements (e) in ppb above seasonal minimum and (c) by percentage of enhancement. The legend represents the source categories of the 4-factor PMF solution……... 98

Figure 4.12 Factor profiles of resolved PMF source factors denoting major source categories influencing the chemical composition of each profile during spring of 2013 (Apr 6 – May 31). The sum of the scaled mass fractions of all species adds up to unity for each profile. The VOCs with an asterisk sign may have minor contributions from other VOCs detected at the same *m/z* depending on the season (see text)…….100

Figure 4.13 Mean diurnal distribution plots apportioned by PMF generated source factors for spring 2013 period (Apr 6 - May 31). The plots include source-wise distribution of methane enhancements (a) in ppb above seasonal minimum and (c) by percentage; source-wise distribution of nitrous oxide enhancements (b) in ppb above seasonal minimum and (d) by percentage, and (e) source-wise distribution of methanol enhancements above seasonal minima. The legend represents the factor source categories of the 5-factor PMF solution for spring 2013 season……..……101

Figure 4.14 Factor profiles of resolved PMF source factors denoting major source categories influencing the chemical composition of each profile during summer of 2013 (Jun 1 – Aug 4). The sum of the scaled mass fractions of all species adds up to unity for each profile. The VOCs with an asterisk sign may have minor contributions from other VOCs detected at the same *m/z* depending on the season (see text)……...104

Figure 4.15 Mean diurnal distribution plots apportioned by PMF generated source factors for summer 2013 period (Jun 1 – Aug 4). The plots include source-wise distribution of methane enhancements (a) in ppb above seasonal minimum and (c) by percentage; source-wise distribution of nitrous oxide enhancements (b) in ppb above seasonal minimum and (d) by percentage, and (e) source-wise distribution of methanol enhancements above seasonal minima. The legend represents the factor source categories of the 6-factor PMF solution for summer 2013……..……105

Figure 4.16 Factor profiles of resolved PMF source factors denoting major source categories influencing the chemical composition of each profile during summer of 2012 (Jun 16 – Aug 31). The sum of the scaled mass fractions of all species adds up to unity for each profile. The VOCs with an asterisk sign may have minor contributions from other VOCs detected at the same *m/z* depending on the season (see text)……...108

Figure 4.17 Mean diurnal distribution plots apportioned by PMF generated source factors for summer 2012 period (Jun 16 – Aug 31). The plots include source-wise distribution of methane enhancements (a) in ppb above seasonal minimum and (c) by percentage and (c) source-wise distribution of methanol enhancements above seasonal minima. The legend represents the factor source categories of the 6-factor PMF solution for summer 2012……109

Figure 4.18 (a) An additional source factor attributed to forest fires results from splitting of the urban + oil / gas factor in a 7-factor PMF solution during summer of 2012; vertical mean diurnal profile of biomass burning tracer acetonitrile during (b) summer of 2012 and (c) summer of 2013 showing accumulation of large emissions in the upper part of the mixed layer from significantly higher forest fire activity in the Sierra Nevada mountains during this period (Jun – Aug) in 2012 versus 2013. The Rush Fire in northeastern California (second largest wildfire in California recorded history) took place in August 2012……..110

Figure 5.1 Diurnal cycles of mean hourly (PST) measured $CH_4$ mixing ratio obtained for 91 and 483 m sampling heights on the WGC tower for the period from June 2012 to August 2013 (7 different seasons). ..……...……127

Figure 5.2 A *priori* scaled $CH_4$ emission map based on CALGEM emission map (top left), a prior scaled $N_2O$ emission map based on EDGAR 4.2 emission map (top right) and region classification map (bottom). The location of the WGC tower is marked with an "x" near longitude = 121ºW, latitude = 38ºN……..129

Figure 5.3 WRF initial boundary set up with three-level nested domains. The ratio of spatial resolution between the three levels is 3. The resolutions for d01, d02, d03 and d04/d05 are 36, 12, 4 and 1.3 km, respectively……131

Figure 5.4 Seasonally averaged footprint maps over 11-19 (PST) for 7 different seasons of summer at 2012, early fall, late fall, winter, winter-spring, spring and summer at 2013……..137

Figure 5.5 3-hour mean $CH_4$ mixing ratio comparison: measured $CH_4$ mixing ratio during noon - afternoon hours used in the first inversion (gray open circle), measured $CH_4$ mixing ratio used in the final inversion (black filled circle), WRF-STILT predicted (used in final inversion) $CH_4$ mixing ratio + WRF-STILT predicted $CH_4$ background (NOAA background) mixing ratio during noon – afternoon hours used for the final inversion (blue open circle), and WRF-STILT predicted $CH_4$ background mixing ratio using the 3-D NOAA curtain (red dots)……138

Figure 5.6 Comparison of $CH_4$ mixing ratios between measurements and predictions based on the final source inverse optimization using NOAA background for summer at 2012,

early fall, late fall, winter (from left to right at top) and winter-spring, spring and summer at 2013 (from left to right at bottom)…….141

Figure 5.7 *Posterior* $CH_4$ emissions in region 3, region 7 and region 8 by different sources from source inversion analysis (left) and region inversion analysis (right) based on NOAA background……...142

Figure 5.8 3-hour $N_2O$ mixing ratio as a function of time (mm/yy): measured $N_2O$ mixing ratio during noon - afternoon hours used in the first inversion (gray open circle), measured $N_2O$ mixing ratio used in the final inversion (black filled circle), WRF-STILT predicted (used in final inversion) $N_2O$ mixing ratio + WRF-STILT predicted $N_2O$ background (NOAA background) mixing ratio during noon – afternoon hours used for the final inversion (blue open circle), and WRF-STILT predicted $N_2O$ background mixing ratio using the 3-D NOAA curtain (red dots)……..….146

Figure 5.9 Comparison of $N_2O$ mixing ratios between measurements and predictions based on the final source inverse optimization using NOAA background for late fall (top left), winter (top right), spring (bottom left) and summer at 2013 (bottom right)……148

Figure 5.10 *Posterior* $N_2O$ emissions in region 3, region 7 and region 8 by different sources from source inversion analysis (left) and region inversion analysis (right). Source sectors include agricultural soils (AGS), manure management (livestock) (MNM), agricultural waste burning (AWB), industrial processes and product use (IPU), energy manufacturing transformation (EMT), indirect emissions from $NO_x$ and $NH_3$ (IDE), indirect $N_2O$ emissions from agriculture (N2O), oil production and refineries (OPR), buildings (residential and others) (RCO), waste (solid and waste water) (WST), non-road transportation (TNR) and road transportation (TRO)……..148

Figure 6.1 Pie charts representing (a) 2008 CALGEM $CH_4$ emissions from regions 3, 7 and 8 scaled to match 2012 ARB state totals for anthropogenic emission sectors; and (b) 2008 EDGAR v4.2 $N_2O$ distribution over Regions 3,7 and 8 scaled to 2012 ARB inventory total……..……....157

Figure 6.2 Pie charts representing PMF-derived source-wise $CH_4$ emissions distribution at Walnut Grove tower during (a) early fall 2012, (b) late fall 2012, (c) winter, (d) winter-spring 2013, (e) spring 2013, and (f) summer 2013…….……....158

Figure 6.3 Pie charts representing PMF-derived source-wise $N_2O$ emissions distribution at Walnut Grove tower during (a) late fall 2012, (b) winter, (c) spring 2013, and (d) summer 2013…… 161

Figure 6.4 Pie charts illustrating the distribution of $CH_4$ emissions (percentage of total) from regional sources (Region 3, 7 and 8) using Bayesian inverse analysis as described in Chapter 5. The pie charts represent (a) early fall 2012, (b) late fall 2012, (c) winter, (d) winter-spring 2013, (e) spring 2013, and (f) summer 2013……...163

Figure 6.5 Pie charts illustrating the distribution of $N_2O$ emissions (percentage of total) from regional sources (Regions 3, 7 and 8) using Bayesian inverse analysis as described in Chapter 5. The pie charts represent (a) late fall 2012, (b) winter, (c) spring 2013, and (d) summer 2013……...…..164

Figure 7.1 Mean vertical concentration gradient diurnal profiles for 48 selected ions measured by PTR-ToF-MS at WGC from February 12 to February 20, 2013. The color scale represents concentration (ppb) of the selected ion, x-axis represents local time of day and y-axis represents height (a.g.l)..…….173

**LIST OF TABLES**

Table 1.1 Mean distribution (%) of $CH_4$ enhancements in different seasons in the 2012-13 annual cycle at WGC by source category as determined using PMF analysis…….3

Table 1.2 Mean distribution (%) of $N_2O$ enhancements in different seasons in the 2012-13 annual cycle at WGC by source category as determined using PMF analysis…...….4

Table 2.1 Global Warming Potential (GWP; $gCO_2eq/g$) values and atmospheric lifetimes for important greenhouse gases from International Panel for Climate Change (IPCC) 4th (2007) and 5th (2013) Assessment Reports (AR)……..……..7

Table 2.2 Sector-wise breakdown of 2013 California $CH_4$ and $N_2O$ emissions inventory (Source: CARB GHG Inventory Tool, Nov 2015)…….……10

Table 3.1 Summary of information for seven seasonal sampling periods chosen for PMF analysis along with average temperatures during this period, data coverage and list of measured tracers…….30

Table 3.2 List of ions (protonated *m/z*) routinely measurable by PTR-MS with ascribed compounds and most significant known sources……..…….39

Table 4.1 Comparison of PMF urban and oil / gas source factor benzene and toluene emission ratios relative to carbon monoxide with those derived from urban measurements and gasoline speciation profiles. Relative emission ratios of toluene to benzene are also included as an indicator of aging of emission plumes arriving at WGC……74

Table 5.1 *A priori* methane emissions (Tg $CH_4$ $yr^{-1}$) for eight source sectors for 7 seasons and annual mean. …….…...128

Table 5.2 Estimated model-data mismatch errors at different months for $CH_4$ and $N_2O$ [Jeong et al., 2012a and 2012b]……...……135

Table 5.3 Final *posterio*r scaling factors for source inversions for each season obtained using the NOAA background…….……140

Table 5.4 *A priori* and *posterior* annual $CH_4$ emissions (Tg $CH_4$ $yr^{-1}$) by source sector…….143

Table 5.5 *Posterior* scaling factors (from final inversion) for $N_2O$ by season and source...…146

Table 5.6 *A priori* and *posterior* annual $N_2O$ emissions (Tg $N_2O$ $yr^{-1}$) by source sectors……... 149

## ABSTRACT

This work investigates the seasonal variability of $CH_4$ and $N_2O$ source apportionment from year-long measurements of GHGs, CO and a suite of VOCs in California's Central Valley from summer 2012 through early fall 2013. We apply the statistical technique of positive matrix factorization (PMF) on the combined GHG - VOC data set over seven separate periods that are representative of broad seasonal patterns observed in the region. We also compare our results to inverse modeling estimates at WGC for the same time-period.

Livestock are the largest regional source of $CH_4$, accounting for a majority of total emissions over different seasons. A second source of $CH_4$ is observed from microbially-mediated temperature-dependent emissions influenced by land / soil management practices and natural wetland ecosystems. A third 'urban and oil / gas source', containing $CH_4$ but no $N_2O$ is theorized to be emitted from an aggregation of upwind sources in the San Francisco Bay Area and the Rio Vista natural gas fields. Only two significant source categories of $N_2O$ are discerned from the PMF analysis – an 'agriculture + soil management + delta' source containing microbe-driven soil emissions of $N_2O$ resulting from fertilizer application and a dairy / livestock manure-management source. Seasonality has a strong influence on $CH_4$ and $N_2O$ biological emissions and this phenomenon is clearly observed using a top-down measurement approach.

# 1 EXECUTIVE SUMMARY

## 1.1 Background

The 2006 AB32 law requires the state of California to regulate and reduce its GHG emissions. The law directs the state's chief air quality regulatory agency, the California Air Resources Board (ARB), to be the lead agency in implementing AB32. The ARB maintains an annual statewide GHG inventory that includes estimates of human-related GHG emissions in the state. The GHG inventory is an important policy and guidance tool for AB32 implementation. Hence, there is an essential need for the ARB to verify and validate the accuracy of emissions reported in the GHG inventory through actual top-down measurements, whenever possible. Most GHGs are emitted from multiple anthropogenic sources that simultaneously emit additional chemicals like Volatile Organic Compounds (VOCs), which can serve as tracers for those specific source categories. Thus, local and regional GHG emission sources impacting a monitoring site during a specific time period can be constrained through simultaneous measurements of GHGs and specific VOCs. Previous direct measurements of GHGs in the state have relied on inverse modeling experiments (Zhao et al., 2009; Jeong et al., 2012b) from tall towers at annual time scales; or employed simultaneous and collocated measurements of VOCs to identify GHG sources but over a relatively smaller spatial and temporal scale (Guha et al., 2015). An integrated campaign which combines the merits of both the above-mentioned approaches was desired by the ARB to determine the suitability of the VOC-based source apportionment techniques to understand temporal distribution of GHG sources impacting a receptor site in the Central Valley over an annual time frame.

## 1.2 Methods

This contract was developed to meet the above-mentioned need by performing statistical source apportionment on a combined GHG - VOC data set measured at the Walnut Grove tower (WGC) near the Sacramento - San Joaquin River Delta region in California's Central Valley. The field campaign funded by this contract took place from the start of summer of 2012 through the end of summer of 2013. The field campaign was preceded by thorough preparation and intensive development of the PTR-MS instrument to ensure accurate identification and collection of many unique molecular entities (*m/z*) or VOCs. The year-long measurements were divided into seven unique periods that are representative of broad temperature / precipitation regimes encountered in this region, Following post-processing, the refined data sets were analyzed using the statistical source apportionment technique of Positive Matrix Factorization (PMF) to investigate the sources of $CH_4$ and $N_2O$ influencing the measured signals at this site. The PMF analysis applied to the GHG-VOC data set is explained in detail in Chapter 4. The team's analysis resulted in novel results that are being prepared for publications, have been documented in a PhD dissertation (Guha et al., 2014), and are summarized in this report (Chapter 4).

## 1.3 Results

Mean percentage contributions to $CH_4$ apportionment in different seasons have been summarized in Table 1.1. We find that dairies and livestock operations in the region surrounding WGC are the largest contributor to the observed $CH_4$ enhancements accounting for 55 – 90 % of the emissions depending on time of the year. The seasonal variation in range of $CH_4$ enhancements ascribed to this source is mainly caused by the varying contribution from the 'agriculture + soil management + delta' source, that varied substantially over the course of the

year. This source contains anaerobically mediated emissions from a combination of wetlands, peatland pastures and flooded / drained agricultural systems in the surrounding Delta. The $CH_4$ contribution from this sector is temperature driven with peak contributions in the summer season (20 - 40 % of enhancements) as opposed to negligible contributions in late fall and winter. $CH_4$ contributions from a third source, the 'urban and oil / gas' source, were observed in all seasonal periods. This source contains emissions possibly from the upwind urban core and natural gas operations in the Delta and generally accounts for 10 - 20 % of the total $CH_4$ enhancements. This sources' relative contribution was highest during the early fall period (up to 30 %) when the temperature-dependent $CH_4$ emissions from the Delta emissions are decreasing, and in the late fall period (up to 35 %) when $CH_4$ emissions from the Delta are absent and observed wind speeds and directions are more variable increasing the influence of the nearby Rio Vista gas fields on the apportioned signals at WGC.

**Table 1.1.** Mean distribution (%) of $CH_4$ enhancements in different seasons in the 2012-13 annual cycle at WGC by source category as determined using PMF analysis.

| Source* | Dairy and Livestock | Ag (rice) + Soil + Delta | Urban + Oil and Gas |
|---|---|---|---|
| early Fall | 64 | 10 | 26 |
| late Fall | 71 | < 1 | 29 |
| Winter | 90 | ND# | 10 |
| Winter-Spring | 66 | 19 | 15 |
| Spring | 69 | 21 | 10 |
| Summer 2013 | 61 | 28 | 11 |

* This table does not convey the uncertainties in apportioning $CH_4$ to the dominant sources and correspondingly little significance in attribution to weak or distant sources.
# ND – not detected

Mean percentage contributions to $N_2O$ apportionment in different seasons have been summarized in Table 1.2. $N_2O$ is measured in four periods (late fall, winter, mid-spring and summer) in this study (Chapter 4). There are two apportioned sources contributing to the $N_2O$ enhancements. One of the sources is the 'agricultural + soil management' source arising from the

N fertilizer application for intensive crop cultivation in the Delta. This $N_2O$ source is very seasonal with peak contributions occurring in the spring and summer season (~ 80 – 90 %) coinciding with the cycle of fertilizer use in the first half of the growing season. In the late part of the fall season, as agricultural activities around WGC are winding down and so is the fertilizer N input to farmlands, this source only accounts for about 20 % of the observed $N_2O$ enhancements with the dominant share (~ 80 %) being attributed to $N_2O$ emissions from the dairy and livestock sector. In the winters, there is much less agricultural activity taking place around WGC, and the 'ag +soil management' source factor is not observed in the PMF of the wintertime data. Almost all of the $N_2O$ in winter is attributed to the dairy and livestock sector.

**Table 1.2.** Mean distribution (%) of $N_2O$ enhancements in different seasons in the 2012-13 annual cycle at WGC by source category as determined using PMF analysis.

| Source* | Dairy and Livestock | Ag (rice) + Soil + Delta | Biogenics# |
|---|---|---|---|
| late Fall 2012 | 78 | 21 | < 1 |
| Winter | 97 | < 1 | 3 |
| Spring | 17 | 83 | < 1 |
| Summer 2013 | 13 | 69 | 18 |

* This table does not convey the uncertainties in apportioning $N_2O$ to the dominant sources and correspondingly little significance in attribution to weak or distant sources.
# Phenomenon of mixing and splitting of emissions from collocated sources results in emissions of soil $N_2O$ being attributed to the biogenics factors (explained in Chapter 6).

In this report, we also present inverse model estimates of $CH_4$ and $N_2O$ emissions (Chapter 5) for the June 2012 - August 2013 period for comparison with results derived from PMF analysis of co-varying multispecies VOC measurement. Both the source and region inversion analyses of $CH_4$ show clear seasonality in emissions. The present study shows that Dairy Livestock (DLS), Landfill (LF) and Crop Agriculture (CP) are the main contributors to emissions around the WGC tower and this is broadly in agreement with the PMF-based results presented in Chapter 4. The posterior emissions resulting from inversions for $N_2O$ show clear seasonal variations, with maxima in late fall and summer, and lower emissions in winter and

spring, perhaps due to reduced agricultural (AGS) emissions in the north valley (e.g. see Figure 5.10). From the results in Chapter 5, it can be seen that the posterior emissions of most $N_2O$ sub-sectors are higher than the prior estimates in most seasons.

## 1.4 Conclusions

In Chapter 6, we conclude that, for $CH_4$, the seasonally resolved apportionment of major sources at WGC is, in general, consistent with the distribution in a regional inventory. The relative contribution of $CH_4$ emissions from wetlands / land management practices in the Delta to the overall apportionment at WGC is substantial in warm temperature periods (e.g. summers) and hence accounting for seasonality in GHG emissions is necessary when using field measurements to validate the emission inventory. The consistent lack of $N_2O$ in the 'urban' source factor in all seasonal PMF analyses highlights the insignificant contribution of vehicle emissions to ambient $N_2O$ observations, compared to agricultural sources, in the region influencing the WGC tower. This finding is consistent with other work done by the authors (Guha et al., 2015) at Bakersfield in southern SJV which represents a mix of agricultural, industrial and urban emissions sources. Based on our observations and the need to address uncertainties in the statewide $N_2O$ emissions inventory, we recommend a direct evaluation of $N_2O$ emissions in the urban regions through on-road source-specific emission factor studies.

The PMF-based regional apportionment for $CH_4$ and $N_2O$ is consistent and in broad agreement with the results from inverse modeling on the same dataset. There are remarkable similarities in the seasonal variation of relative distribution of GHG emissions from major sources from these two completely independent estimation techniques. Data from short term ground-based studies, 'snapshot' airborne measurements and back-trajectory analysis on

temporally-limited data are not able to capture the complete seasonal cycle of emissions produced from these sources leading to bias in estimates resulting from such studies. Measurements made to confirm the bottom-up inventory must account for the seasonality in emissions; therefore year-round studies are generally required. In light of our findings, we propose long-term source-specific ground-measurements as a more representative method to account for $CH_4$ and $N_2O$ emissions from sources that can be expected to have seasonally varying emissions.

# 2 Introduction

## 2.1 Background

The dominant greenhouse gas (GHG) emitted across the globe is carbon dioxide ($CO_2$) which accounts for about 72 % of the total anthropogenic GHG radiative forcing (2.77 $Wm^{-2}$) since the pre-industrial era (year 1750) (IPCC, 2007; Montzka et al., 2011). The remaining GHG radiative forcing is attributed to non-carbon dioxide (non-$CO_2$) GHG's methane ($CH_4$, 21 %), nitrous oxide ($N_2O$, 7 %), and halocarbons (< 1 %).

**Table 2.1**. Global Warming Potential (GWP; $gCO_2eq/g$) values and atmospheric lifetimes for important greenhouse gases from International Panel for Climate Change (IPCC) 4th (2007) and 5th (2013) Assessment Reports (AR).

| **Trace GHG** | **Lifetime (years)** (IPCC AR4 2007 | **GWP time horizon** | | | |
|---|---|---|---|---|---|
| | | **20 years** (IPCC AR5 2013)* | **100 years** (IPCC AR5 2013)* | **20 years** (IPCC AR4 2007) | **100 years** (IPCC AR4 2007) |
| Carbon Dioxide ($CO_2$) | - | 1 | 1 | 1 | 1 |
| Methane ($CH_4$) | 12 | 86 | 34 | 72 | 25 |
| Nitrous Oxide ($N_2O$) | 114 | 268 | 298 | 289 | 298 |

* with climate-carbon feedbacks incorporated

These GHG's have more significant climate change effects than $CO_2$ on a per-ton basis due to their higher Global Warming Potential (GWP), calculated based on the intensity of infrared absorption by each GHG and their atmospheric lifetimes as shown in Table 2.1. The atmospheric lifetime of 12 years and large infrared absorption at unique spectral wavelengths gives $CH_4$ a large GWP of 25 (Forster et al., 2007; Montzka et al., 2011). Anthropogenic global $CH_4$ emissions are emitted by agricultural activities like enteric fermentation and manure management in livestock (Owen and Silver, 2014) and rice cultivation (McMillan et al., 2007), energy sector emissions from oil and gas operations and coal mining (USEPA, 2014), waste management (landfills and waste water treatment), and biomass burning (some of which is

natural) (Smith et al., 2007; Pacala et al., 2010). $N_2O$ has a much longer lifetime in the atmosphere (114 years; Table 2.1) and a very high GWP of 298 (Montzka et al., 2011). Agriculture is the biggest source of anthropogenic $N_2O$ emissions since the use of synthetic fertilizers and manure leads to microbial $N_2O$ emissions from soil (Crutzen et al., 2007; Galloway et al., 2008). Management of livestock and animal waste is another important agricultural source of $N_2O$, while industrial processes including fossil fuel combustion have been estimated to account for 15 % of total global anthropogenic $N_2O$ emissions (Denman et al., 2007). Owing to its shorter lifetime than $CO_2$, reducing $CH_4$ emissions globally can have a more rapid effect on reduction of climate forcing although, in the long-term, $CO_2$ should be the primary focus of GHG emission reduction efforts since it accounts for about 85% of our current GHG inventory. Top-down assessment of $N_2O$ emissions and better quantification will also contribute to the long term success of climate change mitigation efforts since $N_2O$ is removed from the atmosphere much more slowly than $CH_4$ and has a much higher GWP (Montzka et al., 2011).

With the passage of California Global Warming Solutions Act (AB 32), California became the first state in the nation to adopt an ambitious climate change strategy to reduce its GHG emissions. AB32 requires the state to meet a short-term target of reduction of its GHG emissions to 1990 levels by the year 2020, representing a 15 % decrease from business-as-usual scenario emissions projection of 509 million metric tonnes (MMT) $CO_2$-eq to 431 MMT$CO_2$eq. This is to be achieved using a combination of regulatory and reformative measures. California also has a long-term target of reducing GHG emissions to 80% below 1990 levels by the year 2050, signed in 2005 by Governor Schwarzenegger in Executive Orders S-3-05.

The state's chief air quality regulatory agency, the California Air Resources Board (ARB), is entrusted with the responsibility and authority to create regulations to achieve the targets defined in AB32. As part of their AB32 implementation process, the ARB's initial regulatory efforts focused on those major point sources of $CO_2$ that are fairly well-quantified and can bring about large scale GHG reductions e.g. power plant (through market based regulations like Cap and Trade program) and vehicle emissions (through programs like Low Carbon Fuel Standard). The stricter regulation of these sectors has contributed to the state's efforts to achieve the 2020 GHG goal. Because of $CH_4$'s shorter lifetime and an even larger GWP on a 20-year scale (72; Forster et al., 2007), there is increased attention within the science and regulatory community to quantify $CH_4$ emissions using 'top-down' methods and explore meaningful emission reduction opportunities. Besides aiding the state's pursuit of achieving the year 2020 GHG reduction goal, these $CH_4$ reduction efforts have the capability of effectively slowing the near-term rate of climate change if adopted on a global scale. There is also a drive to utilize assessments of $N_2O$ using 'top-down' ambient monitoring methods to verify ARB's 'bottom-up' inventory and identify/inform potential areas for emission reduction opportunities.

A statewide GHG emissions inventory (CARB, 2015) is used to measure progress towards meeting the AB32 goals. In 2013, $CH_4$ accounted for 41.1 MMT$CO_2$eq representing 9 % of the statewide GHG emissions while $N_2O$ emissions totaled 13.1 MMT $CO_2$-eq representing about 3 % of the GHG emissions inventory (Table 2.2 and Figure 1.1). The $CH_4$ emissions total represents a more than 25 % increase from its previous estimate in the inventory (CARB, 2013). California is the most populous state in the United States, home to one out of eight people who live in the nation with a total of 38 million people. It is also the leading agricultural state accounting for more than half of the fruits produced in the nation, and a major source of milk

products and vegetables, in all generating more than $43 billion in revenue (CASR 2011). Agriculture is the major source of non-$CO_2$ GHG emissions in California as well as nationally (USEPA, 2014). Nationwide, in 2013, $CH_4$ accounted for 10 % of the total GHG emissions inventory while $N_2O$ accounted for 5 % of the emissions. The statewide GHG inventory for $CH_4$ is similar to the national inventory although the largest source in California (dairy and livestock) differs from that in the national inventory (natural gas and petroleum systems). Statewide $N_2O$ emissions constitute a lesser fraction of total GHG emissions than that in the national inventory even though the state's agriculture sector is so prolific.

**Table 2.2.** Sector-wise breakdown of 2013 California $CH_4$ and $N_2O$ emissions inventory (Source: CARB GHG Inventory Tool, Nov 2015).

| major source sector (> 1% of total emissions) | Methane | | Nitrous Oxide | |
|---|---|---|---|---|
| | Emissions (× $10^6$ tonnes $CO_2$-eq) | % of total emissions | Emissions (× $10^6$ tons $CO_2$-eq) | % of total emissions |
| Electricity generation | - | - | 0.4 | 3 |
| Enteric fermentation | 11.8 | 29 | - | - |
| Fugitive emissions | 2.4 | 6 | | |
| Other industrial emissions | - | - | 0.2 | 1 |
| Landfills | 8.3 | 20 | - | - |
| Manure management | 10.6 | 26 | 1.5 | 12 |
| Natural gas pipelines | 3.8 | 9 | - | - |
| Rice cultivation | 1.2 | 3 | - | - |
| Soil management[a] | - | - | 7.9 | 65 |
| Transportation | - | - | 1.5 | 12 |
| Wastewater treatment[b] | 2.1 | 5 | 0.9 | 7 |

[a] includes residential and commercial landscaping and related application of fertilizers (~ 10%)
[b] includes solid waste composting

According to the state GHG inventory, enteric fermentation (direct ruminant emission from cattle) is the largest source of $CH_4$ in the state accounting for about 29 % of all $CH_4$ emissions. Manure management (anaerobic lagoons, liquid slurry etc.) is not only the next most important $CH_4$ source (26 %) but is also a significant source of $N_2O$ emissions (12 %). Waste

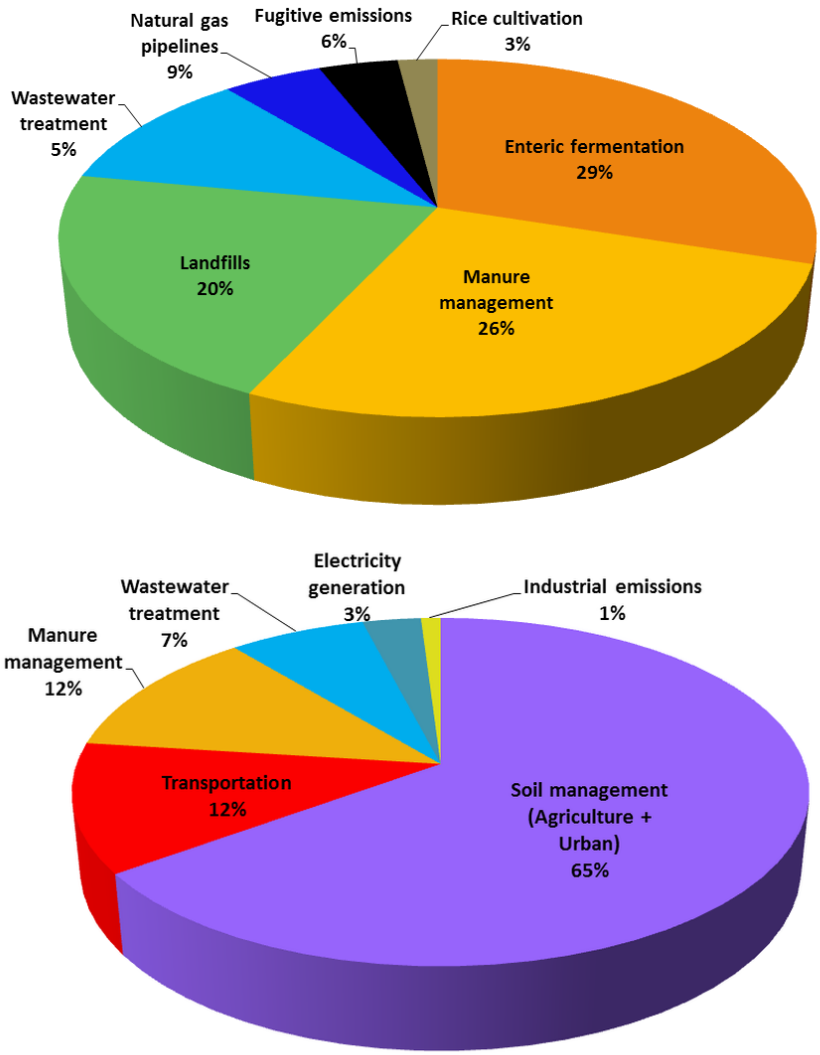


**Figure 1.1.** 2013 California emissions inventory for (top) methane ($CH_4$) - 41.1 million ton $CO_2$eq at GWP = 25; and (bottom) nitrous oxide ($N_2O$) - 13.1 million ton $CO_2$eq at GWP = 298 (Source: CARB GHG Inventory Tool, Nov 2015).

management is an important $CH_4$ source sector. Landfill gas contributes 20 % of the $CH_4$ inventory while waste water management processes account for 5 % of the $CH_4$ inventory and about 7 % of the state $N_2O$ inventory. There are differences in the distribution of major source categories in the nationwide and the state GHG inventories, which primarily reflect very large $CH_4$ emissions from dairies in California and differences in industry make-up. While $CH_4$ emissions from natural gas and petroleum systems (29 %) is very significant in the USEPA

inventory, in the state inventory, the industry accounts for a smaller fraction of just above 15 % (Figure 1.1). It should be noted that California is the fourth largest oil producing state in the country and one of the largest consumers of natural gas. Also, the current $CH_4$ estimates from O&G industry represent a 50 % increase from the same in the previous version of the inventory (CARB, 2013) which demonstrates that inventory estimates of this sector are in flux and improving. On the other hand, while the transportation sector only accounts for 4 % of annual $N_2O$ emissions in the national inventory; this sector has a much larger contribution in the statewide $N_2O$ inventory (Figure 1.1) accounting for 12 % of the total $N_2O$ emissions. This is true even after the latest revisions to the previous version of the inventory which had the contribution to $N_2O$ from the transportation sector at 18 %. It should be noted that direct and indirect soil emissions of $N_2O$ from agricultural management processes along with residential and commercial fertilizer use is, by far, the dominant source of $N_2O$ in both the state (65 %) and the nationwide inventory. Top-down estimation methods can provide a valuable tool to verify, validate and, in some cases, to update the ARB inventory which has seen significant revisions for some $CH_4$ and $N_2O$ source sectors in its latest edition.

## 2.2 Literature Review

The success of ARB's GHG emission reduction efforts is contingent on accurate accounting of emissions. A majority of $CH_4$ emissions are produced by agricultural sources namely enteric fermentation from cattle and management of animal waste (~ 60 %) and if decomposition of waste from landfills and waste water treatment is included, a vast majority of the emissions originate from microbially-mediated biological pathways (~ 83 %; CARB, 2015). Such emissions sources are more likely to be area sources that are spatially and temporally variable, and thus difficult to quantify. For instance, differences in manure management practices

in dairies from that in feedlots have been reported to result in drastically different $CH_4$ emissions (Owen and Silver, 2014). The GHG inventory compiled by ARB for emission accounting is based on a 'bottom-up' emission factor (EF) approach. This approach utilizes weighted average EFs (e.g. methane conversion factor for different animal waste management systems) which account for several process and meteorological factors (e.g. seasonal changes in temperatures, long-term retention time etc. for animal waste systems). These weighted EFs may still not be completely accurate or adequate for estimating emissions from source categories like dairies and livestock, landfills, rice cultivation etc. that have a large annual range of emissions that depend on a number of factors and management practices, some of which may not be resolved (or even possible to quantify) using the ARB methodology. Emission factors derived from ground-based and airborne measurements from rice agriculture in California suggest an underestimation of this source category in the ARB GHG inventory (McMillan et al., 2007; Peischl et al., 2012) even after accounting for rice residue management practices in winter and using the significantly revised new seasonally weighted emission factors. Previous literature, mostly evolving from studies conducted in California, has demonstrated the spatiotemporal nature and seasonal dependence of $CH_4$ emissions from dairy and livestock (Owen and Silver, 2014), natural and restored peatlands / wetlands (Cicerone et al., 1983; Teh et al., 2011; Hatala et al., 2012; Knox et al., 2014), and from agriculture (including rice) (Salas et al., 2006; Knox et al., 2014; McMillan et al., 2007). Currently, the oil and natural gas (O&G) production / extraction sector accounts for about 6 % of the state's total $CH_4$ emissions. A comprehensive spatially resolved state $CH_4$ emissions inventory for the oil production and natural gas system sector, generated from an assortment of public information and US-EPA (Environmental Protection Agency) emission factors, estimates emissions that are 3-7 times larger than the state inventory (Jeong et al., 2014)

pointing to the need to address uncertainties in the latter. Emissions from major $N_2O$ sources of agricultural soil management and livestock manure management (Figure 1.1 b) are also controlled by microbial activity that scale to a number of environmental factors like N fertilizer application rate, soil organic matter content, moisture, management practices, meteorological conditions etc. (Guo et al., 2011). In the light of so many variables, it is important to verify the emission factors which the ARB inventory uses to compute emissions from these $N_2O$ sources, using measurement-based approaches.

A series of 'top-down' measurement campaigns conducted in Southern California report a range of $CH_4$ emissions from oil and natural gas activities, all of which are larger than that is currently attributed to this region in the ARB GHG inventory (Wunch et al., 2009; Peischl et al., 2013). Inverse modeling of airborne CalNex 2010 observations over California suggest underestimation of the $CH_4$ emissions from landfills and wastewater and the oil and gas sector in the GHG inventory (Wecht et al., 2014). Most or all of these studies suffer from some limitations. Inverse modeling from aircraft observations or direct airborne flux computation can estimate surface $CH_4$ emissions but are unable to capture temporal variations in the absence of long term monitoring. Ground based flux towers (Baldocchi et al., 2012; Hatala et al., 2012; Knox et al., 2014) are very suitable and representative measurement methods over homogenous area source configurations (e.g. wetlands, rice etc.) but not so much over O&G production areas and dairy / livestock regions. Inverse dispersion of either tower or remote sensing observations can provide continuous long term monitoring but are constrained by potential inaccuracies in the transport model and *a priori* emission maps. It is difficult to evaluate the inventory at regional scales accurately in the absence of continuous measurements over long periods of time covering large areas. Year-long WRF-STILT inversion of atmospheric $CH_4$ observations have been

performed at the Walnut Grove tower (WGC) in the Central Valley of California to estimate seasonally averaged $CH_4$ emissions that show clear patterns of seasonal variations along with 55 – 84 % higher emissions than California-specific *a priori* models (Jeong et al., 2012a). These measurements, when executed over a network of tall towers, allow for constraining emissions from individual sub-regions over a larger regional scale with lower uncertainties (Jeong et al., 2013).

Global atmospheric concentrations of $N_2O$ have been steadily increasing at a rate of 0.2 - 0.3 % per year (Denman et al., 2007) with current global background levels in excess of 325 ppb. Significant portions of this atmospheric increase have been attributed to extensive use of nitrogen-based fertilizers (Park et al., 2012). The Central Valley of California is a major agricultural region with a per capita output that surpasses any other region in the world (CASR, 2011). The Valley has a multitude of agricultural and biological sources of $N_2O$ including synthetic and organic fertilizer application, manure management, wetlands, wastewater treatment, and crop residue management (Xiang et al., 2013). Emissions of $N_2O$ from agricultural soils are estimated in the ARB inventory using an emission factor approach (Guo et al., 2011). $N_2O$ emissions from the soil are microbially-driven and are affected by numerous environmental factors like N fertilizer application rate, soil organic matter content, moisture, management practices, meteorological conditions etc., which make these emissions spatially and temporally variable, and thus challenging to characterize (van Groenigen et al., 2010; Guo et al., 2011; Hoben et al., 2011; Linquist et al., 2012). Large uncertainties exist in the bottom-up regional estimation of $N_2O$ emissions (NRC, 2010). Very few regional 'top-down' assessments of the $N_2O$ inventory in the US exist, and even fewer over the Central Valley of California. A top down inverse approach based on STILT LPDM back trajectory analysis of aircraft observations

across the US reported under-prediction of $N_2O$ emissions in the EDGAR and GEIA inventory by a factor of ~ 2.6 to 3.0, respectively (Kort et al., 2008). There were, however, no airborne flask samples collected over the Central Valley in this study and the estimates were limited to the early summer period. Atmospheric column-based abundance studies in the Los Angeles region have reported significant underestimation of $N_2O$ by EDGAR and ARB GHG inventories but with high uncertainties. Jeong et al. (2012b) reported the first top-down inverse estimates of $N_2O$ emissions measured at a tall tower based on the WRF-STILT framework that captured the complete annual cycle of $N_2O$ emissions in the Central Valley of California. Spatially averaged $N_2O$ emissions from regions within ~ 150 km of the tower with a large agriculture and dairy / livestock influence were higher than EDGAR inventories by a factor of about 1.6 - 2.5 over different seasons. A comprehensive account of $N_2O$ emissions from field-scale measurements conducted in dairies worldwide show a great discrepancy with modeled emissions derived using inventory emission factors (Owen and Silver, 2014). The PMF results in Guha et al., 2015 indicate that statistically no $N_2O$ is apportioned to the vehicle emissions source factor in the semi-urban Bakersfield region even though it is included as a significant source in the ARB inventory.

## 2.3 Rationale and Objectives

Most of the important GHGs are relatively long lived in the atmosphere, allowing them to mix globally. The global mixing thereby generates background GHG concentrations on top of which any regional variations must be measured hence requiring very precise and accurate measurements. GHGs are emitted from multiple anthropogenic sources that simultaneously emit additional volatile organic compounds (VOCs), some of which have sufficiently long life times to enable their detection at a downwind receptor point after being locally emitted from a source.

Many of the major sources of $CH_4$ and $N_2O$ in California inventory have fairly interpretable signatures of VOC emissions that can serve as tracers for those specific source categories. Hence, GHG emission inventories from multiple sources can be constrained through simultaneous measurements of GHG's and VOC gas species that, otherwise, are difficult to apportion based on stand-alone GHG measurements and modeling. This project is not the first to use VOC tracers to ascribe observed enhancements of atmospheric $CH_4$ to specific sources. For example, the project investigator (Goldstein) was involved in an analysis by Shipham et al. (1995) in which VOC tracers were used to quantify contributions from different methane sources in New England. A more recent study by Lanz et al. (2009) used Positive Matrix Factorization of measured VOCs as tracers to define factors corresponding to four different source categories and then obtained good correlation for some of those factors with observed $CH_4$ concentrations. Multiple studies have measured simultaneous emissions of methane and VOCs for livestock and manure management (e.g. Ngwabie et al. 2008; Shaw et al. 2007) presenting correlations and emission ratios of $CH_4$ versus individual VOCs. Results from these and other related studies could, in theory, be used to guide our analysis of the observations for GHGs and VOCs at any fixed site.

This report describes a collaborative project that built on an existing infrastructure of GHG measurements at a tall tower site in California. The specific objectives of this study were:

1) To perform continuous and high-accuracy mixing ratio and vertical profile measurements of a suite of VOCs and $N_2O$, coordinated with the ongoing continuous measurements of $CO_2$, $CH_4$, and combustion tracer CO over a complete annual cycle at the Walnut Grove tall tower site (WGC; Andrews et al., 2013) in California's Central Valley to assess the apportionment of GHG sources in this region.

2) To analyze the mixing ratio time series of GHGs and VOC tracers using a statistical source apportionment tool called Positive Matrix Factorization (PMF), in order to distinguish individual source category contributions to the regional $CH_4$ and $N_2O$ emissions.
3) To evaluate the temporal dependence (if any) in the relative distribution of the apportioned GHG source contributions through PMF analysis on shorter season-specific time periods.
4) To compare the statistical source apportionment results from the PMF analysis with that derived from an already existing inverse modeling analysis framework (developed for previously collected data at the Walnut Grove tower to ascribe regional emission estimates to specific source sectors), and also to any regional 'bottom-up' GHG inventory for the source regions in the vicinity of and influencing the GHG observations at this site.

In this report we describe in detail how each of these objectives were met, the results obtained, and their implications and significance. Measurements include vertical profiles from the ground to near the top of the WGC tower (525 m) for most species. We parse the year-round measurements into smaller data sets representative of the prevailing season and applied PMF analysis on subsets of combined GHG - VOC data representing unique temporal periods. To determine the major categories of emissions sources contributing to the apportionment of $CH_4$ and $N_2O$ in this region, we used the simultaneous apportionment of VOCs as potential source markers, wind rose plots, and diurnal and vertical profiles to identify and categorize the PMF-generated statistical combinations (factors) as 'sources' or combinations of 'collocated sources'. We hypothesized that the regional dairy and cattle industry will have a significant imprint on the

apportionment of both $CH_4$ and $N_2O$ while the vast expanse of agriculture around the site is likely to have a dominant impact on $N_2O$ signals. We investigate the seasonal variation of the $CH_4$ and $N_2O$ emissions distribution over seven different time periods from mid-2012 until mid-2013. This study provides advantages over short term GHG measurement studies in multi-source regions that only provide a snapshot in time like airborne flux measurements, or back-trajectory analysis on aircraft observations. We hypothesized the $N_2O$ emissions from agriculture will show a seasonal trend that coincides with the primary agricultural growing season in the Central Valley while no major seasonal dependence will be observed for $CH_4$ originating from dairies and cattle feedlots.

This project also established the first long-term baseline measurements of certain GHG source marker VOCs in the Central Valley of California, facilitating the establishment of GHG source category based emission estimates. Together with the accompanying inverse model analysis, these data will provide regionally appropriate GHG concentration and emissions estimates for the Central Valley, against which the effectiveness of future GHG emission control measures, can be quantified. This project also provides data to show the importance of long term monitoring of vertical profiles for a broad suite of tracers on a tall tower as a tool for assessing regional air pollution emissions in California, and thus provides a template for implementing a larger scale network of sites.

## 2.3 References

AB32, 2006. California Global Warming Solutions Act summary document. http://www.leginfo.ca.gov/pub/05-06/bill/asm/ab_00010050/ab_32_bill_20060927_chaptered.pdf

Andrews, A. E., J. D. Kofler, M. E. Trudeau, J. C. Williams, D. H. Neff, K. A. Masarie, D. Y. Chao, D. R. Kitzis, P. C. Novelli, C. L. Zhao, E. J. Dlugokencky, P. M. Lang, M. J. Crotwell, M. L. Fischer, M. J. Parker, J. T. Lee, D. D. Baumann, A. R. Desai, C. O. Stanier, S. F. J. De Wekker, D. E.Wolfe, J. W. Munger, and P. P. Tans (2014), CO2, CO, and CH4 measurements from tall towers in the NOAA Earth System Research Laboratory's Global Greenhouse Gas Reference Network: instrumentation, uncertainty analysis, and recommendations for future high-accuracy greenhouse gas monitoring efforts, Atmospheric Measurement Techniques, 7(2), 647-687.

Baldocchi, D., Detto, M., Sonnentag, O., Verfaillie, J., Teh, Y. A., Silver, W. and Kelly, N. M.: The challenges of measuring methane fluxes and concentrations over a peatland pasture, Agric. For. Meteorol., 153, 177–187, doi:10.1016/j.agrformet.2011.04.013, 2012.

CARB (2013), California Greenhouse Gas Inventory for 2000-2012 - by IPCC Category. http://www.arb.ca.gov/cc/inventory/data/data.htm. accessesd on September 23, 2014.

CARB (2015), California Greenhouse Gas Inventory for 2000-2013 - by IPCC Category. http://www.arb.ca.gov/cc/inventory/data/data.htm. accessesd on Novemeber 9, 2015.

CASR (2011), California Agricultural Statistics Crop Report, 2011. created by California Department of Food and Agriculture, Sacramento, CA and United States Department of Agriculture.

Cicerone, R. J. and Shetter, J. D.: Sources of atmospheric methane: Measurements in rice paddies and a discussion, J. Geophys. Res., 86(C8), 7203, doi:10.1029/JC086iC08p07203, 1981.

Crutzen, P. J., Mosier, a. R., Smith, K. a. and Winiwarter, W.: $N_2O$ release from agro-biofuel production negates global warming reduction by replacing fossil fuels, Atmos. Chem. Phys. Discuss., 7(4), 11191–11205, doi:10.5194/acpd-7-11191-2007, 2007.

Denman, K.L., G. Brasseur, A. Chidthaisong, P. Ciais, P.M. Cox, R.E. Dickinson, D. Hauglustaine, C. Heinze, E. Holland, D. Jacob, U. Lohmann, S Ramachandran, P.L. da Silva Dias, S.C. Wofsy and X. Zhang, 2007: Couplings Between Changes in the Climate System and Biogeochemistry. In: Climate Change 2007: The Physical Science Basis. Contribution of Working Group I to the Fourth Assessment Report of the Intergovernmental Panel on Climate Change [Solomon, S., D. Qin, M. Manning, Z. Chen, M. Marquis, K.B. Averyt, M.Tignor and H.L. Miller (eds.)]. Cambridge University Press, Cambridge, United Kingdom and New York, NY, USA.

Forster, P. ., Ramaswamy, V. ., Artaxo, P. ., Berntsen, T. ., Betts, R. ., Fahey, D. W. ., Haywood, J. ., Lean, J. ., Lowe, D. C. ., Myhre, G. ., Nganga, J. ., Prinn, R. ., Raga, G. ., Schulz, M. . and Dorland, R. V.: 2007: Changes in Atmospheric Constituents and in Radiative Forcing, in Climate Change 2007: The Physical Science Basis. Contribution of Working Group I to the Fourth Assessment Report of the Intergovernmental Panel on Climate Change, edited by S. Solomon, D.

Galloway, J. N., Townsend, A. R., Erisman, J. W., Bekunda, M., Cai, Z., Freney, J. R., Martinelli, L. a, Seitzinger, S. P. and Sutton, M. a: Transformation of the nitrogen cycle: recent trends, questions, and potential solutions., Science, 320(5878), 889–92, doi:10.1126/science.1136674, 2008.

Gentner, D. R., Isaacman, G., Worton, D. R., Chan, A. W. H., Dallmann, T. R., Davis, L., Liu, S., Day, D. A., Russell, L. M., Wilson, K. R., Weber, R., Guha, A. and Harley, R. A.:

Elucidating secondary organic aerosol from diesel and gasoline vehicles through detailed characterization of organic carbon emissions, , doi:10.1073/pnas.1212272109/-/DCSupplemental.www.pnas.org/cgi/doi/10.1073/pnas.1212272109, 2012.

Guha, A., Gentner, D. R., Weber, R. J., Provencal, R., and Goldstein, A. H.: Source apportionment of methane and nitrous oxide in California's San Joaquin Valley at CalNex 2010 via positive matrix factorization, Atmos. Chem. Phys., 15, 12043-12063, doi:10.5194/acp-15-12043-2015, 2015.

Guo, L., Luo, D., Li, C. and Fitzgibbon, M.: Development of Spatial Inventory of Nitrous Oxide Emissions from Agricultural Land Uses in California Using Biogeochemical Modeling, 2011.

Hatala, J. A., Detto, M., Sonnentag, O., Deverel, S. J., Verfaillie, J. and Baldocchi, D. D.: Greenhouse gas (CO2, CH4, H2O) fluxes from drained and flooded agricultural peatlands in the Sacramento-San Joaquin Delta, Agric. Ecosyst. Environ., 150, 1–18, doi:10.1016/j.agee.2012.01.009, 2012.

Hoben, J. P., Gehl, R. J., Millar, N., Grace, P. R. and Robertson, G. P.: Nonlinear nitrous oxide (N2O) response to nitrogen fertilizer in on-farm corn crops of the US Midwest, Glob. Chang. Biol., 17(2), 1140–1152, 2011.

IPCC, 2007. Climate Change 2007: Working Group I: The Physical Science Basis. Intergovernmental Panel on Climate Change. Solomon, S., D. Qin, M. Manning, Z. Chen, M. Marquis, K.B. Averyt, M. Tignor and H.L. Miller (eds.) Cambridge University Press, Cambridge, United Kingdom and New York, NY, USA.

Jeong, S., Millstein, D. and Fischer, M. L.: Spatially Explicit Methane Emissions from Petroleum Production and the Natural Gas System in California, 2014.

Jeong, S., Zhao, C., Andrews, A. E., Bianco, L., Wilczak, J. M. and Fischer, M. L.: Seasonal variation of CH 4 emissions from central California, J. Geophys. Res., 117(D11), D11306, doi:10.1029/2011JD016896, 2012a.

Jeong, S., Zhao, C., Andrews, A. E., Dlugokencky, E. J., Sweeney, C., Bianco, L., Wilczak, J. M. and Fischer, M. L.: Seasonal variations in N 2 O emissions from central California, Geophys. Res. Lett., 39(16), n/a–n/a, doi:10.1029/2012GL052307, 2012b.

Kort, E. a., Eluszkiewicz, J., Stephens, B. B., Miller, J. B., Gerbig, C., Nehrkorn, T., Daube, B. C., Kaplan, J. O., Houweling, S. and Wofsy, S. C.: Emissions of CH 4 and N 2 O over the United States and Canada based on a receptor-oriented modeling framework and COBRA-NA atmospheric observations, Geophys. Res. Lett., 35(18), L18808, doi:10.1029/2008GL034031, 2008.

Knox, S. H., Sturtevant, C., Matthes, J. H., Koteen, L., Verfaillie, J. and Baldocchi, D.: Agricultural peatland restoration: effects of land-use change on greenhouse gas (CO2 and CH4 ) fluxes in the Sacramento-San Joaquin Delta., Glob. Chang. Biol., 1–16, doi:10.1111/gcb.12745, 2014.

Linquist, B., Van Groenigen, K. J., Adviento-Borbe, M. A., Pittelkow, C. and Van Kessel, C.: An agronomic assessment of greenhouse gas emissions from major cereal crops, Glob. Chang. Biol., 18(1), 194–209, 2012.

McMillan, A. M. S., Goulden, M. L. and Tyler, S. C.: Stoichiometry of CH 4 and CO 2 flux in a California rice paddy, J. Geophys. Res., 112(G1), G01008, doi:10.1029/2006JG000198, 2007.

Misztal, P. K., Karl, T., Weber, R., Jonsson, H. H., Guenther, a. B. and Goldstein, a. H.: Airborne flux measurements of biogenic volatile organic compounds over California, Atmos. Chem. Phys. Discuss., 14(6), 7965–8013, doi:10.5194/acpd-14-7965-2014, 2014.

Montzka, S. A., Dlugokencky, E. J. and Butler, J. H.: Non-CO2 greenhouse gases and climate change., Nature, 476(7358), 43–50, doi:10.1038/nature10322, 2011.

NRC (2010), National Research Council, Verifying Greenhouse Gas Emissions: Methods to Support International Climate Agreements, National Academies Press, Washington, D. C.

Ngwabie, N. M., Schade, G. W., Custer, T. G., Linke, S. and Hinz, T.: Abundances and Flux Estimates of Volatile Organic Compounds from a Dairy Cowshed in Germany, J. Environ. Qual., 37(2), 565, doi:10.2134/jeq2006.0417, 2008.

Owen, J. J. and Silver, W. L.: Greenhouse gas emissions from dairy manure management: a review of field-based studies., Glob. Chang. Biol., doi:10.1111/gcb.12687, 2014.

Pacala, Stephen W., et al.(2010): Verifying Greenhouse Gas Emissions: Methods to Support International Climate Agreements, The National Academies Press, Washington, DC, 124 pp., 2010.

Park, J.-H., Goldstein, a H., Timkovsky, J., Fares, S., Weber, R., Karlik, J. and Holzinger, R.: Active atmosphere-ecosystem exchange of the vast majority of detected volatile organic compounds., Science, 341(6146), 643–7, doi:10.1126/science.1235053, 2013.

Peischl, J., Ryerson, T. B., Brioude, J., Aikin, K. C., Andrews, a. E., Atlas, E., Blake, D., Daube, B. C., de Gouw, J. a., Dlugokencky, E., Frost, G. J., Gentner, D. R., Gilman, J. B., Goldstein, a. H., Harley, R. a., Holloway, J. S., Kofler, J., Kuster, W. C., Lang, P. M., Novelli, P. C., Santoni, G. W., Trainer, M., Wofsy, S. C. and Parrish, D. D.: Quantifying

sources of methane using light alkanes in the Los Angeles basin, California, J. Geophys. Res. Atmos., 118(10), 4974–4990, doi:10.1002/jgrd.50413, 2013.

Salas, W., P. Green, S. Frolking, C. Li, and S. Boles (2006), Estimating irrigation water use for California agriculture: 1950s to present, Rep. CEC-500-2006-057, Public Interest Energy Res. Program, California Energy Commission, Sacramento, California.

Santoni, G. W.; Xiang, B.; Kort, E. A.; Daube, B.; Andrews, A. E.; Sweeney, C.; Wecht, K.; Peischl, J.; Ryerson, T. B.; Angevine, W. M.; Trainer, M.; Nehrkorn, T.; Eluszkiewicz, J.; Wofsy, S. C. (2012) California's Methane Budget derived from CalNex P-3 Aircraft Observations and the WRF-STILT Lagrangian Transport Model. AGU Fall Meeting 2012, San Francisco, CA.

Shaw, S. L., Mitloehner, F. M., Jackson, W., Depeters, E. J., Fadel, J. G., Robinson, P. H., Holzinger, R. and Goldstein, A. H.: Volatile organic compound emissions from dairy cows and their waste as measured by proton-transfer-reaction mass spectrometry., Environ. Sci. Technol., 41(4), 1310–6 [online] Available from: http://www.ncbi.nlm.nih.gov/pubmed/17593735, 2007.

Smith, P., D. Martino, Z. Cai, D. Gwary, H. Janzen, P. Kumar, B. McCarl, S. Ogle, F. O'Mara, C. Rice, B. Scholes, O. Sirotenko, 2007: Agriculture. In Climate Change 2007: Mitigation. Contribution of Working Group III to the Fourth Assessment Report of the Intergovernmental Panel on Climate Change [B. Metz, O.R. Davidson, P.R. Bosch, R. Dave, L.A. Meyer (eds)], Cambridge University Press, Cambridge, United Kingdom and New York, NY, USA.

Teh, Y. A., Silver, W. L., Sonnentag, O., Detto, M., Kelly, M. and Baldocchi, D. D.: Large Greenhouse Gas Emissions from a Temperate Peatland Pasture, Ecosystems, 14(2), 311–325, doi:10.1007/s10021-011-9411-4, 2011.

USEPA, 2014. Inventory of U.S. Greenhouse Gas Emissions and Sinks 1990-2012, USEPA . http://www.epa.gov/climatechange/ghgemissions/usinventoryreport.html#fullreport

van Groenigen, J. W., Velthof, G. L., Oenema, O., Van Groenigen, K. J. and Van Kessel, C.: Towards an agronomic assessment of N2O emissions: A case study for arable crops, Eur. J. Soil Sci., 61(6), 903–913, 2010.

Wecht, K. J., Jacob, D. J., Sulprizio, M. P., Santoni, G. W., Wofsy, S. C., Parker, R., Bösch, H. and Worden, J.: Spatially resolving methane emissions in California: constraints from the CalNex aircraft campaign and from present (GOSAT, TES) and future (TROPOMI, geostationary) satellite observations, Atmos. Chem. Phys., 14(15), 8173–8184, doi:10.5194/acp-14-8173-2014, 2014.

Wunch, D., Wennberg, P. O., Toon, G. C., Keppel-Aleks, G. and Yavin, Y. G.: Emissions of greenhouse gases from a North American megacity, Geophys. Res. Lett., 36(15), L15810, doi:10.1029/2009GL039825, 2009.

Xiang, B., Miller, S. M., Kort, E. a., Santoni, G. W., Daube, B. C., Commane, R., Angevine, W. M., Ryerson, T. B., Trainer, M. K., Andrews, A. E., Nehrkorn, T., Tian, H. and Wofsy, S. C.: Nitrous oxide ($N_2O$) emissions from California based on CalNex airborne measurements, J. Geophys. Res. Atmos., 118(7), 2809–2820, doi:10.1002/jgrd.50189, 13.

Zhao, C., Andrews, A. E., Bianco, L., Eluszkiewicz, J., Hirsch, A., MacDonald, C., Nehrkorn, T. and Fischer, M. L.: Atmospheric inverse estimates of methane emissions from Central California, J. Geophys. Res., 114(D16), D16302, doi:10.1029/2008JD011671, 2009.

# 3. Measurements

## 3.1. Site, Greenhouse Gas Sources and Meteorology

The GHG and VOC measurements were made at Walnut Grove tower (WGC; Andrews et al., 2013) near Walnut Grove, California (121.49°W, 38.27°N, and 0 m above sea level). WGC is a tall TV signal transmission tower extending 525 m above ground level (a.g.l). WGC is located about 50 km south of the Sacramento metropolitan area and about 50 - 100 km west-southwest from various urban cores within the extended San Francisco Bay Area as seen in the land cover and potential source map of the region in Figure 3.1. WGC is located at the eastern edge of the ~ 3800 $km^2$ Sacramento - San Joaquin River Delta (referred to as the Delta from here on), an expansive inland river delta and estuary. Much of the land in the Delta, through the past century, has been reclaimed through construction of levee barriers and subsequently drained and used for agriculture. Currently, the Delta serves as an agricultural hotspot of California producing $500 million/year worth of crops that include corn, walnuts, pears, tomatoes, nursery stock, hay and importantly, dairy and livestock (CCCR 2013; SacCR 2013; SCR 2013). As seen in Figure 3.1 created using the National Land Cover Database (Homer et al., 2007), cultivated crop land is ubiquitous around WGC especially to the west and south west of the site, which is the predominant wind direction during a major part of the annual cycle as evidenced in the seasonal day time and night time wind rose plots in Figures 3.2 and 3.3, respectively. Thus we can expect strong influence of biogenic VOC tracers on signals measured at WGC during the growing season. Fertilizer use on farm lands is a major source of $N_2O$, and thus the intensive agriculture around WGC is expected to be a significant contributor to $N_2O$ signals measured at

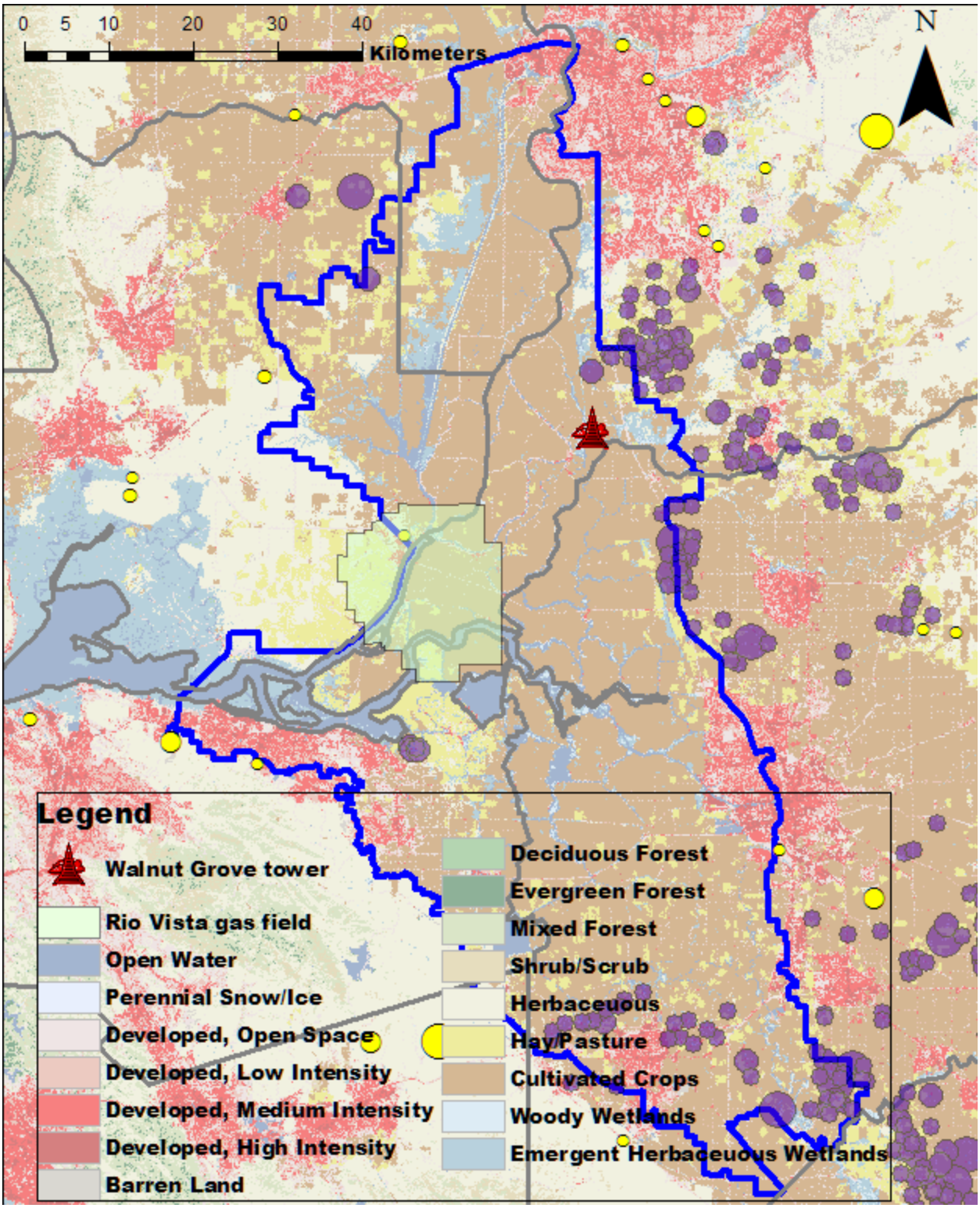


**Figure 3.1.** Walnut Grove tower (WGC) site map showing land cover (Homer et al., 2007) and location of local $CH_4$ and $N_2O$ sources, including dairies (solid purple circles) and landfills (solid yellow circles).The increasing size of the purple and yellow circles represent increasing number of cows and amount of waste treated, respectively. The solid blue boundary line represents the extent of the Sacramento-San Joaquin River Delta.

WGC. The site is in close proximity to many dairy and livestock operations, providing an additional major $CH_4$ and $N_2O$ source. Immediately to the south of WGC lies the San Joaquin County which is home to more than 240,000 dairy and livestock cattle (CASR, 2013). Some portions of the Delta exist as natural wetlands (Figure 3.1), while some of the low lying islands are being converted and restored as wetlands by permanent flooding (Miller et al., 2008) to reverse land subsidence due to peat oxidation. Alongside the relatively newer practice of flooded agricultural systems (like rice) in the Delta (Hatala et al., 2012; Knox et al., 2014), these wetland / peatland ecosystems are a $CH_4$ source (Le Mer and Roger, 2001; Miller, 2011; Teh et al., 2011) and such signals if large enough may be detected at WGC due to its proximity. The intensive rice agriculture in the Sacramento Valley, much of which lies around 100 km north-northwest of WGC, is a known $CH_4$ source that can be a significant contributor to the local $CH_4$ budget during the growing season (McMillan et al., 2007; Peischl et al., 2012). One of the major natural gas fields in California, the Rio Vista gas field, is located 15 - 25 km immediately upwind from WGC in the Delta. Though a number of smaller landfills exist in and around the urban regions, there are no landfills in the Delta.

WGC experiences a Mediterranean climate characterized by hot and dry summers and mild and rainy winters. In summers (Jun - Aug), the seasonal mean daytime temperatures (at 10 m a.g.l) reach a high of ~ 30°C with early morning lows of about ~ 14°C (Table 3.1). In winters (Dec - Feb), the seasonal daytime highs are ~ 14°C and nighttime lows are about 4°C. From annual precipitation records of the nearby town of Lodi located ~ 25 km southeast of WGC (CIMIS, 2013), the bulk of precipitation in the reported measurement period (Jun 2012 - Aug 2013; 14 inches) occurred during Dec 2012 – Jan 2013 with minor rain events during Feb - Mar 2013. A low-level day time marine inflow moves air inland from the San Francisco Bay Area

**Table 3.1.** Summary of information for seven seasonal sampling periods chosen for PMF analysis along with average temperatures during this period, data coverage and list of measured tracers.

| Season | Start/End date | Hourly average temperature range[a] (° C) | Species not measured[b] | Number of hourly samples[c] |
|---|---|---|---|---|
| Summer 2012 | Jun 16 / Aug 31 | 14 - 30 | $N_2O$ | 1583 |
| Early Fall 2012 | Sep 1 / Oct 16 | 13 - 28 | $N_2O$ | 1061 |
| Late Fall 2012 | Oct 17 / Nov 30 | 9 - 20 | N.A. | 774 |
| Winter / Wet season | Dec 1 / Jan 29 | 4 - 13 | MeOH | 744 |
| Winter/ Spring 2013 | Feb 16 / Apr 4 | 4 - 17 | $N_2O$ , MeOH | 1072 |
| Spring 2013 | Apr 6 / May 31 | 12 - 25 | N.A. | 1151 |
| Summer 2013 | Jun 1 / Aug 4 | 15 - 30 | N.A. | 1056 |

[a] range reflects average daily low and average daily high over the sampling period measured at 10 m a.g.l.
[b] N.A. - not applicable; all 13 tracers measured and included in PMF analysis; measured tracers include $CH_4$, $N_2O$, CO, benzene, toluene, acetonitrile, methanol, acetaldehdye, acetone, methyl ethyl ketone, methyl vinyl ketone + methacrolein, isoprene and monoterpenes.
[c] rows of data containing extended periods of missing VOCs removed all together.

into the Central Valley through the Carquinez Straits and along the Delta (Bao et al., 2007). This synoptic onshore wind provides the prevalent wind direction at WGC (91 m a.g.l) during the spring, summer and early fall season (Apr – Sep) that is driven by intense daytime heating in the Central Valley that creates a low pressure over WGC as compared to the coast (Figure 3.2). The day time air flow is strongest in the late afternoon hours and weakest during the morning. This flow can transport pollution from the San Francisco Bay Area into the Central Valley past WGC (Zhong et al., 2004). These dominant flows are likely to bring GHG and VOC emissions from the upwind sources in the greater San Francisco Bay Area and the Delta to WGC.

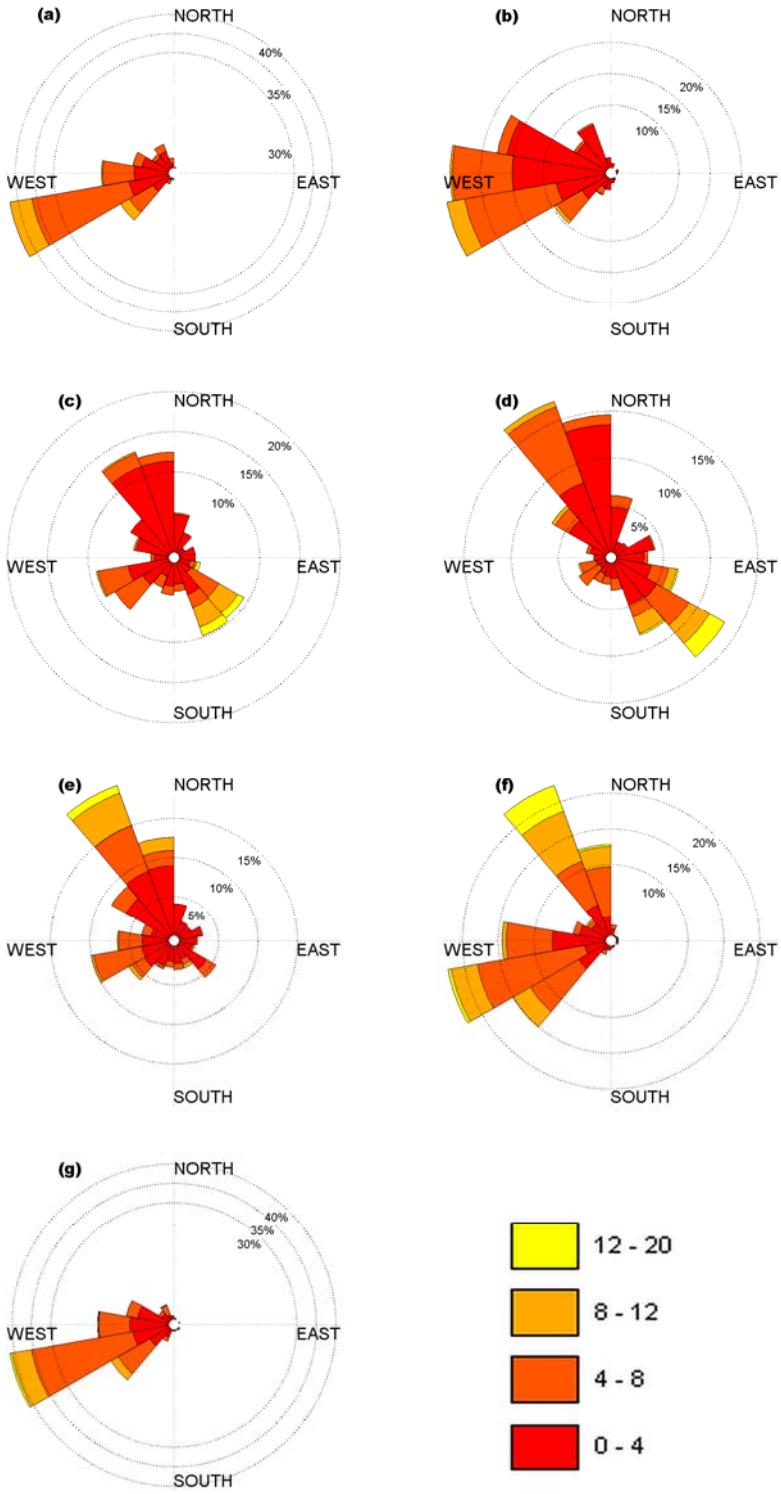


**Figure 3.2.** Daytime distribution of wind speed and direction at WGC during (a) Summer 2012; (b) early Fall 2012 (Sep 1 – Oct 15); (c) late Fall 2012 (Oct 16- Nov 30); (d) Winter (Dec-Jan); (e) Winter/Spring 2013 (Feb- Mar); (f) Spring 2013 (Apr- May); and (g) Summer 2013 (Jun- Aug). The values are measured at 91 m a.g.l, the color scale denotes wind speeds (in m/s) and the concentric circles represent the intensity subdivisions (in percent).

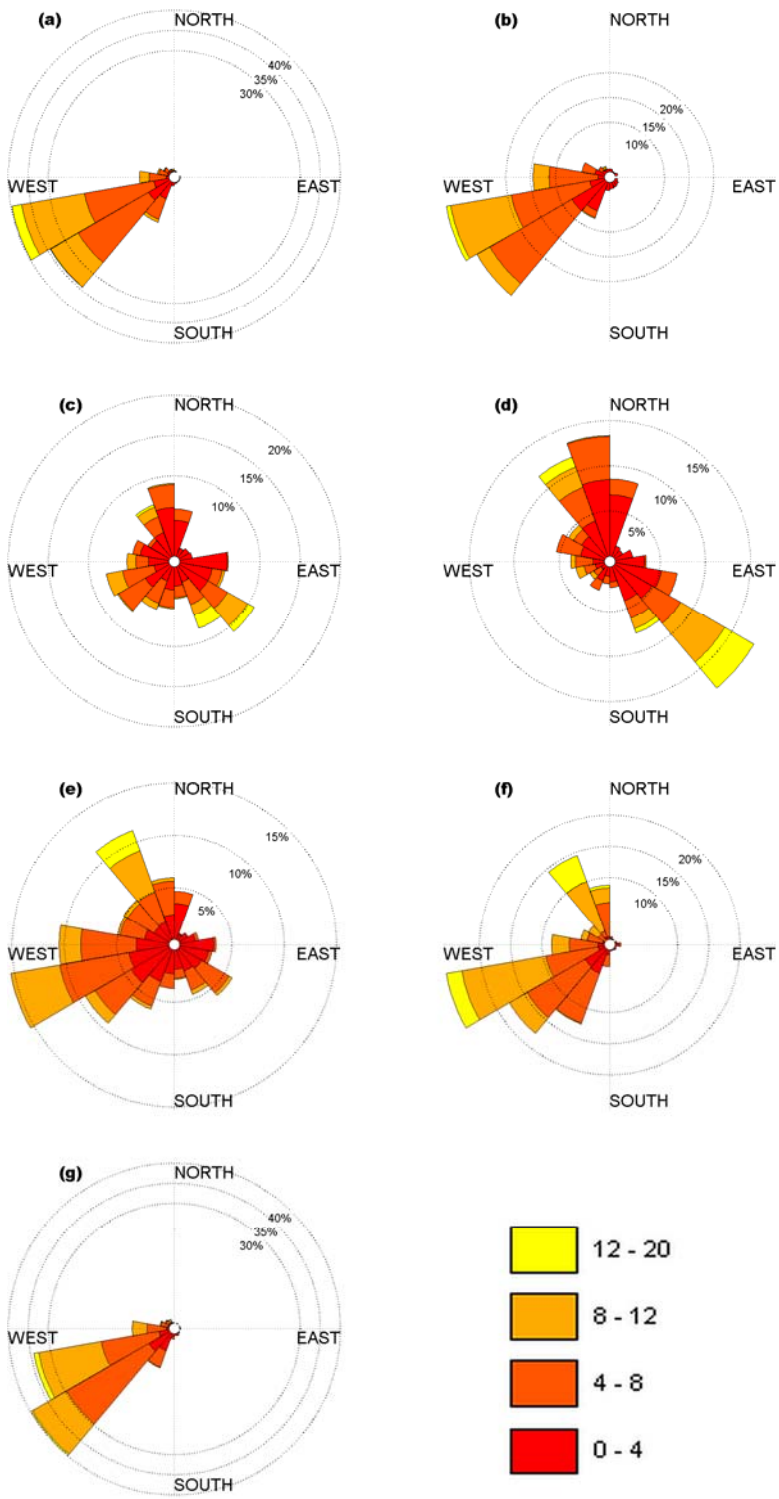


**Figure 3.3.** Nighttime distribution of wind speed and direction at WGC during (a) Summer 2012; (b) early Fall 2012 (Sep 1 – Oct 15); (c) late Fall 2012 (Oct 16- Nov 30); (d) Winter (Dec-Jan); (e) Winter/Spring 2013 (Feb- Mar); (f) Spring 2013 (Apr- May); and (g) Summer 2013 (Jun- Aug). The values are measured at 91 m a.g.l, the color scaledenotes wind speeds (in m/s) and the concentric circles represent the intensity subdivisions (in percent).

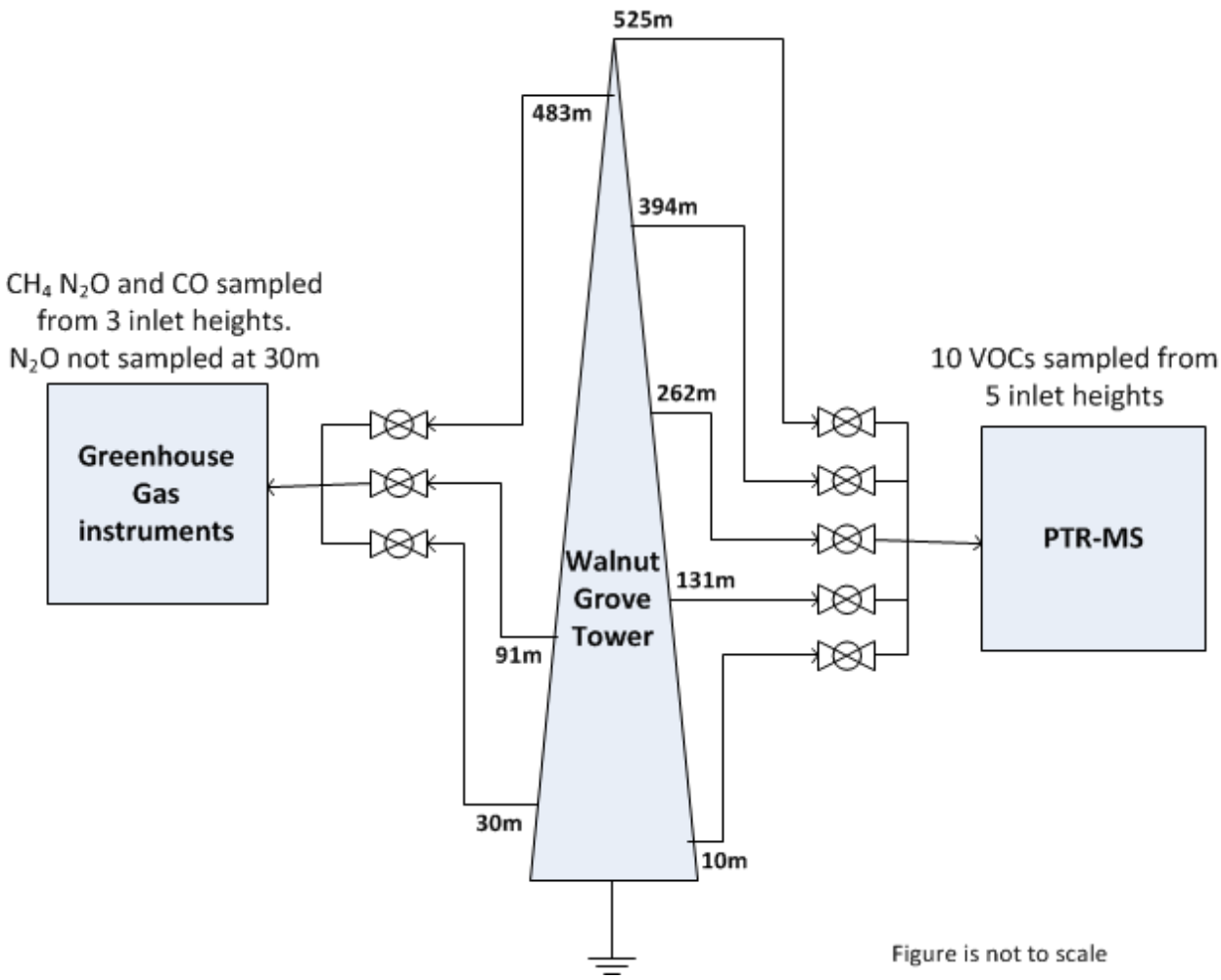


**Figure 3.4.** Simplified schematic at Walnut Grove tower showing location of sampling inlets for the GHG and PTR-MS instruments.

The intensity of this flow is reduced in the night due to nocturnal cooling such that down-valley flows and down-slope flows are observed over the plains and the eastern edges of the Central Valley, respectively. At WGC, however, at least during the warmer months (Apr - Sep), the coast - inland temperature gradient is still significant enough that the westerly upslope flows are maintained even during the nighttime (Figure 3.3). Higher up in the PBL, where the top air inlet was at 525 m a.g.l (Figure 3.4), downslope drainage flows brings air down the Sierra Nevada mountains from the east, thereby biogenic emissions from oak and coniferous forests and their oxidation products (not shown) accumulate in the residual layer at night and mix down

during the morning when vertical mixing begins (Misztal et al., 2014). In the absence (or rather, weakening) of diurnal surface radiative heating/cooling cycle in the late fall, winter and early spring months (Figures 3.2 c-e and 3.2 c-e), the mean flows at WGC are more variable and diffused, with confluence of down-valley winds from both the Sacramento Valley in the north and the San Joaquin Valley to the south at WGC. The site, thus, experiences mean flows from a directionally broader but more local (hence smaller) zone of influence during the cooler / wetter months (Oct-Mar). The fall / winter south-easterly flows make the dairy and livestock intensive regions of San Joaquin County directly upwind of WGC.

## 3.2. Instrumentation for GHGs and CO

The GHG measurements were made using a long-term set up and suite of instruments that are being used for inverse emissions estimates of $CH_4$ (and later $N_2O$) at WGC since 2007. More details about the instrumentation set-up can be found in literature emanating from previous studies at WGC (Zhao et al., 2009; Jeong et al., 2012a, 2012b). Briefly, the GHG measurements are made using a sampling and analysis system that combines pumps, air driers, and gas analyzers. Air samples are drawn from three heights (30, 91 and 483 m a.g.l) as seen in Figure 3.4 on the tower sequentially, then dried first to a water vapor dew point of 5°C using a condensing system and then on a temperature stabilized membrane drier to - 33°C dew point before being supplied to the gas analyzers. When switching between the three heights, the first 4.5 minutes of each sampling period is allowed for equilibration of the gas concentrations and instrument response, and thereafter the last 30 seconds is used as the actual measurement. $CH_4$ is measured using a cavity ring-down spectrometer (Picarro EnviroSense 1301) with an accuracy and precision of 0.3 ppb over a 30 second averaging period. The offset and gain are measured periodically and corrected for every six hours using NOAA primary gas standards. In addition to

this, ambient air is drawn from a separate line at 91 m a.g.l into flask samples that are collected every other day at 1400 PST and later analyzed at NOAA-ESRL to provide further quality check on the in-situ measurements. For $CH_4$, the measurement accuracy determined using the synchronized flask and in-situ measurements is ~ 1 ppb (Jeong et al., 2012a) which is significantly less than the daily range of atmospheric variations seen at WGC.

$N_2O$ was measured using an off-axis Integrated Cavity Output Spectroscopy (ICOS) analyzer (Model 907-0015; Los Gatos Research Inc. - LGR). The offset and gain of the LGR instrument were measured every 3 hours using two secondary standards tied to the NOAA calibration scale and checked using a third standard as a target gas, offset in time by 1.5 hr from the calibration gases. As with the $CH_4$ measurements, the in-situ $N_2O$ measurements are compared with $N_2O$ determined from the 1400 PST NOAA flask samples and 6-month mean offsets (typically < 0.3 ppb) are removed to minimize residual differences from NOAA background $N_2O$ used for inverse estimation. Following periodic calibration, individual $N_2O$ measurements have precision near 0.05 ppb on 2 minute averages and accuracy near 0.1 ppb, which is limited by the uncertainties in propagating the NOAA scale from the primary calibration gases to the in-situ measurements.

CO was measured using a gas filter correlation analyzer (48C Trace Level, Thermo Electron Corporation - TEC) as part of the NOAA Earth System Research Laboratory's (ESRL) Tall Tower GHG Observing Network (Andrews et al., 2013). Typical long term analytical uncertainty for the CO measurements is ~ 6 ppb which is reasonably precise to resolve variability on timescales used in this analysis (1 h). In addition, the LGR ICOS instrument also measures CO with precision of near 1 ppb. The CO data from the coincident measurements (TEC and LGR) were compared over the campaign and showed a high correlation ($R^2 > 0.99$). We are,

thereby, confident about the accuracy of the TEC CO measurements. We fill gaps in the CO time series using measurements from the LGR analyzer. The $CH_4$, CO and $N_2O$ data are finally averaged to hourly intervals to create a series with similar time resolution as the VOC measurements.

## 3.3. Measurement of VOCs

### 3.3.1. PTRMS Instrument and Measurement approach

Major progress in analytical capabilities for measuring atmospheric VOCs in real time with low detection limits has been achieved in the last decade using chemical ionization mass spectrometry. Proton Transfer Reaction Mass Spectrometry (PTR-MS) is a chemical ionization technique based on soft chemical ionization by hydronium ions ($H_3O^+$) in which a wide variety of VOCs (with a proton affinity higher than water) can be measured simultaneously with high time resolution (e.g. seconds) (de Gouw and Warneke, 2007; Blake et al., 2009). VOCs are measured with a mass spectrometer at their parent ion detected on the mass-to-charge (*m/z*) ratio equivalent to its protonated molecular mass (e.g. methanol which has atomic mass 32 is measured at *m/z* 33). Furthermore, the dominant constituents of air including $O_2$, $N_2$, $CO_2$, and $CH_4$ do not interfere with measurements since their proton affinities are lower than that of water. Because of its low detection limits and fast VOC sensing, PTR-MS instrumentation has been extensively deployed in atmospheric measurements worldwide over the past decade and has been included in major collaborative ground and airborne measurement missions such as CABERNET, INDOEX, TEXAQS2000, TEXAQS2006, ITCT2001, MINOS, NEAQS, MILAGRO, ITCT2004, BLODGETT, CABERNET (e.g., Holzinger et al., 2007; Karl et al., 2004; de Gouw et al., 2003; Misztal et al., 2014; Karl et al., 2013).

Automated in-situ measurement of VOCs was performed using a Proton Transfer Reaction Mass Spectrometer (PTR-MS) (IONICON Analytik, Innsbruck, Austria). Details on the detection limits and calibration approach of the PTR-MS instrument used at WGC can be found in previous literature (Holzinger et al., 2005; Fares et al., 2012; Park et al., 2013). At WGC, a 9.4 L/min (20 CFH) air sample stream was drawn from five separate Teflon sample intakes at different heights (10, 131, 262, 394, and 525 m a.g.l) as seen in Figure 3.4. Air was drawn continuously through all the five tubes and sub-samples were sequentially drawn from these tubes into the PTR-MS instrument for VOC analyses. A set of Teflon solenoid valves performed this switch of sample flow every two minutes thus requiring a 10 minute total cycle for one vertical profile measurement consisting of each of the five heights (10 m, 131 m, 262 m, 394 m, and 525 m a.g.l). After switching to a new inlet height, the first 30 s of a two minute period were discarded leaving 90 s of sample flow that was analyzed for ambient tracers. There were 6 of such two-minute periods in each hour of measurement and so effectively 540 s of data per hour was averaged from each inlet level in order to achieve detection limits in the lower pptv range. The instrumental background was evaluated every 3 hours for 5 minutes by sampling zero air created by automated drawing of ambient air through a heated $Pt/Al_2O_3$ (to 350°C) catalyst to remove VOCs. Regular automated calibrations with certified gas standards were performed twice daily for all the reported ions (*m/z*). The standards contained the compounds at 1 ppm each which were diluted by a custom-built dilution system using the catalyst zero air (of the similar humidity to ambient) to obtain sensitivities from multipoint calibration curves for each compound. The PTR-MS was configured to measure approximately 20 masses. The losses in the lines were assessed several times by using a separate line to push air containing known concentrations of VOCs to the second level (131 m) at different residence times. These tests

demonstrated that for all non-sticky compounds the losses were negligible and independent of the residence times simulated at the tower. The sticky compounds (e.g. organic acids) were not included in the reported masses.

### 3.3.2. VOCs of interest

A majority of sources of $CH_4$ in the California inventory (see Chapter 2) have fairly unique signatures of VOC emissions. In addition, other potential sources such as biomass burning which are considered to be minor contributors in the state $CH_4$ inventory (but are thought to be important in the global $CH_4$ inventory) also have unique VOC signatures. Here we review some of what is known about the VOC emission signatures for these sources. We also demonstrate in the next section (Section 3.4 – Pilot Measurements) that VOC tracers can be used as $CH_4$ source indicators at this site. We focus the discussion on those VOCs and related trace gases that can be measured continuously in-situ using the specified configuration ($H_3O^+$ mode) of the above-mentioned PTR-MS while also having a significantly long lifetime to act as a GHG source tracer (> few days and more).

Table 3.2 provides a list of the currently known tracers that can be measured by the PTR-MS and attributed to certain $CH_4$ sources, or are indicative of sources that will help us understand the origin and photochemical history of air masses observed at the Walnut Grove tower. Many of these source categories are unique to specific compounds, while other source categories can be indicated by specific combinations of these compounds. Examples of known VOC emissions from major $CH_4$ sources are briefly described below.

**Table 3.2. List of ions (protonated *m/z*) measured by PTR-MS with ascribed compounds and most significant known sources.**

| Protonated *m/z* | Compound/group of compounds | Significant source(s) |
|---|---|---|
| 33 | Methanol | Livestock, Manure management, Vegetation, Biomass Burning |
| 35 | Hydrogen sulfide | Landfills, Manure management |
| 42 | Acetonitrile | Biomass burning |
| 45 | Acetaldehyde | Rice cultivation, Biomass burning, Vegetation, Photooxidation, Manure Management |
| 47 | Ethanol + Formic acid | Rice cultivation, Livestock (fermenting feed), Gasoline |
| 49 | Methanethiol | Fugitive emissions, Natural gas leakage |
| 59 | Acetone + Propanal | Livestock, Rice cultivation, Vegetation, Photoxidation |
| 61 | Acetic acid + Propanol | Rice cultivation, Livestock |
| 63 | DMS + Ethanethiol | Landfills, Livestock, Rice cultivation, Fugitive Emissions |
| 69 | Isoprene, MBO | Vegetation (Mainly Oak trees-isoprene, Pine trees-MBO) |
| 71 | MVK + MACR | Isoprene photooxidation products |
| 73 | MEK | Manure Management, Landfills, photooxidation of anthropogenic VOCs |
| 79 | Benzene | Fugitive emissions, Gasoline, Biomass burning |
| 81 | Monoterpenes + Hexenals | Vegetation |
| 83 | Hexanals | Vegetation |
| 87 | MBO, C-5 hydrocarbons, Pentanones | Livestock, Rice cultivation, Vegetation |
| 93 | Toluene | Fugitive emissions, Gasoline |
| 107 | C8 aromatics, ethyl benzenes, xylenes | Fugitive emissions, Gasoline |
| 109 | Cresols | Livestock |
| 113 | Oxidation product | Isoprene and terpene photooxidation product |
| 121 | C-9 aromatics, TMB | Fugitive emissions, Gasoline |
| 137 | Monoterpenes | Vegetation |
| 143 | Nonanal | Rice cultivation |

### *Dairies*

In previous research funded by the ARB, VOCs emitted from dairy cows were identified and quantified (Shaw et al., 2007). The experiments were performed at UC Davis by putting cows in a room and measuring the VOCs in air entering and leaving the room at a fixed air exchange velocity so emission rates could be directly calculated. Measurements of VOCs were made using PTR-MS with simultaneous measurements of $CH_4$ and $CO_2$. VOC emissions from dairy cows included methanol, ethanol, acetone + propanal, dimethyl sulfide (DMS), *m/z* 109 (likely p-cresol) and acetic acid amongst others, and there were strong correlations between these VOC tracers and $CH_4$ and $CO_2$. Detection of such VOCs in the sampled air at Walnut Grove will be critical in identifying emissions from dairies, which is assumed in current inventories to be the single largest $CH_4$ source in the state (Figure 1.1). Other dairy studies (e.g. Filipy et al., 2006), also have demonstrated that ethanol and DMS are prominent VOCs produced by lactating cows while slurry waste lagoons can produce certain ketones such as methyl ethyl ketone (MEK).

### *Landfills*

Municipal solid waste landfills are known to emit specific VOCs, and the EPA has documented emission factors for this source (AP 42, USEPA). The AP 42 reports procedures to calculate emission factors for many VOCs including compounds measurable by PTR-MS such as hydrogen sulfide, acetone, and MEK.

### *Natural Gas Leakage*

Methanethiol ($CH_3$-SH) is an odorant added to natural gas before distribution and fugitive losses and leaks can be detected by the presence of this VOC.

***Fugitive Emissions***

Oil and gas extraction and refining activities emit specific tracer compounds that are also emitted by gasoline fuel use. Tracers that can be measured by PTR-MS which indicate fugitive emissions or gasoline emissions include ethanethiol, benzene, toluene, C8 aromatics (xylenes+ethylbenzenes), and C9 aromatics (trimethylbenzenes etc).

***Rice cultivation***

As an initial step to obtain a VOC fingerprint of the emissions from rice cultivation areas, liquid suspensions were extracted from rice wetlands in the Sacramento-San Joaquin Delta and their headspaces were analyzed by PTR-MS (Goldstein and Baldocchi labs, 2011). The most unique VOC indicators of rice cultivation are likely to be a combination of nonanal, acetic acid, acetaldehyde, propionic acid, and DMS.

### 3.3.3. Quality Analysis and Quality Control

Semi-processed data and raw data collected on a continuous basis were used in post-processing. Height-segregated normalized counts per second (ncps), averaged zero air data (one per 3 hours), sensitivities (1 per day) and preliminary ppb (60 min averages) were subjected to quality control procedures and resulted in changes to yield the final 60 min concentration dataset from WGC.

The quality control included zero air validation and reprocessing, sensitivity revalidation, filtering of bad periods based on PTR-MS and tower logs and on the visual inspection of each dataset looking at drift pressure, *m/z* 21, *m/z* 32, *m/z* 37, room temperature. Comparison of

diurnal trends and distribution frequencies of the preliminary and the final data was performed for each *m/z* to check how changes affected statistics and generally to see if the data made sense.

***Zero air (ZA) dataset revalidation***

The revalidation involved:

1) Visual inspection of ZA variability and negatives after subtraction.

2) Marking the periods when zero air was i) not working completely (immediate breakthrough or no data); ii) partially working but breakthroughs at high concentration; iii) working with no breakthroughs observed, iv) contamination from ZA air catalyst, v) internal interference (e.g. O2H+).

3) Selecting an approach individually for each *m/z* to include only the valid ZA points (where breakthrough was unlikely and no interference was apparent). In some cases (e.g. isoprene) occasional negatives at the minimum ambient concentrations were noted. These occasional areas, if within the instrumental accuracy, were nudged to the neighboring minimal zero air level to ensure all-positive datasets without biasing the overall mean or variance.

4) Final zero air dataset was obtained by either a) re-interpolating (linear) the valid zero air points (perfect zero) or b) re-interpolating the daily running minima (when partial breakthrough was observed)

***Sensitivity revalidation.***

This included information from a simultaneous PTR-ToF-MS (Time of Flight PTRMS instrument; February 2013) to exclude or estimate relative contribution from interfering masses. If the interference was found which was not subtracted with ZA, the sensitivity was derived

based on the dominant contribution. In some cases it resulted in *m/z* being specified as the sum of VOC (e.g. acetone+propanal calibrated as acetone). As normalization of count rates includes water clusters, additional check was needed to identify spikes in *m/z* 37 apart from spike inspection in *m/z* 21, and drift pressure. In case of methanol spikes in *m/z* 32 were also investigated.

***Final filtering of resulting concentration***

This was conducted based on information from *m/z* 32 (O2+) [mostly relevant for methanol], presence of gradients and meaningful structures, spike reinspection (e.g. all masses vs acetonitrile, benzene), tower log (Dave Bush) and PTR (log).

The final calibrated dataset was derived for each mass provided it has passed the quality criteria. The daily and monthly figures looking at comparison of semi-processed with post-processed concentrations, potential temperature, *m/z* 21, O2+ and water clusters were saved including Matlab variables and the codes for reference. The periods when drift pressure significantly deviated from 2.0 mbar were rejected for all masses.

After intensive quality checks and post-processing of data, the following masses, represented here by their mass-to-charge ratios (*m/z*), were high quality and included in the subsequent PMF analysis: methanol (*m/z* 33), acetonitrile (*m/z* 42), acetaldehyde (*m/z* 45), acetone + propanal (*m/z* 59), isoprene (*m/z* 69), methyl vinyl ketone (MVK) + methacrolein (MAC) (*m/z* 71), methyl ethyl ketone (MEK) (*m/z* 73), benzene (*m/z* 79), toluene (*m/z* 93), and monoterpenes (*m/z* 137). Acetonitrile (*m/z* 42) is a tropospheric tracer of biomass burning (Lobert et al., 1990; Lobert et al., 1991; Holzinger et al., 1999; Bange and Williams, 2000) but a minor contribution from alkanes during pollution episodes to *m/z* 42 is possible (Dunne et al.,

2012). Similarly, *m/z* 93 (toluene) can see small contributions from biogenic monoterpene fragments if the concentration of the latter is high. Two more masses, green leaf volatiles (*m/z* 83) and C-9 aromatics (*m/z* 121), were available but their quality was only medium to medium-high (due to their multi-compound character, and/or more frequent interferences). Therefore, they have not been included in the PMF analysis but have been utilized for independent comparison with and verification of PMF source factors (in Chapter 4).

## 3.4. Pilot Measurements

To demonstrate the utility of measuring a wider variety of VOC tracers continuously for differentiating between GHG sources, and to show the advantages of having vertical profile data for these tracers, we collected pilot data during preparation of the project proposal with the PTR-MS instrument at the Walnut Grove tower from June through August 2011. Nine of the VOC tracers that we measured are shown as diurnal average vertical profiles in Figures 3.5a-m along with CO, $CO_2$, and $CH_4$. The VOCs were measured at five heights (10, 131, 282, 394, and 525 m above ground level (a.g.l)) and CO, $CO_2$ and $CH_4$ were measured at three heights (30, 91, and 483 m a.g.l).

The diurnal average figures of the tracers show extremely distinct patterns that indicate different source categories and processes contributing (and not contributing) to the GHGs observed at this site. A detailed analysis of such data is presented (in Chapter 4) as part of the project work, and here we point out a few key features relating the $CH_4$ diurnal cycle and vertical profile to some of the key VOC tracers. The complete $CH_4$ vertical distribution and diurnal cycle looks distinct from any of the individual tracers, but it does look like a combination of some of the tracers. $CH_4$ builds up in the nocturnal inversion layer near the ground, similar to tracers

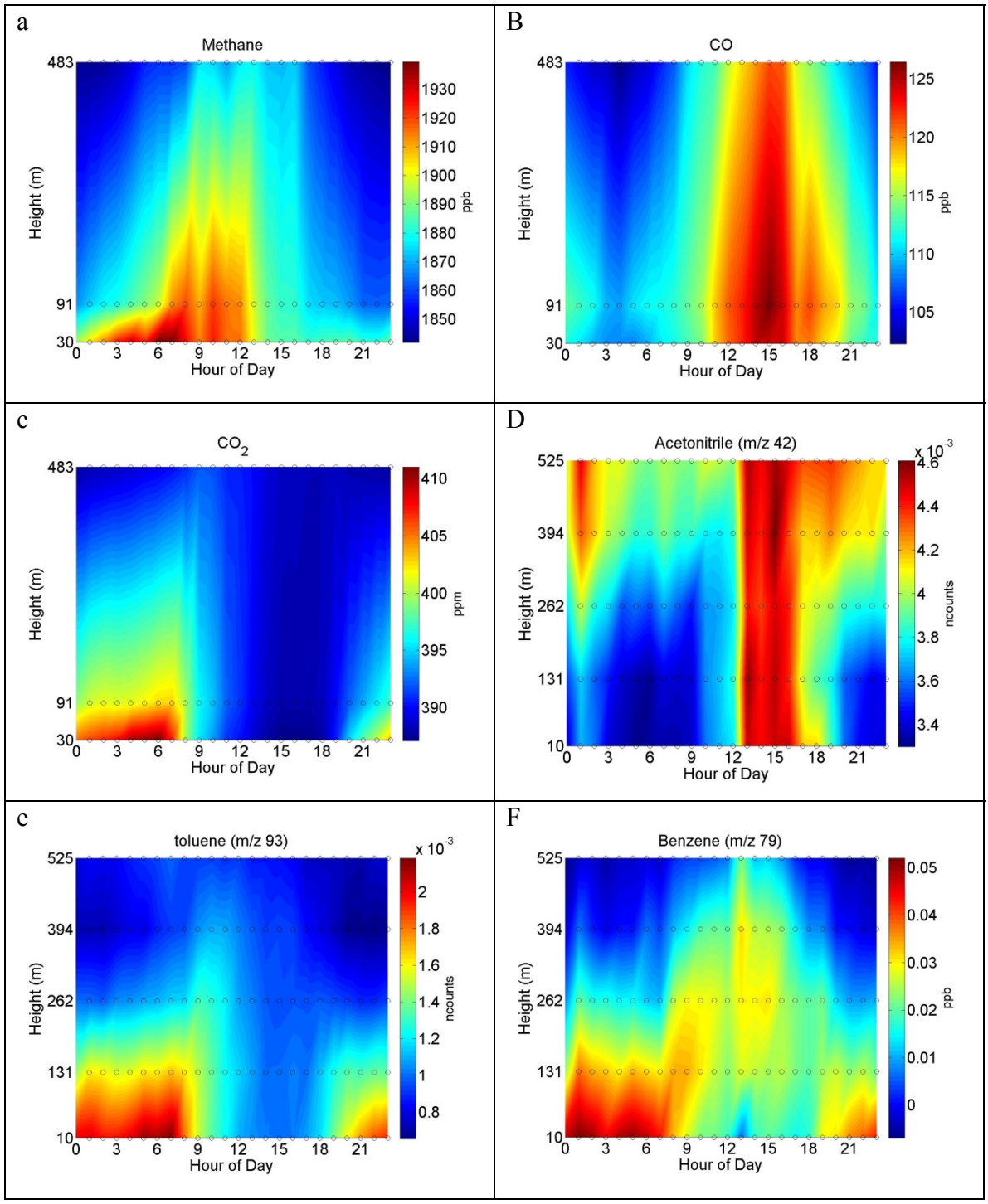


**Figure 3.5.** Average diurnal cycles of vertically resolved GHG and VOC profiles measured at Walnut Grove tower during pilot deployment of UCB PTR-MS: (a) $CH_4$, (b) CO (tracer of fuel combustion, biomass burning), and (c) $CO_2$ measured by LBNL and NOAA at the Walnut Grove tower from June 15-August 21, 2011. VOCs shown include (d) acetonitrile (biomass burning), (e) toluene (gasoline, fugitive emissions), (f) benzene (fugitive emissions, gasoline, biomass burning) - continued next page.

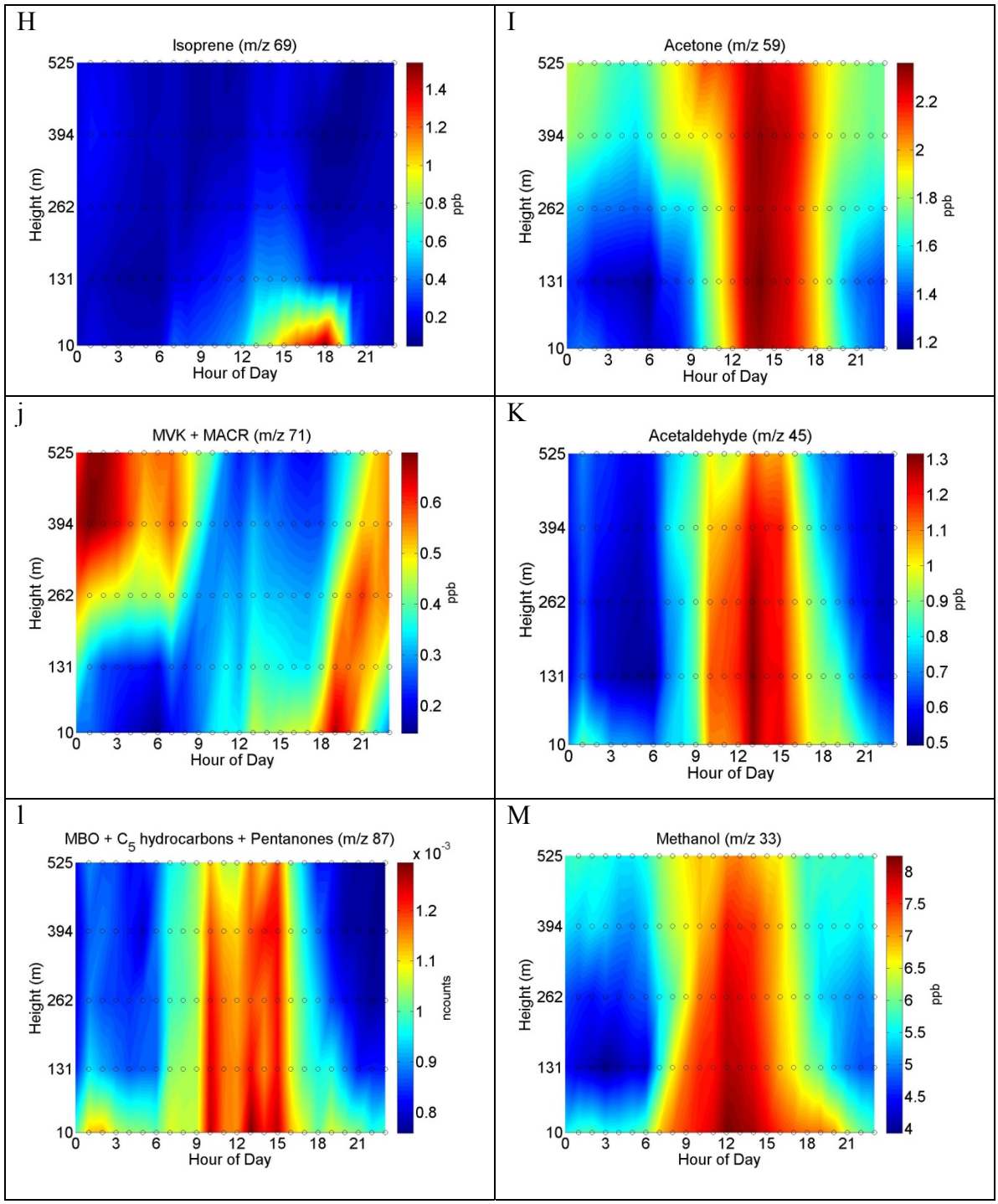


**Figure 3.5 continued.** (h) isoprene (biogenic emission), (i) acetone (livestock, rice, vegetation, photooxidation), (j) methylvinylketone + methacrolein (isoprene photooxidation products), (k) acetaldehyde (rice, biomass burning, vegetation), (l) mixture of MBO + C5 hydrocarbons + pentanones (livestock, rice, vegetation), and (m) methanol (livestock, manure management, vegetation, biomass burning) .

toluene and benzene which are indicative of gasoline and fugitive emissions. However, when the inversion layer breaks in the morning between hour of day 8-9, the toluene and benzene

concentrations decline rapidly while the $CH_4$ concentrations started to become larger after hour of day 6 and then remained high until about hour 13. This morning increase in $CH_4$ looks to be related to at least some of the methanol sources which cause methanol to begin increasing just after hour 6 and have a very similar vertical profile to $CH_4$ until about hour 13, and also have some similar features into the late afternoon. We believe this correspondence of methanol and $CH_4$ is mainly a signature from dairy emissions in the region. Note also that the methanol concentrations at night are low; clearly showing that the high nighttime $CH_4$ near the ground is NOT coming from the dairy operations. Thus, the major features of $CH_4$ variability at this site are likely driven by a combination of emissions from dairy and fossil fuel sources. It is also likely that emissions from rice are influencing the observations at the tower and they may be represented to some degree by *m/z* 87 (e.g. pentanones). During times when the biomass burning tracer acetonitrile is high and vertically well mixed (hours 12-16), CO is also high indicating biomass burning is an important CO source, but $CH_4$ (and $CO_2$) were not significantly elevated at these times demonstrating that even though biomass burning is a source of $CH_4$ (and $CO_2$) there are other larger sources that dominate the observed variability of $CH_4$ averaged over this two month period.

While the fossil fuel tracers toluene and benzene are maximized near the ground (below 250 m) and at night, the biogenic VOC isoprene is maximum in the afternoon from hours 15-18 and only very close to the ground, while the isoprene oxidation products MVK+MACR increase following the isoprene near the ground but then are maximum at night high above the ground (above 250 m). The high MVK+MACR at night above 250m is due to isoprene oxidation products flowing downslope from the Sierra Nevada mountains into the valley, and downslope flow is stopped by the nighttime inversion layer over the valley. Thus, there is a

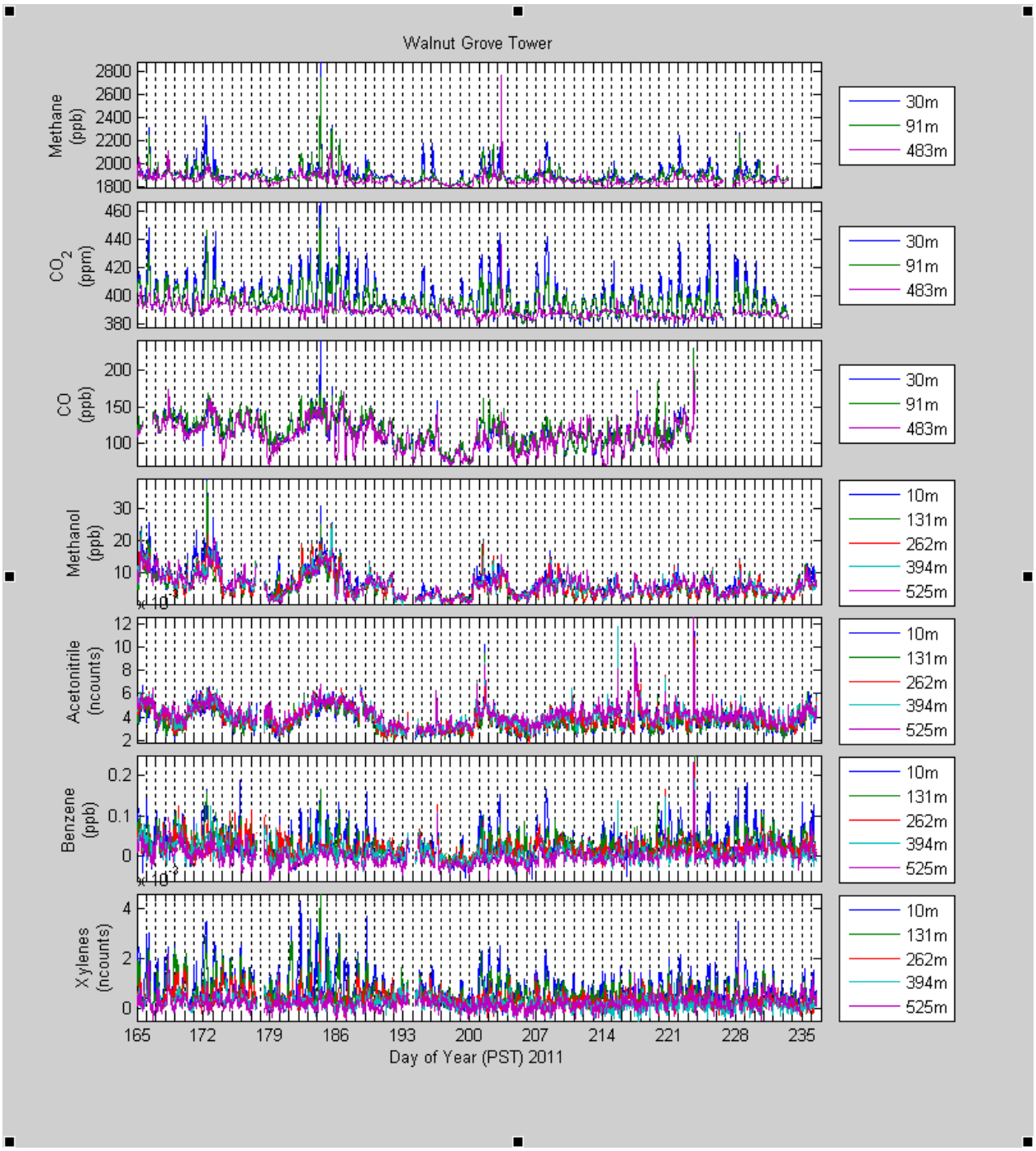


**Figure 3.6.** Time series GHG and pilot PTR-MS VOC measurements at the Walnut Grove tower (June 15-August 21, 2011).

dramatic separation between highly anthropogenic-influenced air mass near the ground at night and highly biogenic-influenced air mass from the surrounding mountains above the inversion layer. While this is not directly related to understanding the GHG emissions in the region, it does demonstrate a tremendous co-benefit of performing coincident VOC measurements in terms of

improving understanding of the vertical and temporal distribution of biogenic and anthropogenic VOCs which affect ozone and aerosol formation chemistry in the region.

A time series of the measurements at the Walnut Grove tower for $CH_4$, $CO_2$ and a small subset of the measured VOCs measured are shown in Figure 3.6 for June 15 to August 21, 2011. These timelines make it clear that there is a tremendous amount of day to day variability which carries rich information about source contributions beyond what can be seen in the daily averages shown in Figure 3.5. Each of the increases in $CH_4$ concentrations can be compared to simultaneous changes in concentrations for the entire suite of measured VOCs to extract information about the sources that contributed (or did not contribute) to the observed increase in $CH_4$. In Figure 3.7 we zoom in to examine three specific events that clearly demonstrate how the VOC tracers can be used to differentiate sources contributing to individual high $CH_4$ events. The first event (Figure 3.7a) demonstrates a fossil fuel signature where increases of $CH_4$ occur simultaneously with CO, benzene, and xylenes, without a significant increase in methanol (dairy tracer) or acetonitrile (fire tracer). The second event (Figure 3.7b) demonstrates the influence of a dairy source where enhanced concentrations are observed for $CH_4$, $CO_2$, and methanol, without an increase in acetonitrile, CO, benzene, or xylene (fire and fossil fuel tracers). The third event (Figure 3.7c) demonstrates a fire event showing a relatively small but still significant enhancement in $CH_4$ with a large increase in acetaldehyde, CO, methanol, acetonitrile, and benzene signals, without a significant increase in xylenes (emission of benzene is much higher than emission of xylene from fires, while the xylene emission from gasoline is an order of magnitude larger than benzene).

The data shown in Figures 3.5 through 3.7 is indicative of what we expected to observe with a yearlong set of observations. This description of the pilot data is qualitative, but it does

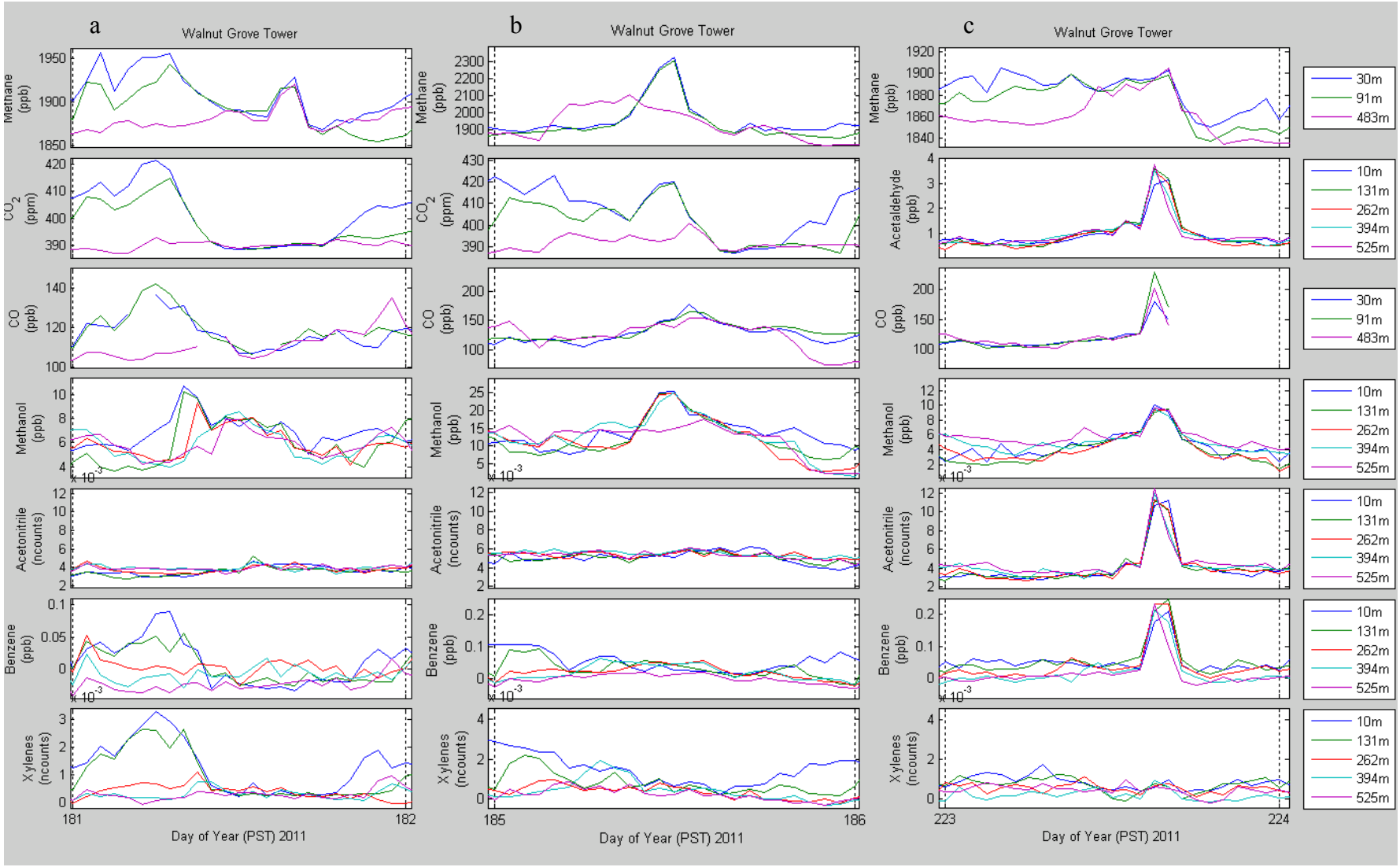


**Figure 3.7**. Example events highlight 3 different species specific GHG and VOC enhancements. Specific events include (a) fossil fuel signatures of $CH_4$, $CO_2$, CO, benzene, and xylenes, (b) likely dairy source with enhanced $CH_4$, $CO_2$, and methanol, and (c) a fire event showing a small enhancement in $CH_4$ with a significant of acetaldehyde, CO, methanol, acetonitrile, and benzene signals.

demonstrate that specific VOC tracers measured simultaneously with GHGs provide indicators for the sources contributing to observed concentrations at the Walnut Grove tower. It shows that although individual VOCs are not unique to individual sources, given the range of compounds that the PTR-MS can measure and our knowledge of source-specific VOC tracers, source apportionment techniques like primary matrix factorization analysis can be used with a suite of tracers to determine the proportion of $CH_4$ and $N_2O$ emissions that can be attributed to a specific source. A report on the conducted analysis using positive matrix factorization for the 2012-2013 measurements is presented in Chapter 4. This chapter also reports our corresponding investigation to determine seasonal changes in the distribution of GHG emissions sources over the annual cycle. In Chapter 5, we report the simultaneous but independent application of the existing inverse modeling approach to ascribe specific amounts of $CH_4$ and $N_2O$ emissions to each of the source categories determined from an *a priori* model to quantitatively constrain emissions of GHGs. In Chapter 6 of the project, the results of the inverse modeling approach are compared with the VOC speciated GHG source contributions from the PMF analysis to further validate the project findings.

## 3.5. References

Andrews, A. E., J. D. Kofler, M. E. Trudeau, J. C. Williams, D. H. Neff, K. A. Masarie, D. Y. Chao, D. R. Kitzis, P. C. Novelli, C. L. Zhao, E. J. Dlugokencky, P. M. Lang, M. J. Crotwell, M. L. Fischer, M. J. Parker, J. T. Lee, D. D. Baumann, A. R. Desai, C. O. Stanier, S. F. J. De Wekker, D. E.Wolfe, J. W. Munger, and P. P. Tans (2014), CO2, CO, and CH4 measurements from tall towers in the NOAA Earth System Research Laboratory's Global Greenhouse Gas Reference Network: instrumentation, uncertainty

analysis, and recommendations for future high-accuracy greenhouse gas monitoring efforts, Atmospheric Measurement Techniques, 7(2), 647-687.

Blake, R. S., Monks, P. S., and Ellis, A. M.: Proton-Transfer Reaction Mass Spectrometry, *Chemical Reviews, 109, 861-896, doi:10.1021/cr800364q*, 2009.

CASR (2013), California Agricultural Statistics Crop Report, 2013. created by California Department of Food and Agriculture, Sacramento, CA and National Agricultural Statistics Service, United States Department of Agriculture. http://www.nass.usda.gov/Statistics_by_State/California/Publications/California_Ag_Statistics/2013cas-all.pdf

CCCR (2013), Contra Costa County Annual Crop Report, 2013. Created by California Department of Food and Agriculture, Concord, CA. http://www.co.contra-costa.ca.us/DocumentCenter/View/34207. Accessed on November 23, 2014.

CIMIS (2013), California Irrigation Management Information System daily station report, Station 166, Lodi West. http://wwwcimis.water.ca.gov/WSNReportCriteria.aspx. Accessed on August 27, 2014.

de Gouw, J., Warneke, C., Karl, T., Eerdekens, G., van der Veen, C., and Fall, R.: Sensitivity and specificity of atmospheric trace gas detection by proton-transfer-reaction mass spectrometry, *International Journal of Mass Spectrometry, 223, 365-382,* 2003.

de Gouw, J., and Warneke, C.: Measurements of volatile organic compounds in the earth's atmosphere using proton-transfer-reaction mass spectrometry, *Mass Spectrometry Reviews, 26, 223-257, 10.1002/mas.20119,* 2007.

Dunne, E., Galbally, I. E., Lawson, S., and Patti, A.: Interference in the PTR-MS measurement of acetonitrile at m/z 42 in polluted urban air—A study using switchable reagent ion PTR-MS, International Journal of Mass Spectrometry, 319, 40-47, 2012.

Fares, S., Park, J.-H., Gentner, D. R., Weber, R., Ormeño, E., Karlik, J. and Goldstein, a. H.: Seasonal cycles of biogenic volatile organic compound fluxes and concentrations in a California citrus orchard, Atmos. Chem. Phys., 12(20), 9865–9880, doi:10.5194/acp-12-9865-2012, 2012.

Filipy, J., B. Rumburg, G. Mount, H. Westberg, and B. Lamb (2006), Identification and quantification of volatile organic compounds from a dairy, Atmos. Environ., 40(8), 1480–1494, doi:10.1016/j.atmosenv.2005.10.048.

Hatala, J. a., Detto, M., Sonnentag, O., Deverel, S. J., Verfaillie, J. and Baldocchi, D. D.: Greenhouse gas (CO2, CH4, H2O) fluxes from drained and flooded agricultural peatlands in the Sacramento-San Joaquin Delta, Agric. Ecosyst. Environ., 150, 1–18, doi:10.1016/j.agee.2012.01.009, 2012.

Holzinger, R., D.B. Millet, B. Williams, A. Lee, N.M. Kreisberg, S.V. Hering, J.L. Jimenez, J. Allan, D.R. Worsnop, and A.H. Goldstein: Emission, oxidation, and secondary organic aerosol formation of volatile organic compounds as observed at Chebogue Pt, Nova

Scotia, *Journal of Geophysical Research-Atmospheres, doi:10.1029/2006JD007599,* 2007.

Holzinger, R., A. Lee, K. T. Paw U and A. H. Goldstein, Observations of oxidation products above a forest imply biogenic emissions of very reactive compounds, Atmospheric Chemistry and Physics, 5: 67-75, 2005

Homer, C., Dewitz, J., Fry, J., Coan, M., Hossain, N., Larson, C., Herold, N., McKerrow, A., VanDriel, J. N. and Wickham, J.: Completion of the 2001 National Land Cover Database for the Counterminous United States, Photogramm. Eng. Remote Sensing, 73(4), 337–341[online]. Available from: http://www.ncbi.nlm.nih.gov/pmc/articles/PMC3339477/pdf/ehp.120-a152.pdf, 2007.

Jeong, S., Zhao, C., Andrews, A. E., Bianco, L., Wilczak, J. M. and Fischer, M. L.: Seasonal variation of CH 4 emissions from central California, J. Geophys. Res., 117(D11), D11306, doi:10.1029/2011JD016896, 2012a.

Jeong, S., Zhao, C., Andrews, A. E., Dlugokencky, E. J., Sweeney, C., Bianco, L., Wilczak, J. M. and Fischer, M. L.: Seasonal variations in N 2 O emissions from central California, Geophys. Res. Lett., 39(16), n/a–n/a, doi:10.1029/2012GL052307, 2012b.

Karl, T., Potosnak, M., Guenther, A., Clark, D., Walker, J., Herrick, J. D., and Geron, C.: Exchange processes of volatile organic compounds above a tropical rain forest: Implications for modeling tropospheric chemistry above dense vegetation, Journal of Geophysical Research-Atmospheres, 109, 24, D18306, 10.1029/2004jd004738, 2004.

Karl, T., Misztal, P. K., Jonsson, H. H., Shertz, S., Goldstein, A. H., and Guenther, A. B.: Airborne Flux Measurements of BVOCs above Californian Oak Forests: Experimental Investigation of Surface and Entrainment Fluxes, OH Densities, and Damkohler Numbers, J Atmos Sci, 70, 3277-3287, Doi 10.1175/Jas-D-13-054.1, 2013.

Knox, S. H., Sturtevant, C., Matthes, J. H., Koteen, L., Verfaillie, J. and Baldocchi, D.: Agricultural peatland restoration: effects of land-use change on greenhouse gas (CO2 and CH4 ) fluxes in the Sacramento-San Joaquin Delta., Glob. Chang. Biol., 1–16, doi:10.1111/gcb.12745, 2014.

Lobert, J.M., D.H. Scharffe, W.M. Hao, and P.J. Crutzen, 1990. Importance of biomass burning in the atmospheric budgets of nitrogen-containing gases. Nature 346 (6284):552–554. doi:10.1038/346552a0, 1990.

Lobert, J.M.; Scharffe, D.H.; Weimin Hao; Kuhlbusch, T.A.; Seuwen, R.; Warneck, P.; Crutzen, P.J.: Experimental evaluation of biomass burning emissions: Nitrogen and carbon containing compounds: (Max-Planck-Inst. for Chemistry, Mainz (West Germany)): from Levine, J.S. (ed.); 599 p; 1991; p. 289-304: Massachusetts Inst. of Tech. Press; Cambridge, MA (United States) : Chapman conference on global biomass burning: atmospheric, climatic, and biospheric implications : Williamsburg, VA (United States); 19-23 Mar 1990; CONF-900355—Publication Date 1991.

le Mer, J. and Roger, P.: Production, oxidation, emission and consumption of methane by soils : A review, Eur. J. Soil Biol., 37(1), 25–50 [online] Available from: http://cat.inist.fr/?aModele=afficheN&cpsidt=978757 (Accessed 28 October 2014), 2001.

McMillan, A. M. S., Goulden, M. L. and Tyler, S. C.: Stoichiometry of CH 4 and CO 2 flux in a California rice paddy, J. Geophys. Res., 112(G1), G01008, doi:10.1029/2006JG000198, 2007.

Miller, R. L.: Carbon Gas Fluxes in Re-Established Wetlands on Organic Soils Differ Relative to Plant Community and Hydrology, Wetlands, 31(6), 1055–1066, doi:10.1007/s13157-011-0215-2, 2011.

Misztal, P. K., Karl, T., Weber, R., Jonsson, H. H., Guenther, A. B., and Goldstein, A. H.: Airborne flux measurements of biogenic isoprene over California, Atmos Chem Phys, 14, 10631-10647, DOI 10.5194/acp-14-10631-2014, 2014.

Park, J.-H., Goldstein, a H., Timkovsky, J., Fares, S., Weber, R., Karlik, J. and Holzinger, R.: Active atmosphere-ecosystem exchange of the vast majority of detected volatile organic compounds., Science, 341(6146), 643–7, doi:10.1126/science.1235053, 2013.

Peischl, J., Ryerson, T. B., Holloway, J. S., Trainer, M., Andrews, a. E., Atlas, E. L., Blake, D. R., Daube, B. C., Dlugokencky, E. J., Fischer, M. L., Goldstein, a. H., Guha, a., Karl, T., Kofler, J., Kosciuch, E., Misztal, P. K., Perring, a. E., Pollack, I. B., Santoni, G. W., Schwarz, J. P., Spackman, J. R., Wofsy, S. C. and Parrish, D. D.: Airborne observations of methane emissions from rice cultivation in the Sacramento Valley of California, J. Geophys. Res., 117, D00V25, doi:10.1029/2012JD017994, 2012.

SacCR (2013), Sacramento County Crop and Livestock Report, 2013. created by California Department of Food and Agriculture, Sacramento, CA. Accessed on November 23, 2014. www.agcomm.saccounty.net/Documents/CropandLivestockReports/2013Report.pdf.

SCR (2013), Solano County Crop and Livestock Report, 2013. created by California Department of Food and Agriculture, Fairfield, CA. Accessed on November 23, 2014. . www.solanocounty.com/civicax/filebank/blobdload.aspx?BlobID=18405.

Shaw, S. L., Mitloehner, F. M., Jackson, W., Depeters, E. J., Fadel, J. G., Robinson, P. H., Holzinger, R. and Goldstein, A. H.: Volatile organic compound emissions from dairy cows and their waste as measured by proton-transfer-reaction mass spectrometry., Environ. Sci. Technol., 41(4), 1310–6 [online] Available from: http://www.ncbi.nlm.nih.gov/pubmed/17593735, 2007.

Teh, Y. A., Silver, W. L., Sonnentag, O., Detto, M., Kelly, M. and Baldocchi, D. D.: Large Greenhouse Gas Emissions from a Temperate Peatland Pasture, Ecosystems, 14(2), 311–325, doi:10.1007/s10021-011-9411-4, 2011.

Zhao, C., Andrews, A. E., Bianco, L., Eluszkiewicz, J., Hirsch, A., MacDonald, C., Nehrkorn, T. and Fischer, M. L.: Atmospheric inverse estimates of methane emissions from Central California, J. Geophys. Res., 114(D16), D16302, doi:10.1029/2008JD011671, 2009.

Zhong, S., Whiteman, C. and Bian, X.: Diurnal evolution of three-dimensional wind and temperature structure in California's Central Valley, J. Appl. …, (1962), 1679–1699 [online] Available from: http://journals.ametsoc.org/doi/abs/10.1175/JAM2154.1 (Accessed 6 March 2013), 2004.

# 4. Positive Matrix Factorization (PMF) Analysis

## 4.1. Experiment

### 4.1.1. Principles of PMF

Source apportionment techniques like PMF have been used in the past to apportion ambient concentration datasets into mutually co-varying groups of species. PMF is especially suitable for studies where *a priori* knowledge of the number of sources impacting the measurements, the chemical nature of source profiles and relative contribution of each source to the concentration time series of a measured compound are unknown or cannot be assumed. PMF has been applied to ambient particulate matter studies (Lee et al., 1999; Kim et al., 2004); to determine sources of atmospheric organic aerosols (OA) (Ulbrich et al., 2009; Slowik et al., 2010; Williams et al., 2010); and to gas phase measurements of VOCs in major metropolitan cities (Brown et al., 2007; Bon et al., 2011) and over long time spans on continental scales (Lanz et al., 2009). PMF is a receptor-only unmixing model which breaks down a measured data set containing time series of a number of compounds into a mass balance of an arbitrary number of constant source factor profiles (FP) with varying concentrations over the time of the data set (time series or TS) (Ulbrich et al., 2009).

In real world ambient scenarios, sources of emissions are often not known or well-understood. PMF technique requires no *a priori* information about the number or composition of factor profiles or time trends of those profiles. The constraint of non-negativity in PMF ensures that all values in the derived factor profiles and their contributions are constrained to be positive leading to physically meaningful solutions. PMF attributes a measure of experimental uncertainty (or weight) to each input measurement. Data point weights allow the level of

influence to be related to the level of confidence the analyst has in the measured data (Hopke, 2000). In this way, problematic data such as outliers, below-detection-limit, or altogether missing data can still be substituted into the model with appropriate weight adjustment (Comero et al., 2009) allowing for a larger input data set, and hence a more robust analysis. PMF results are quantitative; it is possible to obtain chemical composition of sources determined by the model (Comero et al., 2009). PMF can be applied to data sets that are not homogenous and/or require normalization without introducing artifacts as long as relative numerical magnitudes of input time series data streams for various compounds are comparable.

### 4.1.2. Choice of sampling periods

In this study, we began with the assumption that we would perform PMF-based source apportionment over four separate periods consistent with local seasonal distinctions, as opposed to one composite PMF analysis through the entire measurement period (June 2012 – August 2013). There were two principal reasons behind this choice. Firstly, the factor profiles produced in a PMF analysis represent constant linear source configurations that do not change over the whole analysis cycle. Some VOCs included in this study have principally light and temperature driven sources (e.g. isoprene) and have non-linear dependence on such parameters. Similarly, for some compounds, emissions from their largely biological sources would depend and vary with the stage of vegetative growth or microbial activity (e.g. methanol, acetone, $N_2O$). Hence, we anticipate that the fractional composition of certain source categories can vary significantly during different times in the annual cycle and as such, a single factor profile representing a source category for the entire year may result in an inaccurate PMF fitting with a higher residual error. This constraint can be overcome to a reasonable extent by performing unique PMF analyses over shorter time periods when the meteorological variables (like light, temperature and

rainfall) impacting the site are more homogenous. Hence, the optimal choice of total number of separate PMF analyses to be performed on the larger dataset seemed to be four. These study periods are summer (Jun-Aug), fall (Sep-Nov), winter (Dec-Feb), and spring (Mar-May). Secondly, this choice of sampling period made more sense as it was consistent with those used in previous evaluation of $CH_4$ and $N_2O$ emissions from inverse dispersion analysis of atmospheric observations at WGC (Jeong et al., 2012a, 2012b). The choice of four seasonal study periods would, hence, allow for a potential comparison of PMF results with WRF-STILT derived $CH_4$ emissions (being evaluated currently).

We, however, did not have complete data coverage of all tracers through the course of the entire campaign as seen in Table 3.1. Two key compounds in the PMF analysis are $N_2O$ and methanol (MeOH). It was vital to perform PMF analyses over extended periods of time when $N_2O$ data was not missing since one of the primary objective of this study is to perform PMF-based apportionment of $N_2O$ sources in the region. We conducted the first $N_2O$ measurements at WGC from mid-October 2012 until end of January 2013 and then after a significant period of missing data, measurements continued from start of April until mid-August 2013. Additionally, having continuity in MeOH measurements was important as it served as a primary indicator of $CH_4$ from dairy and livestock sources as opposed to fugitive and/or urban sources. To comply with the assumptions of seasonality and similar meteorological conditions over a sampling period, and at the same time ensure minimal missing data of $CH_4$, CO (combustion / industrial tracer), $N_2O$ and methanol, we decided to perform PMF analyses over seven distinct periods based on continuous times of consistent sets of tracers being available, and seasons. Table 3.1 lists the meteorological characteristics at WGC and a summary of the tracers included in the PMF analysis during each of these periods.

### 4.1.3 Mathematical Framework of PMF

In the recent past, PMF has been utilized to perform ambient source apportionment of organic aerosols (Ulbrich et al., 2009; Slowik et al., 2010; Williams et al., 2010) as well as VOCs (Brown et al., 2007; Bon et al., 2011; Yuan et al., 2012). In this study, the PMF technique is applied to the combined data set of GHGs, CO, and VOCs to apportion their contributions to major source categories influencing the WGC site. The fundamentals of the PMF technique are based on the principles laid out in relevant literature (Paatero and Tapper, 1994; Paatero, 1997; Comero et al., 2009; Ulbrich et al., 2009). We will briefly mention some concepts relevant to the understanding of the analysis carried out in this study. PMF is a multivariate factor analysis tool that breaks down a dataset of speciated trace gas measurements into two matrices. The PMF input parameters involve a m × n data matrix X with *i* rows containing mixing ratios at sampling time $t_i$ and *j* columns containing time series of each $tracer_j$. A corresponding uncertainty matrix S reports measurement precision (uncertainty) of the signal of each $tracer_j$ at every $t_i$ ($s_{ij}$). The PMF model can then be resolved into two matrices as:

$$\boldsymbol{X}_{ij} = \sum_{p} g_{ip} f_{pj} + e_{ij} \tag{1}$$

where p refers to the number of contributing factors in the solution as determined by the analyst (discussed below), $g_{ij}$ (mass concentration) are elements of a m × p matrix G whose columns represent the factor time series while $f_{ij}$ (mass fraction) are elements of a p × n matrix F whose rows represent the factor chemical profiles. Thus, one resultant matrix represents the factor profiles (F) while the second matrix contains the factor contributions (G) or the total mass

contributed by each factor at each time step in the data series. $e_{ij}$ are the elements of a m × n matrix E containing residuals not fit by the model matrix at each data point.

The PMF algorithm uses a least-squares algorithm to iteratively fit the values of **G** and **F** by minimizing a "quality of fit" parameter *Q* (Bon et al., 2011), defined as:

$$Q = \sum_{i=1}^{m}\sum_{j=1}^{n}\left(e_{ij}/s_{ij}\right)^2 \tag{2}$$

In this way, PMF minimizes the sum of squares of error-weighted model-measurement deviations. The theoretical value of *Q*, denoted by *Q*-expected ($Q_{exp}$) can be estimated as:

$$Q_{exp} \equiv (m \times n) - p \times (m + n) \tag{3}$$

If all the errors have been estimated within the uncertainty of the data points (i.e. $e_{ij}\ s_{ij}^{-1} \sim 1$) and the model fits the data perfectly, then *Q* should be approximately equal to $Q_{exp}$. The PMF technique does not require assumption of any *a priori* information regarding the composition of source factors and does require the constraint of non-negativity of the factor solutions.

A custom software (PMF Evaluation Tool v2.06, PET) developed by Ulbrich et al. (2009) was used to perform the multivariate analysis. Time series of 13 tracers (two GHGs $CH_4$ and $N_2O$, CO and 10 VOCs) were initially combined into a unified data set. An account of the statistics of the year-long measurements of each of these tracers is listed in Table 3.1. A number of data preparation steps, described in the next three sections, are involved prior to application of PMF to smaller seasonal datasets derived from the unified data matrix based on our choice of PMF sampling periods. For this study, post-processed measurements from the Picarro $CH_4$

instrument, LGR $N_2O$/CO analyzer and the PTRMS (for VOCs) were combined into a unified data set to create matrices **X** and **S**.

### 4.1.4 Choice of measurement height for PMF analysis

GHGs and VOCs are measured at different heights on the tower with different inlets and separate, dedicated sampling lines. Figure 3.4 lists the measurement height and species data that are available at each of those heights. $N_2O$ data was available at two inlet heights (91 m and 483 m a.g.l) with no measurements at the bottom-most level (30 m a.g.l). Additionally, $CH_4$ data at the bottom-most level was more likely to be influenced by nearby sources than data at upper heights, potentially biasing the measurements. Hence, it was decided to not utilize the GHG data observed at the bottom-most height for the purpose of PMF analysis, and to use the more regionally relevant data from a higher inlet height instead. The hourly diurnal patterns of $CH_4$, $N_2O$ and CO enhancements at the middle (91 m a.g.l) and top (483 m a.g.l) inlet heights, during different seasons, were found to be consistent and similar (Figures 4.1 a-d, 4.3 i-l and 4.1 e-h, respectively). We, thus, conclude that the variability of GHGs and CO signals measured at the middle inlet height (91 m a.g.l) is very similar to what would be measured at 131 m a.g.l (since it lies between 90 and 483 m a.g.l), which is one of the inlet heights at which VOCs were measured. Thus, GHG and CO measurements from the 91 m a.g.l inlet height were paired with PTRMS-derived VOC measurements from the nearest inlet height (131 m a.g.l) to create the unified GHG-VOC data matrix. Past inverse dispersion studies at the Walnut Grove tower have utilized $CH_4$ and $N_2O$ observations from the 91 m a.g.l inlet (Jeong et al., 2012 a,b), and thus we also chose this height to be consistent with previous work. In chapter 5 we describe inverse analysis done for the same time period on GHG data measured from the 91 m.a.g.l inlet (same as PMF analysis) and a comparison of results from these approaches is provided in chapter 6.

The choice of sampling heights and the use of data collected over full diurnal cycles affects the spatial region where the PMF analysis is sensitive. This is because the spatial domain over which a PMF analysis accurately represents emissions is a function of meteorology and areal distribution of emission sources (Guha et al., 2015). Following previous work, we assume that the PMF technique is best utilized to apportion local sources at distances of < ~ 50 km radius from the tower. In particular, this implies that the PMF is unlikely to provide sensitive attribution for weak local sources that will be enveloped in signals from strong local, or sources that are carried by winds from significant distances and do not produce a strong diurnal variation in signal at the site because the diurnal variation in boundary layer depth at the site is no longer a strong factor controlling signal strength.

### 4.1.5 Background concentrations of GHG, CO and VOC tracers

Background concentration time series for each tracer were determined based on interpolated running 10 day 0.05 quantile curves at the measurement height (91 m a.g.l) chosen for PMF analysis (read below) and subtracted from the mixing ratio time series to generate enhancements of individual VOCs at each hourly time stamp. For three tracers that had a relatively short life-time of the order of few hours or less, e.g. isoprene, methyl vinyl ketone plus methacrolein (MVK / MAC), and, monoterpenes, no background was assumed (0 ppt). All the other VOC tracers in the PMF study had variable season-dependent atmospheric lifetimes that range from a few days (e.g. toluene in summer) or longer and their backgrounds can be a significant percentage of the absolute mixing ratios (e.g. benzene in winter). $CH_4$, $N_2O$ and CO, have longer lifetimes than the VOCs in this study and have background curves which either have a seasonality (like $CH_4$ and CO) and / or are steadily increasing with time (e.g. $N_2O$). The sources of $CH_4$, $N_2O$ and CO are predominantly primary (not secondary production) and surface-

based hence for these three tracers, the running 10 day 0.05 quantile curve at the upper height (483 m a.g.l) was assumed as the background for 91 m a.g.l.

The enhancements in each time series were scaled by applying scaling coefficients (SC). This scaling process allowed for a consistent scheme to represent tracers with vastly different absolute concentrations (e.g. high ppb scale for $CH_4$ vs low ppt level for monoterpenes) and improve the visual attributes of PMF output plots to follow. The scaling coefficients were determined to assure that variability of all input data for each species was comparable. The background-adjusted mixing ratio enhancements are used as the input data ($x_{ij}$) in the PMF data matrix.

$$x_{ij} = SC \times \left(Mixing\ ratio_{ij} - Background_j\right), \text{ if } x_{ij} > \text{LOD} \quad (4a)$$

$$x_{ij} = SC \times (LOD/2), \text{ if } x_{ij} <= \text{LOD} \quad (4b)$$

$$x_{ij} = SC \times (GM), \text{ if } x_{ij} \text{ is not known} \quad (4c)$$

where SC –scaling coefficient; LOD –limit of detection; GM – geometric mean.

For each tracer time series, there are small enhancements below the limits of detection (LOD, see next section) and also negative enhancements arising from concentrations whose values fall below the interpolated background curves. In these cases $x_{ij}$ was assumed to be half the value of LOD.

### 4.1.6 Uncertainty matrix

To determine the uncertainties associated with data at each time stamp for each tracer, 3σ limit of detection (LOD) for hourly averaged data were determined for each tracer from the raw data. For the VOCs, guidelines set forth by Williams et al. (2010) were adopted to calculate the

uncertainty estimates. An analytical uncertainty ($AU$) of 10 % combined with above-mentioned limits of detection (LOD) was used to calculate the total uncertainty for each $x_{ij}$:

$$s_{ij} \equiv \left(\left(AU \times x_{ij}\right)^2 + (LOD)^2\right)^{0.5}, \text{ if } x_{ij} > \text{LOD}, \tag{5a}$$

$$s_{ij} \equiv \left(\left(x_{ij}\right)^2 + (2 \times LOD)^2\right)^{0.5}, \text{ if } x_{ij} <= \text{LOD} \tag{5b}$$

$$s_{ij} \equiv 10 \times x_{ij}, \text{ if } x_{ij} \text{ is not known} \tag{5c}$$

Using this approach, the detection limit dictates the errors for small enhancements (~ LOD) while errors for larger enhancements in the time series are tied more to the magnitude of the data value ($x_{ij}$) itself. To maintain the robustness of PMF analysis, outliers, missing values and below detection limit values were selectively down-weighted by increasing their uncertainty in proportion to the uncertainty of other data points.

The impact of different levels of uncertainty that arise from using different instruments based on unique scientific techniques (e.g. laser spectrometry versus chemical ionization) has been noted to be significant in determining the quality of fit of the PMF model to the data from the respective instruments. Slowik et al. (2010) have reported that differences in signal-to-noise ratio of different instruments do lead to PMF solutions being skewed and biased. The GHG and CO measurements have high precision and significantly lower detection limits than ambient levels. The relatively low values of uncertainties in the GHG data, compared to VOCs, are substituted with those calculated using a custom approach. The GHG and CO uncertainties are assumed to be proportional to the square root of the data value and an arbitrary scaling factor was determined through trial and error to produce lower values of $Q\ Q_{exp}^{-1}$:

$$s_{ij} \equiv A \times \left(x_{ij}\right)^{0.5}, \tag{6}$$

where A = 1 (for $CH_4$ and CO), 2 (for $N_2O$)

This method attributes larger percentage uncertainties to smaller enhancements and hence lesser weight in the final solution and vice versa. This approach leads to an uncertainty matrix that attributes relatively similar percentage errors to both GHGs and VOCs, which should lead to a better fitting of the data in PMF. This is also experimentally verified through numerous PMF iterations (not shown here) where assigning comparable uncertainties to both GHG and VOC input data is observed to provide PMF solutions that have more a more balanced representation of species from all instruments in the output factor profiles.

Missing values are replaced by the geometric mean of the tracer enhancement time series and their accompanying uncertainties are set at ten times this geometric mean (Polissar et al., 1998) to decrease their weight in the solution. Based on the *a priori* treatment of the entire input data (scaling) and the corresponding outputs of the PMF analysis, a weighting approach (for measurements from different instruments) as used in (Slowik et al., 2010) is not found to be necessary.

#### 4.1.7 PMF factor number, rotations and error analysis

A detailed account of how to arrive at a user-defined optimal PMF solution, rotations of factors to generate factor profiles with higher degree of plausibility albeit at a higher "quality of fit" parameter Q value, and bootstrapping analysis to determine quantitative uncertainties of the chosen PMF solution is described in Section 2.2.6 of the PhD dissertation of a co-author in this report (Guha et al., 2014). We will avoid repeating those details here but instead summarize the overall procedures performed for each of the seven different PMF analyses. Specific results of these operations, if relevant, are reported in the description of the PMF results in Section 4.3.

PMF factor numbers (p) were explored from 1-8 for each PMF analysis to determine the optimal or "best explained" combination of factor profiles. Care was taken to avoid considering a p-factor solution where a clear splitting of an existing factor from a (p-1)-factor solution into two resulting factors was observed, such that the two factors in the p-factor solution had similar diurnal profiles and time series but with different constituents. At each p, different random starting points (SEEDs) were tested (from 1-10) to find the local minimum of a particular p-factor PMF solution (Paatero, 1997). This gave a better idea of the existence of additional "real" factors in the ultimate solution. The rotational ambiguity was explored using the FPEAK parameter that was varied from -1.0 to +1.0 at 0.2 unit increments without changing p to explore solutions which may present more physically realistic combinations of factor profiles (Paatero et al., 2002) as opposed to that in the base solution (at FPEAK = 0). It should be noted that there were a maximum of 13 tracers in certain PMF runs but when $N_2O$ and/or MeOH were missing completely, these tracers were not included in the PMF analysis for that seasonal period, hence decreasing the actual number of included tracers (Table 3.1). This directly impacts the degrees of freedom in each successive higher p-factor solution. Such high p-factor solutions may have a significantly lower Q but may represent apportionment of individual tracers completely and exclusively to separate factors that does not make physical sense and defeats the purpose of performing PMF analysis. Hence, we are cautious in considering and accepting solutions at higher numbers of factors unless they make clear physical sense to the analyst and can be attributed to a source category.

In traditional PMF literature, uncertainties in mass fractions derived from PMF analysis are often not reported at all. A detailed description of how the uncertainty in the relative apportionment of a particular tracer, say $CH_4$, in a specific source factor is calculated for this

study can be found in related work of the authors (Section S3; Guha et al., 2015). A bootstrapping analysis of the chosen p-factor solution was performed (Norris et al., 2008; Ulbrich et al., 2009) with 100 runs. The 1-sigma standard deviation of the mean mass fraction of a tracer (e.g. $CH_4$) in a particular source factor, for a particular season, calculated from 100 bootstrapping runs is reported as 'uncertainty' in the abstract and the rest of this chapter (Section 4.2.2). The percentage range for $CH_4$ and $N_2O$ that is also reported throughout the text, for each source type and for each season, is not related to the uncertainties calculated using the bootstrap runs. The percentage range reported originates from the source-apportioned time series of hourly samples computed by using the $CH_4$ and $N_2O$ mass fraction from each factor profile for a chosen p-factor solution. This range often demonstrates the variation of the tracer concentration typically observed in each season due to meteorological and diurnal variations.

## 4.2. Results and Discussion

### 4.2.1. Description of PMF source factors

In this sub-section, we present the composition of the different factors that result from the PMF analysis on seven individual sampling periods from June 2012 to Aug 2013 at WGC. The PMF source factors are statistical combinations of co-varying signal contributions and as such, covariance due to diurnal changes in vertical mixing and shifts in wind direction may result in contributions of coincidentally located sources being apportioned to the same source factor. This is also known as factor 'splitting' and 'mixing' and has been discussed in Section 2.2.6 in Guha et al. (2014). Our choice of source factor nomenclature reflects our interpretation of the dominant source contributions to the composition of each factor resulting from VOC source marker evaluation, comparison of relative emission rates and diurnal trends. The factors reveal a

break-down of the major $CH_4$ and $N_2O$ source categories that can be deconstructed from the input data matrix based on the input uncertainties ascribed to each data value in the time series.

For each sampling period related to a particular season, we identify the number of factors in the 'best case' PMF solution based on the guidelines in Guha et al. (2014). The PMF source factors that were observed at WGC in different seasons over the 2012-13 annual cycle were 'Dairy and Livestock', 'Urban + Oil and Gas', 'Primary Biogenics and Secondary Organics', 'Agriculture + Soil Management + Delta', 'Fresh Isoprene', 'Isoprene Oxidation products' and likely 'Forest Fires' (see Summer 2012; Section 4.2.2). In the following paragraphs, we list and describe all the source factors that make up the factor profiles resulting from one or multiple PMF analyses. The specific factor profiles resulting from the apportionment of each unique seasonal PMF run are shown in Figures 4.4, 4.6, 4.8, 4.10, 4.12, 4.14, and 4.16.

***Dairy and Livestock emissions***

This source factor is represented in all plots and figures in orange color. The major contributors to this factor are $CH_4$ and $N_2O$ (whenever included in the PMF analysis). This factor contains some contributions from oxygenated VOCs like methanol, acetaldehyde, acetone + propanal and MEK in seasonally varying proportions over the seven PMF periods. These VOCs have been reported to be emitted from various processes within dairy and feedlot operations in significant quantities (Filipy et al., 2006; Shaw et al., 2007; Ngwabie et al., 2008; Chung et al., 2010). The presence of methanol in this factor points to the essentially biological origin of emissions from this source as opposed to a combustion / fugitive source. This source factor is a minor contributor to the enhancements of the included aromatics (benzene and toluene) and combustion tracer CO. The minor contributions of aromatics to this source have been detected in

all the above-mentioned studies. The *m/z* 93 can also potentially be a fragment from monoterpenes as opposed to toluene. The CO can also result from the large-scale industrialized nature of dairy agriculture in the Central Valley where a lot of commercial motor-driven equipment is used. The MeOH / $CH_4$ (mmol $mol^{-1}$) relative emission rates (ER) derived from different seasonal 'dairy and livestock' factor profiles in this study range from 3.4 to 9.3. This is in general agreement with emission rates reported from dairy and feedlot studies in Table 2.4 in of Guha et al. (2014). Particularly, our range of observed emission rates show conformity with cow chamber studies (Shaw et al., 2007), regression slopes from dairy plumes measured by aircraft (Gentner et al., 2014a) and the lower end of slopes observed in flights over the Central Valley in Figure 3.12b of Guha et al. (2014). The $N_2O$ / $CH_4$ emission rate range of 2.8 – 12.8 (mmol $mol^{-1}$) over four different seasonal PMF periods in this study is similar to that of the dairy and livestock factor in the PMF analysis at Bakersfield of 5.5 mmol $mol^{-1}$ (Chapter 2; Guha et al., 2014). Hence, we demonstrate that the principal contributor to the orange factor is emissions from intensive dairy and livestock operations surrounding WGC and $CH_4$ and $N_2O$ are the principal constituents of this source factor.

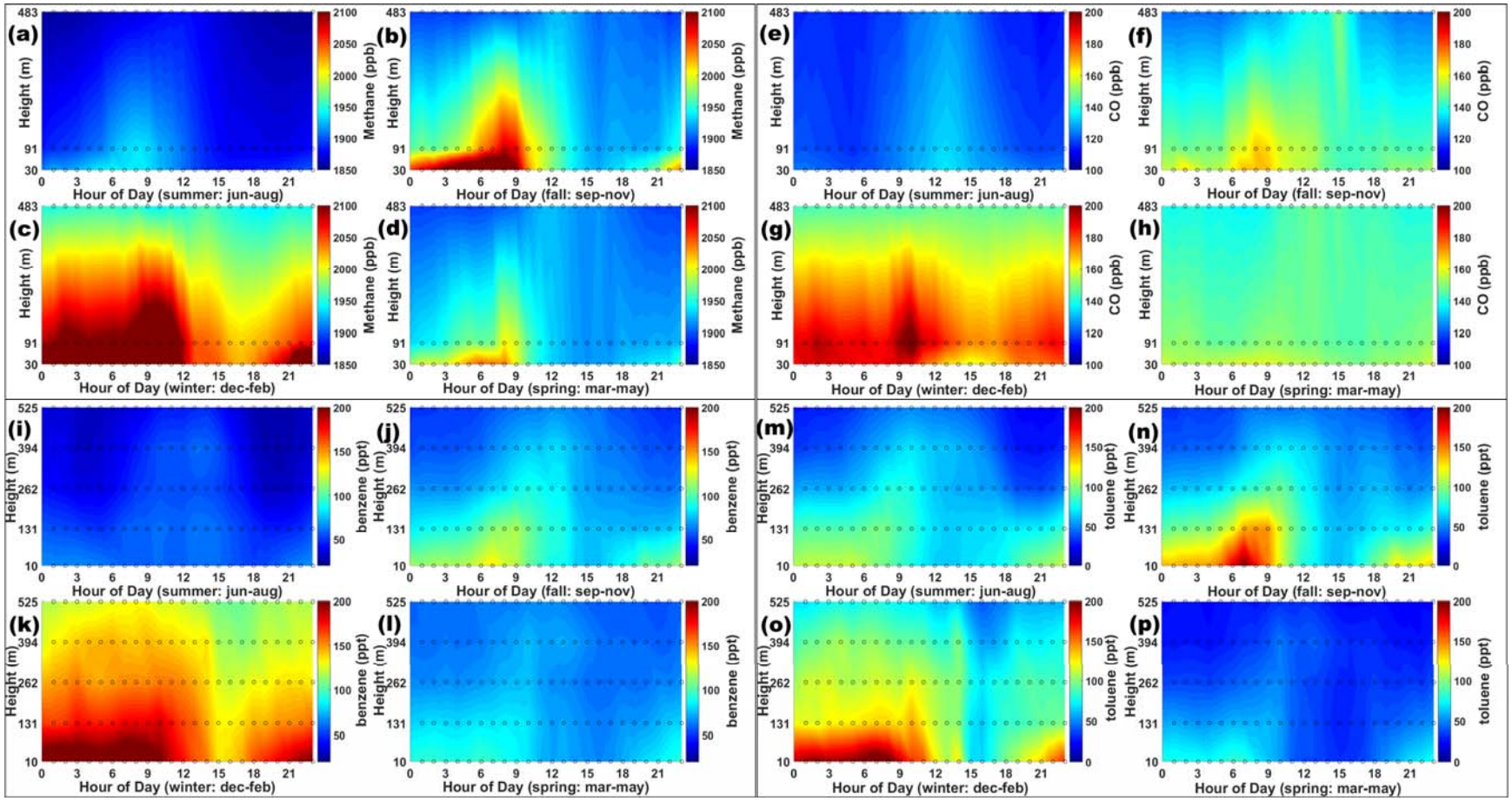


**Figure 4.1.** Mean diurnal distribution (x-axis) of $CH_4$, combustion tracer CO and aromatic VOCs showing interpolated vertical profiles across all measured heights (y-axis) during different seasons at WGC. The color axis represents the mixing ratio of each compound. Species shown include (a-d) $CH_4$, (e-h) CO, (i-l) benzene, and (m-p) toluene. The x-axis of each figure lists the season for which the concentrations have been plotted. The horizontal dotted lines in each plot represent the height (m a.g.l) on WGC at which the measurements are made.

***Urban and Oil & Gas emissions***

This source factor is represented in black color in all factor profiles and diurnal distribution plots. This source factor is by far the dominant source of CO and aromatics like benzene and toluene. This suggests that the sources contributing to this factor have an imprint of combustion-related emissions. The rural location of WGC and absence of any major highways immediately upwind of the site suggests that these emissions are not dominated by a local vehicle combustion source. This can also be deduced from the toluene to benzene molar ratios reported in Table 4.1 which is used as an indicator of traffic emissions. A range of 1.5 to 4.3 (mol $mol^{-1}$) has been suggested as typical emission ratios of toluene to benzene from fresh plumes in various urban environments (Warneke et al., 2007; Baker et al., 2008; Liu et al., 2009; Bon et al., 2011; Borbon et al., 2013; Lan and Minh, 2013). Photochemical aging of a fresh plume depletes emitted toluene faster than benzene owing to the difference in their OH radical rate constants, the OH removal process being the principal atmospheric loss mechanism for these aromatics (Gelencsér et al., 1997; Warneke et al., 2007). Hence, toluene / benzene ratios are expected to decrease with time (distance) from the source and, as a consequence, be lower in rural environments than in urban environments as seen in a study conducted at multiple urban and rural sites located unique traffic-equivalent distances (hours) apart (Gelencsér et al., 1997). The range of toluene/benzene ratios we observe in this PMF factor is 0.4 – 1.1 (with lower end of the ratios during winters) which is significantly less than typical urban emission ratios and gasoline-speciation profiles observed in Table 4.2. This indicates that a significant contribution to aromatics and CO attributed to this factor may be emitted from sources in the upwind urban regions in the outer San Francisco Bay Area that get photochemically depleted (more toluene depletion versus benzene depletion) as they are transported to WGC and hence the difference in

**Table 4. 1**. Comparison of PMF urban and oil / gas source factor benzene and toluene emission ratios relative to carbon monoxide with those derived from urban measurements and gasoline speciation profiles. Relative emission ratios of toluene to benzene are also included as an indicator of aging of emission plumes arriving at WGC.

| Study | Source | benzene / CO (pptv $ppbv^{-1}$) | toluene / CO (pptv ppbv-1) | toluene / benzene (pptv pptv-1) |
|---|---|---|---|---|
| WGC PMF urban and oil/gas factor[a] | This study | 1.1 - 1.8 | 0.4 - 1.5 | 0.4 - 1.1 |
| Mexico city 2006 | Bon et al. (2011) | 4.2 ± 0.4 | 1.21 ± 0.06 | 3.5 ± 0.4 |
| CalNex Los Angeles ambient emission ratios[b] | Borbon et al. (2013) | 1.30 | 3.18 | 2.40 |
| New England 2004 | Warneke et al. (2007) | 0.62 | 2.62 | 4.2 |
| 28 US cities (1999-2005)[c] | Baker et al. (2008) | 0.7 | 2.7 | 3.9 |
| Berkeley liquid gasoline speciation 2010[d] | Gentner et al. (2012) | NA | NA | 9.708 ± 1.375 |
| Berkeley evaporative gasoline speciation 2010[e] | Gentner et al. (2012) | NA | NA | 2.906 ± 0.246 |

[a] Range of mean ratios over seven unique PMF experiments for different seasonal periods.
[b] Derived from Linear Regression Fit slope of scatterplot from CalNex Pasadena supersite samples.
[c] Ratios represent average of emission ratios from 28 cities.
[d] Ratios calculated from Table S9, Gentner et al., 2012; uncertainties are ± standard deviation.
[e] Ratios calculated from Table S11, Gentner et al., 2012; uncertainties are ± standard deviation.

the observed emission rates originate from a multitude of sources including five O&G refineries in the North Bay area (< 60 km from WGC), a couple of landfills, fugitive emissions from urban natural gas pipeline distribution network etc.

The largest natural gas producing field in California, Rio Vista, is located about 15 - 25 km south-west of WGC. It is possible that the emissions contributing to this factor are predominantly from industrial operations in this field and the associated $CH_4$ is due to fugitive losses. A large enhancement of $CH_4$ (up to 120 ppb) was observed while flying over this field during the CABERNET campaign (Section 3.2.2; Guha et al., 2014) pointing to fugitive emissions that could very well be responsible for the $CH_4$ apportioned to this factor. Additionally, no $N_2O$ is present in the chemical profile in even minor fractions which adds weight to the possibility of the 'black' factor being dominantly an Oil and Gas fugitive + combustion source. In a measurement study of VOCs and $CH_4$ in 43 Chinese cities, significantly higher $CH_4$ mixing ratios were observed in 15 cities where toluene / benzene ratios were < 1 (mol $mol^{-1}$) and not typical of the 10 "traffic-related cities" where the ER was ~ 1.7 or higher (Barletta et al., 2005). Additionally, the abundance of light alkane fraction of ethane (associated with natural gas leakage), relative to other hydrocarbons, was significantly higher in these 15 cities. This suggests that fugitive $CH_4$ emissions along with VOC emissions from related natural gas extraction process at the Rio Vista field is likely to have lower toluene / benzene ratios in line with our observations in this factor. In the absence of measurements of light alkanes like ethane and propane which can serve as excellent source tracers for fugitive $CH_4$ emissions from the O&G sector, it is difficult to verify and validate the exact source / origin of the emissions contributing to this factor. Lower toluene / benzene ratios (< 1) have also been reported from biofuel / wood burning (~ 0.58), forest fires and agricultural residue burning (~ 0.82) (Andreae and Merlet, 2001; Jordan et al., 2009). Since upwind emissions plumes from the Bay Area will always flow over the gas field and croplands before arriving at WGC, we conclude it is best to

define this source factor as a combination of fugitive / combustion emissions from the urban core and the O&G sector.

Secondary production of acetaldehyde from photo-oxidation of light alkanes is the largest global source of acetaldehyde (Millet et al., 2009) and a minor source of acetone (Goldstein and Schade, 2000; Schade and Goldstein, 2006; Hu et al., 2013). Urban / O&G plumes are likely to contain light alkane emissions and hence, expectedly, we see acetaldehyde and some acetone apportioning on to this factor. This source factor also contains some contributions of *m/z* 42 which are potentially alkanes emitted into the polluted plumes arriving at WGC. In winters, this factor sees some anthropogenic contributions on masses that have traditionally dominant biogenic contributions in summers. Some *m/z* 69, which is predominantly isoprene in summers, apportions on to this factor. These are mostly contributions from pentadienes and cyclopentenes which are by-products in petroleum industry plumes. Similarly, *m/z* 137 contribution during winters is from known anthropogenic monoterpenes while *m/z* 71 potentially contains contributions from refinery by-products like pentenes and 2-methyl-2-butene. No methanol is apportioned to this factor in any seasonal PMF analysis.

***Primary Biogenics and Secondary Organics***

This source factor is one of the three that is produced in all of the seven PMF evaluations and is shown in green color in all plots. This source factor is the dominant contributor of oxygenated VOCs all of which have major primary biogenic and secondary photochemical sources surrounding WGC. This includes methanol (Baker et al., 2001; Schade and Goldstein, 2001, 2006; Harley et al., 2007; Hu et al., 2011), acetaldehyde (Kesselmeier and Staudt, 1999; Karl et al., 2002), acetone ( Kirstine et al., 1998; Goldstein and Schade, 2000; Hu et al., 2013) and methyl ethyl ketone (Kirstine et al., 1998; de Gouw et al., 1999). A number of studies have

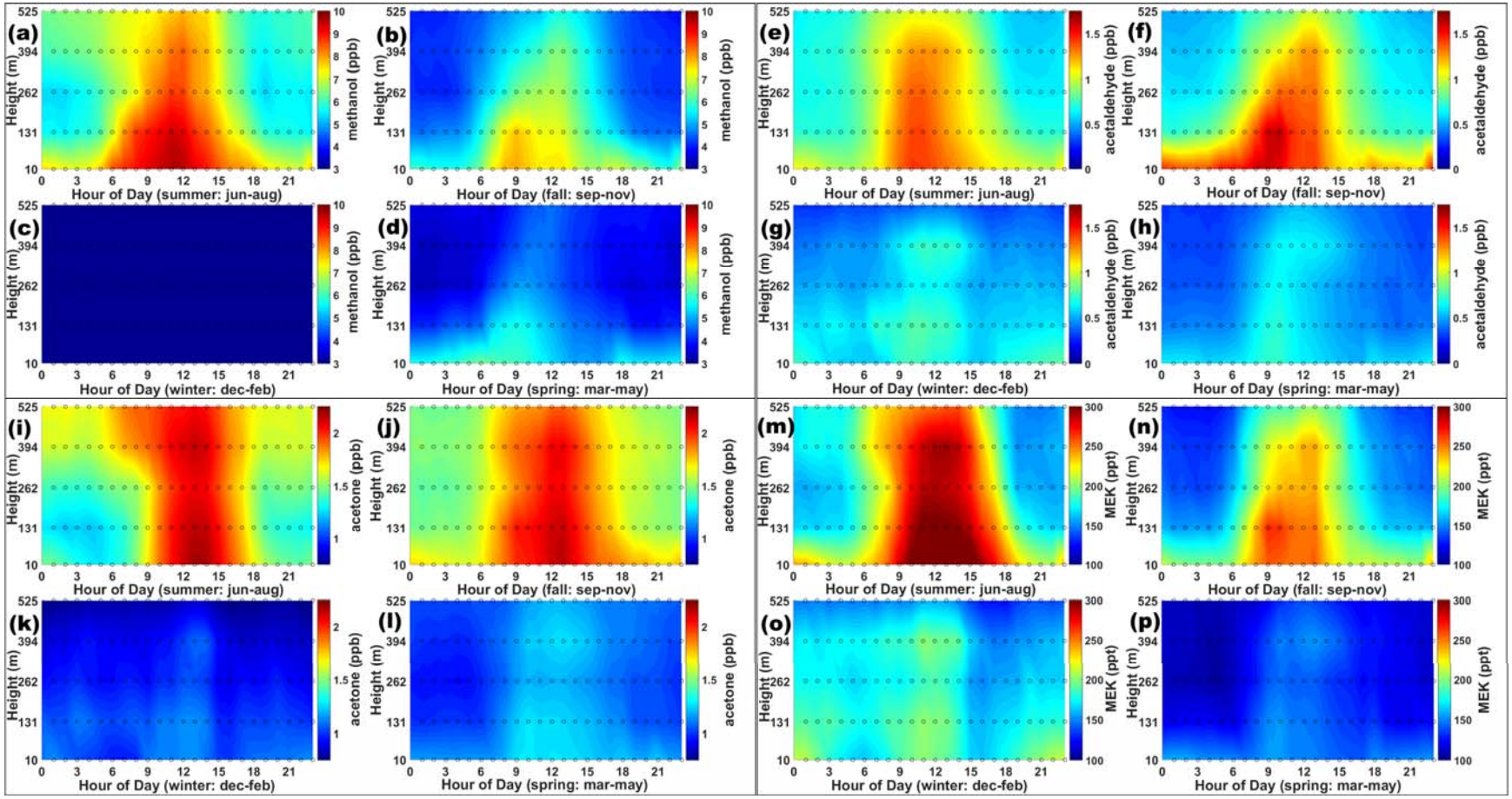


**Figure 4.2.** Mean diurnal distribution (x-axis) of oxygenated VOCs showing interpolated vertical profiles across all measured heights (y-axis) during different seasons at WGC. The color axis represents the mixing ratios of each VOC. Species shown include (a-d) methanol, (e-h) acetaldehyde, (i-l) acetone, and (m-p) methyl ethyl ketone (MEK). The x-axis of each figure lists the season for which the concentrations have been plotted. The horizontal dotted lines in each plot represent the height (m a.g.l) on WGC at which the measurements are made. There were no methanol measurements in the winter season at any height (Figure c).

reported significant fluxes of these compounds from Central Valley agriculture (Fares et al., 2011, 2012; Park et al., 2013). The diurnal profiles of these oxygenated VOCs (Figure 4.2) are generally consistent with that from year-round measurements at a largely rural site in New Hampshire (Jordan et al., 2009). The vertical profiles in Figure 4.2 and diurnal cycle in Figure 4.10c indicates that these compounds are predominantly produced from local ground-based sources with maximum emissions during daytime. As mentioned in Section 3.1, the region surrounding WGC is predominantly farm land with a variety of cultivated crops. Primary biogenic VOC emissions from nearby agriculture reach a maximum during the day. Secondary VOCs produced from surrounding biogenic precursor sources are primarily photochemically-driven so would also peak during daytime. Prevailing daytime winds arriving at WGC contain a combination of these two above-mentioned categories of emissions (Figure 4.2). There is no noticeable apportionment of CO, aromatics and acetonitrile to the factor profile and this confirms the majorly biogenic nature of the sources influencing this factor. There is no $CH_4$ and $N_2O$ (except in summer 2013 PMF; Section 4.2.2 and explained later) apportioned to this factor. This is an expected outcome, based on our knowledge of $CH_4$ and $N_2O$ emissions sources.

The rise and decline of the peak enhancements at the measurement height (131 m a.g.l) occur at slightly different times for different oxygenated VOCs e.g. the peak of methanol during summers (Figure 4.2 a) occurs at 1100 PST, which is one hour after the peak occurs for acetaldehyde (Figure 4.2 e) but a couple of hours before peak concentrations are achieved for acetone (Figure 4.2 i). Different emission mechanisms and biological triggers within the plant system have been previously proposed. For instance, large methanol emissions result from leaves controlled by opening and closing of the stomata (Harley et al., 2007; Hüve et al., 2007) and higher methanol emissions occur due to pectin-hardening during stages of rapid plant growth

(Galbally and Kirstine, 2002; Hüve et al., 2007) in late spring/early summer. Also, acetaldehyde is released throughout the day in forest canopies under varying light conditions (Karl et al., 2002), while MEK is the largest VOC released from grass and clover pastures (Kirstine et al., 1998) located farther from the site compared to crop lands (Figure 3.1) followed by methanol and acetone. Acetone can be emitted from primary biogenic emissions that are light and temperature dependent and simultaneously occur from photochemical production thus peaking in mid to late summer time (Hu et al., 2013; Jacob et al., 2002; Schade and Goldstein, 2006). The apportionment through PMF analysis is based on simultaneous linear covariance of enhancements. At WGC, differences in release mechanisms of the oxygenated VOCs from their biogenic sources and photochemical reaction rates lead to staggering of diurnal timelines. In spite of this, the collective similarity in the non-linear enhancement features in the diurnal profiles result in major portions of oxygenated VOC signals being apportioned to a common source factor which we describe as 'Primary Biogenics and Secondary Organics'.

Even during winters, agricultural residues in the post-harvested fields, and potential double cropping may result in some biogenic emissions that lead to this factor appearing in the PMF analysis even as other biogenic / agriculture related factors are not identified (Figure 4.8).

***Agriculture + Soil Management + Delta emissions***

This source factor is represented in purple color in all factor profile and PMF diurnal distribution plots. This factor is a major contributor to $N_2O$ enhancements in all seasonal PMF runs where $N_2O$ is measured and included. In addition, most of the monoterpene emissions (*m/z* 137) are attributed to this factor along with minor contributions of oxygenated VOCs (OVOCs), isoprene and MVK / MAC, all of which have mostly biogenic sources around WGC. A similar

factor was observed in the PMF analysis at Bakersfield (Section 2.3.2 and Figure 2.7; Guha et al., 2014). In this source factor, we principally see microbially-mediated soil emissions of $N_2O$ arising from the use of synthetic and organic fertilizers on nearby agricultural farmlands that include corn, a variety of fruits and vegetables and large swaths of rice agriculture (~ 100 km from WGC), all of which require N fertilizer input (van Groenigen et al., 2010; Hoben et al., 2011; Linquist et al., 2012; Rosenstock et al., 2013). As discussed later in Section 4.2.2, the $N_2O$ signal apportioned to this factor varies seasonally and depends on the annual cycle of agriculture and corresponding use of fertilizers. Collocated with the soil $N_2O$ emissions are minor VOC contributions from agricultural crops. The emissions of $N_2O$ are primary in nature and result in minor enhancements above a large tropospheric background. The diurnal profile is mostly governed by daytime dilution in an increasing volume of the expanding boundary layer followed by accumulation of emissions in the shrinking boundary layer and night time inversion (Figure 4.3 i-l). The emissions of OVOCs from crops, on the other hand, are dependent on various factors with a major exponential dependence on temperature (and in some cases light) and vary non-linearly. Hence the majority of crop OVOC emissions get apportioned to the 'green' factor profile (**F**) with exponentially varying factor contributions (**G**) in the time series. In addition to this, minor contributions of primary OVOCs co-vary with collocated emissions due to boundary layer dynamics rather than temperature and light dependence. These contributions, mostly minor, also help explain the reconstructed PMF time series and get apportioned to the 'purple' factor. This 'purple' factor would contain other similarly varying tracers in the air parcels that arrive at WGC simultaneously e.g. coincident emissions of $N_2O$ and monoterpenes. Biogenics like monoterpenes (*m/z* 137) are emitted from crops and have a diurnal profile, which is different from other oxygenated VOCs (explained in the next section). Its diurnal profile is, however,

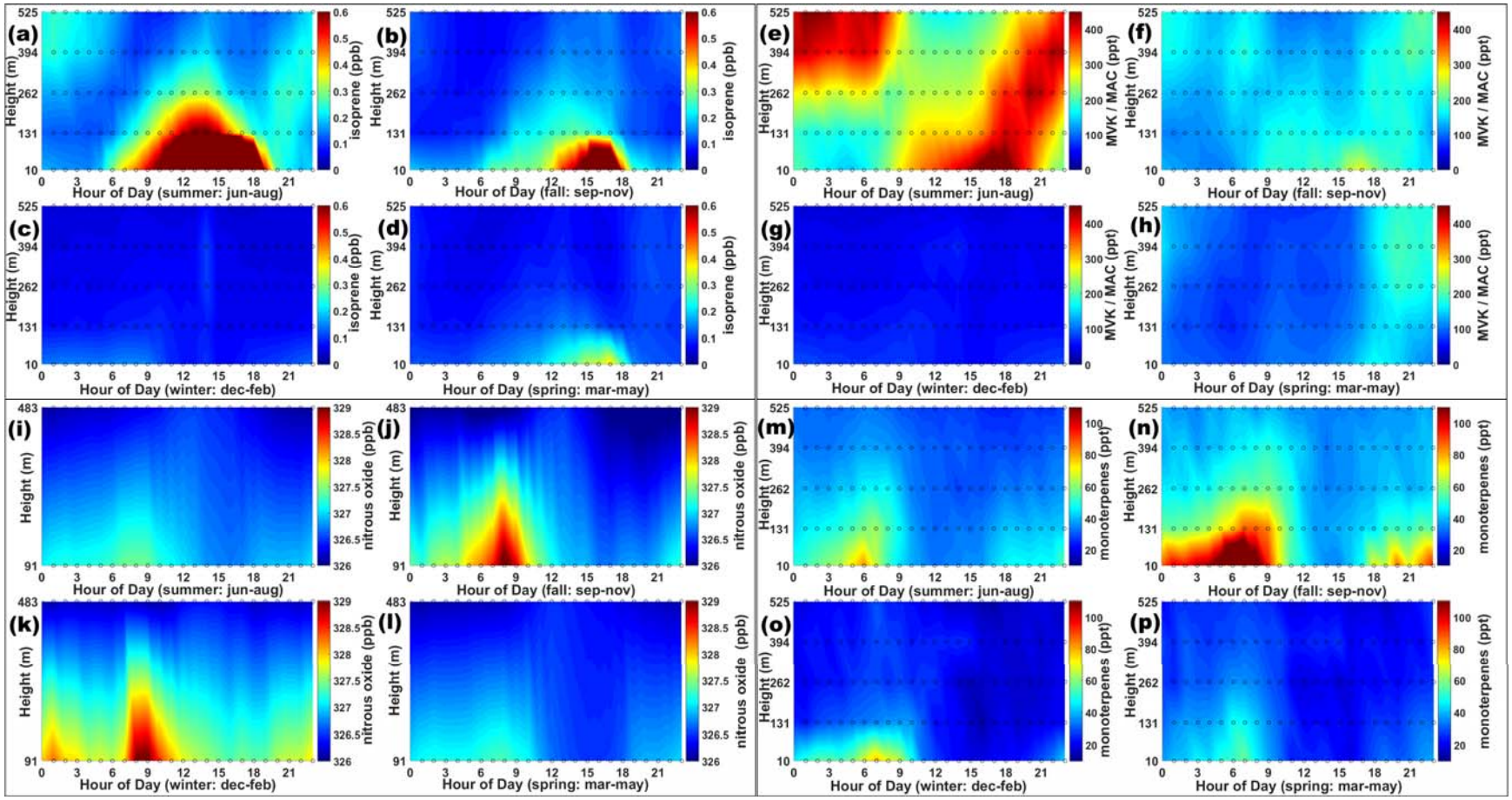


**Figure 4.3.** Mean diurnal distribution (x-axis) of primary and secondary biogenic VOCs along with $N_2O$ showing interpolated vertical profiles across all measured heights (y-axis) during different seasons at WGC. The color axis represents the mixing ratios of each VOC. Species shown include (a-d) isoprene, (e-h) methyl vinyl ketone (MVK) + methacrolein (MAC), (i-l) $N_2O$, and (m-p) monoterpenes (*m/z* 137). The x-axis of each figure lists the season for which the concentrations have been plotted. The horizontal dotted lines in each plot represent the elevation (m a.g.l) on WGC at which the measurements are made. $N_2O$ was not measured at 30 m a.g.l, hence measurements begin at 91 m a.g.l.

similar to that of $N_2O$ and a major proportion of the monoterpene enhancements are apportioned to this source category.

This source factor also contains some contributions from *m/z* 93 which is calibrated to toluene in this experiment. The *m/z* 93 diurnal profile (named toluene in Figure 4.1 m) is similar to that of $N_2O$ (Figure 4.3 i) and monoterpenes (Figure 4.3 m) during the summer season. The diurnal profile of benzene (Figures 4.1 i-l) and CO (Figures 4.1 e-h) are similar to each other in all seasons. But a comparison with seasonal diurnal profiles of toluene (Figure 4.1 m-p) reveals that in the summer season, the diurnal profile of toluene is quite different. This points to an additional summertime source of toluene (or another VOC detected on *m/z* 93) that masks the general expected non-biological emission profile of toluene similar to that of benzene and CO if they had completely similar emissions sources. This additional enhancement is coming from the 'purple' source factor. Similar observations at a rural site in New Hampshire have been observed for summertime toluene and local vegetative emissions have been estimated to have a significant contribution to the enhancements (White et al., 2008). Some methanol also gets apportioned to this factor. Methanol, monoterpenes and toluene emissions from corn and corn harvesting has been reported to be significant (Graus et al., 2013) with some minor emissions of benzene. Methanol and monoterpenes are also emitted in significant quantities during harvesting of managed grasslands (Ruuskanen et al., 2011). The region around WGC has a lot of corn plantations and large areas at the edge of the Delta are managed grasslands and pastures (Figure 3.1). The literature on the emissions of the above-mentioned VOCs conforms well to our observed chemical apportionment of this factor. Monoterpenes are stored by plants in storage pools and are released in large amounts during damage and stress (like during harvesting and early growth). We find that mass fraction of monoterpenes attributed to this factor is

significantly larger in the PMF apportionments during early fall and late fall seasons (Figures 4.4 and 4.6), which coincide with the harvesting season and also during early spring (Figure 4.10), which coincides with the planting season. This reaffirms the agricultural origin of this source factor. A small mass fraction of $CH_4$ is apportioned to this factor. Most of the upwind regions around WGC are part of the Sacramento – San Joaquin Delta and as such, contain large tracts of lands that are periodically flooded and drained like peatland pastures, natural and restored wetlands, and some rice agriculture (Figure 3.1). This land cover is ubiquitous and coterminous with agricultural farm lands and as such, any GHG and VOC emissions from the two above mentioned land-types is coincident in the plumes arriving at WGC. If the diurnal profile of these emissions is essentially controlled by boundary layer dynamics and meteorology, these emissions will be attributed to a common factor even though they may represent separate source categories. $CH_4$ (as well as $N_2O$) fluxes have been reported from a variety of flooded / drained ecosystems in the Delta like restored wetlands, peatland pastures and rice cultivation (Teh et al., 2011; Hatala et al., 2012; Knox et al., 2014). Hence, we explain the origin of the methane attributed to this factor as that coming from anaerobic mechanisms (both man-made and natural) in the Delta region around WGC. We understand that this factor is influenced by an aggregation of these collocated sources and best represented by a statistical combination of their contributions as a unique factor in the PMF analysis and we therefore define this source factor as 'Agriculture + Soil management + Delta'.

***Fresh Isoprene emissions***

This factor is highly seasonal, and is observed as an output of PMF analysis in the late spring, summer and early fall. This factor is represented in 'light blue' color in the plots. This

factor mostly contains fresh isoprene emissions with minor contributions from oxygenated VOCs. The diurnal profile of isoprene has a peak during the day and the concentrations reach a low during the evenings and stay close to being negligible before beginning to rise in the morning again as seen in the diurnal profile plots for isoprene (Figures 4.3 a-d). Isoprene comprises a third of annual global VOC emissions from all natural and anthropogenic sources with > 90% of the emissions coming from terrestrial plant foliage (Guenther et al., 2006). Isoprene is mostly emitted by chloroplasts as a function of light and temperature (Steeghs et al., 2004). Hence its emissions occur during the day and stop at night. Isoprene has a short lifetime (~ 1 h), as compared to some of the other coincident OVOCs, the reaction with OH radicals being its principal sink. Due to differences in emission sources and loss processes such as chemical reactions, advection, and vertical dilution, isoprene almost exclusively gets apportioned to its own PMF factor. Emissions of isoprene are much higher in the summer time as compared to winter and early spring and hence this factor is not produced in those respective PMF runs. There is no $CH_4$ or $N_2O$ attributed to this factor.

Monoterpenes (Figure 4.3 m-p) have a different diurnal profile than isoprene with peak concentrations occurring in the night time / early morning and daytime minima. This is also observed in forest environments and rural agricultural locations alike (Bouvier-Brown et al., 2009; Jordan et al., 2009; McKinney et al., 2011). Monoterpene emissions from surrounding tree crops (and nearby deciduous forests) and grasses are primarily a function of temperature (from stored pools within resin ducts) and not light. During the summer and fall, monoterpene emissions during the night time are enhanced due to warmer night time temperatures resulting in continued emissions that build up in a shallow boundary layer.

***Isoprene oxidation products***

This source factor is represented in 'navy blue' color in the PMF-related plots. This factor principally contains methyl vinyl ketone (MVK) and methacrolein (MAC) (measured as a sum by PTR-MS), which are atmospheric oxidation products of isoprene. Hence, this factor is closely associated with the 'fresh isoprene' factor and shows up in the PMF apportionment only when isoprene emissions are significant, which occurs in the summer season only. The diurnal profile of MVK and MAC follows and lags behind the isoprene diurnal profile reaching peak concentrations around 1800 PST. A visual analysis of the observed diurnal concentration plots (Figures 4.3 e-h) reveal that a part of the MVK / MAC signal directly results from oxidation of locally emitted isoprene at the ground level while another part of the signal measured at 131 m a.g.l at WGC is a result of entrainment of advected MVK / MAC from upper levels at WGC (see Figure 4.3 e). This MVK / MAC prevalent at the upper levels of WGC is contained in oxidized biogenic plumes in the easterly downslope winds blowing from the oak forests along the foothills in the Sierra Nevada mountain range to the east of the site (Misztal et al., 2014). No observable $CH_4$ or $N_2O$ is apportioned to this source factor or observed at the upper levels in the diurnal profiles of $CH_4$ (Figures 4.5 a-d) or $N_2O$ (Figures 4.3 i-l). Hence it is clear that the biogenic plumes from the forested regions in the foothills do not have any $CH_4$ or $N_2O$ imprint.

### 4.2.2 Seasonal PMF results

We herein present the relative strength of $CH_4$ and $N_2O$ sources in the region as determined using PMF. One of the objectives of this analysis is to investigate the seasonal distribution of the relative contributions of major GHG sources over a complete annual cycle. We present the diurnal profiles of $CH_4$ and $N_2O$ enhancements apportioned by source strength for each seasonal PMF analysis and discuss the reasons behind the variability in the relative

source strengths between seasons, if observed. As is seen in the seasonal absolute concentration diurnal plots (Figures 4.1 a-d, 4.3 i-l), both $CH_4$ and $N_2O$ mixing ratios have a diurnal pattern resulting from primary sources that emit into an expanding boundary layer during the day time as atmospheric mixing increases, followed by a shallow boundary layer in stable atmospheric conditions during the nighttime. Observed absolute concentrations are lower in the summertime as boundary layers are deeper while wintertime concentrations are higher due to a shallower boundary layer. From the visual analysis of the source-apportioned relative diurnal distribution plots accompanying the absolute diurnal plots for each season, we do not observe a rectifier effect forcing of boundary layer dynamics on the PMF apportionment of $CH_4$ and $N_2O$ enhancements as is typically observed in the correlation between diurnal / seasonal boundary layer dynamics and ecosystems $CO_2$ fluxes. The relative contributions of a source to $CH_4$ and $N_2O$ enhancements is driven by relative strengths of emissions sources in different seasons and meteorology (e.g. high westerly winds in summers versus low along-valley winds in winters).

The GHG and VOC measurements were conducted over a complete annual cycle from mid-2012 to mid-2013 with data from the summers of 2012 and 2013 analyzed separately (Table 3.1). Since, we do not have $N_2O$ measurements during summer 2012 (measurements of $N_2O$ only begin in mid-Oct), we consider the PMF apportionment during summer of 2013 to complete the annual cycle that begins in early Fall 2012. We do include the PMF analysis results from summer of 2012 in order to compare $CH_4$ apportionment results from two consecutive summers and to evaluate any anomalies, if present.

***Early Fall 2012 (Sep 1 – Oct 15)***

A 6-factor solution is able to optimally describe the apportionment of GHGs and VOCs during the first half of fall 2012 as shown in Figure 4.4. $N_2O$ was not measured during this

period. Most of the $CH_4$ signal (~ 55 - 80 % ) is apportioned to the 'dairy and livestock' source depending on the time of day as seen in the PMF diurnal distribution plots in Figures 4.5 a and c. The uncertainty attached to the mean $CH_4$ mass fraction of this factor from the bootstrapping analysis is +/- 9 %. The diurnal profile of reconstructed $CH_4$ resembles that of emissions with primary sources whose concentrations vary with boundary layer depth and vertical mixing. The 'urban and oil/gas' source is responsible for about 15 to 30 % of the daily enhancements with uncertainty in the mean $CH_4$ mass fraction apportioned to this source from the bootstrapping analysis being about 46 %. It should be noted that both daytime and nighttime winds (Figures 3.2 b and 3.3 b) are predominantly arriving from the west-southwest. This is expected to increase the influence of sources upwind of WGC, namely the urban core of San Francisco Bay Area and Rio Vista gas fields. The proportion of $CH_4$ apportioned to the 'urban and oil/gas' source is less in the later seasons when winds are more multi-directional (Figure 4.9 c). A minor contribution to the $CH_4$ enhancements (5 - 15 %) is also observed from the 'ag soil and delta' source factor with a relatively high uncertainty of 58 % in the mean $CH_4$ mass fraction attributed to this source factor. Temperatures during this season are fairly warm and the emissions of $CH_4$ from wetlands / peatlands (and possibly rice agriculture) can certainly contribute to the $CH_4$ observed in this factor. As is seen later in the PMF plots for seasons where $N_2O$ is included in the analysis (e.g. 4.6 d), this source is a significant contributor to $N_2O$ enhancements. Most of the monoterpenes are essentially biogenic in nature (Bouvier-Brown et al., 2009) and are attributed to this factor. Monoterpenes have been reported to be emitted in significant quantities during the harvesting season (Ruuskanen et al., 2011; Graus et al., 2013) and this confirms the agriculture origin of this source. We distinguish this factor from the 'primary biogenics and secondary organics' source by including the PMF-based source-wise diurnal distribution of methanol (in Figure 4.9 b). This

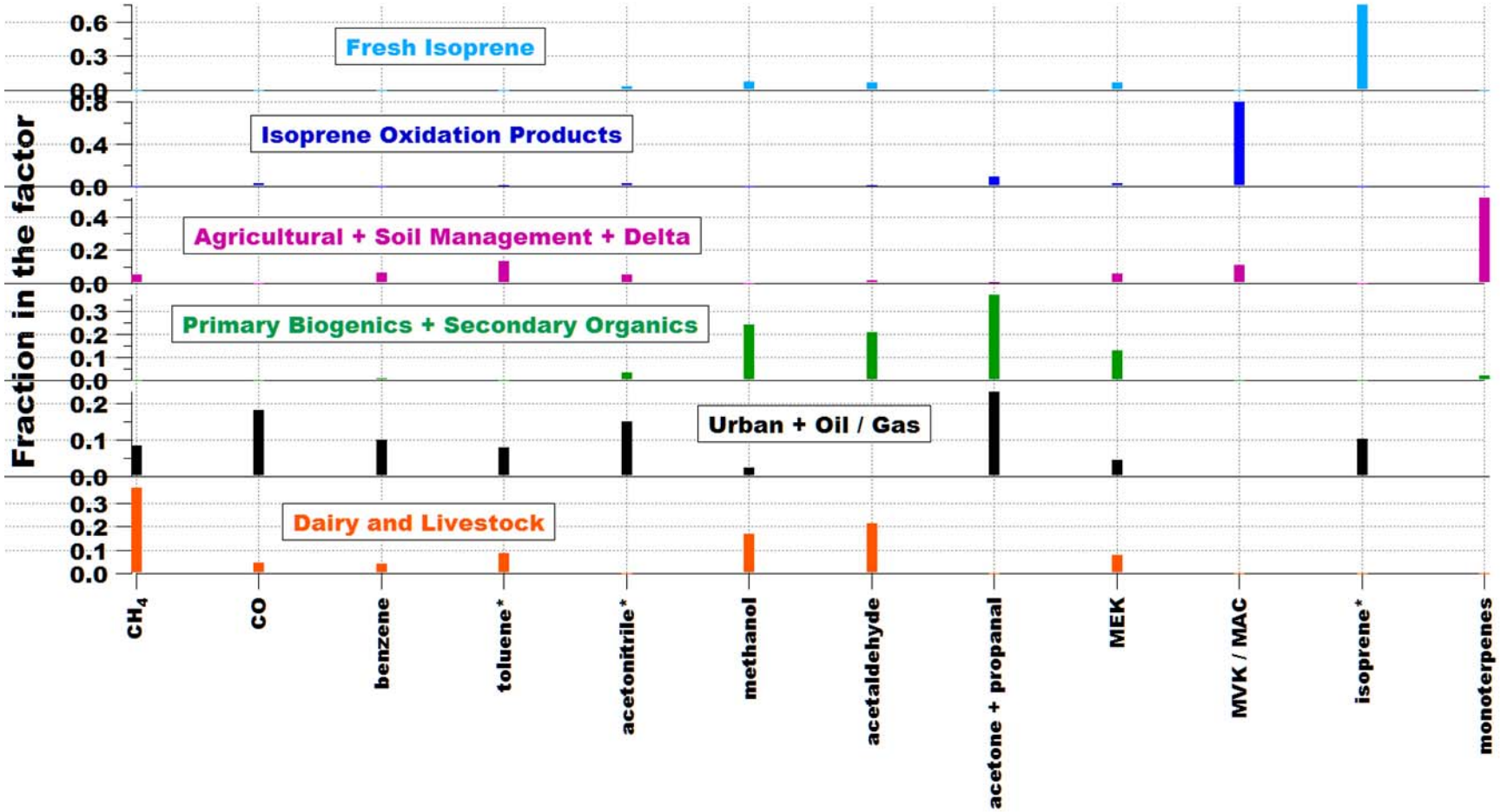


**Figure 4.4.** Factor profiles of resolved PMF source factors denoting major source categories influencing the chemical composition of each profile during early fall of 2012 (Sep 1 – Oct 16). The sum of the scaled mass fractions of all species adds up to unity for each profile. The VOCs with an asterisk sign may have minor contributions from other VOCs detected at the same *m/z* depending on the season (see text).

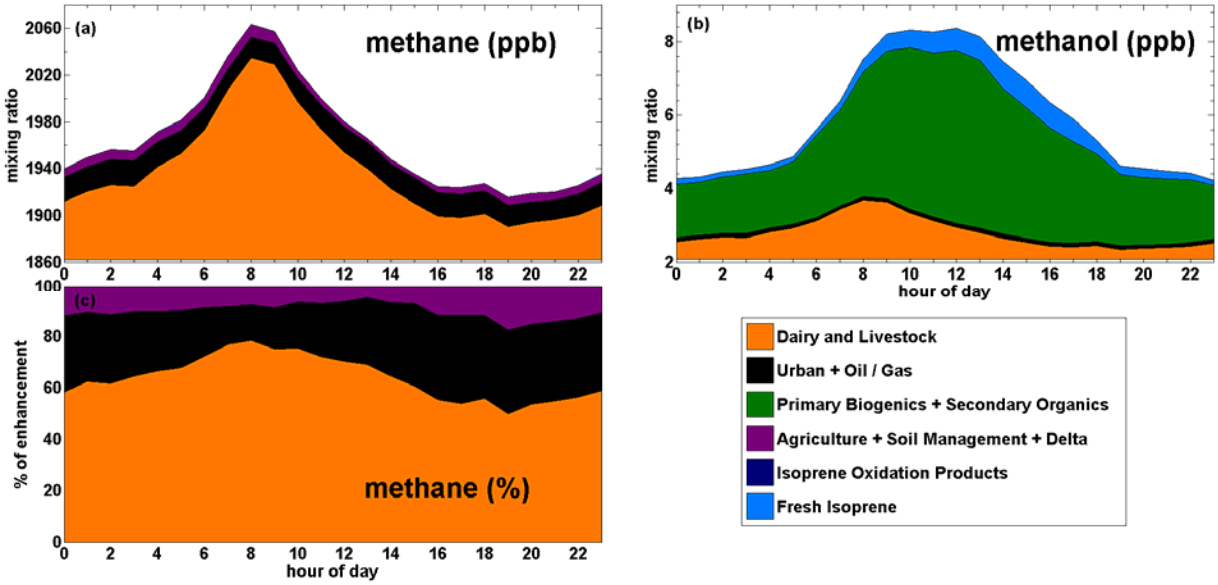


**Figure 4.5.** Mean diurnal distribution plots apportioned by PMF generated source factors for early Fall 2012 period (Sep 1 – Oct 16). The plots include (a) source-wise distribution of methane enhancements above seasonal minimum, (b) source-wise distribution of methanol enhancements, and (c) source-wise distribution of methane enhancements by percentage. The legend represents the factor source categories of the 6-factor PMF solution for early Fall 2012.

figure shows that the majority of emissions for methanol and oxygenated VOCs, which mostly apportion to this source, peak during day time. This is in contrast with the 'ag + soil + delta' diurnal profile (also shown in Figures 4.15 c-d) even though these sources are probably collocated. The multi-source apportionment of methanol in Figure 4.9 b shows that PMF can distinguish between different sources having varied influence on the measured signal depending on factors like timing of active source mechanisms, advection, meteorology etc.

In summary, three sources of $CH_4$ are identified in the fall 2012 PMF sampling period with 'dairies and livestock' as the dominant source, followed by the 'urban and oil / gas' source and a minor contribution from the 'ag + soil management + delta' source.

***Late Fall 2012 (Oct 16 – Nov 30)***

The apportionment of the latter half of the fall 2012 season can be best explained by a 4-factor solution (Figure 4.6). As compared to the period preceding it (early fall 2012), temperatures drop significantly (Table 3.1) and hence the isoprene emissions decrease substantially to the extent that a separate source factor containing fresh isoprene emissions is not reproduced in the PMF analysis for this period. Consequently, there is no 'isoprene oxidation products' factor either in the solution. During this period, $N_2O$ was also measured at WGC. $CH_4$ is apportioned to two factors: the 'dairy and livestock' source which accounts for ~ 65 - 80% of the daily variation with the uncertainty from the bootstrapping analysis being about 9 % of the mean $CH_4$ mass fraction for this source factor; and the 'urban and oil/gas' source which accounts for ~ 20 - 35 % of the observed enhancements (Figures 4.7 a and c) with 17 % uncertainty in the mean $CH_4$ mass fraction for this source factor. As opposed to early fall, there is no contribution to $CH_4$ enhancements from the 'ag soil and delta' source factor. This is most likely due to cooler temperatures during this period (Table 3.1) as average highs drop by about 8°C as compared to early fall season thus reducing production of $CH_4$ from wetland and drained agricultural systems in the Delta (Baldocchi et al., 2012; Hatala et al., 2012; Knox et al., 2014). Dairy and livestock operations, on the other hand, are a year round activity and even though $CH_4$ emissions from manure management may be reduced during this relatively cooler period, the overall $CH_4$ enhancements resulting from this sector remain high and the dominant contributor to the $CH_4$ apportionment in the absence of other competing sources. Winds are more variable in this period (Figures 3.2 c and 3.3 c) and the contributions from local sources may be more important. This suggests that the 'urban and oil / gas' factor may contain significant contributions from the nearby Rio Vista gas field.

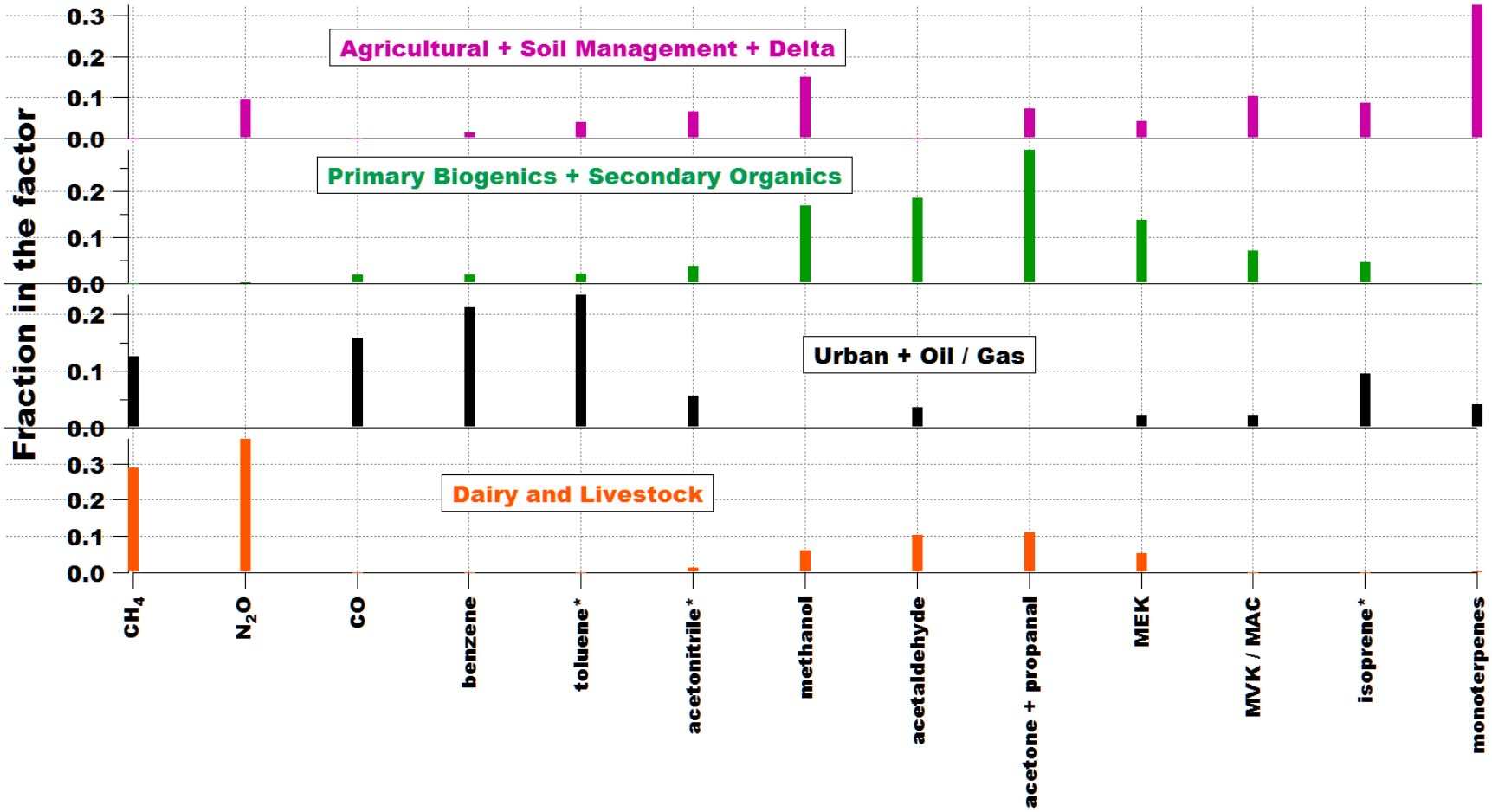


**Figure 4.6.** Factor profiles of resolved PMF source factors denoting major source categories influencing the chemical composition of each profile during late fall of 2012 (Oct 17 – Nov 30). The sum of the scaled mass fractions of all species adds up to unity for each profile. The VOCs with an asterisk sign may have minor contributions from other VOCs detected at the same *m/z* depending on the season (see text).

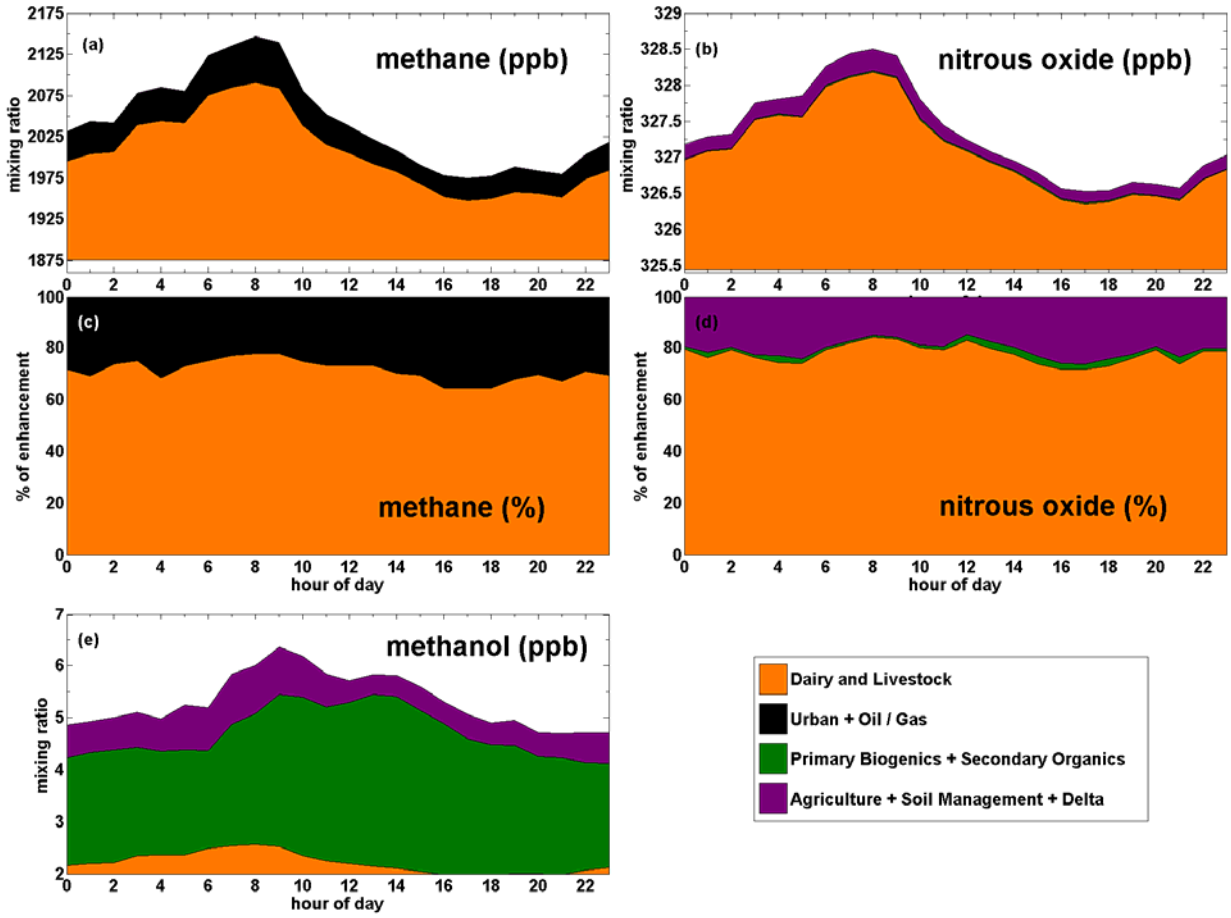


**Figure 4.7.** Mean diurnal distribution plots apportioned by PMF generated source factors for late Fall 2012 period (Oct 17 – Nov 30). The plots include source-wise distribution of methane enhancements (a) in ppb above seasonal minimum and (c) by percentage; source-wise distribution of nitrous oxide enhancements (b) in ppb above seasonal minimum and (d) by percentage, and (e) source-wise distribution of methanol enhancements above seasonal minima. The legend represents the factor source categories of the 4-factor PMF solution for late Fall 2012.

For $N_2O$, we observe that the 'dairy and livestock' sector is the largest contributor to $N_2O$ emissions accounting for ~ 80 % of the total daily enhancements (Figures 4.7 b and d) with less than 7 % uncertainty in the mean $N_2O$ mass fraction for this source factor in this season. The remaining $N_2O$ (~ 20 %) is mostly attributed to the 'agriculture' source factor, which is also the main source for monoterpene emissions, possibly resulting from the vast harvesting activity during this season. The mean $N_2O$ mass fraction attributed to the 'agriculture' source factor has a large uncertainty of 90 % associated with it in the corresponding bootstrapping analysis. It is

important to recognize that the relative amounts of these two sources will differ regionally, and may not be the same in the northern and southern ends of the Central Valley due to the relative distributions of dairy / livestock / fertilizer use. The $N_2O$ apportionment to the 'dairy and livestock' sector is somewhat higher than the proportion of $N_2O$ attributed to the dairy source in Bakersfield (Figure 2.11; Guha et al., 2014). In this case, this is likely due to less fertilizer input as the agricultural season winds down (Oct - Nov) which would significantly decrease the $N_2O$ emissions resulting from and attributed to the agricultural sector, as compared to the relatively unchanging $N_2O$ emissions from manure management in the dairy sector. By that logic, we expect the proportion of $N_2O$ to be higher during the growing season and we visit this hypothesis in the later sections.

***Winter / Wet season (Dec 1, 2012 – Jan 29, 2013)***

During the winter season, a 3-factor PMF solution (Figure 4.8) is most suitable to describe the apportionment of $CH_4$ and $N_2O$ (Figures 4.9 a-d). In the winters, there is substantially less active agriculture in the region as most of the crops have been harvested in the fall. This means that fertilizer use and subsequent $N_2O$ emissions from crop agriculture should be negligible. Additionally, low temperatures in the inland Central Valley (Table 3.1) means that microbially mediated $CH_4$ emissions from wetlands and peatland pastures should be low too and possibly below the level of detection within the framework of input uncertainties. This hypothesis is validated in the PMF solution as it does not reproduce the 'agriculture + soil management + delta' source factor from the previous period. The $CH_4$ enhancements (Figures 4.9 a and c) are predominantly attributed to the 'dairy and livestock' source which accounts for ~ 90 % of the enhancements with a bootstrapping uncertainty of only 7 % in the mean $CH_4$ mass fraction. The remaining 10 % of the emissions come from the 'urban and oil / gas' source with a

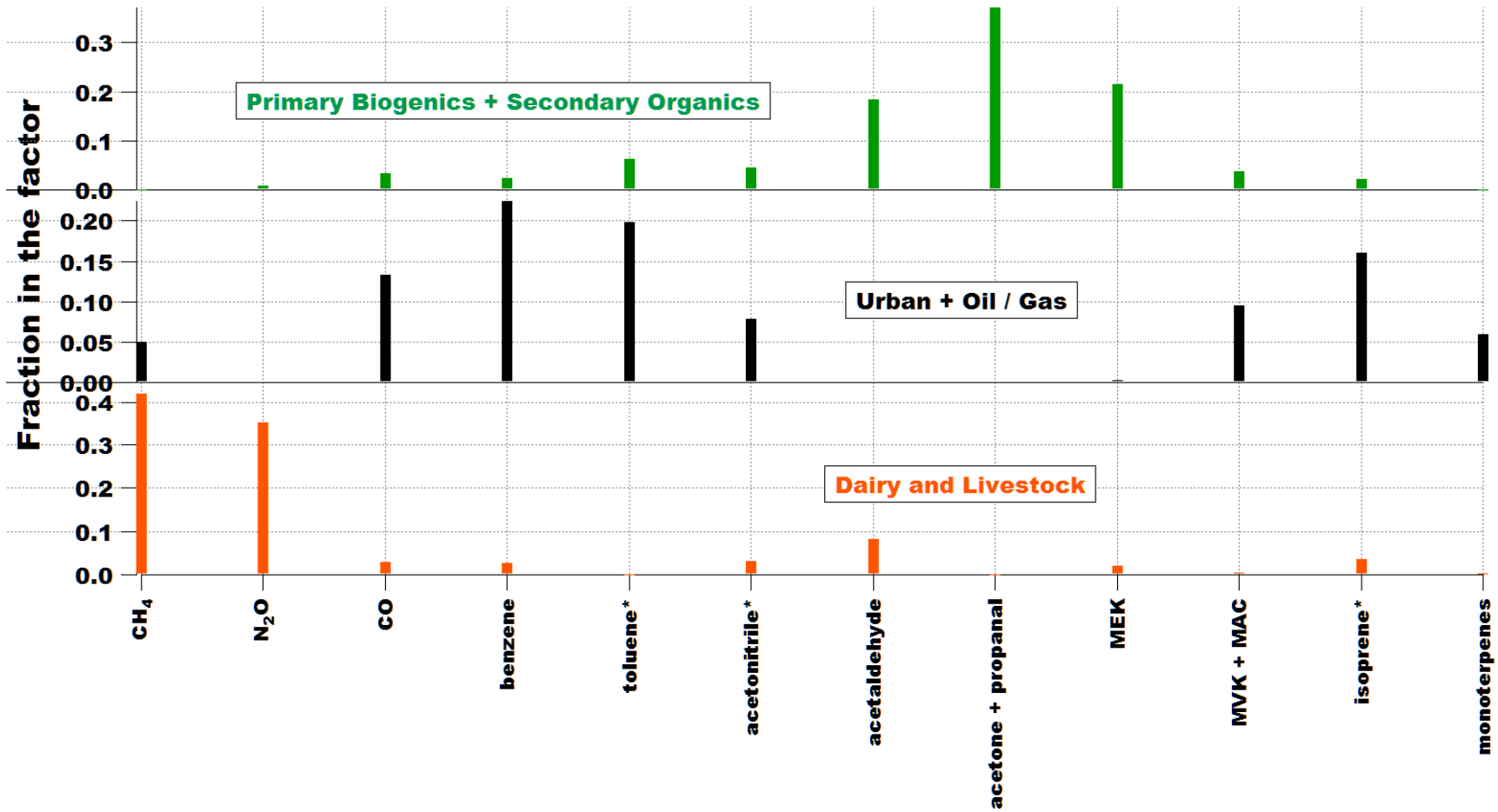


**Figure 4.8.** Factor profiles of resolved PMF source factors denoting major source categories influencing the chemical composition of each profile during winter / wet season (Dec 1 – Jan 29). The sum of the scaled mass fractions of all species adds up to unity for each profile. The VOCs with an asterisk sign may have minor contributions from other VOCs detected at the same *m/z* depending on the season (see text).

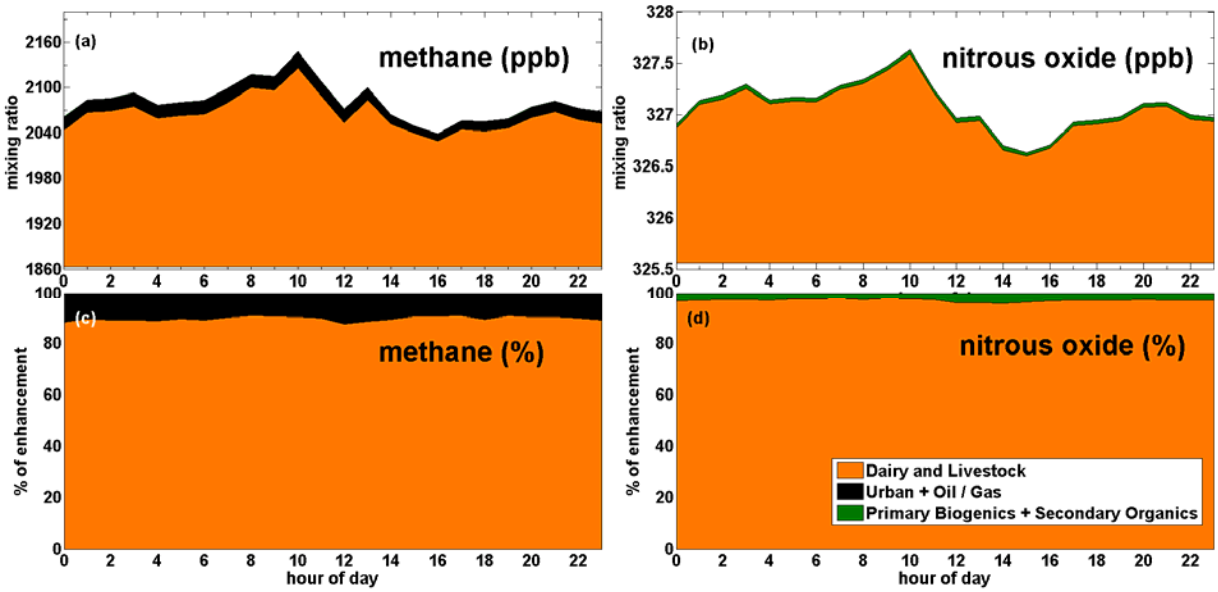


**Figure 4.9.** Mean diurnal distribution plots apportioned by PMF generated source factors for winter (wet season) period (Dec 1 – Jan 29). The plots include source-wise distribution of methane enhancements (a) in ppb above seasonal minimum and (c) by percentage; source-wise distribution of nitrous oxide enhancements (b) in ppb above seasonal minimum and (d) by percentage. The legend represents the factor source categories of the 3-factor PMF solution for this season.

relatively high uncertainty of 45 % in the mean $CH_4$ mass fraction used to compute the contribution of this sector. This is a reasonable outcome as the dominant wind direction during the winters is along the floor of the Central Valley (northwest and southeast) as seen in Figures 3.2 d and 3.3 d. The prevailing winds causes the densely concentrated dairy and feedlot complex in the San Joaquin County (to the southeast of the site) to become directly upwind of the site for majority of this period. The above-mentioned reason coupled with reduced or almost absent contributions from agriculture related $N_2O$ emissions causes the observed $N_2O$ enhancements to be almost exclusively attributed to the dairy and livestock sector (Figures 4.9 b and d). A very tiny (< 5 %) of the emissions are attributed to the 'biogenics' factor and this may be related to precipitation-driven $N_2O$ release from left-over soil N on fallow crop lands in the post-harvesting

period or a small amount of ongoing regional agricultural activity, although this contribution is well-within the bounds of uncertainties ascribed to the $N_2O$ data.

***Late Winter / early Spring season 2013 (Feb 15 – Apr 5)***

The source apportionment during late winter and early spring period is best described by a 4-factor PMF solution for this period (Figure 4.10) which resembles a similar factor solution observed during the late fall period (Figure 4.6) with the exception that $N_2O$ was missing from the input data set during this period. The diurnal plots of the scaled factor mass distribution (Figures 4.11 a-d) give a glimpse into the differences in the diurnal patterns which PMF analysis is able to suitably resolve. We observe that even though the 'dairy and livestock', 'urban and oil / gas' and the 'agriculture and delta-related' sources have early morning peaks in concentrations followed by daytime lows (Figure 4.11 a, b and d, respectively), there are finer differences in their diurnal profiles (like timing of peaks and lows), which allow the PMF tool to analyze and resolve these non-covarying features in the time series, and apportion combinations of tracers with similar features into distinct factors. Also, the 'primary biogenics and secondary organics' source has peak concentrations during the early afternoon period coincident with periods of highest temperature and sunlight received (Figure 4.11 c) and this reaffirms our understanding of the biogenic origin of this source factor.

The bulk of the $CH_4$ (~ 60 - 70 %) enhancements are attributed to the 'dairy and livestock' source with less than 10 % uncertainty in the $CH_4$ mass fraction apportioned to this source. Smaller contributions are observed from the 'urban and oil / gas' source (~ 20 %; standard deviation of 78 % in the average $CH_4$ mass fraction) and the 'ag soil management + delta' source (15 - 25 %; standard deviation of 40 % in the average $CH_4$ mass fraction) in Figures

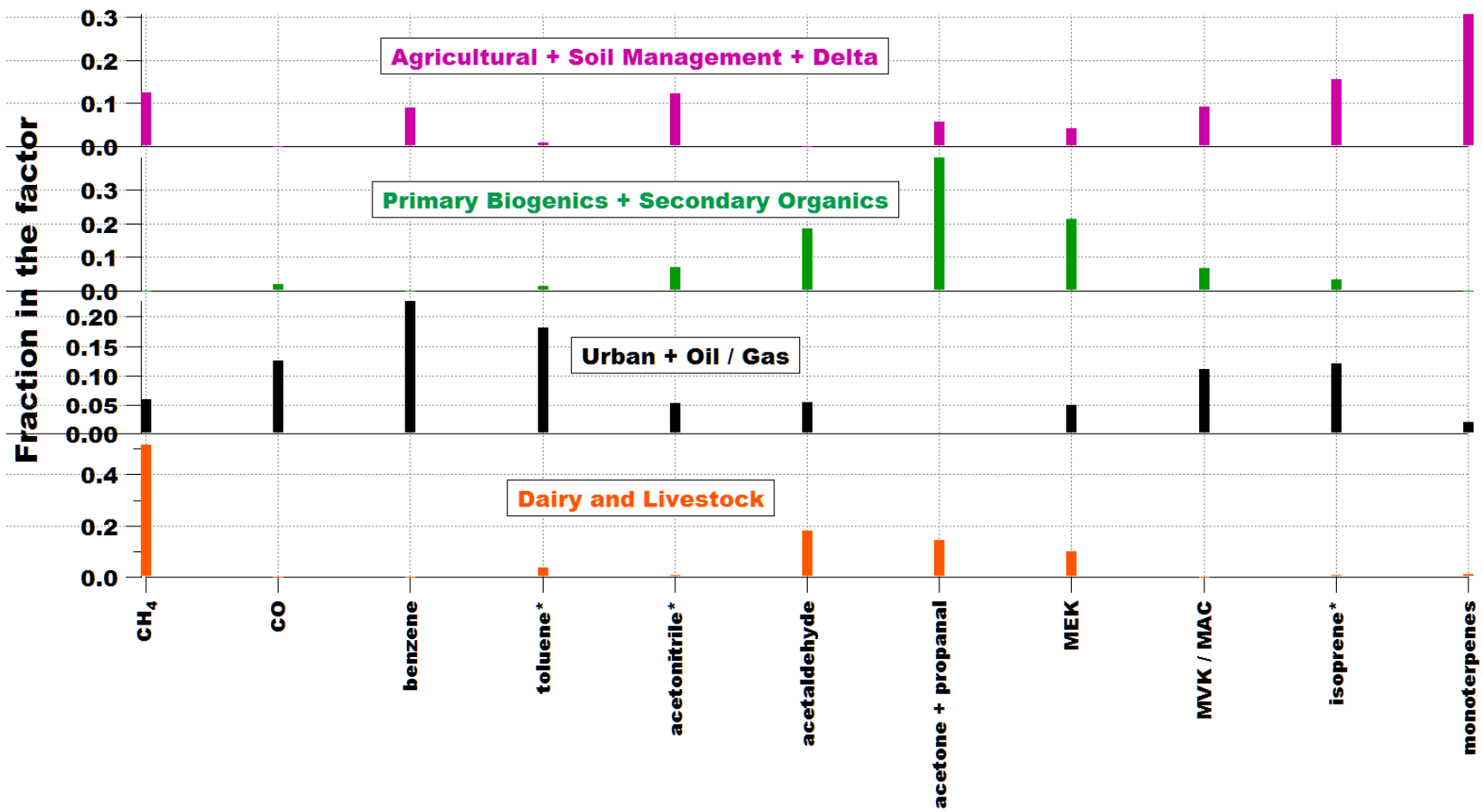


**Figure 4.10.** Factor profiles of resolved PMF source factors denoting major source categories influencing the chemical composition of each profile during winter / early spring of 2013 (Feb 16 – Apr 4). The sum of the scaled mass fractions of all species adds up to unity for each profile. The VOCs with an asterisk sign may have minor contributions from other VOCs detected at the same *m/z* depending on the season (see text).

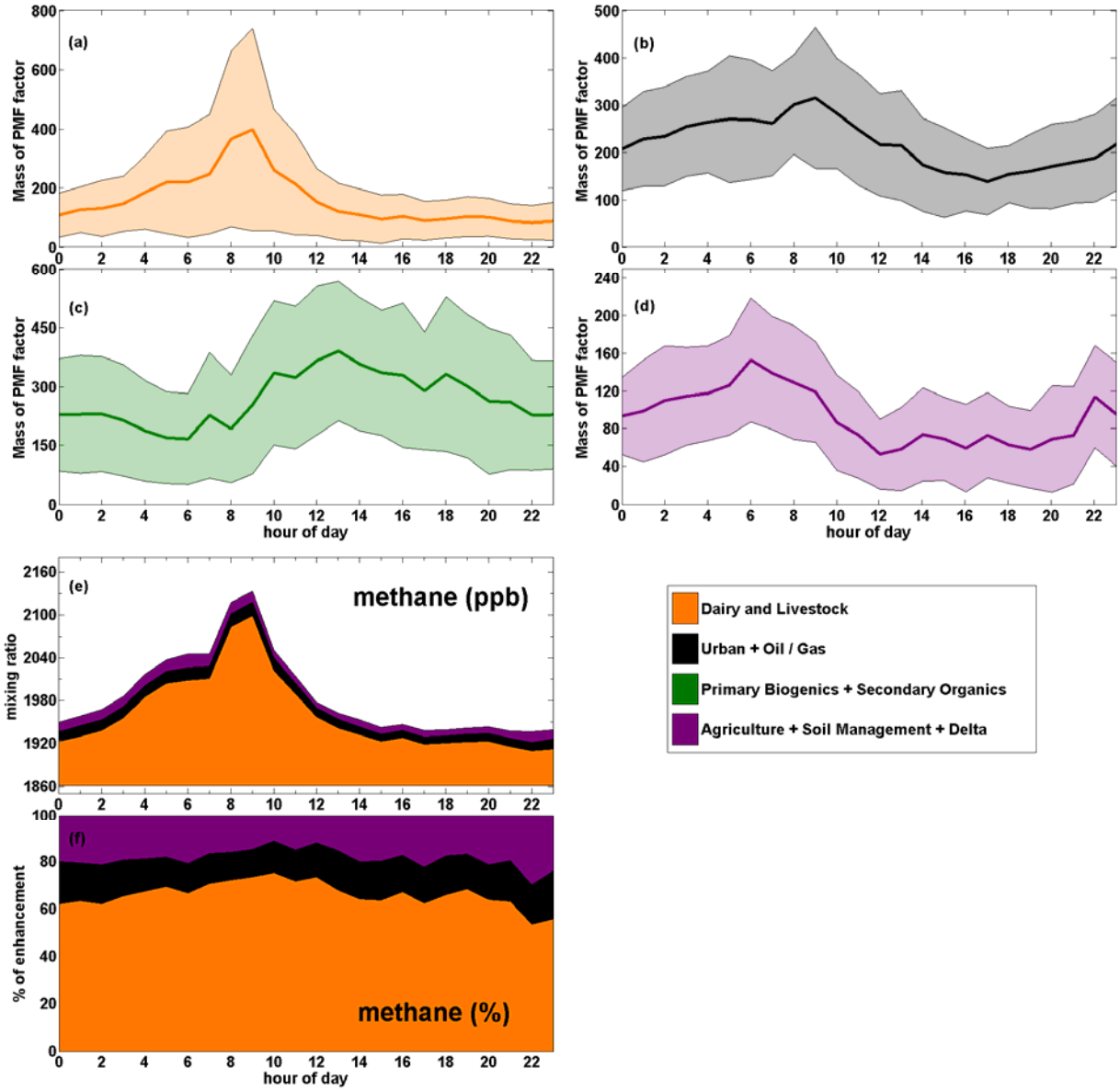


**Figure 4.11.** Mean diurnal distribution plots apportioned by PMF generated source factors for the late winter / early spring season (Feb 16 – Apr 4). The plots include mass distribution of (a) scaled 'dairy and livestock' factor concentrations, (b) scaled 'urban + oil / gas' factor concentrations, (c) scaled 'primary biogenics and secondary organics' factor concentrations, and (d) scaled 'agriculture + soil management + delta' factor concentrations. The solid colored line represents the average concentration for that hour of day while the semi-transparent shaded region represents the 1σ standard deviation. The remaining plots show source-wise distribution of methane enhancements (e) in ppb above seasonal minimum and (c) by percentage of enhancement. The legend represents the source categories of the 4-factor PMF solution.

4.11 e-f. Higher daily temperatures during this period compared to the immediately preceding winter period (Table 3.1) results in an increase in anaerobic activity of microbes in the Delta

wetlands (Miller, 2011). It should be noted that the % contribution from the 'ag + delta' source to the $CH_4$ apportionment (Figure 4.11 e) is somewhat larger than that observed from the same source in early fall 2012 (4.5 c). This cannot be reasonably explained on the basis of average ambient temperatures as temperatures in this period are cooler than that observed in early fall 2012 (Table 3.1). Drainage of agricultural fields (including rice paddy) in preparation for new plantings has been reported to be responsible for large releases of $CH_4$ (Hatala et al., 2012; Knox et al., 2014). In this season, the dominant day time wind direction is from the northwest (Figure 3.2 e) where 90% of California's rice crop is grown in the upwind Sacramento Valley This is the season when large amounts of flooded rice paddy fields with huge amounts of plant residue are drained before seeds of the new crop are sown, and this could be responsible for the $CH_4$ seen in this 'ag + delta' source factor. Drainage of water-logged fields (from the rainy season) containing agricultural residues in the Delta, in preparation for the growing season can also lead to $CH_4$ emissions that apportion to this source.

***Spring 2013 (Apr 6 – May 31)***

The PMF analysis during the spring season results in a 5-factor solution with an additional factor related to 'isoprene and oxidation products' being produced in this seasonal period (Figure 4.12) as compared to the winter / spring 2013 period (Figure 4.10). This is primarily due to significantly warmer temperatures in this period along with greater sunlight input which increases isoprene emissions from vegetation surrounding WGC. Isoprene and its oxidation products, apportion into their own factor owing to a sharp diurnal cycle resulting from their different source distribution as compared to other oxygenated VOCs.

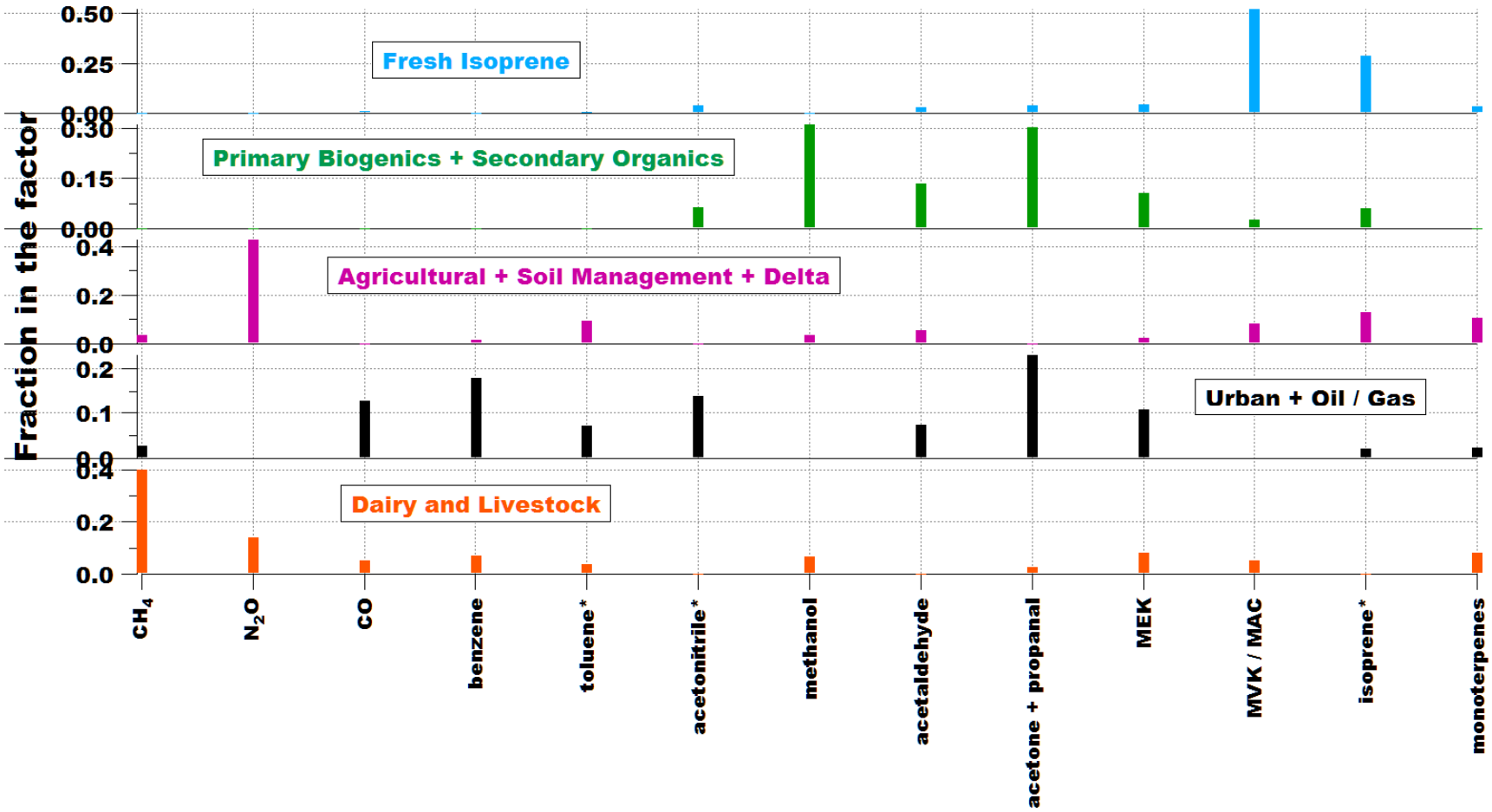


**Figure 4.12.** Factor profiles of resolved PMF source factors denoting major source categories influencing the chemical composition of each profile during spring of 2013 (Apr 6 – May 31). The sum of the scaled mass fractions of all species adds up to unity for each profile. The VOCs with an asterisk sign may have minor contributions from other VOCs detected at the same *m/z* depending on the season (see text).

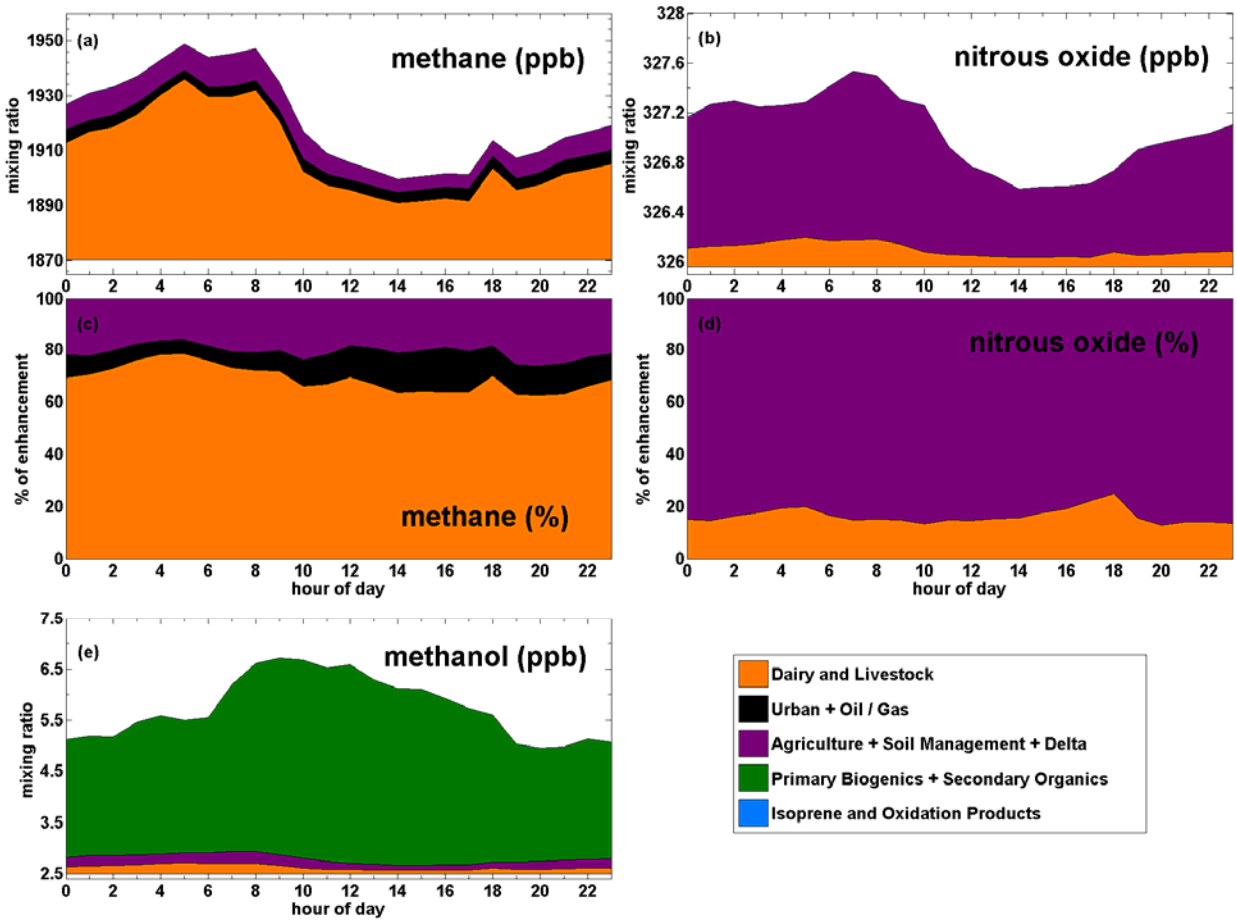


**Figure 4.13.** Mean diurnal distribution plots apportioned by PMF generated source factors for spring 2013 period (Apr 6 - May 31). The plots include source-wise distribution of methane enhancements (a) in ppb above seasonal minimum and (c) by percentage; source-wise distribution of nitrous oxide enhancements (b) in ppb above seasonal minimum and (d) by percentage, and (e) source-wise distribution of methanol enhancements above seasonal minima. The legend represents the factor source categories of the 5-factor PMF solution for spring 2013 season.

The majority of the $CH_4$ signals, ~ 70 %, are apportioned to the 'dairy and livestock' factor (Figure 4.13 c) with an uncertainty of 14 % in estimating the $CH_4$ mass fraction belonging to this source factor. About 10 to 15 % of the $CH_4$ enhancements are apportioned to the 'urban and oil / gas' source factor with an uncertainty of 63 % in the factor $CH_4$ mass fraction. Contributions from the 'ag + soil management + delta' source factor to the $CH_4$ enhancements remain relatively high at 20 – 25 % (standard deviation of 36 % about the mean $CH_4$ mass fraction) and this conforms with increasing $CH_4$ emissions from wetland ecosystems in Delta

(Figure 6; Knox et al., 2014). The $CH_4$ fluxes observed from these wetland ecosystems during the spring and summer season (Knox et al., 2014) are on the same scale as that reported from the airborne flux measurements over the dairy intensive regions in the Central Valley in the CABERNET study (Table 3.2; Guha et al., 2014). This indicates there are significant natural and anthropogenic (managed lands) sources of $CH_4$ in the Delta with predominantly microbially-mediated emission pathways that are more active in warmer temperature regimes with saturated soil conditions. As also indicated by the wind rose plots (Figure 3.2 f and 3.3 f), there is a marked change in mesoscale meteorology in this season as the up and down valley flow pattern gives way to land-sea breezes and the prevailing wind direction is more westerly (Zhong et al., 2004; Bao et al., 2007). This should increase the influence of the 'urban and oil / gas' factor on the $CH_4$ signals given their upwind location. We do not, however, observe any increase in the $CH_4$ apportionment to this factor, possibly due to simultaneous and larger input from $CH_4$ emissions occurring in the Delta ecosystem which masks the influence of the 'urban + oil/gas' source on $CH_4$ apportionment.

There is a significant difference in $N_2O$ source apportionment in the spring season (Figures. 4.13 b and d) as compared to the late fall (Figures. 4.7 b and d) and winter season (Figures 4.9 b and d). In this season, the 'agriculture + soil management + Delta' source factor is the overwhelming contributor to the $N_2O$ enhancements (~ 80 %) with only ±10 % uncertainty in estimating the mean $N_2O$ mass fraction (in Figure 4.12) using the bootstrapping method. The 'dairy and livestock' sector accounts for the remaining 20 % emissions. This is in sharp contrast with the apportionment in the above-mentioned seasons when the 'dairy and livestock' sector was the dominant source of $N_2O$ emissions. Manure management practices that are the principal source of $N_2O$ from dairies are not expected to widely vary over the annual cycle. Additionally,

$CH_4$ emissions from dairies are relatively unchanged over the course of the year and this indicates that dairies and feedlots generally operate in the same manner through the annual cycle. Hence, the higher proportion of $N_2O$ enhancements from the 'ag + soil management' factor can be attributed to a tremendous increase in emissions from this sector. Most of the inorganic / organic fertilizer and animal manure application to the farms take place early in the growing season that can range from Mar -Apr (for rice) to May-Jun (for corn and other crops). Hence major $N_2O$ emissions can be expected in these months as the fields are flooded and irrigated which acts as a trigger for subsequent denitrification and $N_2O$ emissions (Rosenstock et al., 2013). Thus, we note that $N_2O$ emissions from the 'ag + soil management' sector show a strong pattern of seasonality with much higher contribution to the apportionment of the measured signals during the spring (and as we see later, in the summer season) as opposed to the end of the growing season (in late fall) or winter when application of N fertilizer for agriculture is at its minimum in California.

Figure 4.13 e indicates that most of the methanol emissions in the spring season arise from 'biogenic and secondary' sources far outweighing the contribution from the 'dairy and livestock' sector. This is consistent with literature on biogenic methanol emissions which point to springtime pectin biosynthesis during plant and leaf growth as a principal methanol source (Galbally and Kirstine, 2002; Karl, 2003; Schade and Goldstein, 2006). The exponential variance of methanol emissions with temperature (Harley et al., 2007) during the spring and summer months seen in this work agree well with the trends observed in a similar year-round tall-tower measurement at a semi-rural site (Hu et al., 2011) and previous studies in California (Schade and Goldstein, 2006). The lack of $CH_4$, in this source factor, though not surprising, is a confirmation that there are major plant biogenic sources of methanol that do not contribute any methane.

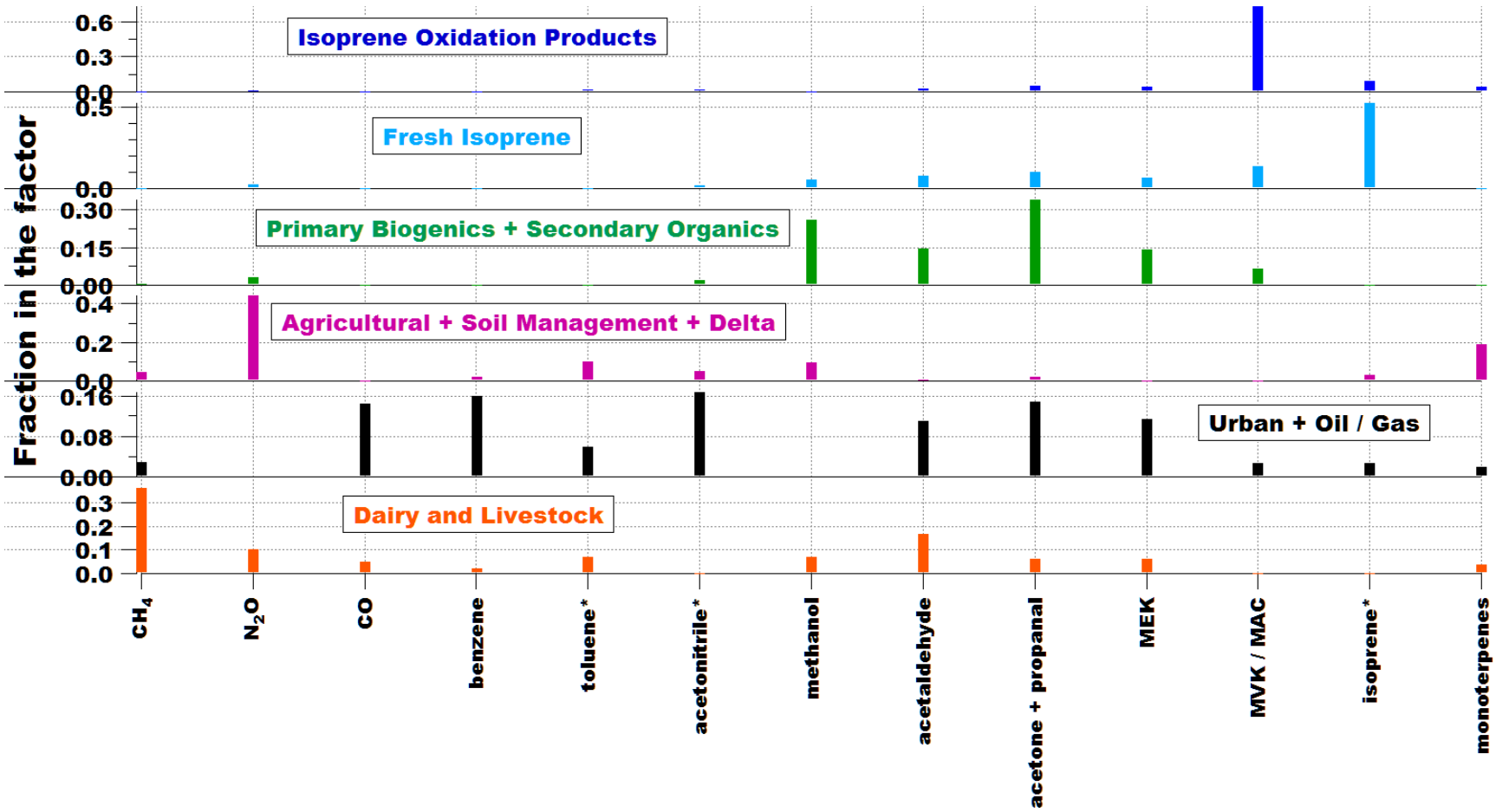


**Figure 4.14.** Factor profiles of resolved PMF source factors denoting major source categories influencing the chemical composition of each profile during summer of 2013 (Jun 1 – Aug 4). The sum of the scaled mass fractions of all species adds up to unity for each profile. The VOCs with an asterisk sign may have minor contributions from other VOCs detected at the same *m/z* depending on the season (see text).

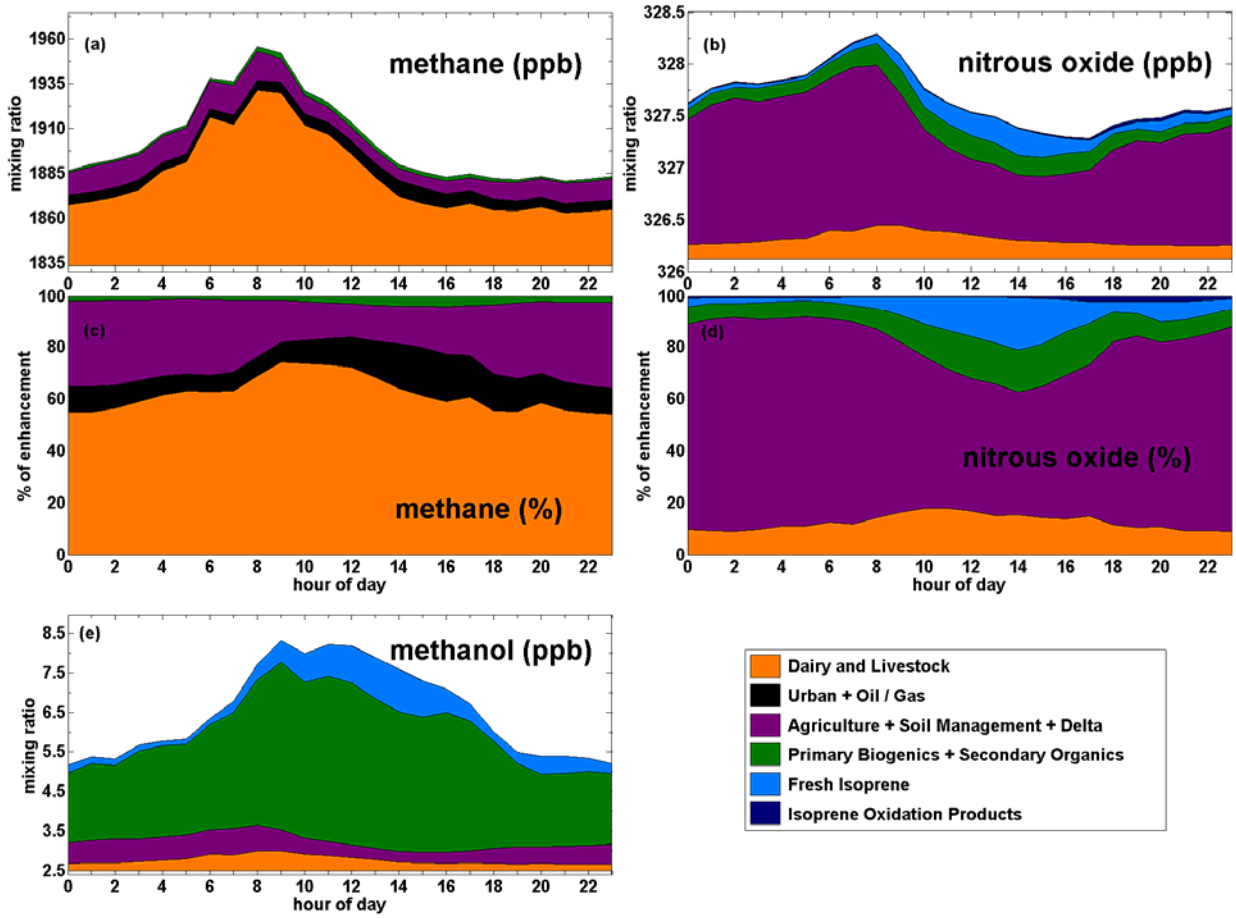


**Figure 4. 15.** Mean diurnal distribution plots apportioned by PMF generated source factors for summer 2013 period (Jun 1 – Aug 4). The plots include source-wise distribution of methane enhancements (a) in ppb above seasonal minimum and (c) by percentage; source-wise distribution of nitrous oxide enhancements (b) in ppb above seasonal minimum and (d) by percentage, and (e) source-wise distribution of methanol enhancements above seasonal minima. The legend represents the factor source categories of the 6-factor PMF solution for summer 2013.

### *Summer 2013 (Jun 1 – Aug 4)*

The factor profiles in the 6-factor PMF solution for the summer 2013 season are represented in Figure 4.14. The 'dairy and livestock', 'urban and oil / gas', and 'agriculture + soil management + delta' source factors look similar in composition to the same factors from the preceding spring analysis (Figure 4.12). In terms of source apportionment, a majority of $CH_4$ emissions are still apportioned to the 'dairy' factor (~ 55 – 70 %; 10% uncertainty in

the averaged $CH_4$ mas fraction ) even though its relative share is reduced. The delta-related $CH_4$ emissions are responsible for about 20 - 40 % of the observed enhancements (Figure 4.15 c) which is the maximum amongst all the PMF sampling periods for this source. The uncertainty in the mean $CH_4$ mass fraction for the delta source is +/- 11 %. The relatively high contribution of this source to the PMF apportionment can be partly due to wind directions as winds are primarily westerly and south-westerly during the summer season (Figures 3.2 g and 3.3 g) and this makes WGC directly downwind of the Delta region. The core reason is most probably increased $CH_4$ emissions from wetlands, peatlands and rice cultivation in the upwind Delta. The contributions from wetland and flooded agricultural systems scale with temperature and hence peak during the summers (Hatala et al., 2012; Knox et al., 2014). We observe that the source contribution of the 'ag + soil + delta' factor to the apportionment of $CH_4$ signals peaks during this season and then decreases in the early fall season as ambient temperatures drop (Figure 4.5 c) before reducing to undetectable proportions in the late fall (Figure 4.7 c) and winter season (Figure 4.9 c). Contributions from urban and oil / gas sources remain about 10 %.

The bulk of the $N_2O$ signal is apportioned to the 'agriculture-related' source factor (Figures 4.15 b and d). In this analysis, we observe the 'splitting of factors' phenomena explained in Section 2.2.6 in Guha et al. (2014). A portion of the $N_2O$ enhancements gets apportioned to the 'biogenics' and the 'isoprene' factors. A 'splitting' phenomena is likely to be observed in high-factor solutions with fewer degrees of freedom (total included species in the data set) when contributions from collocated sources may get apportioned between them. It should be noted that both the 'biogenics' and the 'isoprene' factor are originating from natural plants and non-woody and woody crops being grown on agricultural farmlands in the Delta in the vicinity of WGC. These farm lands are the major source of soil emissions of $N_2O$ being

apportioned to the 'ag soil management + delta' factor. Hence the total contribution of the agriculture-related $N_2O$ emissions to the observed enhancements should be looked upon as the sum of the contributions of the three above-mentioned factors which amounts to 80 - 90% ( < 6% uncertainty in the 'ag + soil' mean $N_2O$ mass fraction from bootstrapping analysis) with the rest being attributed to the 'dairy and livestock' factor. The current $N_2O$ source apportionment, along with a similar apportionment in the spring season, underlines the importance of fertilizer-related emissions of $N_2O$ from the agricultural sector during the growing season (Apr – Oct). We do not have $N_2O$ measurements during early Fall but in late fall of 2012, we observe that the proportion of agriculture-related $N_2O$ in the total enhancements reduces to 20 % coinciding with decreasing inputs of fertilizers to farm lands as the growing season draws to a close and crops are harvested. As is observed during spring, methanol emissions are dominated by the 'biogenic' factors with a minor contribution from the 'dairy' source (Figure 4.15 e).

***Summer 2012 (Jun 15 – Aug 31)***

The profiles in the 6-factor PMF solution in summer 2012 (Figure 4.16) are similar to those from summer 2013 (Figure 4.14), with the exception that $N_2O$ measurements were not present in the 2012 analysis. $N_2O$ is the dominant constituent of the 'ag + soil + delta' profile, and in its absence, the mass fractions of other tracers in this factor are reasonably larger. The $CH_4$ source apportionment result (Figures 4.17 a and c) from summer 2012 has three contributing sources: the 'dairy and livestock' source, 'ag + soil + delta' source, and the 'urban and oil / gas source' in nearly the same proportions as seen in the summer 2013 analysis.

The chemical composition of the 'urban and oil /gas' source factor, at first glance, does not look similar for the two summer periods as acetonitrile and acetone + propanal fractions in the summer 2012 solution look significantly larger. A deeper investigation leads to an interesting

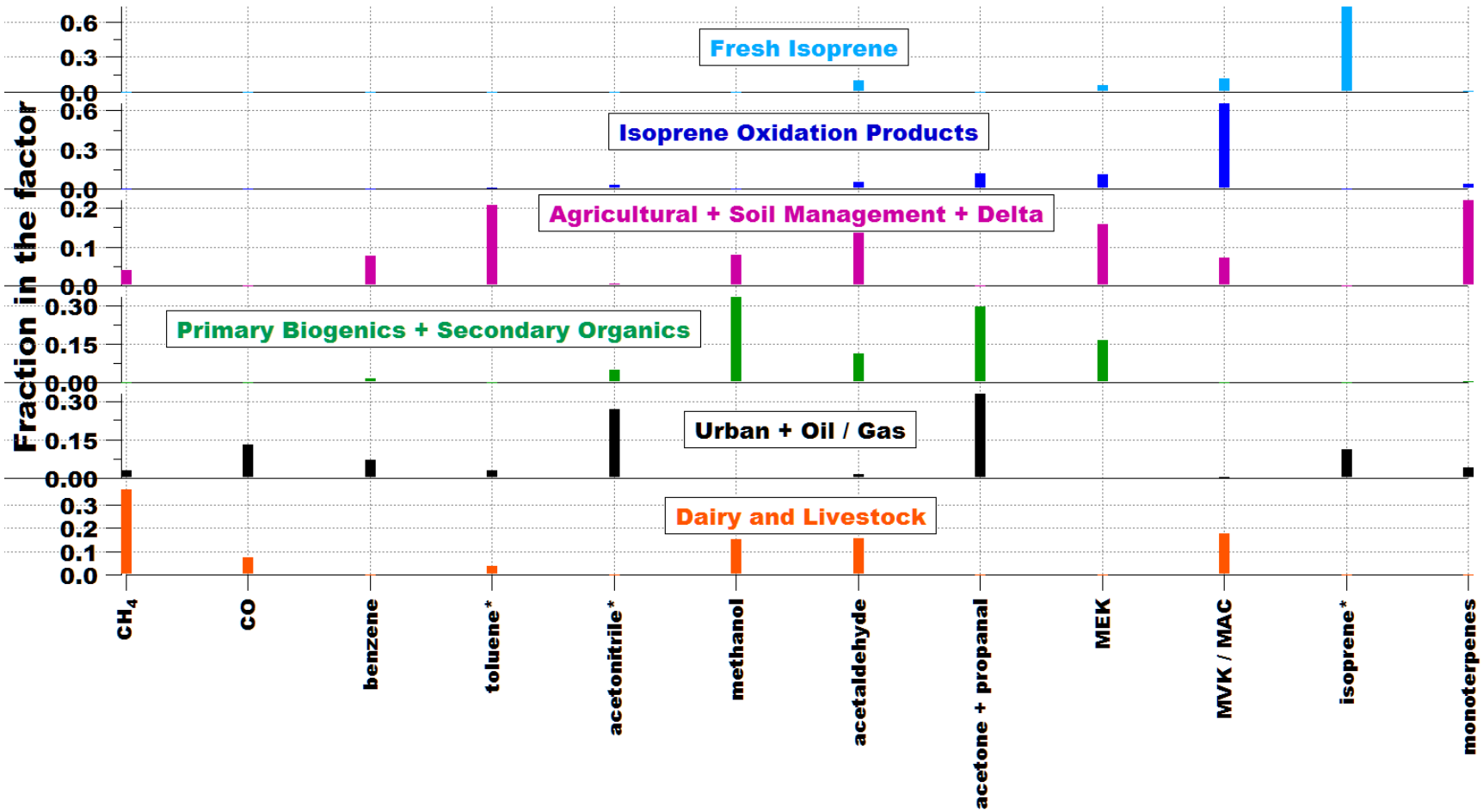


**Figure 4.16.** Factor profiles of resolved PMF source factors denoting major source categories influencing the chemical composition of each profile during summer of 2012 (Jun 16 – Aug 31). The sum of the scaled mass fractions of all species adds up to unity for each profile. The VOCs with an asterisk sign may have minor contributions from other VOCs detected at the same *m/z* depending on the season (see text).

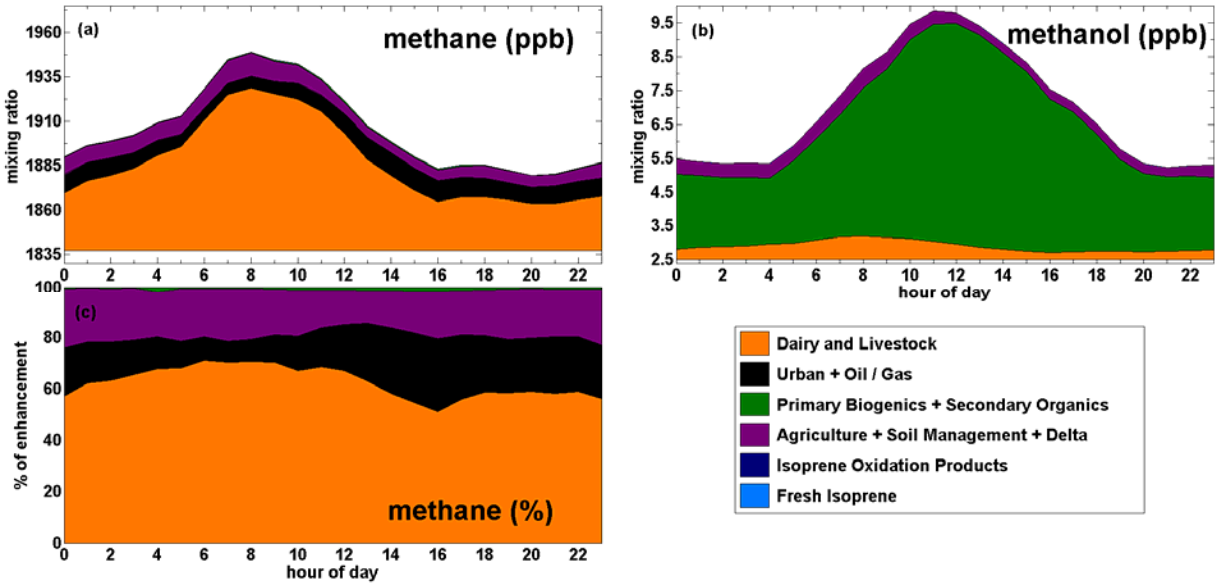


**Figure 4.17.** Mean diurnal distribution plots apportioned by PMF generated source factors for summer 2012 period (Jun 16 – Aug 31). The plots include source-wise distribution of methane enhancements (a) in ppb above seasonal minimum and (c) by percentage and (c) source-wise distribution of methanol enhancements above seasonal minima. The legend represents the factor source categories of the 6-factor PMF solution for summer 2012.

finding. A 7-factor solution (not shown here explicitly) produces an additional factor which is mostly dominated by acetonitrile and acetone (Figure 4.18 a) that was formerly present in the 'urban and oil / gas' factor in the 6-factor solution. This new factor also has minor mass fractions attributed to combustion tracers CO, benzene and a minor amount of $CH_4$. Acetonitrile is a well-known biomass burning tracer (Bange and Williams, 2000; de Gouw, 2003). On analyzing the average vertical diurnal profile of measured acetonitrile in summer 2012, we find that huge concentrations of acetonitrile were present in the upper levels of WGC at all times of the day (Figure 4.18 b), and they were transported down during the day time when vertical mixing is rapid. Significant amounts of acetone were also present in the upper parts of the mixed layer (Figure 4.2 i) and vertical mixing during the day caused this signal to be detected at the 131 m a.g.l level. The source of this acetonitrile and acetone was the large forest fire in northeastern California that occurred in August 2012 known as the Rush Fire. This wildfire at the time was

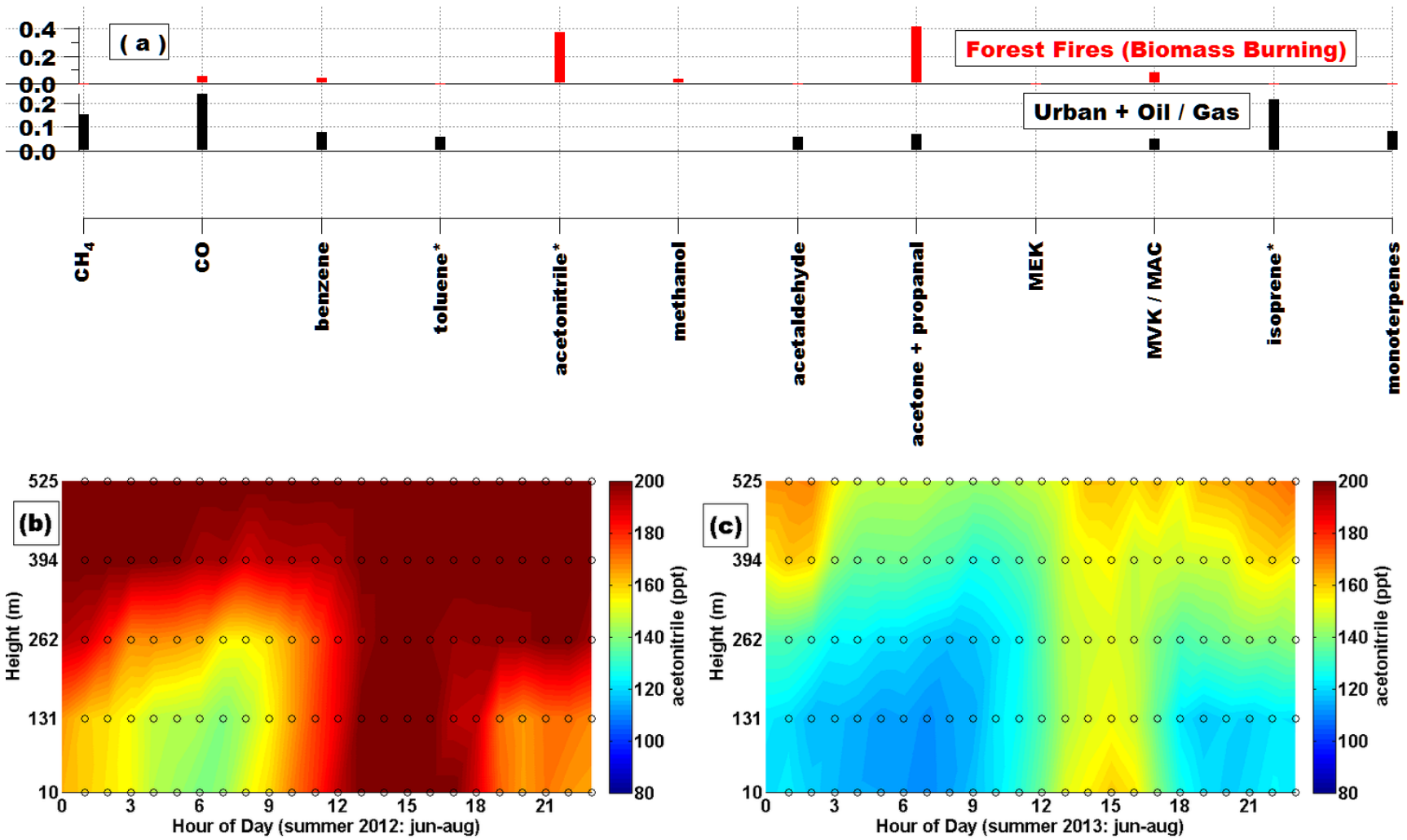


**Figure 4.18.** (a) An additional source factor attributed to forest fires results from splitting of the urban + oil / gas factor in a 7-factor PMF solution during summer of 2012; vertical mean diurnal profile of biomass burning tracer acetonitrile during (b) summer of 2012 and (c) summer of 2013 showing accumulation of large emissions in the upper part of the mixed layer from significantly higher forest fire activity in the Sierra Nevada mountains during this period (Jun – Aug) in 2012 versus 2013. The Rush Fire in northeastern California (second largest wildfire in California recorded history) took place in August 2012.

the second largest in the state's recorded history (since 1932). Since forest fires are associated with intensely hot plumes, the VOCs in the fire emissions plumes are carried aloft above the boundary layer quickly by the rising hot air. These emissions arrive at the 131 m a.g.l measurement level on WGC during the middle of the day when peak vertical mixing occurs. This is also the time of day when emissions contained in 'urban and oil /gas plumes' arrive at the site with the day time westerly sea breeze. This is the reason that the 6-factor solution 'mixes' both these unique source contributions (from two vertically divergent directions) into a single factor. With a total of only 12 apportioned tracers in the whole time series, we observe 'splitting' of other source factors (not shown and as described above and in Chapter 2 of Guha et al., 2014), if we try to use the 7-factor solution as the 'best case' solution. Hence we do not choose the 7-factor solution as our final solution but instead present the 'urban and oil/gas' factor profile and the 'forest fires' factor profile from the 7-factor solution separately (in Figure 4.18 a) to explain the observed chemical profile of the 'urban and oil / gas factor' in the 6-factor solution (Figure 4.16). It should be noted that in summer 2013, acetonitrile concentrations in the upper elevations of the mixed layer were significantly lower in the absence of a large fire like the one in August 2012. The 'infamous' Rim Fire in Yosemite National Park occurred in August 2013 following the conclusion of our summer 2013 PMF analysis and is hence not captured in our analysis. Detection of an acetonitrile-containing 'biomass burning' factor associated with large wildfires is an important finding that confirms the applicability and effectiveness of the PMF method to apportion GHG sources containing unique source tracers. The contribution of $CH_4$ from the forest fires source factor was found to be insignificant compared to other regional sources and well-within the range of ascribed uncertainties.

Tables 1.1 and 1.2 included in Chapter 1 (Executive Summary) summarize the mean percentage source-specific distribution of $CH_4$ and $N_2O$ enhancements over different seasons. The contrast in the PMF apportionment between different seasons and with the inverse modeling approach is discussed in more detail in Chapter 6.

## 4.3. References


Andreae, M. O. and Merlet, P.: Emission of trace gases and aerosols from biomass burning, Global Biogeochem. Cycles, 15(4), 955–966, doi:10.1029/2000GB001382, 2001.

Baker, B., Guenther, A., Greenberg, J. and Fall, R.: Canopy level fluxes of 2-methyl-3-buten-2-ol, acetone, and methanol by a portable relaxed eddy accumulation system, Environ. Sci. Technol., 35(9), 1701–1708, 2001.

Baldocchi, D., Detto, M., Sonnentag, O., Verfaillie, J., Teh, Y. A., Silver, W. and Kelly, N. M.: The challenges of measuring methane fluxes and concentrations over a peatland pasture, Agric. For. Meteorol., 153, 177–187, doi:10.1016/j.agrformet.2011.04.013, 2012.

Bange, H. W. and Williams, J.: New Directions: Acetonitrile in atmospheric and biogeochemical cycles, Atmos. Environ., 34(28), 4959–4960, doi:10.1016/S1352-2310(00)00364-2, 2000.

Bao, J.-W., Michelson, S. a., Persson, P. O. G., Djalalova, I. V. and Wilczak, J. M.: Observed and WRF-Simulated Low-Level Winds in a High-Ozone Episode during the Central California Ozone Study, J. Appl. Meteorol. Climatol., 47(9), 2372–2394, doi:10.1175/2008JAMC1822.1, 2007.

Barletta, B., Meinardi, S., Sherwood Rowland, F., Chan, C.-Y., Wang, X., Zou, S., Yin Chan, L. and Blake, D. R.: Volatile organic compounds in 43 Chinese cities, Atmos. Environ., 39(32), 5979–5990, doi:10.1016/j.atmosenv.2005.06.029, 2005.

Bon, D. M., Ulbrich, I. M., de Gouw, J. a., Warneke, C., Kuster, W. C., Alexander, M. L., Baker, a., Beyersdorf, a. J., Blake, D., Fall, R., Jimenez, J. L., Herndon, S. C., Huey, L. G., Knighton, W. B., Ortega, J., Springston, S. and Vargas, O.: Measurements of volatile organic compounds at a suburban ground site (T1) in Mexico City during the MILAGRO 2006 campaign: measurement comparison, emission ratios, and source attribution, Atmos. Chem. Phys., 11(6), 2399–2421, doi:10.5194/acp-11-2399-2011, 2011.

Borbon, A., Gilman, J. B., Kuster, W. C., Grand, N., Chevaillier, S., Colomb, a., Dolgorouky, C., Gros, V., Lopez, M., Sarda-Esteve, R., Holloway, J., Stutz, J., Petetin, H., McKeen, S., Beekmann, M., Warneke, C., Parrish, D. D. and de Gouw, J. a.: Emission ratios of anthropogenic volatile organic compounds in northern mid-latitude megacities: Observations versus emission inventories in Los Angeles and Paris, J. Geophys. Res. Atmos., 118(4), 2041–2057, doi:10.1002/jgrd.50059, 2013.

Bouvier-Brown, N. C., Goldstein, A. H., Gilman, J. B., Kuster, W. C. and de Gouw, J. A.: In-situ ambient quantification of monoterpenes, sesquiterpenes, and related oxygenated compounds during BEARPEX 2007 – implications for gas- and particle-phase chemistry, Atmos. Chem. Phys. Discuss., 9(2), 10235–10269, doi:10.5194/acpd-9-10235-2009, 2009.

Brown, S. G., Frankel, A. and Hafner, H. R.: Source apportionment of VOCs in the Los Angeles area using positive matrix factorization, Atmos. Environ., 41(2), 227–237, doi:10.1016/j.atmosenv.2006.08.021, 2007.

Chung, M. Y., M. Beene, S. Ashkan, C. Krauter, and A. S. Hasson (2010), Evaluation of non-enteric sources of non-methane volatile organic compound (NMVOC) emissions from dairies, Atmos. Environ., 44(6), 786–794, doi:10.1016/j.atmosenv.2009.11.033.

Comero, S., Capitani, L., and Gawlik, B. M.: Positive Matrix Factorization - An introduction to the chemometric evaluation of environmental monitoring data using PMF, JRC Scientific and Technical Reports, EUR 23946 EN-2009.

de Gouw, J. A.: Emission sources and ocean uptake of acetonitrile (CH 3 CN) in the atmosphere, J. Geophys. Res., 108(D11), 4329, doi:10.1029/2002JD002897, 2003.

de Gouw, J. A., Howard, C. J., Custer, T. G. and Fall, R.: Emissions of volatile organic compounds from cut grass and clover are enhanced during the drying process, Geophys. Res. Lett., 26(7), 811–814, 1999.

Fares, S., Gentner, D. R., Park, J.-H., Ormeno, E., Karlik, J. and Goldstein, A. H.: Biogenic emissions from Citrus species in California, Atmos. Environ., 45(27), 4557–4568, doi:10.1016/j.atmosenv.2011.05.066, 2011.

Fares, S., Park, J.-H., Gentner, D. R., Weber, R., Ormeño, E., Karlik, J. and Goldstein, a. H.: Seasonal cycles of biogenic volatile organic compound fluxes and concentrations in a California citrus orchard, Atmos. Chem. Phys., 12(20), 9865–9880, doi:10.5194/acp-12-9865-2012, 2012.

Filipy, J., B. Rumburg, G. Mount, H. Westberg, and B. Lamb (2006), Identification and quantification of volatile organic compounds from a dairy, Atmos. Environ., 40(8), 1480–1494, doi:10.1016/j.atmosenv.2005.10.048.

Galbally, I. E., and Kirstine, W.: The Production of Methanol by Flowering Plants and the Global Cycle of Methanol, Journal of Atmospheric Chemistry, 43, 195-229, 10.1023/A:1020684815474, 2002.

Gelencsér, A., Siszler, K. and Hlavay, J.: Toluene-benzene concentration ratio as a tool for characterizing the distance from vehicular emission sources, Environ. Sci. …, 31(10),

2869–2872 [online] Available from: http://pubs.acs.org/doi/abs/10.1021/es970004c (Accessed 30 November 2014), 1997.

Gentner, D. R., Ford, T. B., Guha, a., Boulanger, K., Brioude, J., Angevine, W. M., de Gouw, J. a., Warneke, C., Gilman, J. B., Ryerson, T. B., Peischl, J., Meinardi, S., Blake, D. R., Atlas, E., Lonneman, W. a., Kleindienst, T. E., Beaver, M. R., Clair, J. M. St., Wennberg, P. O., VandenBoer, T. C., Markovic, M. Z., Murphy, J. G., Harley, R. a. and Goldstein, a. H.: Emissions of organic carbon and methane from petroleum and dairy operations in California's San Joaquin Valley, Atmos. Chem. Phys., 14(10), 4955–4978, doi:10.5194/acp-14-4955-2014, 2014.

Gentner, D. R., Isaacman, G., Worton, D. R., Chan, A. W. H., Dallmann, T. R., Davis, L., Liu, S., Day, D. A., Russell, L. M., Wilson, K. R., Weber, R., Guha, A. and Harley, R. A.: Elucidating secondary organic aerosol from diesel and gasoline vehicles through detailed characterization of organic carbon emissions, , doi:10.1073/pnas.1212272109/-/DCSupplemental.www.pnas.org/cgi/doi/10.1073/pnas.1212272109, 2012.

Goldstein, A. H. and Schade, G. W.: Quantifying biogenic and anthropogenic contributions to acetone mixing ratios in a rural environment, Atmos. Environ., 34(29-30), 4997–5006, doi:10.1016/S1352-2310(00)00321-6, 2000.

Graus, M., Eller, A. S. D., Fall, R., Yuan, B., Qian, Y., Westra, P., de Gouw, J. and Warneke, C.: Biosphere-atmosphere exchange of volatile organic compounds over C4 biofuel crops, Atmos. Environ., 66, 161–168, doi:10.1016/j.atmosenv.2011.12.042, 2013.

Guenther, A., Karl, T., Harley, P., Wiedinmyer, C., Palmer, P. I. and Geron, C.: Estimates of global terrestrial isoprene emissions using MEGAN (Model of Emissions of Gases and

Aerosols from Nature), Atmos. Chem. Phys. Discuss., 6(1), 107–173, doi:10.5194/acpd-6-107-2006, 2006.

Guha, A., Gentner, D. R., Weber, R. J., Provencal, R., and Goldstein, A. H.: Source apportionment of methane and nitrous oxide in California's San Joaquin Valley at CalNex 2010 via positive matrix factorization, Atmos. Chem. Phys., 15, 12043-12063, doi:10.5194/acp-15-12043-2015, 2015.

Guha, A. (2014). Sources of methane and nitrous oxide in California's Central Valley estimated through direct airborne flux and positive matrix factorization source apportionment of ground-based and regional tall tower measurements (Doctoral Dissertation). Retrieved from UC Berkeley Library database.

Harley, P., Greenberg, J., Niinemets, Ü. and Guenther, A.: Environmental controls over methanol emission from leaves, Biogeosciences Discuss., 4(4), 2593–2640, 2007.

Hatala, J. a., Detto, M., Sonnentag, O., Deverel, S. J., Verfaillie, J. and Baldocchi, D. D.: Greenhouse gas (CO2, CH4, H2O) fluxes from drained and flooded agricultural peatlands in the Sacramento-San Joaquin Delta, Agric. Ecosyst. Environ., 150, 1–18, doi:10.1016/j.agee.2012.01.009, 2012.

Hoben, J. P., Gehl, R. J., Millar, N., Grace, P. R. and Robertson, G. P.: Nonlinear nitrous oxide (N2O) response to nitrogen fertilizer in on-farm corn crops of the US Midwest, Glob. Chang. Biol., 17(2), 1140–1152, 2011.

Hopke, P.: A guide to positive matrix factorization, Department of Chemistry, Clarkson University, Potsdam, N, pp 1–16 , http://www.epa.gov/ttnamti1/files/ambient/pm25/workshop/laymen.pdf

Hu, L., D. B. Millet, S. Y. Kim, K. C. Wells, T. J. Griffis, E. V. Fischer, D. Helmig, J. Hueber, and a. J. Curtis (2013), North American acetone sources determined from tall tower measurements and inverse modeling, Atmos. Chem. Phys., 13(6), 3379–3392, doi:10.5194/acp-13-3379-2013.

Hu, L., Mohr, M. J., Wells, K. C., Griffis, T. J., Helmig, D. and Millet, D. B.: Sources and seasonality of atmospheric methanol based on tall tower measurements in the US Upper Midwest, Atmos. Chem. Phys. Discuss., 11(6), 17473–17505, doi:10.5194/acpd-11-17473-2011, 2011.

Hüve, K., Christ, M. M., Kleist, E., Uerlings, R., Niinemets, Ü., Walter, A. and Wildt, J.: Simultaneous growth and emission measurements demonstrate an interactive control of methanol release by leaf expansion and stomata, J. Exp. Bot., 58(7), 1783–1793, 2007.

Jacob, D. J., Field, B. D., Jin, E. M., Bey, I., Li, Q., Logan, J. A., Yantosca, R. M. and Singh, H. B.: Atmospheric budget of acetone, J. Geophys. Res. Atmos., 107(D10), ACH 5–1–ACH 5–17, doi:10.1029/2001JD000694, 2002.

Jeong, S., C. Zhao, A. E. Andrews, L. Bianco, J. M. Wilczak, and M. L. Fischer (2012a), Seasonal variation of CH 4 emissions from central California, J. Geophys. Res., 117(D11), D11306, doi:10.1029/2011JD016896.

Jeong, S., C. Zhao, A. E. Andrews, E. J. Dlugokencky, C. Sweeney, L. Bianco, J. M. Wilczak, and M. L. Fischer (2012b), Seasonal variations in N 2 O emissions from central California, Geophys. Res. Lett., 39(16), n/a–n/a, doi:10.1029/2012GL052307.

Jordan, C., Fitz, E., Hagan, T., Sive, B., Frinak, E., Haase, K., Cottrell, L., Buckley, S., and Talbot, R.: Long-term study of VOCs measured with PTR-MS at a rural site in New

Hampshire with urban influences, Atmos. Chem. Phys., 9, 4677-4697, doi:10.5194/acp-9-4677-2009, 2009

Karl, T.: Seasonal variation of biogenic VOC emissions above a mixed hardwood forest in northern Michigan, Geophys. Res. Lett., 30(23), 2186, doi:10.1029/2003GL018432, 2003.

Karl, T., Curtis, A. J., Rosenstiel, T. N., Monson, R. K. and Fall, R.: Transient releases of acetaldehyde from tree leaves-products of a pyruvate overflow mechanism?, Plant, Cell Environ., 25(9), 1121–1131, 2002.

Kesselmeier, J. and Staudt, M.: Biogenic volatile organic compounds (VOC): An overview on emission, physiology and ecology, J. Atmos. Chem., 33(1), 23–88, 1999.

Kirstine, W., Galbally, I., Ye, Y. and Hooper, M.: Emissions of volatile organic compounds (primarily oxygenated species) from pasture, J. Geophys. Res., 103(D9), 10605, 1998.

Kim, E., Hopke, P. K. and Edgerton, E. S.: Improving source identification of Atlanta aerosol using temperature resolved carbon fractions in positive matrix factorization, Atmos. Environ., 38(20), 3349–3362, doi:10.1016/j.atmosenv.2004.03.012, 2004.

Knox, S. H., Sturtevant, C., Matthes, J. H., Koteen, L., Verfaillie, J. and Baldocchi, D.: Agricultural peatland restoration: effects of land-use change on greenhouse gas (CO2 and CH4 ) fluxes in the Sacramento-San Joaquin Delta., Glob. Chang. Biol., 1–16, doi:10.1111/gcb.12745, 2014.

Lan, T. T. N. and Minh, P. A.: BTEX pollution caused by motorcycles in the megacity of HoChiMinh, J. Environ. Sci. (China), 25(2), 348–356, 2013.

Lanz, V.A., Henne, S., Staehelin, J., Hueglin, C., Vollmer, M.K., Steinbacher, M., Buchmann, B., and Reimann, S.: Statistical analysis of anthropogenic non-methane VOC variability

at a European background location (Jungfraujoch, Switzerland): Atmos. Chem. Phys., 9, 3445-3459, doi:10.5194/acp-9-3445-2009.

Linquist, B., Van Groenigen, K. J., Adviento-Borbe, M. A., Pittelkow, C. and Van Kessel, C.: An agronomic assessment of greenhouse gas emissions from major cereal crops, Glob. Chang. Biol., 18(1), 194–209, 2012.

Liu, J., Mu, Y., Zhang, Y., Zhang, Z., Wang, X., Liu, Y. and Sun, Z.: Atmospheric levels of BTEX compounds during the 2008 Olympic Games in the urban area of Beijing, Sci. Total Environ., 408(1), 109–116, 2009.

Lee, E., Chan, C. K. and Paatero, P.: Application of positive matrix factorization in source apportionment of particulate pollutants in Hong Kong, Atmos. Environ., 33(19), 3201–3212, doi:10.1016/S1352-2310(99)00113-2, 1999.

McKinney, K. a., Lee, B. H., Vasta, a., Pho, T. V. and Munger, J. W.: Emissions of isoprenoids and oxygenated biogenic volatile organic compounds from a New England mixed forest, Atmos. Chem. Phys., 11(10), 4807–4831, doi:10.5194/acp-11-4807-2011, 2011.

McMillan, A. M. S., Goulden, M. L. and Tyler, S. C.: Stoichiometry of CH 4 and CO 2 flux in a California rice paddy, J. Geophys. Res., 112(G1), G01008, doi:10.1029/2006JG000198, 2007.

Millet, D. B., Guenther, A., Siegel, D. A., Nelson, N. B., Singh, H. B., de Gouw, J. A., Warneke, C., Williams, J., Eerdekens, G., Sinha, V., Karl, T., Flocke, F., Apel, E., Riemer, D. D., Palmer, P. I. and Barkley, M.: Global atmospheric budget of acetaldehyde: 3-D model analysis and constraints from in-situ and satellite observations, Atmos. Chem. Phys. Discuss., 9(6), 24225–24279, doi:10.5194/acpd-9-24225-2009, 2009.

Misztal, P. K., Karl, T., Weber, R., Jonsson, H. H., Guenther, a. B. and Goldstein, a. H.: Airborne flux measurements of biogenic volatile organic compounds over California, Atmos. Chem. Phys. Discuss., 14(6), 7965–8013, doi:10.5194/acpd-14-7965-2014, 2014.

Norris, G., Vedantham, R., Wade, K., Brown, S., Prouty, J., and Foley, C.: EPA Positive Matrix Factorization (PMF) 3.0 Fundamentals and User Guide, Washington DC, USA, 2008.

Ngwabie, N. M., Schade, G. W., Custer, T. G., Linke, S. and Hinz, T.: Abundances and Flux Estimates of Volatile Organic Compounds from a Dairy Cowshed in Germany, J. Environ. Qual., 37(2), 565, doi:10.2134/jeq2006.0417, 2008.

Paatero, P. (1997), Least squares formulation of robust non-negative factor analysis, Chemom. Intell. Lab. Syst., 37(1), 23–35, doi:10.1016/S0169-7439(96)00044-5.

Park, J.-H., Goldstein, a H., Timkovsky, J., Fares, S., Weber, R., Karlik, J. and Holzinger, R.: Active atmosphere-ecosystem exchange of the vast majority of detected volatile organic compounds., Science, 341(6146), 643–7, doi:10.1126/science.1235053, 2013.

Paatero, P., and U. Tapper (1994), Positive matrix factorization: A non-negative factor model with optimal utilization of error estimates of data values, Environmetrics, 5(April 1993), 111–126.

Peischl, J., Ryerson, T. B., Holloway, J. S., Trainer, M., Andrews, a. E., Atlas, E. L., Blake, D. R., Daube, B. C., Dlugokencky, E. J., Fischer, M. L., Goldstein, a. H., Guha, a., Karl, T., Kofler, J., Kosciuch, E., Misztal, P. K., Perring, a. E., Pollack, I. B., Santoni, G. W., Schwarz, J. P., Spackman, J. R., Wofsy, S. C. and Parrish, D. D.: Airborne observations of methane emissions from rice cultivation in the Sacramento Valley of California, J. Geophys. Res., 117, D00V25, doi:10.1029/2012JD017994, 2012.

Polissar, A.V., Hopke, P.K., Malm, W.C., and Sisler, J.F.: Atmospheric aerosol over Alaska 1. Spatial and seasonal variability: JGR, Vol 13, No. D15j, 19,305-19,044: DOI: 10.1029/98JD01365 Aug 20, 1998.

Rosenstock T, Liptzin D, Six J, Tomich T. 2013. Nitrogen fertilizer use in California: Assessing the data, trends and a way forward. Calif Agr 67(1):68-79. DOI: 10.3733/ca.E.v067n01p68. http://californiaagriculture.ucanr.edu/landingpage.cfm?article=ca.E.v067n01p68&fulltext=yes

Ruuskanen, T. M., Müller, M., Schnitzhofer, R., Karl, T., Graus, M., Bamberger, I., Hörtnagl, L., Brilli, F., Wohlfahrt, G. and Hansel, A.: Eddy covariance VOC emission and deposition fluxes above grassland using PTR-TOF., Atmos. Chem. Phys., 11(2), 611–625, doi:10.5194/acp-11-611-2011, 2011.

Schade, G. W. and Goldstein, A. H.: Seasonal measurements of acetone and methanol: Abundances and implications for atmospheric budgets, Global Biogeochem. Cycles, 20(1), n/a–n/a, doi:10.1029/2005GB002566, 2006.

Schade, G. W. and Goldstein, A. H.: Fluxes of oxygenated volatile organic compounds from a ponderosa pine plantation, J. G. Res., 106(D3), 3111, doi:10.1029/2000JD900592, 2001.

Shaw, S. L., Mitloehner, F. M., Jackson, W., Depeters, E. J., Fadel, J. G., Robinson, P. H., Holzinger, R. and Goldstein, A. H.: Volatile organic compound emissions from dairy cows and their waste as measured by proton-transfer-reaction mass spectrometry., Environ. Sci. Technol., 41(4), 1310–6 [online] Available from: http://www.ncbi.nlm.nih.gov/pubmed/17593735, 2007.

Slowik, J. G., Vlasenko, a., McGuire, M., Evans, G. J. and Abbatt, J. P. D.: Simultaneous factor analysis of organic particle and gas mass spectra: AMS and PTR-MS measurements at an urban site, Atmos. Chem. Phys., 10(4), 1969–1988, doi:10.5194/acp-10-1969-2010, 2010.

Steeghs, M., Bais, H. P., de Gouw, J., Goldan, P., Kuster, W., Northway, M., Fall, R. and Vivanco, J. M.: Proton-transfer-reaction mass spectrometry as a new tool for real time analysis of root-secreted volatile organic compounds in Arabidopsis., Plant Physiol., 135(1), 47–58, 2004.

Teh, Y. A., Silver, W. L., Sonnentag, O., Detto, M., Kelly, M. and Baldocchi, D. D.: Large Greenhouse Gas Emissions from a Temperate Peatland Pasture, Ecosystems, 14(2), 311–325, doi:10.1007/s10021-011-9411-4, 2011.

Ulbrich, I. M. et al. (2009), Interpretation of organic components from Positive Matrix Factorization of aerosol mass spectrometric data, Atmos. Chem. Phys., 9(9), 2891–2918, doi:10.5194/acp-9-2891-2009.

van Groenigen, J. W., Velthof, G. L., Oenema, O., Van Groenigen, K. J. and Van Kessel, C.: Towards an agronomic assessment of N2O emissions: A case study for arable crops, Eur. J. Soil Sci., 61(6), 903–913, 2010.

Warneke, C., McKeen, S. a., de Gouw, J. a., Goldan, P. D., Kuster, W. C., Holloway, J. S., Williams, E. J., Lerner, B. M., Parrish, D. D., Trainer, M., Fehsenfeld, F. C., Kato, S., Atlas, E. L., Baker, a. and Blake, D. R.: Determination of urban volatile organic compound emission ratios and comparison with an emissions database, J. Geophys. Res., 112(D10), D10S47, doi:10.1029/2006JD007930, 2007.

White, M. L., Russo, R. S., Zhou, Y., Ambrose, J. L., Haase, K., Frinak, E. K., Varner, R. K., Wingenter, O. W., Mao, H., Talbot, R. and Sive, B. C.: Are biogenic emissions a significant source of summertime atmospheric toluene in rural Northeastern United States?, Atmos. Chem. Phys. Discuss., 8(3), 12283–12311, doi:10.5194/acpd-8-12283-2008, 2008.

Williams, B. J., Goldstein, a. H., Kreisberg, N. M., Hering, S. V., Worsnop, D. R., Ulbrich, I. M., Docherty, K. S. and Jimenez, J. L.: Major components of atmospheric organic aerosol in southern California as determined by hourly measurements of source marker compounds, Atmos. Chem. Phys., 10(23), 11577–11603, doi:10.5194/acp-10-11577-2010, 2010.

Yuan, B., Shao, M., de Gouw, J., Parrish, D. D., Lu, S., Wang, M., Zeng, L., Zhang, Q., Song, Y., Zhang, J. and Hu, M.: Volatile organic compounds (VOCs) in urban air: How chemistry affects the interpretation of positive matrix factorization (PMF) analysis, J. Geophys. Res. Atmos., 117(D24), n/a–n/a, doi:10.1029/2012JD018236, 2012.

Zhong, S., Whiteman, C. and Bian, X.: Diurnal evolution of three-dimensional wind and temperature structure in California's Central Valley, J. Appl. …, (1962), 1679–1699 [online] Available from: http://journals.ametsoc.org/doi/abs/10.1175/JAM2154.1 (Accessed 6 March 2013), 2004.

# 5. Seasonally varying methane and nitrous oxide emissions using inverse modeling of atmospheric back trajectories

## 5.1. Introduction

At present, $CH_4$ and $N_2O$ are estimated to contribute ~ 9% and 3% of total California GHG emissions, respectively (CARB, 2015). However, the lack of accurate activity data and an incomplete understanding of emission processes result in uncertainty in the bottom-up emissions. This suggests that atmospheric measurements and inverse modeling may provide an independent method to qualify local to regional $CH_4$ and $N_2O$ emissions from California. It should be noted that the inverse modeling work performed in this project (ARB contract # 11-315) is unique and different from the LBNL inverse modeling project (ARB contract # 11-306), which analyzed a data across the state from a later time period ( fall 2013 - spring 2014). This work utilizes data from WGC alone for a different time period (fall 2012-2013), primarily for the purpose of comparing with the coincident VOC-based PMF analysis.

Atmospheric inverse modeling using observed and predicted mixing ratios to estimate the surface flux has become an effective tool to understand GHGs emissions (Houweling et al., 1999; Gimson and Uliasz, 2003; Kort et al., 2008; Zhao et al., 2009; Jeong et al., 2012a). Using this method, Zhao et al. (2009) have estimated $CH_4$ emissions from the central California; Jeong et al. (2012a) have analyzed the seasonal variations of $CH_4$ and Jeong et al. (2012b) estimated $N_2O$ emissions in central California. Also, Jeong et al. (2013) investigated $CH_4$ emissions across California using multiple towers. Applying a similar inverse modeling approach to this study, the multi-tower inverse analysis used atmospheric observations from five sites in California's Central Valley across different seasons (September 2010 to June 2011). Combining the result

from a study of the South Coast Air Basin (Wennberg et al., 2012), Jeong et al. (2013) estimated a state total of 2.0 – 2.7 Tg $CH_4$/yr (at 68% confidence), which is higher than the current state inventory (~1.6 Tg $CH_4$/yr, CARB (2015)).

Following those efforts, we quantify $CH_4$ and $N_2O$ emissions from central California in the June 2012 to August 2013 period using a Bayesian inverse modeling approach driven by measurements from a tall tower near Walnut Grove (WGC, hereafter). We also update the $N_2O$ emission at December 2007 – November 2009 (2008-2009, hereafter) by using the same (used in this study) *a priori* emission maps, NOAA boundary condition and methods to gain surface footprints in springs and summers as the period of 2012 - 2013. In Section 5.2, we describe the measurements and modeling approach including *a priori* $CH_4$ and $N_2O$ emission maps, atmospheric transport modeling, and the Bayesian inverse method and uncertainty analysis. Section 5.3 reports results, including averaged footprints in different seasons, seasonally varying measured $CH_4$ and $N_2O$ mixing ratios and the inferred $CH_4$ and $N_2O$ surface emissions from central California around WGC by source and region. Section 5.4 discusses the results and offers conclusions on $CH_4$ and $N_2O$ emissions in central California for the measurement period.

## 5.2. Data and Models

The Bayesian inversion analysis employed here obtains *posterior* $CH_4$ and $N_2O$ emissions by multiplicatively scaling the *a priori* emission maps to minimize the weighted difference between the measured and predicted GHG signals as described below.

### 5.2.1. Measurements

$CH_4$ and $N_2O$ mixing ratios were measured every 15 minutes at 91 and 483 m on a tall-tower near Walnut Grove, California (WGC, 121.49°W, 38.27°N, 0 m above sea level). As in

previous work from this site (Zhao et al., 2009; Jeong et al., 2012a), dry-molar $CH_4$ mixing ratios are measured with a cavity ring-down (Picarro, G2301) spectrometer. Air was dried to between -25 to -30°C dew point using condensers and Nafion drier, and 4 NOAA primary gas standards were used to calibrate and check the instrument gain and offset every 4 hours (Andrews et al., 2014).

Similarly, dry molar $N_2O$ was measured with an off-axis laser spectrometer (Los Gatos $N_2O$/CO-EP). In this case, calibrations with two secondary standards were performed every 2 hr to maintain ~ 0.05 ppb precision and stability, as judged by stability of interleaved "target" gas measurements. To evaluate and control offsets of measured $CH_4$ and $N_2O$ mixing ratios relative to NOAA calibration scales used to define the mixing ratio of background air inflow to California, the measured *in-situ* mixing ratios were compared with time synchronized flask sampling and analysis by NOAA. Using the *in-situ* to flask comparisons, the measurement accuracy was better than ~ 1 ppbv for $CH_4$, and 0.1-0.2 ppb for $N_2O$, both sufficient to capture measured atmospheric variations. Calibrated mixing ratios were then averaged into 3 hr time bins for comparison with predicted signals. The *in-situ* $CH_4$ and $N_2O$ measurements were compared with analysis of flask samples collected at this site and subsequently analyzed at the NOAA laboratory. A mean offset of 0.3 ± 0.05 ppb of $N_2O$ was subtracted from the *in-situ* data to match the mean of the flask data.

Before use in the inversions, measured GHG signals were selected based upon a "well-mixed" requirement that the vertical gradient in mixing ratio between 91 and 483 m fall within a range typically found for each month. For example, Figure 5.1 shows the difference of hourly mean methane mixing ratios at 91 and 483 m is smallest in spring and the largest in winter with the minimum values of 0 and 118.3 ppb respectively. Here, the seasons are defined as summer

2012 (June 16 – August 31, 2012), early fall (September 01 – October 17, 2012), late fall (October 17 – November 30, 2012), winter (December 14, 2012 – January 29, 2013), winter-spring (February 14 – April 05, 2013), spring (April 07 – June 01, 2013) and summer 2013 (June 01 – August 05, 2013) due to the availability of measured data. Based on this analysis we find the time of convergence near midday. Following previous work at this site, we select data points in time when the $CH_4$ mixing ratio difference between 91 and 483 m is less than 3 standard deviations from the difference of the mean diurnal cycle difference for the 1200-1700 time window.

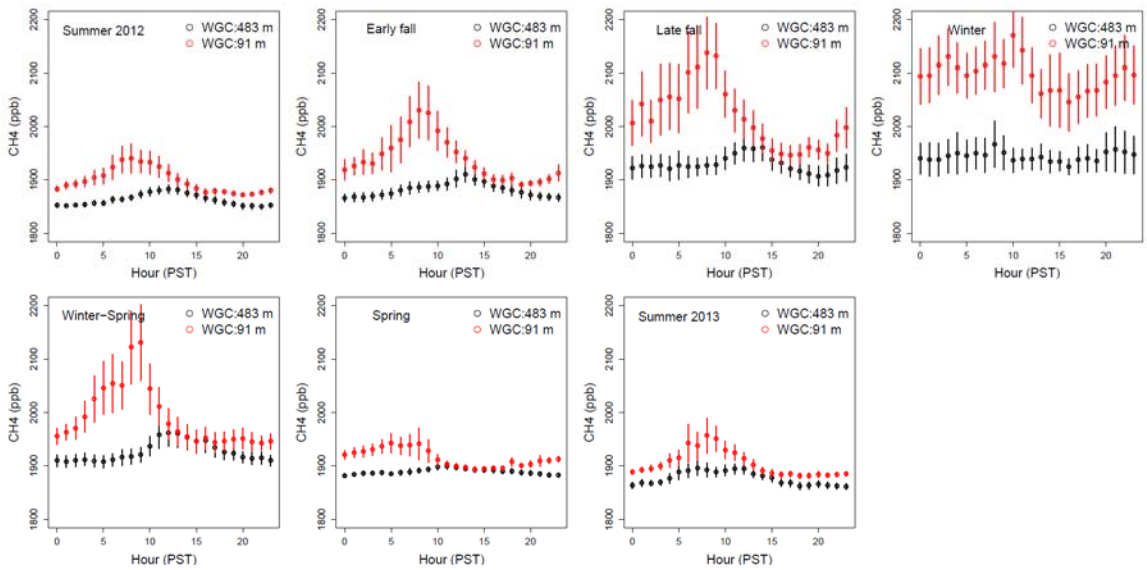


**Figure 5.1**. Diurnal cycles of mean hourly (PST) measured $CH_4$ mixing ratio obtained for 91 and 483 m sampling heights on the WGC tower for the period from June 2012 to August 2013 (7 different seasons).

### 5.2.2. Prior $CH_4$ Emission Map

Following previous work, we apply an update to a 0.1° × 0.1° prior methane emission model shown in Figure 5.2 for California including wastewater (WW), landfills (LF), dairy livestock (DLS), non-dairy livestock (NDLS), the natural gas system (NG, including petroleum

production), petroleum refining and mobile (PL), natural wetlands (WL), and crop agriculture (CP) (see Table 5.1). This work used the California Greenhouse Gas Emission Measurements (CALGEM) project *a priori* $CH_4$ emission model (henceforth CALGEM model, available at calgem.lbl.gov) described by Jeong et al. (2012a, 2013, 2014) with some modifications. The CALGEM emission model provides emissions by sector at a high spatial resolution (0.1º × 0.1º) for California. The CALGEM model has seasonal components for wetlands and crop agriculture only, and these seasonal emissions are combined with non-seasonal emissions to construct monthly emission maps for inversions (Table 5.1). The inversion approach using non-seasonal prior emissions is widely used (e.g., Zhao et al., 2009; Jeong et al., 2012a; 2012b; 2013; Wecht et al., 2014; Cui et al., 2015). In particular, Jeong et al. [2012a; 2012b; 2013] showed non-seasonal priors can provide information on seasonality in the *posterior* emission.

In this study, the CALGEM prior emissions distributions are scaled to match 2012 ARB state totals for anthropogenic emission sectors (CARB, 2014; March 2014 version), with small (< 50 Gg $CH_4$/yr) adjustments for some regions and sectors (per ARB staff private communication). The spatial distribution of the dairy livestock emissions was revised by incorporating the 2012 county-level dairy statistics from USDA

**Table 5.1.** *A Priori methane* emissions (Tg $CH_4$ $yr^{-1}$)* for eight source sectors for 7 seasons and annual mean.

| | Summer 2012 | Early fall | Late fall | Winter | Winter-spring | Spring | Summer 2013 | Annual |
|---|---|---|---|---|---|---|---|---|
| WW | 0.02 | 0.02 | 0.02 | 0.02 | 0.02 | 0.02 | 0.02 | 0.02 |
| LF | 0.10 | 0.10 | 0.10 | 0.10 | 0.10 | 0.10 | 0.10 | 0.10 |
| DLS | 0.26 | 0.26 | 0.26 | 0.26 | 0.26 | 0.26 | 0.26 | 0.26 |
| NDLS | 0.05 | 0.05 | 0.05 | 0.05 | 0.05 | 0.05 | 0.05 | 0.05 |
| NG | 0.08 | 0.08 | 0.08 | 0.08 | 0.08 | 0.08 | 0.08 | 0.08 |
| PL | 0.02 | 0.02 | 0.02 | 0.02 | 0.02 | 0.02 | 0.02 | 0.02 |
| WL | 0.03 | 0.04 | 0.03 | 0.02 | 0.01 | 0.02 | 0.03 | 0.02 |
| CP | 0.14 | 0.07 | 0.00 | 0.00 | 0.00 | 0.02 | 0.14 | 0.05 |
| Total | 0.69 | 0.62 | 0.55 | 0.53 | 0.53 | 0.55 | 0.69 | 0.59 |

*The emission represents the total for Regions 3, 7 and 8 near the WGC tower by season.

(http://www.nass.usda.gov/Statistics_by_State/California/Publications/County_Estimates/2013lvsceF.pdf) using the spatial distribution from Jeong et al. (2013). The spatial distribution of petroleum production and the natural gas system was revised based on Jeong et al. (2014).

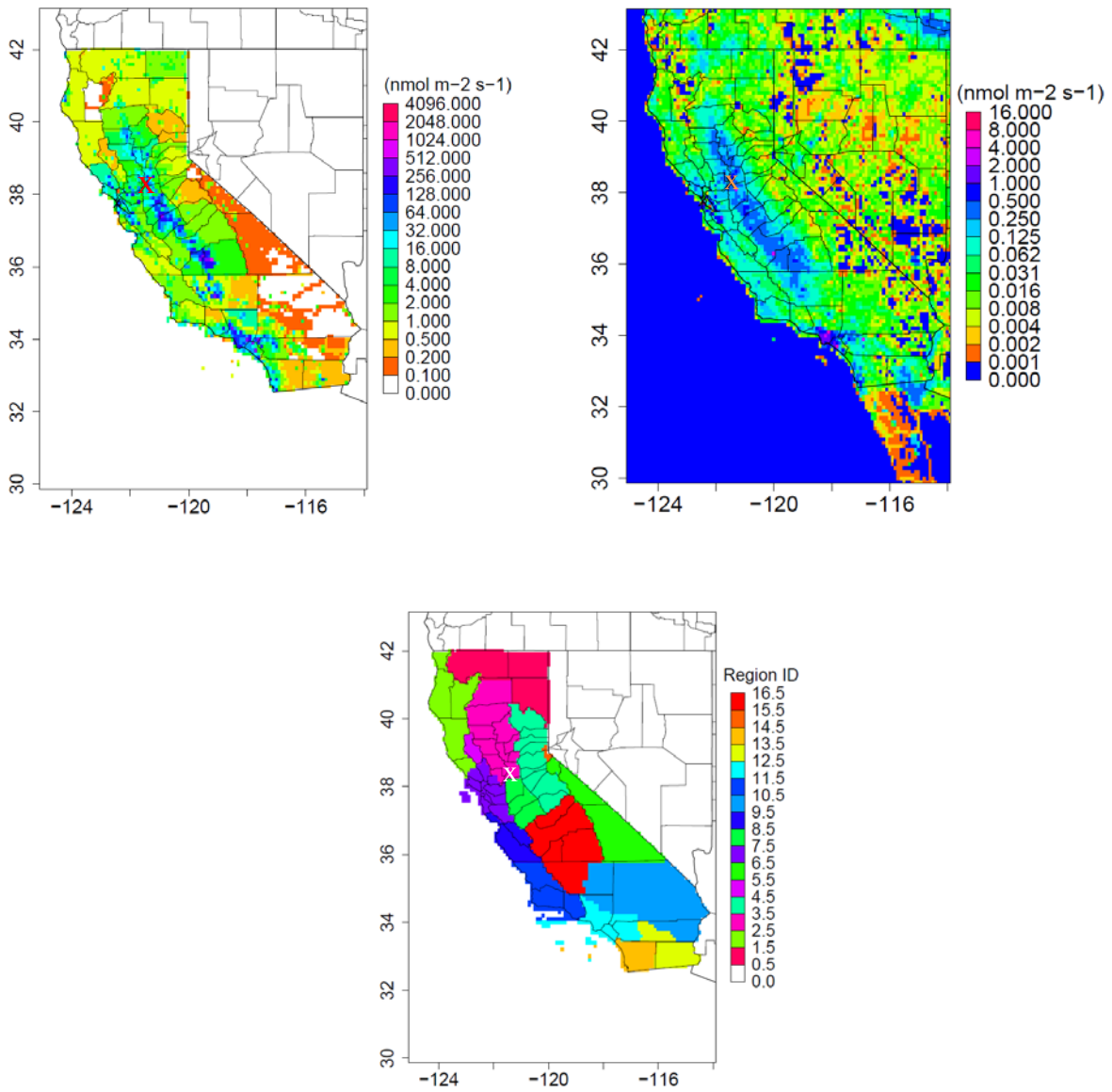


**Figure 5.2**. A *priori* scaled $CH_4$ emission map (nmol/m$^2$/s) based on CALGEM emission map (top left), a prior scaled $N_2O$ emission map (nmol/m$^2$/s) based on EDGAR 4.2 emission map (top right) and region classification map (bottom). The location of the WGC tower is marked with an "x" near longitude = 121ºW, latitude = 38ºN.

Lacking a California specific map for *a priori* $N_2O$ emissions, we apply the 0.1° × 0.1° EDGAR 4.2 $N_2O$ emission (European Commission Joint Research Centre and Netherlands Environmental Assessment Agency, Emission Database for Global Atmospheric Research (EDGAR), release version 4.2, 2011, http://edgar.jrc.ec.europa.eu), after scaling each source sector to match the CARB inventory for 2012 by sector (see Figure 5.2, center). Outside California, the EDGAR 4.2 emission maps are used for both $CH_4$ and $N_2O$ emissions in the remainder of the modeling domain described below.

Kort et al. (2008) and Jeong et al. (2012b) assumed that $N_2O$ emissions from unfertilized natural soils are small compared to emissions from agricultural soils and other anthropogenic sources in California. In this study, we derived the emission map for natural forest based on the Global Emissions InitiAtive (GEIA) emission model (Bouwman et al., 1995) and included it in the inversion. We used the Moderate Resolution Imaging Spectroradiometer (MODIS) land cover type data product (http://e4ftl01.cr.usgs.gov/MOTA/MCD12Q1.051/2012.01.01/, accessed February 2015) to identify natural forest pixels at 0.1° (~ 10 km) resolution. Based on the MODIS-derived natural forest map, we regridded the 1°x1° GEIA emissions from soils under natural vegetation and fertilized agricultural fields to represent 0.1° natural forest emissions. The prior $N_2O$ emission from natural forest is 2.2 Gg $N_2O$/yr, which is 4.5% of the state total $N_2O$ emissions. Similarly, US EPA estimates forest soil emissions are less than 1%. Also, we used ocean $N_2O$ emissions from the GEIA model (Bouwman et al., 1995) to incorporate emissions from ocean along the California coast to the inversion system. While the total $N_2O$ emission from ocean within the entire modeling domain (extending from ~150°W - 90°W) is ~1.4 times the current state total anthropogenic $N_2O$ emission (44 Gg $N_2O$/yr, CARB, 2015), they are distributed over a large area where there is negligible footprint sensitivity, resulting in very small

predicted signal at the WGC tower. The scaled $N_2O$ prior emission map from the EDGAR 4.2 model as well as forest and ocean prior emission maps from GEIA model are applied to update regional inversion during the period of 2008-2009.

### 5.2.3. Atmospheric Transport Modeling

Predicted GHG mixing ratios within the modeling domains are computed as **FE**, where **F** is the footprint and **E** is the prior emission. The footprint **F** is calculated by tracking the parcel dwelling time in each pixel. The parcel transport was simulated by the coupled WRF-STILT (Weather Research and Forecasting and Stochastic Time-Inverted Lagrangian Transport) model (Lin et al., 2003; Skamarock et al., 2008; Nehrkorn et al., 2010). This transport model has been widely implemented in many studies including airborne (Gerbig et al., 2003; Kort et al., 2008) and tower measurement-based (Zhao et al., 2009; Jeong et al., 2012a, 2012b and 2013) inversions.

**Figure 5.3.** WRF initial boundary set up with three-level nested domains. The ratio of spatial resolution between the three levels is 3. The resolutions for d01, d02, d03 and d04/d05 are 36, 12, 4 and 1.3 km, respectively.

The WRF model (version 3.5.1) was used for modeling meteorology with 5 computational domains with the resolution of 36, 12, 4 (d01, d02 and d03) and two 1.3 (d04 and d05) km resolutions as shown in Figure 5.3. The d03 domain of 4 km resolution represents most of California; the d04 and d05 domains of 1.3 km are used to cover the metropolitan area of Los Angeles and the San Francisco Bay Area, respectively. As in Jeong et al. (2013), the WRF model was run with two-way nesting and planetary boundary layer (PBL) heights were resolved with 50 levels over complex terrain features of California. Initial and boundary meteorological conditions are given according to the North American Regional Reanalysis data set (Mesinger et al., 2006). Based on the findings in Jeong et al. (2013), we adopt the Mellor-Yamada-Janjic (MYJ) scheme to model PBL and the NOAA-Noah land surface model (LSM) to model the land surface effects for the late fall to the early spring period (from October to March) and five-layer thermal diffusion LSM scheme to model the land surface for other months. More details on choosing PBL and LSM schemes can be found in Jeong et al. (2013) and not introduced in details here. The WRF run was conducted each day separately for 30 hours including the 6-hour spin-up from the previous day and the output data are saved hourly.

The hourly WRF outputs are used to run the STILT model for particle trajectory simulations. An ensemble of 500 STILT particles are released at the WGC tower located in central California at the height of 91 m above ground every hour from 12 - 17 PST. These particles are run backward for 7 days driven with meteorology from WRF output within the d01, d02, and d03 domains to make sure that most of the particles reach the domain boundary. Model outputs are screened to remove instances when a majority (less than 80%) fails to reach the western edge of the domain at 130ºW longitude. $CH_4$ background signals are computed using

both the NOAA-derived Pacific background (see Jeong et al., 2013 for details) and measurements from the Trinidad Head (THD) station. Measurements at THD were made by flame ionization gas chromatography as part of the Advanced Global Atmospheric Gases Experiment (AGAGE) network (Prinn et al., 2000). AGAGE uses the Tohoku University calibration scale, which is indistinguishable from the NOAA calibration scale used for the Picarro measurements at WGC with a relative scale factor of 1.0003 (Hall et al., 2014). $N_2O$ background is estimated using the NOAA boundary condition.

### 5.2.4. Bayesian Inverse Model

#### *Inversion Approach*

The scaling factor Bayesian inversion (SFBI) method is used to estimate $CH_4$ and $N_2O$ emissions from central California using measured $CH_4$ and $N_2O$ mixing ratios at the tall tower WGC. As in Gerbig et al. (2003) and Jeong et al. (2013), model measurement relations can be expressed as,

$$\mathbf{c} = \mathbf{K}\boldsymbol{\lambda} + \mathbf{v} \tag{5.1}$$

where **c** is background-subtracted 3 hour mean measured mixing ratios at the receptor; **K** = **FE** is the predicted mixing ratio calculated by footprint **F** and prior emission **E**, which was introduced in Section 5.2.3 and Section 5.2.2 respectively**;** $\boldsymbol{\lambda}$ presents scaling factors used to scale *a priori* emissions according to source sectors or region sectors depending on source or region analysis; and **v** is a model-data mismatch vector represented with a covariance matrix **R**. **R** is a diagonal matrix which represents the total uncertainty contributed by all error sources such as the measurement error and the transport error. Based on the Gaussian assumptions, the *posterior* estimate for $\boldsymbol{\lambda}$ is solved as

$$\lambda_{post} = \left(K^T R^{-1} K + Q_\lambda^{-1}\right)^{-1} \left(K^T R^{-1} c + Q_\lambda^{-1} \lambda_{prior}\right) \tag{5.2}$$

where $\boldsymbol{\lambda}_{prior}$ is the *a priori* estimate for $\boldsymbol{\lambda}$, and $\mathbf{Q}_\lambda$ is the error covariance associated with $\boldsymbol{\lambda}_{prior}$. 50% uncertainty is employed for $\boldsymbol{\lambda}_{prior}$ in the present a prior emission for the inversion analysis of $CH_4$ (Pacala et al., 2010) and 100% for $N_2O$ (Jeong et al., 2012b). The *posterior* error covariance for $\boldsymbol{\lambda}$ can be expressed as

$$V_{post} = \left(K^T R^{-1} K + Q_\lambda^{-1}\right)^{-1} \tag{5.3}$$

The SFBI method is used to estimate optimal $CH_4$ emissions for 7 seasons and $N_2O$ emissions for 4 seasons based on the *a priori* emission map described in Section 5.2.2. The inverse modeling approach are implemented for two phases as in Bergamaschi et al. [2005] and Jeong et al. [2012a, 2012b] for both $CH_4$ and $N_2O$ inversions. At first, the inversion is carried out using signals of well-mixed measured signal depicted in Section 5.2.1. The second/final inversion are conducted again using data selected by another criteria $|\mathbf{c}_i - (\mathbf{K}\boldsymbol{\lambda})_i|^2 < \alpha \mathbf{R}_i$, where $\alpha$ is a fixed value for each month depending on the chi-square statistics. Both of the first and second inversions use the original *a priori* emission maps, which means that the first inversion can be recognized as a data selection tool for the atmospheric observations. In the final inversion, the outliers which might otherwise produce biases in the inversion will be removed. Here, we adopt the same method as Jeong et al. (2013) to decide $\alpha$ instead of using $\alpha = 2$ in Bergamaschi et al. (2005). The value of $\alpha$ for each month is decided via an iterative process until that the chi-square values from the final inversion is very close to unity (Tarantola, 1987).

To conduct the regional inversion for the period of 2008-2009, we re-calculated the predicted $N_2O$ mixing ratios using the updated footprints as well as the updated *a priori* $N_2O$

emission maps mentioned above while the measured signal and other settings are same as Jeong et al. (2012b).

***Uncertainty Analysis***

Jeong et al. (2012a; 2012b; 2013) estimated the model-data mismatch matrix **R** for the WGC tower by summing the uncertainties from different sources such as the limited number (500 particles in this study) of particles released ($\mathbf{S}_{part}$), flux aggregation at finite resolution ($\mathbf{S}_{aggr}$), errors in modeled transport winds ($\mathbf{S}_{TransWIND}$) and PBL ($\mathbf{S}_{TransPBL}$), and estimated background ($\mathbf{S}_{bkgd}$), which can be expressed as

$$\mathbf{R}_i = \mathbf{S}_{part} + \mathbf{S}_{aggr} + \mathbf{S}_{bkgd} + \mathbf{S}_{TransPBL} + \mathbf{S}_{TransWIND}, \quad (5.4)$$

In this paper, we adopt the uncertainty analysis result in Jeong et al. (2012a) for $CH_4$ and Jeong et al. (2012b) for $N_2O$. The model-data mismatch used in this study is listed in Table 5.2. The details on the uncertainty analysis are described in Jeong et al. (2012a; 2012b). We also evaluate the sensitivity of the inversion results to the **R** covariance matrix.

**Table 5.2.** Estimated model-data mismatch errors by month for $CH_4$ and $N_2O$ (Jeong et al., 2012a; 2012b).

| **Month** | **1** | **2** | **3** | **4** | **5** | **6** | **7** | **8** | **9** | **10** | **11** | **12** |
|---|---|---|---|---|---|---|---|---|---|---|---|---|
| Model-data mismatch for $CH_4$ (ppb) | 42 | 42 | 22 | 22 | 22 | 22 | 16 | 16 | 22 | 22 | 22 | 42 |
| Model-data mismatch for $N_2O$ (ppb) | 0.63 | 0.63 | 0.4 | 0.4 | 0.4 | 0.48 | 0.48 | 0.48 | 0.41 | 0.41 | 0.41 | 0.63 |

## 5.3. Results

### 5.3.1. Meteorology and Footprints

We compare the WRF predicted wind and the measured wind from the WGC tower to evaluate the wind speed and wind direction difference. The average root-mean-square error

(RMSerr) at four height levels of 122, 244, 366 and 488 m ranges from 2.32 to 4.21 $ms^{-1}$. We found that the averaged RMSerr is much smaller in July and August than in winter. For instance, in the year 2012, the RMSerrs for July and August were 2.32 and 2.45 $ms^{-1}$, respectively. For the same months in 2013, the RMSerrs were 2.70 and 2.47 $ms^{-1}$, which are much smaller than that of December 2012 (4.21 $ms^{-1}$). These results are consistent with the model-data mismatch errors in Jeong et al. (2012a). The predicted-measured wind angle difference is also an important factor influencing the comparison of predicted and measured GHG signals. The averaged values of the mean (standard deviation) of the angle difference at different vertical levels ranged from 18.91 (21.95) to 43.57 (42.59) degrees. The angle differences are also smaller in summer than other seasons. For instance, the mean (standard deviation) angle differences are 52.91(43.52), 65.92 (48.45), 54.65(46), 61.8 (49.74), 49.17 (44.56), 44.63 (37.92) and 52.55 (41.39) degree for seasons of summer in 2012, early fall, late fall, winter, winter-spring, spring and summer in 2013, respectively. To reduce model-data-mismatch errors, data were excluded for time periods when the angle difference was greater than 2 standard deviations of the mean angle difference for each height and each month in the case of $CH_4$ inversion analysis. This had the effect of removing between 3 and 9% of the 3 hourly predicted $CH_4$ signals across the different seasons in this study.

Resulting footprints are shown as midday averaged footprints for the different periods of study in Figure 5.4. The panels show that the footprints vary seasonally due to different wind directions in different seasons. For example, footprints over the San Francisco Bay are stronger than other regions in summer (both of 2012 and 2013) because of sea breeze winds from the Golden Gate into the Sacramento River Delta in summer. In contrast, Central Valley footprints are relatively strong in the late fall to early spring periods. For instance, the footprints are very

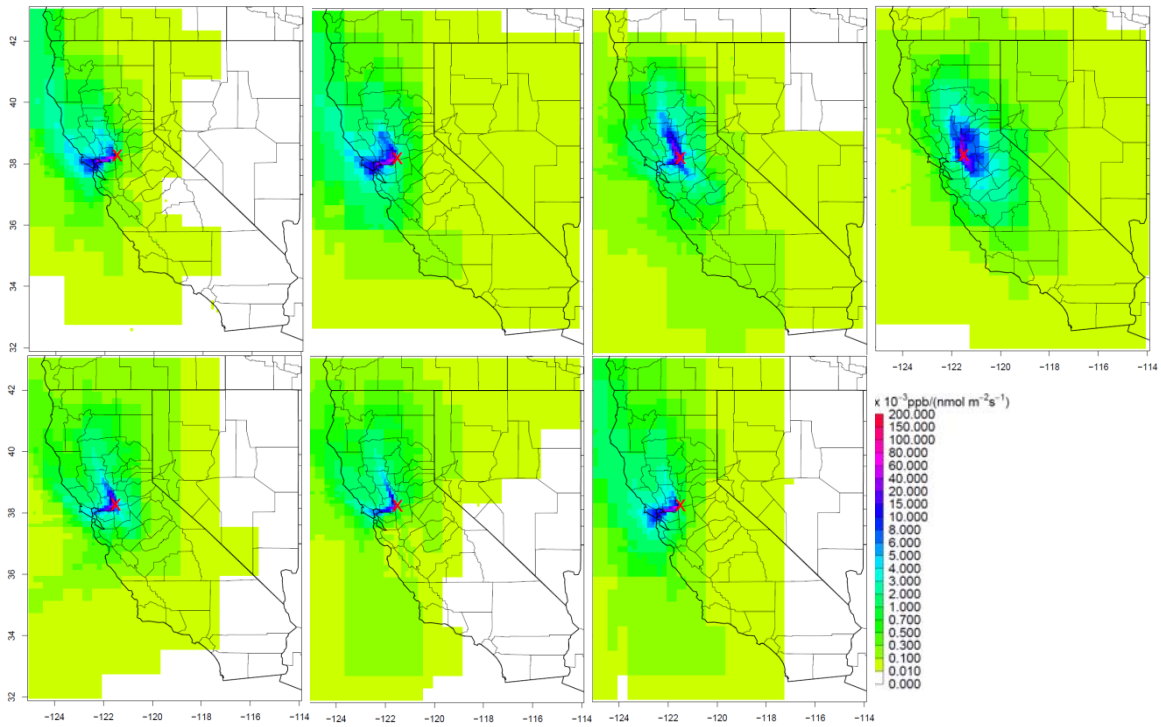


**Figure 5.4.** Seasonally averaged footprint maps over 11-19 (PST) for 7 different seasons of summer at 2012, early fall, late fall, winter, winter-spring, spring and summer at 2013.

strong in the North Central Valley during late fall and winter when the wind blows along the valley.

### 5.3.2. Estimating $CH_4$ emission

#### *$CH_4$ Mixing Ratios*

After screening data as described above, measured mixing ratios are averaged to 3-hour periods and compared with predictions for daytime periods (13-18 PST for summer and 12-17 PST for other seasons).

The mixing ratios are shown in Figure 5.5, which include measured $CH_4$ mixing ratios for the first inversion, measured $CH_4$ mixing ratios for the final version, the predicted signal + background signal for the final inversion and background. The typical amplitude of both of the predicted and observed signals varies with season. For instance, the largest mixing ratios appear

in winter, and mixing ratios increase in the late fall while decreasing in the early spring generally. This is consistent with the variation of the boundary layer depths in central California with the boundary layer highest in late-spring months and lowest in winter (Bianco et al., 2011). Here, the background-subtracted mean values used in the first inversions are 31.1, 57.7, 79.9, 91.4, 61.9, 20.8 and 33.8 ppb in 2012 summer, 2013 early fall, late fall, winter, winter-spring, spring and summer. Additionally, the minimum values of the measured $CH_4$ mixing ratios are close to the NOAA $CH_4$ background with the minimum values in the summer and the maximum in the winter. The approximation of the minimum measured mixing ratios to the background also indicates that the estimated background adopted in this study is reasonable and there is no significant bias in the measured mixing ratios.

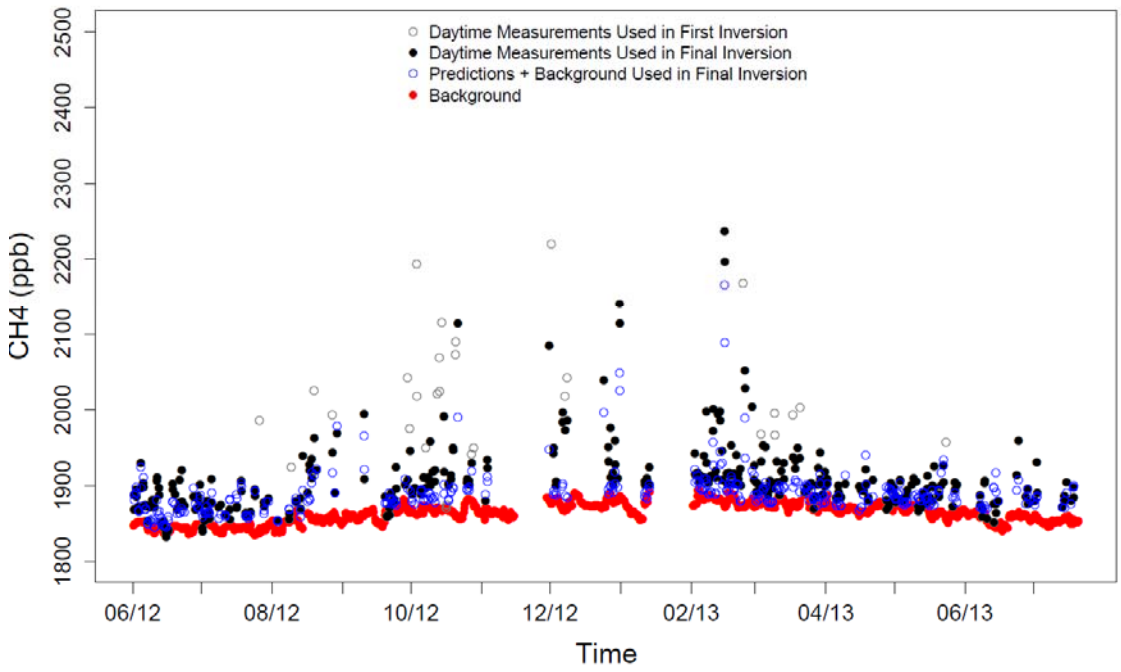


**Figure 5.5.** 3-hour mean $CH_4$ mixing ratio comparison: measured $CH_4$ mixing ratio during noon - afternoon hours used in the first inversion (gray open circle), measured $CH_4$ mixing ratio used in the final inversion (black filled circle), WRF-STILT predicted (used in final inversion) $CH_4$ mixing ratio + WRF-STILT predicted $CH_4$ background (NOAA background) mixing ratio during noon – afternoon hours used for the final inversion (blue open circle), and WRF-STILT predicted $CH_4$ background mixing ratio using the 3-D NOAA curtain (red dots).

***Bayesian Analysis of $CH_4$***

Following prior work, we conduct the Bayesian inverse analysis using scaled CALGEM emission map introduced in Section 5.2 for the 8 source sectors, i.e. waste water (WW), landfill (LF), diary livestock (DLS), non-dairy livestock (NDLS), natural gas (NG), petroleum (PL), wetland (WL), crop agriculture (CP) and emissions from outside CA. Hence, a total of 9 scaling factors $\lambda$ (i.e., 8 sectors and outside California) are solved for each source inversion analysis. For region analysis 17 scaling factors for each region inversion analysis (i.e., 16 regions in CA and region outside CA) are solved. Here, we focus on the source inversion and the total emissions from regions 3, region 7 and region 8 (Fig. 5.2 bottom) because these are the regions with sensitivity in the WGC tower footprints.

After the first inversion, an orthogonal weighted chi-squared linear regression analysis [Press et al., 1992] is conducted. Outlier data are then identified and removed when difference between measured and predicted mixing ratios are larger than a certain value which is a factor $\alpha$ (e.g., $\alpha = 2$) of the estimated error (Bergamaschi et al., 2005). In this study, $\alpha$ is set to 2 - 3 by considering the chi-square statistics close to 1. Depending on the season, the outlier removals vary with season excluding 2.2, 12.9, 29.5, 10.0, 7.7, 0 and 2.3% (mean removal rate = 10.8%). Here, the removal rate is somewhat smaller than our previous studies of 5 - 25% (removal rate = 13.4%) in Jeong et al. (2012a) and 12 - 14% removal rate reported by Bergamaschi et al. (2005).

After outliers are removed, the SFBI is implemented for the second inversion. The slope and RMS error for different seasons after the final inversion are 0.82±0.08 (RMS error = 16.39 ppb), 0.86±0.09 (22.24 ppb), 0.87±0.06 (21.96 ppb), 1.03±0.08 (44.11 ppb), 0.99±0.03 (23.41 ppb), 0.78±0.12 (14.9 ppb) and 0.76±0.25 (20.27 ppb) for summer of 2012, early fall,

late fall, winter, winter-spring, spring and summer of 2013, respectively (Figure 5.6). Before the inversion, the best-fit slopes of predicted vs. measured (RMS error) for individual seasons were 0.65±0.06 (19.15 ppb), 0.56±0.09 (44.3 ppb), 0.28±0.05 (84.89 ppb), 0.49±0.07 (86.33 ppb), 0.64±0.04 (53.08 ppb), 0.72±0.11 (15.18 ppb) and 0.76±0.32 (24.02 ppb). As shown in Figure 5.6, after the inversion, the results for all seasons have improved yielding the best-fit slopes near unity and reducing the RMS errors, in particular in winter and winter-spring. The final *posterior* scaling factors for each season in Table 5.3 show that the *posterior* emissions from all source sectors are slightly smaller or higher than the prior emission, in particular the source sectors of DLS, LF, NDLS and NG. Only the emissions from DLS and CP are smaller than the prior emission in summer 2013. Also, the uncertainties for LF, DLS, NG and CP were significantly reduced depending on the season, suggesting that emissions from these sources are distributed near WGC tower. For instance, the uncertainty of LF is reduced to 38% in late fall, DLS reduced to 10% in winter-spring, NG reduced to 34% in summer 2012, and CP reduced to 25% in summer 2012. However, the *posterior* uncertainties for other sectors are only slightly decreased since most of the emission sources from these sectors are far from the WGC tower and are not constrained by the inversion.

**Table 5.3.** Final *posterior* scaling factors for source inversions for each season obtained using the NOAA background.

| Source* | Summer 2012 | Early Fall | Late Fall | Winter | Winter-spring | Spring | Summer 2013 |
|---|---|---|---|---|---|---|---|
| **WW** | 0.92±0.49 | 1.05±0.5 | 1.13±0.5 | 1.06±0.5 | 1.18±0.5 | 0.98±0.5 | 1.08±0.49 |
| **LF** | 1.12±0.45 | 1.37±0.46 | 1.88±0.38 | 1.23±0.5 | 1.78±0.44 | 1.02±0.46 | 1.24±0.44 |
| **DLS** | 0.94±0.42 | 1.17±0.46 | 1.73±0.37 | 1.81±0.22 | 1.21±0.1 | 1.19±0.43 | 0.6±0.45 |
| **NDLS** | 1.12±0.48 | 1.16±0.49 | 1.45±0.49 | 1.21±0.49 | 1.66±0.48 | 1.17±0.48 | 1.03±0.49 |
| **NG** | 1.14±0.34 | 1.33±0.4 | 2.14±0.42 | 1.35±0.49 | 2.47±0.37 | 1.06±0.42 | 1.27±0.37 |
| **PL** | 0.93±0.49 | 1.07±0.5 | 1.17±0.5 | 1.04±0.5 | 1.26±0.5 | 0.99±0.5 | 1.03±0.5 |
| **WL** | 1.13±0.48 | 1.2±0.49 | 1.34±0.49 | 1.08±0.5 | 1.25±0.5 | 1.05±0.5 | 1.03±0.49 |
| **CP** | 1.21±0.25 | 0.86±0.3 | 0.98±0.5 | 0.99±0.5 | 0.96±0.5 | 0.99±0.45 | 0.53±0.34 |

*Source sectors include wastewater (WW), landfill (LF), dairy livestock (DLS), non-dairy livestock (NDLS), natural gas including petroleum production and local processing (NG), petroleum refining and mobile sources (PL), wetland (WL) and crop (CP, largely rice).

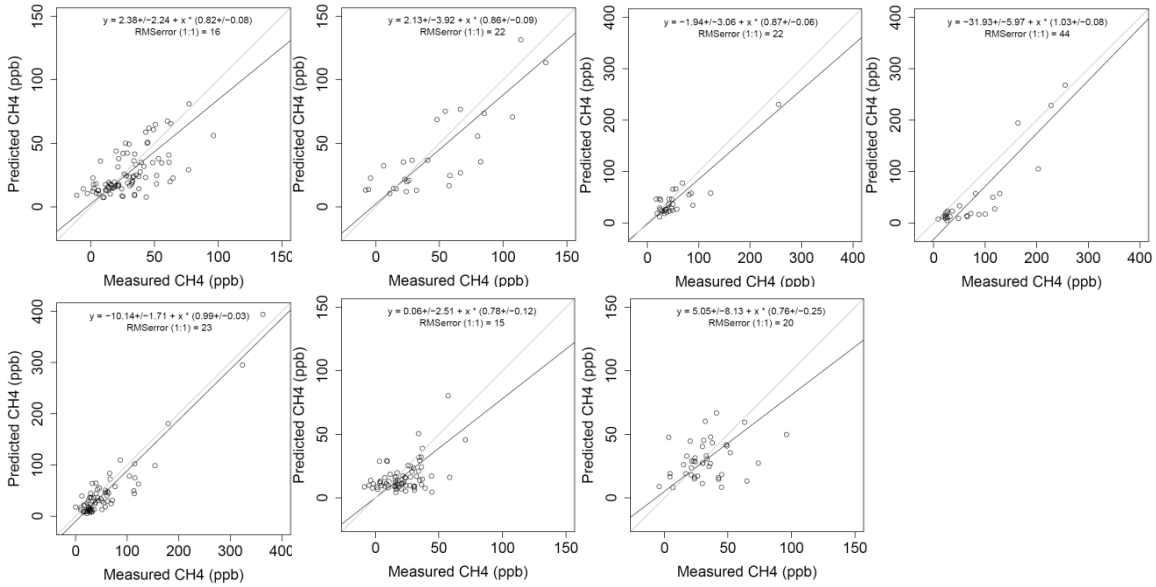


**Figure 5.6**. Comparison of $CH_4$ mixing ratios between measurements and predictions based on the final source inverse optimization using NOAA background for summer in 2012, early fall, late fall, winter (from left to right at top) and winter-spring, spring and summer in 2013 (from left to right at bottom).

We then examine the seasonal variations in *posterior* emissions from the inversion by source sector in each season in Figure 5.7 (left), and from the inversion by region for regions 3, 7 and 8 in Figure 5.7 (right). In general seasonal variations from specific sources are small compared to the *posterior* uncertainties. One exception is agriculture (CP), which is driven by seasonality of rice agriculture in region 3, where higher emissions are expected in summer due to flooding and agricultural production. Summing across source sectors for regions 3, 7, and 8 (regions sensitive to WGC), seasonal variations in total $CH_4$ emissions from these regions are also generally small compared to the *posterior* uncertainties. Using a t-test, we find that total emissions in late fall and winter of 2012 are higher (at 95% confidence) than summer, 2013, but not summer, 2012. Given potential for uncertainties in atmospheric transport and other factors, we recommend further studies to improve understanding of seasonal variations in $CH_4$ emissions from California.

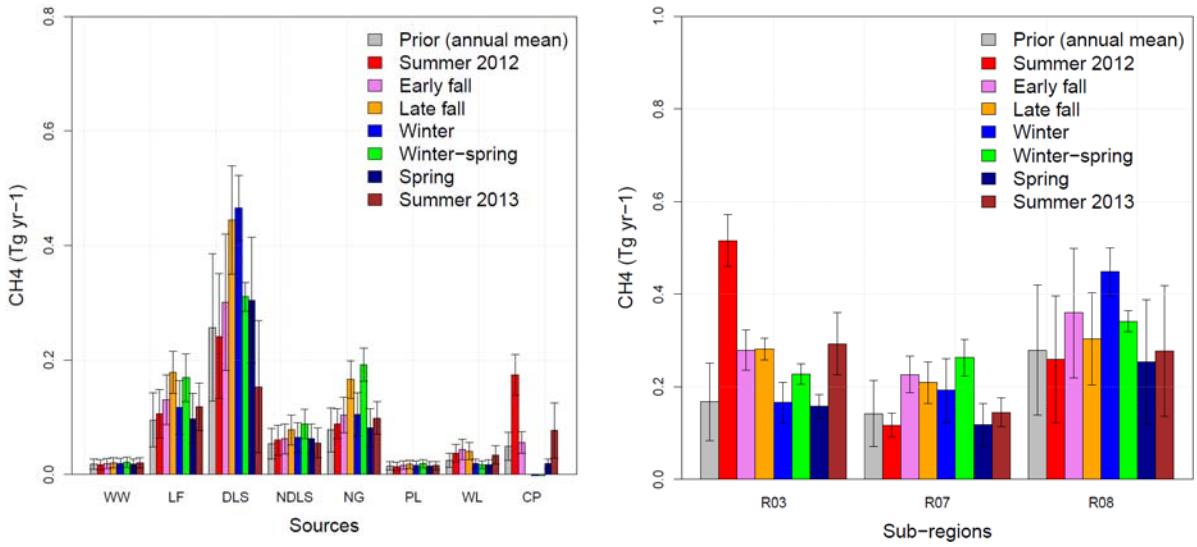


**Figure 5.7**. *Posterior* $CH_4$ emissions in region 3, region 7 and region 8 by different sources from source inversion analysis (left) and region inversion analysis (right) based on NOAA background.

To evaluate the annual total emissions from different source sectors, the annual prior and *posterior* emissions are compared in Table 5.4. For the three regions (3, 7, and 8) in central California, the inverse analysis suggests that actual total $CH_4$ emissions for the three regions are marginally higher (1.1 – 1.5, at 68% confidence) than the prior although most of the individual emission sectors are consistent with those of the prior within error. The main contribution to the *posterior* emission is dairy and non-dairy livestock accounting for about 51% of the total followed by landfills with ~17%, natural gas with ~16% and rice with ~7%. Wetland, petroleum, and wastewater each contributes 3 - 4% of the total. As in Jeong et al. (2012a), we find that there are anti-correlations (i.e., negative correlation coefficients; Tarantola, 1987) between the emissions from different source sectors. For instance, the correlation coefficient between DLS and LF is -0.34 in late fall while it is -0.39 between DLS and NG in summer 2013. This result suggests that the data used to drive these inversions does not allow us to uniquely resolve independent scaling factors such that only a linear combination of those scaling factors can be

**Table 5.4.** *A priori* and *posterior* annual $CH_4$ emissions (Tg $CH_4$ $yr^{-1}$) by source sector.

| Source* | Prior | *Posterior* |
|---|---|---|
| CP | 0.05 | 0.05±0.02 |
| DLS | 0.26 | 0.32±0.09 |
| LF | 0.10 | 0.13±0.04 |
| NDLS | 0.05 | 0.07±0.03 |
| NG | 0.08 | 0.12±0.03 |
| PL | 0.01 | 0.02±0.01 |
| WL | 0.02 | 0.03±0.01 |
| WW | 0.02 | 0.02±0.01 |
| **Total** | **0.59** | **0.76±0.11** |

*Source sectors include crop (CP, largely rice), dairy livestock (DLS), landfill (LF), non-dairy livestock (NDLS), natural gas including petroleum production and local processing (NG), petroleum refining and mobile sources (PL), wetland (WL) and wastewater (WW).

resolved. This highlights the importance of the VOC measurements and analysis in elucidating the relative contributions from different source sectors.

### *Sensitivity analysis*

In this study, we also considered the uncertainty from using different $CH_4$ background inflow data and the varied model-data-mismatch error. For background, in addition to the NOAA curtain product we used measurements from the THD site to represent clean air from the Pacific Ocean. We found that annual total emissions for the combined regions of 3, 7 and 8 are only slightly higher (0.75 +/- 0.12 vs. 0.68 +/- 0.12 Tg $CH_4$/yr) for the NOAA background than for that of THD, and consistent within the *posterior* uncertainties at 68% confidence level. The reason for the slight difference is that the NOAA background is generally slightly lower than THD measurements, resulting in slightly higher *posterior* emissions.

We also conducted a sensitivity test of *posterior* emissions to different model-data mismatch uncertainties in the **R** covariance matrix. Here, we perturbed the values in the **R** matrix by multiplying the original values (i.e., those used in Jeong et al., 2012a) by factors of 0.5 – 1.5.

Summing over source sectors, the annual total *posterior* emissions ranged from 0.74±0.11 to 0.76±0.12 Tg $CH_4$ $yr^{-1}$ with differences less than ~3% of the annual total emission.

### 5.3.3. Estimating $N_2O$ Emissions

#### *$N_2O$ Mixing Ratios*

As mentioned in Section 5.2, $N_2O$ measurements are available for 4 of the 7 seasons used in the $CH_4$ analysis during the period of 2012 - 2013. After applying the similar criteria for data inclusion as $CH_4$, the remaining background-subtracted mean $N_2O$ mixing ratios used in the first inversions are 1.28, 1.06, 0.31 and 0.74 ppb for late fall, winter, spring and summer 2013, respectively. Additionally, as shown in Figure 5.8, the minimum values of the measured $N_2O$ mixing ratios are close to the NOAA $N_2O$ background. We also note that only one data point in the winter season is removed due to a very large predicted signal relative to the measurement.

#### *Inversion analysis of $N_2O$*

Here, we estimate *posterior* emissions using the EDGAR 4.2 emission map scaled to the CARB emission by sector. We estimate $N_2O$ emissions for both sector (sector analysis) and region (region analysis). For source analysis we estimate $N_2O$ emissions for 15 source sectors, i.e. agricultural soils (AGS), indirect $N_2O$ emissions from agriculture (N2O), agricultural waste burning (AWB), manure management (livestock) (MNM), waste (solid and waste water) (WST), non-road transportation (TNR), road transportation (TRO), energy manufacturing transformation (EMT), indirect emissions from $NO_x$ and $NH_3$ (IDE), oil production and refineries (OPR), buildings (Residential and others) (RCO) and industrial processes and product use (IPU), ocean, forest, and other anthropogenic outside California. For region analysis, 19 scaling factors are solved to adjust the prior emissions including 16 regions in CA, region outside CA, ocean and

forest regions. As in $CH_4$, only the emissions in regions 3, 7 and 8 are considered in the *posterior* emissions. Following the first inversion, 16.9%, 7.0%, 0% and 1.6% (mean removal rate = 6.4%) of the data are removed for late fall, winter, spring and summer 2013, respectively. After outliers are removed, the SFBI is implemented for the second inversion. The best-fit slopes (prediction vs. measurement) and RMS errors after the final inversion are 0.94±0.04 (RMS error = 0.45 ppb), 0.89±0.09 (0.57 ppb), 0.63±0.05 (0.27 ppb) and 0.68±0.11 (0.41 ppb) in late fall, winter, spring and summer 2013, respectively. Before inversion, the best-fit slopes were lower and the RMS errors were larger compared to the post-inversion results: 0.52±0.04 (1.03 ppb), 0.56±0.14 (1.25 ppb), 0.48±0.04 (0.29 ppb) and 0.33±0.06 (0.58 ppb).

The scaling factors for individual source sectors are shown in Table 5.5 by season and Figure 5.10. Note that the scaling factor is the ratio of *posterior* to *a priori* emissions and, as described, we use *a priori* $N_2O$ emissions that are constant over time without seasonality. The seasonal variation in $N_2O$ emissions is most strong in the AGS sector as one might expect from the cycle of agricultural activity while other sectors show only small variations (Figure 5.10). This seasonal variation in AGS agrees with that in region 3 (Sacramento Valley) from the region analysis (Figure 5.10 right).

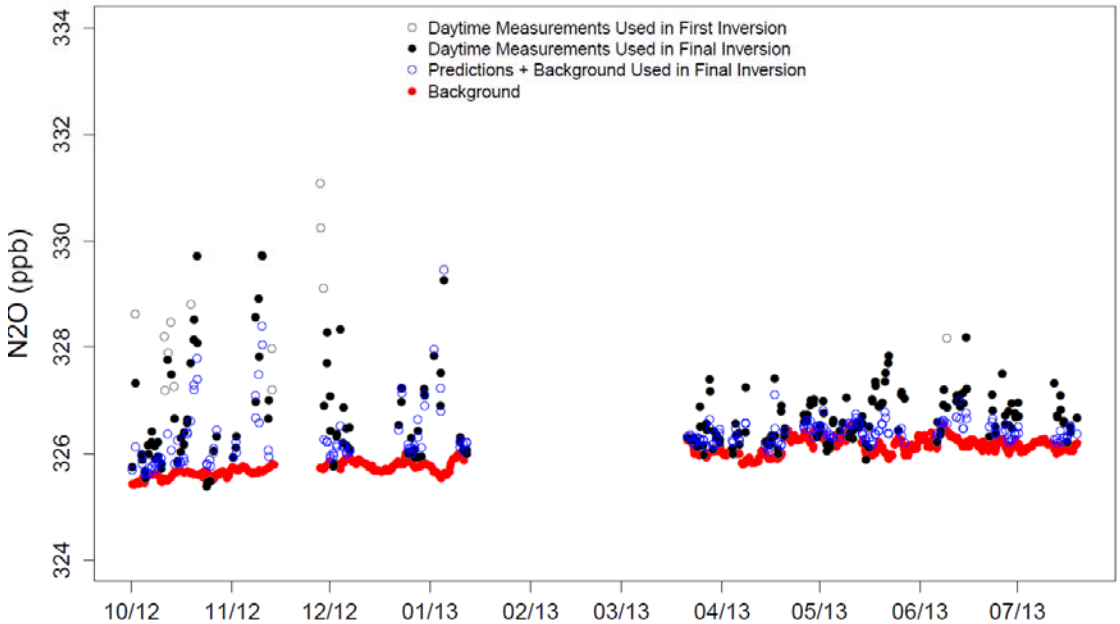


**Figure 5.8.** 3-hour $N_2O$ mixing ratio as a function of time (mm/yy): measured $N_2O$ mixing ratio during noon - afternoon hours used in the first inversion (gray open circle), measured $N_2O$ mixing ratio used in the final inversion (black filled circle), WRF-STILT predicted (used in final inversion) $N_2O$ mixing ratio + WRF-STILT predicted $N_2O$ background (NOAA background) mixing ratio during noon – afternoon hours used for the final inversion (blue open circle), and WRF-STILT predicted $N_2O$ background mixing ratio using the 3-D NOAA curtain (red dots).

**Table 5.5.** *Posterior* scaling factors (from final inversion) for $N_2O$ by season and source.

| Source* | Late Fall | Winter | Spring | Summer 2013 |
|---|---|---|---|---|
| **AGS** | 2.13±0.39 | 1.08±0.48 | 1.41±0.49 | 2.56±0.56 |
| **MNM** | 1.31±0.59 | 1.85±0.83 | 1.58±0.95 | 1.49±0.96 |
| **AWB** | 1.01±1 | 1±1 | 1±1 | 1.02±1 |
| **IPU** | 1.49±0.72 | 0.48±0.62 | 1.27±0.96 | 1.34±0.86 |
| **EMT** | 0.99±1 | 1.02±1 | 1.02±1 | 1.02±1 |
| **IDE** | 1.01±1 | 1±1 | 1.01±1 | 1.01±1 |
| **N2O** | 1.33±0.96 | 1.02±0.97 | 1.12±0.97 | 1.45±0.97 |
| **OPR** | 1±1 | 1±1 | 1±1 | 1±1 |
| **RCO** | 1±1 | 1±1 | 1.01±1 | 1.01±1 |
| **WST** | 1.04±0.97 | 1.06±0.99 | 1.08±0.99 | 1.14±0.98 |
| **TNR** | 1.01±1 | 1±1 | 1.01±1 | 1.01±1 |
| **TRO** | 1.27±0.96 | 0.85±0.97 | 1.24±0.98 | 1.46±0.97 |

*Source sectors include agricultural soils (AGS), manure management (MNM), agricultural waste burning (AWB), industrial processes and product use (IPU), energy manufacturing transformation (EMT), indirect emissions from NOx & $NH_3$ (IDE), indirect $N_2O$ emissions from agriculture (N2O), oil production & refineries (OPR), buildings (residential & others) (RCO), waste (solid & wastewater) (WST), non-road transportation (TNR), and road transportation (TRO).

We note that winter emissions from the AGS sector and region 3 are similar to the annual mean in the prior, which is consistent with the result in Jeong et al. (2012b). For IPU and TRO, the emissions are likely lower in winter than the other seasons, but due to the large uncertainty the seasonality is not easily distinguishable. The *posterior* uncertainty for AGS is significantly reduced for all seasons while the MNM emissions are constrained in late fall and the IPU emissions are somewhat constrained in late fall and winter. This is similar to the results shown in the $CH_4$ analysis where the *posterior* uncertainties vary by season and sector. However, as shown in Figure 5.10, the *posterior* uncertainties for other sectors remain high without much reduction after inversion. This suggests that we need more data to effectively constrain those sources. As with $CH_4$, *posterior* emissions show large anti-correlation between MNM, IPU, N2O and TRO. This result further suggests that the data do not allow the inversion system to independently estimate emissions and only a linear combination of sector emissions may be resolved. This suggests that there could be some trade-offs between regional emissions (e.g., between Region 7 and 8) and the total emission for the three regions can be estimated with more confidence than the individual regions. As in the $CH_4$ analysis, we also tested the sensitivity of estimated emissions to varying model-measurement errors by perturbing the estimates in Jeong et al. (2012b). We find that *posterior* emissions range from $0.022 \pm 0.005$ to $0.023 \pm 0.005$ Tg $N_2O$ per year.

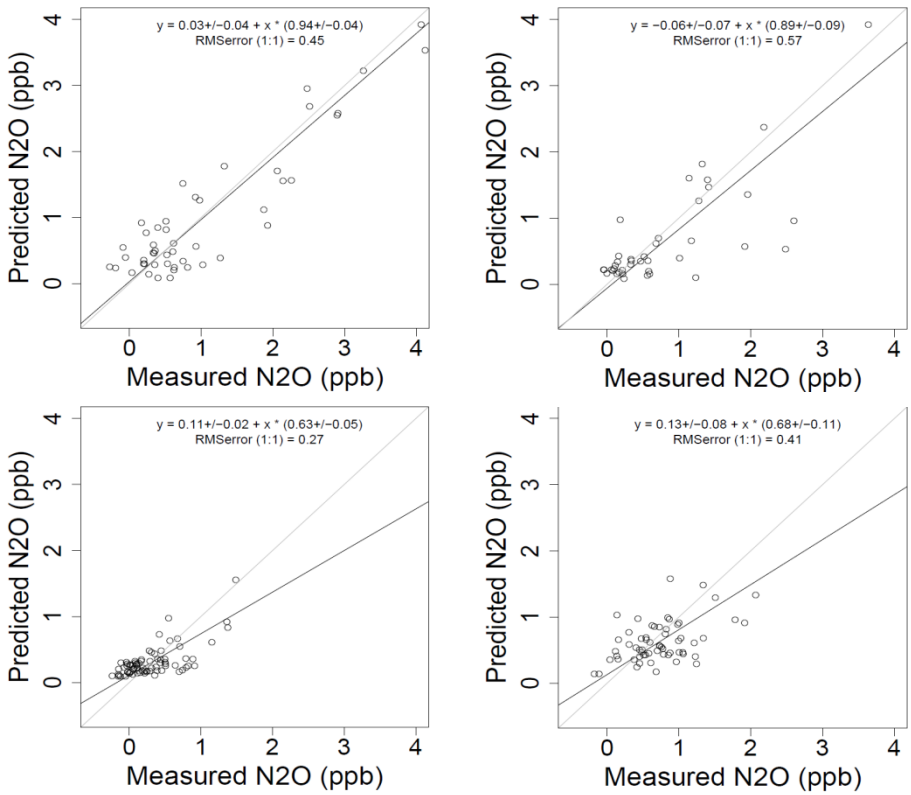


**Figure 5.9.** Comparison of $N_2O$ mixing ratios between measurements and predictions based on the final source inverse optimization using NOAA background for late fall (top left), winter (top right), spring (bottom left) and summer at 2013 (bottom right).

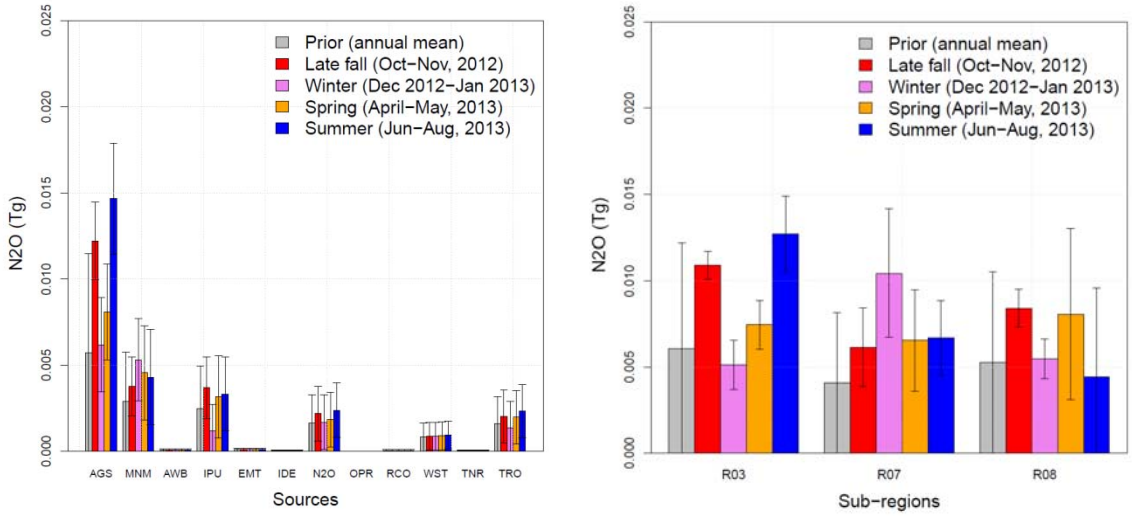


**Figure 5.10.** *Posterior* $N_2O$ emissions in region 3, region 7 and region 8 by different sources from source inversion analysis (left) and region inversion analysis (right). Source sectors include agricultural soils (AGS), manure management (livestock) (MNM), agricultural waste burning (AWB), industrial processes and product use (IPU), energy manufacturing transformation (EMT), indirect emissions from $NO_x$ and $NH_3$ (IDE), indirect $N_2O$ emissions from agriculture (N2O), oil production and refineries (OPR), buildings (residential and others) (RCO), waste (solid and waste water) (WST), non-road transportation (TNR) and road transportation (TRO).

**Table 5.6.** *A priori* and *posterior* annual $N_2O$ emissions (Tg $N_2O$ $yr^{-1}$) by source sectors.*

| Source Sectors | Prior | *Posterior* |
|---|---|---|
| AGS | 0.006 | 0.01±0.003 |
| AWB | 0 | 0±0 |
| EMT | 0 | 0±0 |
| IDE | 0 | 0±0 |
| IPU | 0.002 | 0.003±0.002 |
| MNM | 0.003 | 0.004±0.002 |
| N2O | 0.002 | 0.002±0.002 |
| OPR | 0 | 0±0 |
| RCO | 0 | 0±0 |
| TNR | 0 | 0±0 |
| TRO | 0.002 | 0.002±0.002 |
| WST | 0.001 | 0.001±0.001 |
| **Total** | **0.015** | **0.023±0.005** |

*The emission represents the total for regions 3, 7, and 8 near the WGC tower by source. Source sectors include agricultural soils (AGS), agricultural waste burning (AWB), energy manufacturing transformation (EMT), indirect emissions from NOx & $NH_3$ (IDE), industrial processes and product use (IPU), manure management (MNM), indirect $N_2O$ emissions from agriculture (N2O), oil production & refineries (OPR), buildings (residential & others) (RCO), non-road transportation (TNR), road transportation (TRO), and waste (solid & wastewater) (WST).

Here we note that the *posterior* emissions during 2012 - 2013 are somewhat lower than the previous result of 0.038±0.007 Tg $N_2O$ $yr^{-1}$ reported by Jeong et al. (2012b) for 2008 - 2009. To further investigate this difference, using the same setting as in this study, we conducted regional inversions for the period of 2008 - 2009 using the same prior emissions and $N_2O$ background inflow that is specific to the Eastern Pacific that we use for the current inversion of the 2012 - 2013 period. Using the updated prior emissions and background, we find annual *posterior* 2008 - 2009 $N_2O$ emissions for regions 3, 7, and 8 is 0.028±0.005 Tg $N_2O$ $yr^{-1}$, which is lower than the estimate reported by Jeong et al. (2012b), and consistent with the *posterior* emission estimated for 2012 - 2013.

## 5.4. Discussion

The inferred annual *posterior* emissions in regions 3, 7 and 8 near the WGC tower are 0.75±0.11 Tg $CH_4$ $yr^{-1}$ based on the NOAA background, which is 1.27±0.21 time the prior $CH_4$ emissions, suggesting *posterior* emissions for this region are not significantly different from the prior model. From the source sector perspective, the result suggests that the DLS, LF are the main contributors to the emissions around the WGC tower, with little evidence of statistically significant seasonal variations in $CH_4$ emissions, with the exception of crop agriculture, where seasonal variations of *posterior* emission is likely driven by the seasonality of rice emissions observed in previous work (McMillan et al., 2007; Peischl et al., 2012).

For $N_2O$, the total annual *posterior* emission for regions 3, 7 and 8 is 0.023±0.005 Tg $N_2O$ $yr^{-1}$ for both source and region analyses, which is 1.53 ± 0.33 times larger than the prior estimate used in this study (0.015 Tg $N_2O$ $yr^{-1}$). This suggests $N_2O$ emissions from the region surrounding WGC were only marginally larger than the prior model in 2012 - 2013. Re-examining previous work by Jeong et al. (2012b), we find that applying the updated prior emission model and marine background $N_2O$ specific to the Eastern Pacific used in the current work reduce *posterior* emissions estimated for the earlier 2008 - 2009 period such that they are indistinguishable from emissions in the 2012 - 2013 period given the uncertainties of the two analyses. Last, the inversions suggest there is an observable seasonal pattern to $N_2O$ emissions, with maxima in late fall and summer, and lower emissions in winter and spring that is likely due to variation from agricultural (AGS) sources.

This chapter reported the inverse model estimates of $CH_4$ and $N_2O$ emissions for the June 2012 - August 2013 period conducted at WGC, for the purpose of comparison with PMF-derived

source apportionment results (from Chapter 4). In Chapter 6, the results of inverse modeling are compared with those of the PMF analysis and further discussion is presented. The inverse model results from CARB project # 11-306 for the region surrounding WGC are in the same range as those obtained for the time period (2012-2013) of this project.

## 5.5. References


Andrews, A. E., J. D. Kofler, M. E. Trudeau, J. C. Williams, D. H. Neff, K. A. Masarie, D. Y. Chao, D. R. Kitzis, P. C. Novelli, C. L. Zhao, E. J. Dlugokencky, P. M. Lang, M. J. Crotwell, M. L. Fischer, M. J. Parker, J. T. Lee, D. D. Baumann, A. R. Desai, C. O. Stanier, S. F. J. De Wekker, D. E.Wolfe, J. W. Munger, and P. P. Tans (2014), $CO_2$, CO, and $CH_4$ measurements from tall towers in the NOAA Earth System Research Laboratory's Global Greenhouse Gas Reference Network: instrumentation, uncertainty analysis, and recommendations for future high-accuracy greenhouse gas monitoring efforts, *Atmos. Meas. Tech.Atmospheric Measurement Techniques*, **7**(2), 647-687.

Bergamaschi, P., M. Krol, F. Dentener, A. Vermeulen, F. Meinhardt, R. Graul, M. Ramonet, W. Peters, and E. J. Dlugokencky (2005), Inverse modelling of national and European $CH_4$ emissions using the atmospheric zoom model TM5, *Atmos. Chem. Phys.*, **5**, 2431–2460.

Bianco, L., I. V. Djalalova, C. W. King, and J. M. Wilczak (2011), Diurnal evolution and annual variability of boundary-layer height and its correlation to other meteorological variables in California's Central Valley, *Boundary-Layer Meteorology*, **140**, 491-511, DOI 10.1007/s10546-011-9622-4, 1-21.

Bouwman, A.F., K.W. van der Hoek and J.G.J. Olivier (1995), Uncertainties in the global source distribution of nitrous oxide Journal of Geophysical Research 100, 2785-2800.

CARB (2014), California Greenhouse Gas Emissions Inventory. California Air Resources Board Staff Report, Accessed January 2015 (http://www.arb.ca.gov/cc/inventory/inventory.htm, version March 2014).

CARB (2015), California Greenhouse Gas Emissions Inventory. California Air Resources Board Staff Report, Accessed September 2015 (http://www.arb.ca.gov/cc/inventory/inventory.htm, version April 2015).

Cleveland, C. C., B. W. Sullivan (2012), Biogeochemistry: drought and tropical soil emissions, *Nature*, **489**(7415), 211-2.

Gerbig, C, J. Lin, S. Wofsy, B. Daube, A. E. Andrews, B. Stephens, P. S. Bakwin, and C. Grainger (2003), Toward constraining regional-scale fluxes of $CO_2$ with atmospheric observations over a continent: 2. Analysis of COBRA data using a receptor-oriented framework, *J. Geophys. Res.*, **108**(D24), 10.1029/2003JD003770.

Gimson, N. R. and M. Uliasz (2003), The determination of agricultural methane emissions in New Zealand using receptor-oriented modelling techniques, *Atmos. Environ.*, **37**, 3903-3912.

Hall, B. D., et al. (2014). Results from the International Halocarbons in Air Comparison Experiment (IHALACE), *Atmos. Meas. Tech.*, 7(2), 469–490.

Houweling, S., T. Kaminski, F. Dentener, J. Lelieveld, and M. Heimann (1999), Inverse modeling of methane sources and sinks using the adjoint of a global transport model, *J. Geophys. Res.*, **104**(D21), 26137-26160..

Jeong, S., C. Zhao, A. E.Andrews, L. Bianco, J. M. Wilczak and M. L. Fischer (2012a), Seasonal variation of CH4 emissions from central California. *Journal of Geophysical Research - Atmospheres* **117**, no. D11.

Jeong, S., C. Zhao, A. E., Andrews, E. J. Dlugokencky, C. Sweeney, L. Bianco, J. M. Wilczak,and M. L. Fischer, (2012b), Seasonal variations in N2O emissions from central California, *Geophysical Research Letters* **39**, L16805.

Jeong, S., Y.-K. Hsu, A. E.Andrews, L. Bianco, P.Vaca, J. M. Wilczak, and M. L. Fischer (2013), A multitower measurement network estimate of California's methane emissions, *J. of Geophysical Research: Atmospheres* **118**, 339-351.

Jeong, S., D. Millstein, and M. L. Fischer (2014) Spatially Explicit Methane Emissions from Petroleum Production and the Natural Gas System in California, *Environmental Science & Technology,* **48** (10), 5982-5990.

Kort, E. A., J. Eluszkiewicz, B. B. Stephens, J. B. Miller, C. Gerbig, T. Nehrkorn, B. C. Daube, J. O. Kaplan, S. Houweling, and S. C. Wofsy (2008), Emissions of $CH_4$ and $N_2O$ over the United States and Canada based on a receptor-oriented modeling framework and COBRA-NA atmospheric observations, *Geophy. Res. Lett.*, **35***,* L18808, doi:10.1029/2008GL034031.

Lin, J. C., C. Gerbig, S. C. Wofsy, A. E. Andrews, B. C. Daube, K. J. Davis, and C. A. Grainger (2003), A near-field tool for simulating the upstream influence of atmospheric observations: The Stochastic Time-Inverted Lagrangian Transport (STILT) model, *J. Geophys. Res.*, **108**(D16), 4493, doi:10.1029/2002JD003161.

McMillan, A. M. S., M. L. Goulden, and S. C. Tyler (2007), Stoichiometry of CH4 and CO2 flux in a California rice paddy, *J. Geophys. Res.*, 112, G01008, doi:10.1029/2006JG000198.

Meyer, D., P. L. Price, H. A. Rossow, N. Silva-del-Rio, B. M. Karle, P. H. Robinson, E. J. DePeters, J. G. Fadel (2011), Survey of dairy housing and manure management practices in California, *Journal of Dairy Science*, **94** (9), 4744-4750.

Mesinger, F., et al. (2006), North American Regional Reanalysis, *Bull. Amer. Meteor. Soc.*, **87** (3), 343-360.

Nehrkorn, T., J. Eluszkiewicz, S. C. Wofsy, J. C. Lin, C. Gerbig, M. Longo, and S. Freitas (2010), Coupled weather research and forecasting - stochastic time-inverted lagrangian transport (WRF-STILT) model, *Meteor. Atmos. Phys.*, **107** (1), 51-64, doi:10.1007/s00703-010-0068-x.

Pacala, S. W., C. Breidenich, P. G. Brewer, I. Y. Fung, M. R. Gunson, G. Heddle, B. E. Law, G. Marland, K. Paustian, M. Prather, J. T. Randerson, P. P. Tans, and S. C. Wofsy (2010), *Verifying greenhouse gas emissions: Methods to support international climate agreements*, Committee on Methods for Estimating Greenhouse Gas Emissions, National Research Council.

Peischl, J., et al. (2012), Airborne observations of methane emissions from rice cultivation in the Sacramento Valley of California, *J. Geophys. Res.*, 117, D00V25, doi:10.1029/2012JD017994.

Peischl, J., et al. (2013), Quantifying sources of methane using light alkanes in the Los Angeles basin, California, *J. Geophys. Res. Atmos.*, 118, doi:10.1002/jgrd.50413.

Press, W. H., S. A.Teukolsky, W. T. Vetterling, and B.P. Flannery (1992), *Numerical Recipes, 2nd edition*. Cambridge: Cambridge University Press.

Prinn, R.G., et al (2000), A history of chemically and radiatively important gases in air deduced from ALE/GAGE/AGAGE. *J. Geophys. Res. Atmos.*, 105, D14, 17751–17792.

Skamarock, W.C., J. B. Klemp, J. Dudhia, D.O. Gill, D. M. Barker, X. Z. Huang, W. Wang, and J. G. Powers (2008), A description of the advanced research WRF version 3. Technical Note 475+STR. Mesoscale and Microscale Meteorology Division, NCAR, Boulder,

Colorado.

Tarantola, A. (1987), *Inverse Problem Theory Methods for Data Fitting and Model Parameter Estimation*, 613 pp., Elsevier, New York.

Wennberg, P. O., W. Mui, D. Wunch, E. A. Kort, D. R. Blake, E. L. Atlas, G. W. Santoni, S. C. Wofsy, G. S. Diskin, S. Jeong, and M. L. Fischer (2012), On the Sources of Methane to the Los Angeles Atmosphere. *Environ. Sci. Technol.*, 46 (17), 9282 - 9289, doi:10.1021/es301138y.

Xiang, B., et al. (2013), Nitrous oxide ($N_2O$) emissions from California based on 2010 CalNex airborne measurements, J. Geophys. Res. Atmos., 118, 2809–2820, doi:10.1002/jgrd.50189.

Zhao, C., A. E. Andrews, L. Bianco, J. Eluszkiewicz, A. Hirsch, C. MacDonald, T. Nehrkorn, and M. L. Fischer (2009), Atmospheric inverse estimates of methane emissions from Central California, *J. Geophys. Res.*, **114**, D16302.

# 6. PMF based $CH_4$ and $N_2O$ source apportionment at Walnut Grove

## 6.1. Comparison with inventory source distribution

We herein present a direct comparison of PMF-derived $CH_4$ and $N_2O$ source apportionment with distributions in regional inventories derived from 'bottom-up' sources (Figures 6.1 a and 6.1 b, respectively). Spatially resolved sector-wise 0.1° × 0.1° *a priori* $CH_4$ emissions maps with seasonal components, developed using the CALGEM emission model (Jeong et al., 2013) and scaled to match the 2012 statewide inventory for anthropogenic emission sectors (CARB, 2014; September 2014 version) as described in Section 5.2.2, is used to create the $CH_4$ inventory pie chart (Figure 6.1 a). The PMF analysis that we perform is reflective of regional sources and source contributions. Hence, in the derivation of the annual CALGEM $CH_4$ source distribution pie chart, we only include source contributions from the three zones that surround the WGC site and are expected to have maximum contribution to the observed $CH_4$ enhancements which are regions 3, 7 and 8 in Figure 5.2 (formerly Regions 6,7, and 8; Figure 1; Jeong et al., 2013).

We find that the contribution of $CH_4$ emissions from the dairy and livestock sector remains dominant in the regional CALGEM inventory (58 %). This is generally consistent with the range of PMF-based apportionment across all seasons using averaged seasonal contributions (61- 90 %; Figure 6.2 a-f) though the relative share of $CH_4$ from the dairy and livestock sector is higher during the fall and winter season as compared to summers, when other local sources of $CH_4$ are more active. The waste management source (landfills and waste water treatment combined) is the next largest contributor to the 'bottom-up' inventory (21 %). This source is not separately detected in the season-wise PMF results at WGC as contributions from this primarily

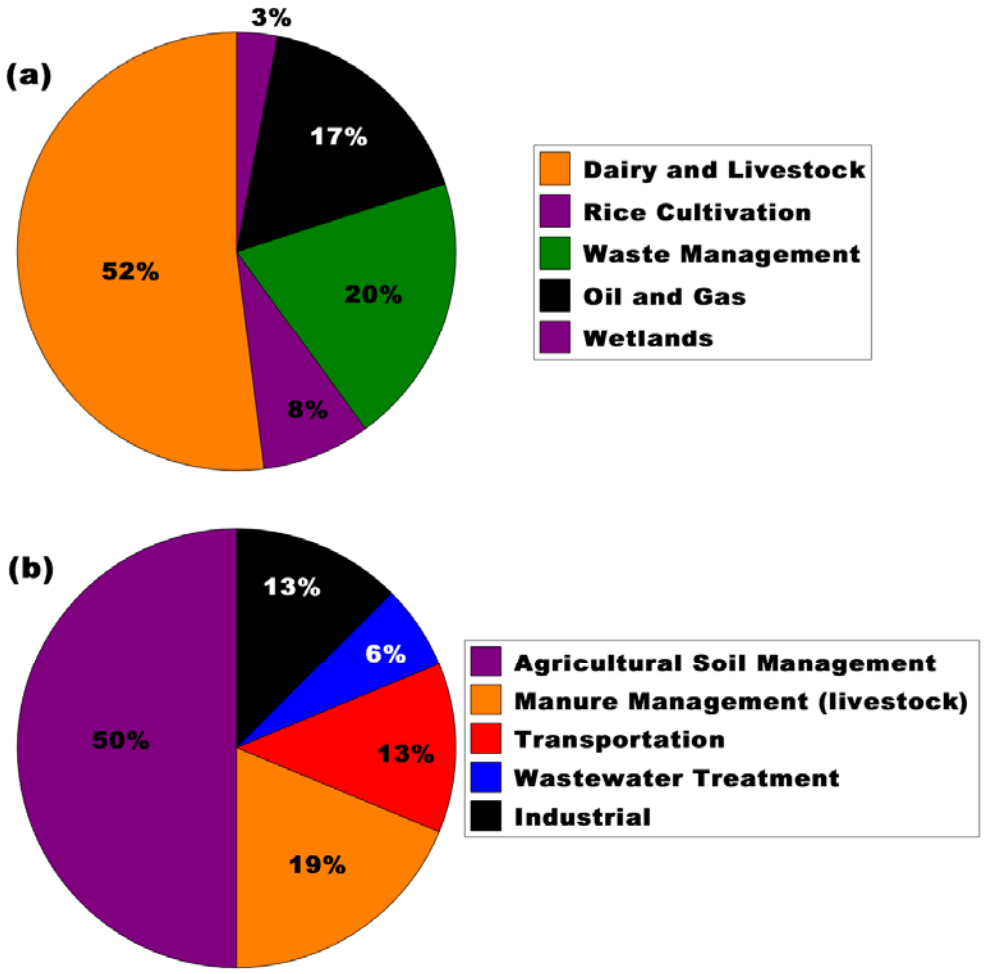


**Figure 6.1.** Pie charts representing (a) 2008 CALGEM $CH_4$ emissions from regions 3, 7 and 8 scaled to match 2012 ARB state totals for anthropogenic emission sectors; and (b)2008 EDGAR v4.2 $N_2O$ distribution over Regions 3,7 and 8 scaled to 2012 ARB inventory total.

urban source is likely beyond the region of influence of this apportionment analysis and even if detected, is likely to be included in the 'urban and oil / gas' source sector (in black color in Figures 6.2 a-f) due to the largely far-upwind and urban location of these landfills.

In the early fall season, the wind directions are predominantly westerly (Figure 3.3 b) which causes the San Francisco Bay Area and its constituent landfills, waste water treatment plants and natural gas distribution $CH_4$ sources to lie upwind of WGC thus increasing the influence of the mostly urban Region 7 defined in Jeong et al. (2013) on WGC signals. We see

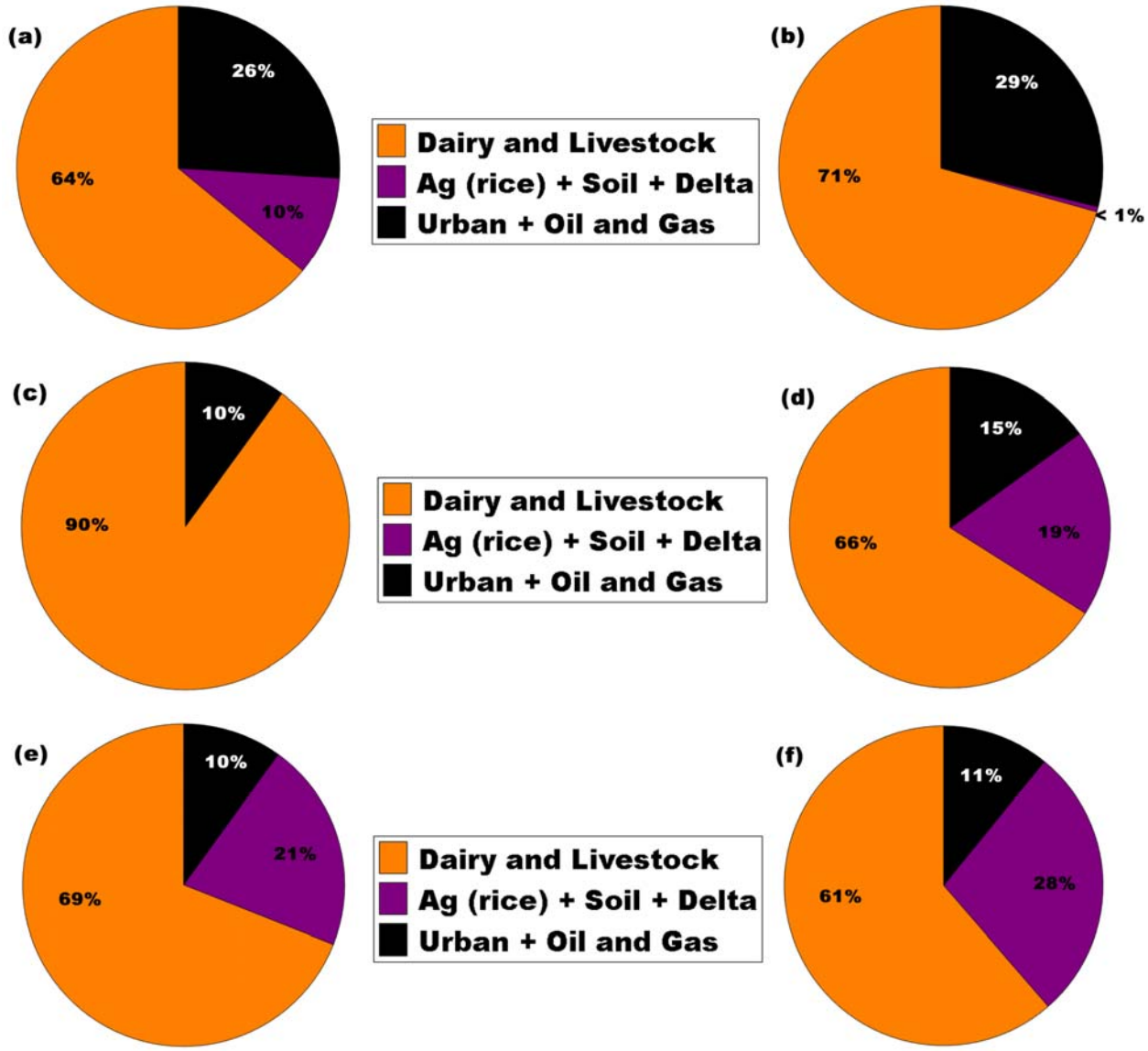


**Figure 6.2.**, Pie charts representing PMF-derived source-wise $CH_4$ emissions distribution at Walnut Grove tower during (a) early fall 2012, (b) late fall 2012, (c) winter, (d) winter-spring 2013, (e) spring 2013, and (f) summer 2013. We note that this figure does not convey the uncertainties in apportioning $CH_4$ to the dominant sources and correspondingly little significance in attribution to weak or distant sources *(see section 4.2.2)*.

that during this season, the relative share of $CH_4$ emissions arising from the 'urban and oil / gas source' (26 %) is similar to that observed from summing of 'waste management' and 'oil and gas' $CH_4$ emissions in the regional CALGEM inventory (31 %). In winters, when prevailing wind directions are generally along the valley floor (Figures 3.2 d and 3.3 d), the 'urban and oil /

gas' source has a lesser influence on $CH_4$ emissions distribution (Figure 6.2 c) while influence of the dairies present in the Central Valley is much more prominent.

The differences we observe in the annual accounting are mostly due to the magnitude of $CH_4$ emissions from wetlands (natural or anthropogenic) which are also accounted for in the CALGEM inventory but without account for seasonality. Together with the $CH_4$ emissions from rice cultivation, the flooded agriculture/wetland ecosystems in the region account for about 11 % of $CH_4$ emissions annually in the CALGEM inventory (purple portions in Figure 6.1 a). We find that $CH_4$ emissions from the equivalent 'ag + soil + delta' source sector are heavily dependent on seasons - with an almost non-existent contribution to the $CH_4$ source apportionment during winter, and up to 28 % of the local $CH_4$ emissions during the summer. In general, the 'bottom-up' inventories for $CH_4$ are in reasonable agreement with the PMF-derived seasonal distribution of $CH_4$ emissions at WGC with respect to the major sources. The variations in the distributions that we encounter principally result from and can be accounted for based on the seasonal nature of certain $CH_4$ sources (e.g. rice cultivation and wetlands), missing / underestimated sources (e.g. natural gas operations in the upwind Rio Vista fields), and prevailing seasonal meteorology ( e.g. for urban sources). $CH_4$ emissions from wetland / soil management processes in the Delta (e.g. flooding of peatland pastures to build carbon and prevent soil subsidence) and rice cultivation are significant contributors to the observed ambient $CH_4$ enhancements at WGC. Top-down California specific assessments to quantify the anthropogenic contribution to $CH_4$ emissions from artificial wetlands will help determine the magnitude of these emissions and account for them in the ARB inventory.

We present regional emissions derived from high- resolution (0.1° × 0.1°) US-totaled $N_2O$ emission model maps EDGAR42 (European Commission Joint Research Centre and

Netherlands Environmental Assessment Agency, Emission Database for Global Atmospheric Research (EDGAR), release version 4.2, 2010, http://edgar.jrc.ec.europa.eu) in Figure 6.1 b. We use the 0.1 degree EDGAR maps to generate source specific emission maps for our prior emission model (in Chapter 5). In this case, we scale each sector to match the 2012 ARB source sector totals at the state level (CARB, 2014). We then sum over the 0.1 degree pixels within Regions 3, 7, and 8 and include those sums in Table 5.6 and in Figure 6.1 b. For reference, the statewide $N_2O$ emissions distribution in the ARB inventory is, in general, consistent with that calculated for the entire country in the EDGAR inventory with respect to major sources with the exception being that $N_2O$ emissions from industrial sources (primarily by-product of industry production of nitric acid and adipic acid) are primarily located outside of California and hence do not feature in the ARB inventory. But there are certain contrasting features that stand out when these 'bottom-up' inventories are compared with the PMF-derived $N_2O$ averaged seasonal source distributions at WGC. We present the seasonally resolved PMF-derived $N_2O$ source distribution pie charts in Figures 6.3 a-d. Firstly, manure management in the dairy and livestock sector is a significantly larger source of $N_2O$ at WGC than the prior emissions in the ARB-scaled EDGAR inventory which is also used for the inverse modeling. Secondly, $N_2O$ emissions from 'agricultural soil management' at WGC display a strong seasonal nature with the emission trend coinciding with that of N fertilizer use during the agricultural growing season. Negligible $N_2O$ emissions are observed during the winter fallow season. This seasonal variability is not represented in the EDGAR inventory. This could potentially result in a different annual emission estimate than that computed using an approach which takes environmental factors causing the seasonality of $N_2O$ emissions into account. This variability may impact inventory verification and validation conclusions for $N_2O$, especially when comparing with emissions

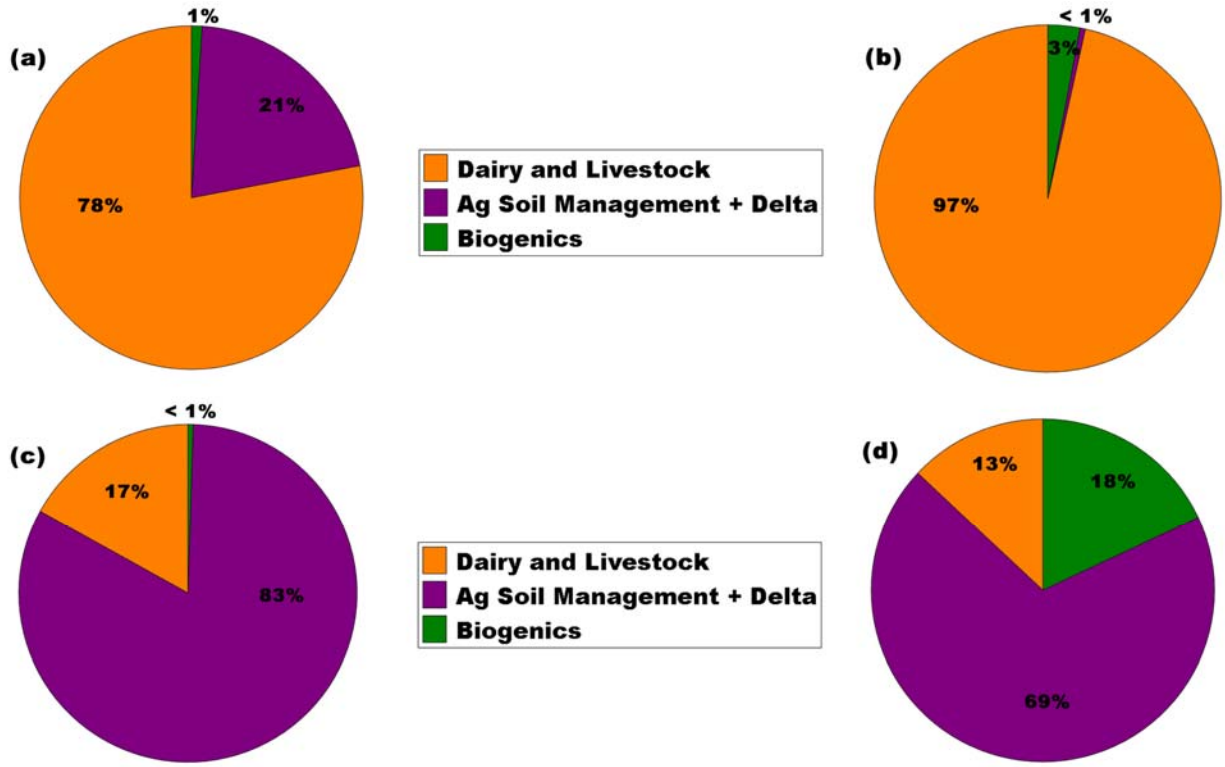


**Figure 6.3.** Pie charts representing PMF-derived source-wise $N_2O$ emissions distribution at Walnut Grove tower during (a) late fall 2012, (b) winter, (c) spring 2013, and (d) summer 2013. We note that this figure does not convey the uncertainties in apportioning $N_2O$ to the dominant sources and correspondingly little significance in attribution to weak or distant sources (see Section 4.2.2).

derived from short-duration studies to annual inventory estimates. Finally, but perhaps most importantly, we do not see evidence of $N_2O$ emissions originating from the transportation sector (primarily from urban regions) influencing the WGC site. The PMF analysis consistently produces an 'urban and oil / gas source' (black factor in Figures 6.2 a-f) that likely contains $CH_4$ contributions from urban sources (including from landfills) but no $N_2O$ is apportioned to this source in any season. This finding is consistent with the absence of $N_2O$ in the 'vehicle emission' source profile observed at Bakersfield (Guha et al., 2015). Both the statewide ARB inventory (CARB, 2015) and the regional EDGAR inventory (Figure 6.1 b) have a substantial fraction of $N_2O$ emissions attributed to the transportation sector. This mismatch highlights a need for further evaluation of the bottom-up statewide inventory of $N_2O$ emissions from the transportation sector.

## 6.2. Comparison with Bayesian inverse analysis based source distribution

The mean data from Figures 5.7 (left) and 5.10 (left) have been used to create the seasonally apportioned, inverse dispersion-derived, source-wise emissions distribution $CH_4$ and $N_2O$ pie charts as seen in Figures 6.4 and 6.4, respectively. It must be noted that the regional emissions represented in the CALGEM $CH_4$ distribution (Figure 6.1 a) are specific to California's Regions 6, 7 and 8 (Jeong et al., 2013) while the analysis conducted in Chapter 5 focuses on Regions 3, 7 and 8. Region 6 in prior analyses (Jeong et al., 2013) is similar to the current Region 3. The current Region 3 is actually Region 6 + Region 11 (small emissions as compared to Region 6) in Jeong et al. (2013) The change has been applied to be consistent with ARB's air basin classification in the most recent work. We combine inverse-analysis regional $CH_4$ emissions from the waste water (WW), landfill (LF), natural gas (NG) and petroleum (PL) sectors into a single category in Figure 6.4. The $CH_4$ emissions sources contributing to this group are mostly located in Region 7, and hence summation of $CH_4$ emissions from this group can be best categorized and represented by the PMF-derived 'urban + oil and gas' source factor.

On comparison of the season-specific plots in Figure 6.2 (a-f) and Figure 6.4 (a-f), we observe that the 'dairy and livestock' source (generated by combining DLS and NDLS sectors from Chapter 5) generally remains the dominant source of $CH_4$ in the Bayesian analysis. The contribution of the 'urban + oil and gas' source to the Bayesian seasonal distribution is also significant throughout the annual cycle and is consistently larger than the same source's contribution to the PMF-derived apportionment for all seasons. At the same time, the contribution of $CH_4$ emissions from the 'agriculture + delta' source is larger in the apportionment based on PMF analysis as compared to the inverse analysis distribution. These observations

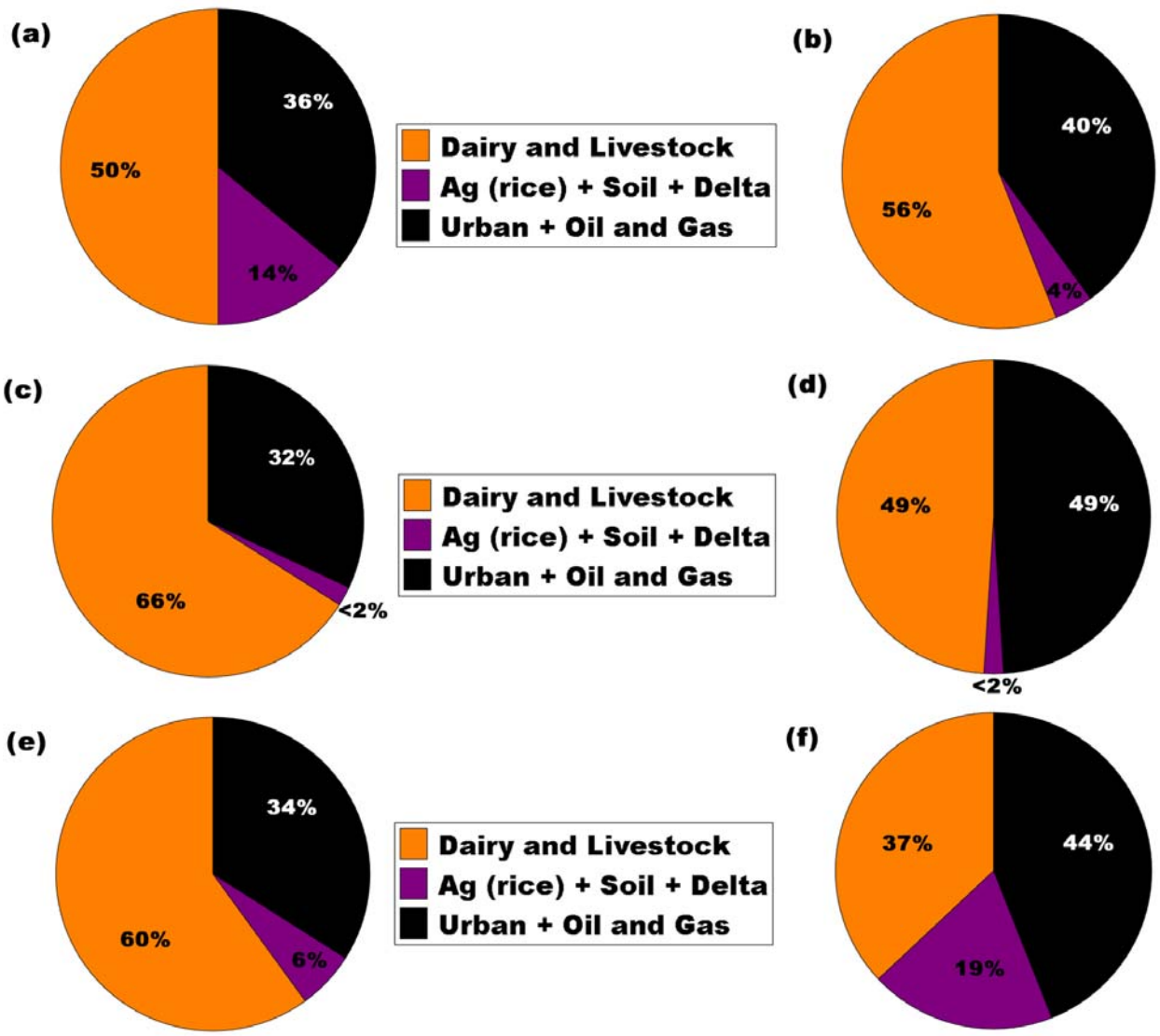


**Figure 6.4.** Pie charts illustrating the distribution of $CH_4$ emissions (percentage of total) from regional sources (Region 3, 7 and 8) using Bayesian inverse analysis as described in Chapter 5. The pie charts represent (a) early fall 2012, (b) late fall 2012, (c) winter, (d) winter-spring 2013, (e) spring 2013, and (f) summer 2013. We note that these figures do not convey uncertainties in the estimates which are presented in Section 5.3.2 and Table 5.3.

suggest that the efficacy of PMF analysis is limited by location of emissions sources with respect to the receptor location. The urban sources of $CH_4$ emissions are far enough from WGC (> 100 km) that $CH_4$ enhancements from the sources in this region (Region 7) are reasonably well-mixed and diluted as they arrive at WGC. Thus, while PMF analysis lacks the statistical power to apportion relatively minor and far away sources, the contribution of the 'urban + oil and gas' source itself seems to be under-represented in the PMF distribution. Using the same logic, we

conclude that emissions from relatively nearby sources such as livestock, wetlands and rice agriculture produce distinct enhancement signals that are distinguishable and can be partitioned using PMF. Hence the PMF-based results illustrated in Figures 6.2 a-f, which apportion a larger share of observed enhancements to nearby sources (like livestock) as compared to farther sources (like urban and oil and gas), is representative of a smaller regional footprint than that which is estimated by the Bayesian inverse analysis in Figures 6.4 a-f. Nonetheless, the relative distribution of three major $CH_4$ source categories in the region estimated from the same receptor location (WGC), over the same annual time frame and using two independent and different apportionment techniques are similar and cannot be clearly distinguished given the uncertainties in both techniques.

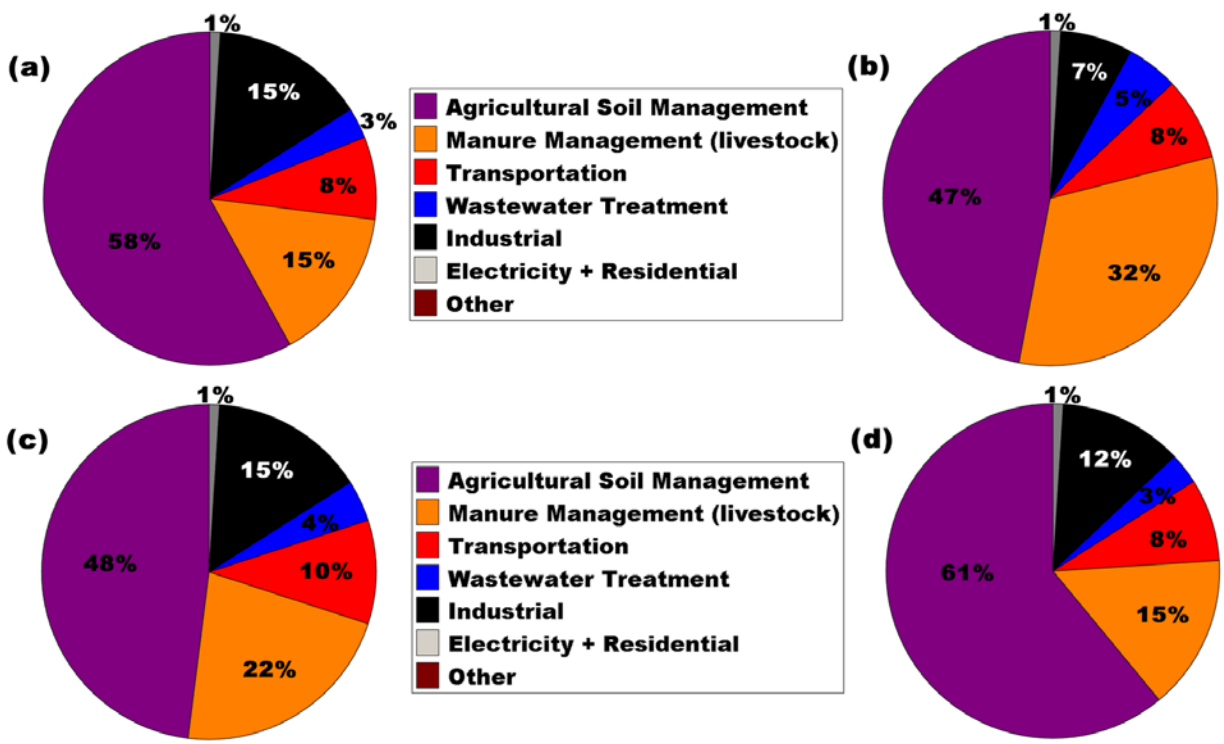


**Figure 6.5.** Pie charts illustrating the distribution of $N_2O$ emissions (percentage of total) from regional sources (Regions 3, 7 and 8) using Bayesian inverse analysis as described in Chapter 5. The pie charts represent (a) late fall 2012, (b) winter, (c) spring 2013, and (d) summer 2013. We note that these figures do not convey uncertainties in estimates which are presented in Section 5.3.3 and Table 5.5. Refer to Figure 5.10 for absolute emissions from each source in each season.

The pie charts in Figure 6.5 a-d represent the season-specific $N_2O$ emissions source distribution, derived using Bayesian inverse analysis (Chapter 5) from WGC tower with a regional footprint representing Regions 3, 7 and 8. A comparison of the PMF-derived plots (Figure 6.3 a-d) and inverse analysis plots (Figure 6.5 a-d) indicates that while PMF is able to detect a clear seasonal pattern to $N_2O$ emissions from the 'ag soil management and delta' source factor, a smaller temporal pattern is captured in the inverse analysis distribution. This may be in part because the *a priori* emission model does not incorporate seasonally varying nitrogen use activity data to that extent of detail that simulates real-time situations. However, it is critical to note that the PMF analysis, which relies on day-night differences in mixing ratio to estimate relative source contributions, is more sensitive to local emissions than the more regionally averaged signals obtained from the daytime measurements used in the Bayesian inverse model analysis. This leads to different footprints affecting the Bayesian and PMF results, with the prevalence of more local valley sources having larger contributions in the PMF analysis. Hence agricultural soils, which can be a very large local $N_2O$ source, appear disproportionately large during the summer. In contrast, manure management source is relatively smaller in the PMF results while it represents a more significant source of $N_2O$ emissions in the inverse analysis. Emissions of $N_2O$ from transportation sector (red), wastewater treatment (blue) and industrial processes (black), originating in the urban core of the San Francisco Bay Area do not create a large day-night difference as they are relatively well-mixed as they arrive at WGC and are hence not differentiated by the PMF analysis and in the corresponding plots (Figure 6.3 a-d). The inverse analysis plots, derived from *a priori* inventory information, do resolve the measured enhancements into contributions from numerous $N_2O$ emissions sources including transportation,

waste treatment, electricity and residential use and industrial processes. PMF and inverse modeling analysis thus each provide analytical resources that are complimentary.

## 6.3. References

CARB (2014), California Greenhouse Gas Inventory for 2000-2012 - by IPCC Category. http://www.arb.ca.gov/cc/inventory/data/data.htm. accessesd on September 23, 2014.

Guha, A., Gentner, D. R., Weber, R. J., Provencal, R., and Goldstein, A. H.: Source apportionment of methane and nitrous oxide in California's San Joaquin Valley at CalNex 2010 via positive matrix factorization, Atmos. Chem. Phys., 15, 12043-12063, doi:10.5194/acp-15-12043-2015, 2015.

Jeong, S., Y.-K. Hsu, A. E.Andrews, L. Bianco, P.Vaca, J. M. Wilczak, and M. L. Fischer (2013), A multitower measurement network estimate of California's methane emissions, *J. of Geophysical Research: Atmospheres* **118**, 339-351.

# 7. Summary and Recommendations

## 7.1. Summary of source speciation work using VOCs

In this report we attempt to understand the spatial and temporal distribution of $CH_4$ and $N_2O$ sources by conducting year-round measurements from a tall television transmission tower in Walnut Grove (WGC) at the eastern edge of the Sacramento – San Joaquin River Delta in the Central Valley of California over 2012-13. In Chapter 4 the mixing ratio measurements are combined with coincident measurements of 10 VOCs and CO serving as potential source markers, and a Positive Matrix Factorization source-apportionment technique is applied to investigate the sources of $CH_4$ and $N_2O$ influencing the measured signals at this site. The year-long measurements were divided up into seven unique periods representative of broad temperature / precipitation regimes encountered in this region, and also to match the data continuity of measured tracers in each individual period. We find that dairies and livestock operations in the region surrounding WGC are the largest contributor to the observed $CH_4$ enhancements accounting for 55 – 90 % of the emissions depending on time of the year. The variation in proportion of $CH_4$ enhancements ascribed to this source is mainly caused by the varying contribution from the 'agriculture + soil management + delta' source, which was the second most important contributor to methane enhancements and varied substantially over the course of the year. This source contains anaerobically mediated emissions from a combination of wetlands, peatland pastures and flooded / drained agricultural systems e.g. rice in the surrounding Delta. The $CH_4$ contribution from this sector is temperature driven with peak contributions in the summer season (20 - 40 % of enhancements) as opposed to late fall and winter season when contributions to $CH_4$ signals from this source are negligible and hence

undetectable by PMF. $CH_4$ contributions from a third source, the 'urban and oil / gas' source, were observed in all seasonal periods. This source contains emissions from the upwind urban core, petroleum refineries, and natural gas operations in the Delta and accounts for 10 - 20 % of the total $CH_4$ enhancements. This sources' relative contribution was highest during the early fall period (up to 30 %) when the temperature-dependent $CH_4$ emissions from the Delta emissions are decreasing, and in the late fall period (up to 35 %) when $CH_4$ emissions from the Delta are absent and observed wind speeds and directions are more variable increasing the influence of the nearby Rio Vista gas fields on the apportioned signals at WGC.

$N_2O$ is measured in four periods (late fall, winter, mid-spring and summer) in this study. $N_2O$ is primarily apportioned to two sources. One of the sources is the 'agricultural + soil management' source arising from the N fertilizer application for intensive crop cultivation in the Delta. This $N_2O$ source is very seasonal with peak contributions occurring in the spring and summer season (~ 80 – 90 %) coinciding with the cycle of fertilizer use in the first half of the growing season. In the late part of the fall season, as agricultural activities around WGC are winding down and so is the added fertilizer N input to farmlands, this source only accounts for about 20 % of the observed $N_2O$ enhancements with the dominant share (~ 80 %) being attributed to $N_2O$ emissions from the dairy and livestock sector. In the winters, there is much less agricultural activity taking place around WGC, and the 'ag +soil management' source factor is not observed in the PMF analysis of the wintertime data. Subsequently almost all of the $N_2O$ in winters is attributed to the dairy and livestock sector. We also observe that a source consisting of contributions from primary biogenics and secondary organics is consistently produced in PMF analysis for all seasonal periods. No detectable contributions of $CH_4$ and $N_2O$ signals come from this source, which reinforces that plants and crops do not emit these GHGs as direct emissions.

We conclude that, for $CH_4$, the seasonally resolved apportionment of major sources at WGC is broadly consistent with the distribution in the regional inventory if the influence of far-away sources (e.g. landfills) is not considered. The relative contribution of $CH_4$ emissions from wetlands / land management practices in the Delta to the overall apportionment at WGC is substantial in warm temperature regimes (e.g. summers) and the bottom-up inventory verification mechanisms and studies need to account for the seasonality in emissions from this sector. The consistent lack of $N_2O$ in the 'urban' source factor in all seasonal PMF analyses highlights the insignificant contribution of vehicle emissions to ambient $N_2O$ observations when measured at this site. Evidence from results of PMF analysis in Bakersfield (Guha et al., 2015) provides a similar conclusion in a region that has a mix of urban and agricultural sources. The seasonal variations we observe in emissions of $CH_4$ and $N_2O$ from certain sources has implications for how data from short-term studies should be used for inventory verification. Data from ground-based studies, 'snapshot' airborne measurements and back-trajectory analysis on temporally-limited data may not be able to capture the complete cycle of emissions produced from these sources leading to bias in estimates resulting from such studies. Short-term studies, thus, cannot yield emission factors that can be used to verify the weighted annual emission factors used in the 'bottom-up' inventories, especially for seasonally varying sources like $N_2O$ from agriculture, $CH_4$ from artificial wetland and rice cultivation etc. In light of our findings, we propose long-term source-specific ground-measurements as a more representative method to account for $CH_4$ and $N_2O$ emissions from sources that can be expected to have a seasonal pattern of variability.

## 7.2. Recommendations on future work

In this report, we have augmented understanding of the relative importance and seasonality of sources for two major GHGs, $CH_4$ and $N_2O$, in the Sacramento-San Joaquin Delta region of Central Valley of California. The Central Valley is one of the most industrialized and high-producing agricultural regions of the world producing ~ 8 % of the nation's agricultural output by value, on less than 1 % of total farmland in the United States (CASR, 2011), thereby rightly earning the nickname 'nation's vegetable and fruit basket'. The San Joaquin Valley also sits on top of rich oil and gas formations that support a vast oil and gas extraction and processing industry. The San Joaquin Valley alone would be ranked fourth in oil production in the nation if it were a state (~ 515,000 barrels of oil per day), while just Kern County has more than 42,000 producing oil wells that account for ~ 68% of the oil produced in California, 10 % of US production, and close to 1 % of total world annual oil production (DOGGR, 2012). This means there are a multitude of significant emissions sources of GHGs and VOCs arising from this extensive agro-industrial complex that are collocated and co-emitting into the same atmospheric boundary layer. Our ability to apportion and resolve these GHG sources into unique combinations using VOC source markers is critical to the success of 'top-down' measurements and also in the verification and validation of the 'bottom-up' GHG inventory. We believe that there are two main conclusions from this work which suggest the need for further research to improve the CARB GHG emission inventory - first, the seasonality of major sources of $CH_4$ and $N_2O$ from agricultural sector, and second, the magnitude of $N_2O$ from the transportation sector. Furthermore, our work has developed a baseline understanding of how to use VOC's as GHG source tracers in top down PMF analysis, and we recommend that ARB invest in further application and development of this approach. The results from this work suggest that more comprehensive (more locations) and consistent longer term studies that rely on tall tower

measurements and include VOCs as measured tracers would be useful for improving the 'state of knowledge' regarding $CH_4$ and $N_2O$ source emission strengths in different regions of California.

With the PTRMS that was used in the current study, we were limited to simultaneous monitoring of about 20 masses at unit mass resolution with an effective upper size limit around 200 m/z due to the scanning speed and sensitivity of the quadrupole mass spectrometer detector. Even more comprehensive measurements are now possible using a newer Proton Transfer Reaction Time of Flight Mass Spectrometer (PTR-TOF-MS). The TOF enables simultaneous measurements of the complete VOC spectrum with mass resolution of >4000 M/ΔM providing separation of even more VOCs, and chemical formula identification from the measured exact masses. With PTR-TOF-MS, hundreds of VOC compounds are observable with high enough time resolution to also calculate fluxes by eddy-covariance (Park et al., 2013). In addition, the PTR-TOF-MS is equipped with a new Switchable Reagent Ions (SRI) system that provides capability for measurements using $NO^+$ or $O_2^+$ in addition to the conventional $H_3O^+$ ionization mode. These ionization modes allow for substantial expansion of the measurable VOC suite to include alkanes (e.g. ethane, propane, butane, which should serve as extremely useful tracers of natural gas emissions) which have lower proton affinities than $H_2O$ and therefore cannot be detected in the conventional $H_3O^+$ mode. Including alkanes and many other VOCs measurable using PTR-TOF-MS with SRI should significantly improve characterization and tracing of GHG emission categories in future studies.

As a demonstration of this new capability, we borrowed National Center for Atmospheric Research (NCAR's) PTR-TOF-MS to measure the gradients at WGC in parallel with the PTR-MS for two weeks in February 2013 (and we now have our own PTR-TOF-MS with SRI at UC Berkeley). As mentioned in Sect. 3.3, these data were already useful for validating the nominal

masses of the PTR-MS and confirming the dominant compound attributions. As an example of the expanded measurement capability, Figure 7.1 shows the average diurnal cycle of concentration gradients from the PTR-ToF-MS for a portion (48) of the more than 300 detected ions at WGC. Diurnal and vertical patterns show behavior consistent with boundary layer dynamics, wind profiles and source activity for a broad array of VOCs from different sources. Mass concentration of oxygenated VOCs with two or more than two oxygen atoms, and with nitrogen + oxygen generally increased with height because these are secondary compounds formed by photochemical production in the atmosphere. The opposite was true for pure hydrocarbons and reduced nitrogen containing VOCs which generally are primary emissions and thus highest near the ground where they were emitted. The remaining species include halogenated as well as other volatile compounds detectable using $H_3O^+$. For example, the highest molecular weight compounds (the last 3 panels) are cyclic volatile methylsiloxanes (cVMS) which have been recently identified as volatile emissions from personal care products such as antiperspirants where they are often a dominant ingredient (Tang et al., 2015), and may also serve as tracers for wastewater treatment facilities where these compounds tend to accumulate following human bathing. At WGC, the observed pattern of cVMS suggests these compounds are emitted locally, accumulating near the ground early in the morning.

To understand the seasonality of emissions from the agricultural sector, ARB should also prioritize smaller spatial scale future studies and experiments. Short-range inverse dispersion techniques, where a backward Lagrangian Stochastic (bLS) atmospheric dispersion model coupled with a Monin-Obukhov similarity theory (MOST) description of near-surface winds can be used to infer source emission rates from upwind and downwind gas concentration

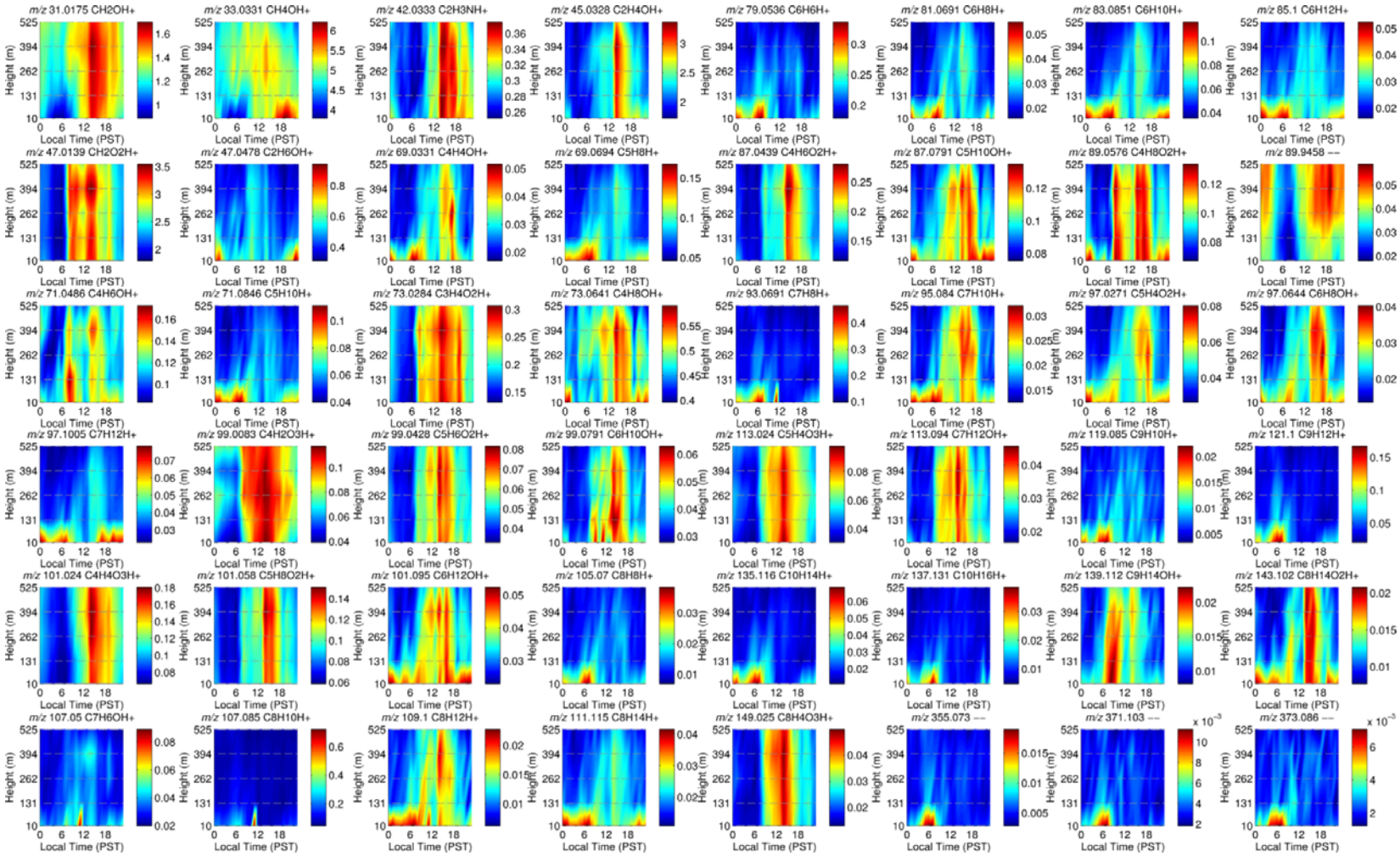


**Figure 7.1.** Mean vertical concentration gradient diurnal profiles for 48 selected ions measured by PTR-ToF-MS at WGC from February 12 to February 20, 2013. The color scale represents concentration (ppb) of the selected ion, x-axis represents local time of day and y-axis represents height (a.g.l).

measurements (Flesch et al., 2004). Experiments based on this technique have been shown to provide reliable long-term estimates of $CH_4$, $NH_3$ and $N_2O$ emissions from a variety of area sources like dairy farms and agricultural fields (McGinn et al., 2006; Turner et al., 2010; Leytem et al., 2011; Ro et al., 2013; VanderZaag et al., 2014). These could also be combined with PTRMS or PTR-TOF-MS measurements to provide clear and useful chemical source signatures for constraining larger scale top down analyses. Ground based eddy covariance, using fast-response analyzers, has been demonstrated to be a robust method to directly measure emissions of $CH_4$ and $N_2O$ over relatively homogenous area sources e.g. rice paddy and wetlands (Teh et al., 2011; Baldocchi et al., 2012; Hatala et al., 2012; Knox et al., 2014). Both the above mentioned techniques can be applied over complete annual cycles to determine unique emission rates representative of different seasons and farm management practices. These direct estimation methods are conducted at facility-level or field-level spatial resolutions. These data would complement the knowledge derived from the regional high spatial resolution (0.1° × 0.1°) long-term multi-tower based WRF-STILT back trajectory analysis (Jeong et al., 2012a, 2012b, 2013) and PMF derived from long term studies using VOC tracers, and together, these methods can be used to constrain the non-$CO_2$ GHG inventory effectively. An expansion of ARB's current $CH_4$ network to a $CH_4$/$N_2O$/VOC framework could be very useful to combine the advantages of inverse dispersion modeling and statistical source apportionment at the same time.

At the scale of individual fields or landfill facilities, a combination of ground-based eddy covariance from small towers and automated chamber measurements offer direct and reliable ways to estimate emissions as they provide either an integrated whole-ecosystem flux (eddy covariance) or spatially resolved measures of gas exchange (e.g. Teh et al., 2011; Zhang et. al., 2014). In this respect, modern analyzers capable of providing high frequency continuous

measurements of $N_2O$ have only recently become available, and can be utilized to provide eddy covariance measurements of $N_2O$ while chambers can provide more detailed information on what part of the soil system (e.g., between, on top of, or on the side of furrows) emits $N_2O$. Year-long flux measurements on crop lands with different major crop types (e.g rice, corn, walnuts, etc.) would allow quantification of fluxes from high-impact events and conditions like fertilizer spraying, application of pesticides, tilling, precipitation, flooded agricultural residues, drainage of fields etc. Projects funded by CARB that share similar goals are already underway in the state. These direct $N_2O$ estimates can provide a wealth of valuable information to verify, validate and improve the inventory and also to assess the agreement with Denitrification-Decomposition (DNDC) and other biogeochemical models.

Direct, continuous, and simultaneous measurements of $CH_4$, $N_2O$, CO, VOCs, and $CO_2$ at fixed sites in confined emissions spaces like tunnels, and also on highways from mobile measurement platforms (like instrument vans) can provide critical constraints on transportation sector emissions in real world operation. These experiments can allow on-road measured $N_2O/CH_4/CO_2/CO/VOC$ vehicle emission ratios to be determined for the California fleet that can be compared with the inventory based EMFAC emission factors. Such approaches will be quite effective in verifying and validating the CARB $N_2O$ emissions inventory for mobile sources and for interpreting source profiles determined from PMF analysis at fixed tall tower sites.

Finally, aircraft scale flux measurements of GHGs, a wide suite of VOCs, NOx, and potentially other air pollutants of interest have recently been proven viable with ~ 2 km spatial resolution (e.g. Misztal et al., 2014; Goldstein et al., 2014; Karl et al., 2013). Flux measurements at this spatial resolution would be extremely useful for mapping actual emission distributions over large areas of California including urban, rural, agricultural, or oil producing regions.

These data could serve as a critical and periodic top down assessment of those non-$CO_2$ GHG sources for which previous top-down observations are scarce and/or for verifying the bottom-up estimates of those GHG sources whose emissions are not microbially-mediated (hence not seasonally varying) and can be reasonably well-defined by scaling up individual sources such as cogeneration plants and refineries. We strongly recommend that the ARB develop this capability in collaboration with the University of California atmospheric science community.

## 7.3. References


CARB (2013), California Greenhouse Gas Inventory for 2000-2012 - by IPCC Category. http://www.arb.ca.gov/cc/inventory/data/data.htm. accessesd on September 23, 2014.

CASR (2011), California Agricultural Statistics Crop Report, 2011. created by California Department of Food and Agriculture, Sacramento, CA and United States Department of Agriculture.

DOGGR (2012), 2011 Preliminary report on California oil and gas production statistics, Department of Conservation's Division of Oil, Gas and Geothermal Resources; Publication No. PR03.

Baldocchi, D., Detto, M., Sonnentag, O., Verfaillie, J., Teh, Y. A., Silver, W. and Kelly, N. M.: The challenges of measuring methane fluxes and concentrations over a peatland pasture, Agric. For. Meteorol., 153, 177–187, doi:10.1016/j.agrformet.2011.04.013, 2012.

Flesch, T. K., Wilson, J. D., Harper, L. a., Crenna, B. P. and Sharpe, R. R.: Deducing Ground-to-Air Emissions from Observed Trace Gas Concentrations: A Field Trial, J. Appl. Meteorol., 43(3), 487–502, doi:10.1175/1520-0450(2004)043<0487:DGEFOT>2.0.CO;2, 2004.

Goldstein, A.H., A. Guenther, T. Karl, R. Woods, H. Jonsson, P.K. Misztal, Improving Regional Biogenic VOC Emission Estimates Using an Airborne PTRMS Eddy Flux Measurement System, Final Report, California Air Resources Board Award No. 09-339, April 16, 2014.

Guha, A., Gentner, D. R., Weber, R. J., Provencal, R., and Goldstein, A. H.: Source apportionment of methane and nitrous oxide in California's San Joaquin Valley at CalNex 2010 via positive matrix factorization, Atmos. Chem. Phys., 15, 12043-12063, doi:10.5194/acp-15-12043-2015, 2015.

Hatala, J. a., Detto, M., Sonnentag, O., Deverel, S. J., Verfaillie, J. and Baldocchi, D. D.: Greenhouse gas (CO2, CH4, H2O) fluxes from drained and flooded agricultural peatlands in the Sacramento-San Joaquin Delta, Agric. Ecosyst. Environ., 150, 1–18, doi:10.1016/j.agee.2012.01.009, 2012.

Jeong, S., Hsu, Y.-K., Andrews, A. E., Bianco, L., Vaca, P., Wilczak, J. M. and Fischer, M. L.: A multitower measurement network estimate of California's methane emissions, J. Geophys. Res. Atmos., 118(19), 11,339–11,351, doi:10.1002/jgrd.50854, 2013.

Jeong, S., Millstein, D. and Fischer, M. L.: Spatially Explicit Methane Emissions from Petroleum Production and the Natural Gas System in California, 2014.

Jeong, S., Zhao, C., Andrews, A. E., Bianco, L., Wilczak, J. M. and Fischer, M. L.: Seasonal variation of CH 4 emissions from central California, J. Geophys. Res., 117(D11), D11306, doi:10.1029/2011JD016896, 2012a.

Jeong, S., Zhao, C., Andrews, A. E., Dlugokencky, E. J., Sweeney, C., Bianco, L., Wilczak, J. M. and Fischer, M. L.: Seasonal variations in N 2 O emissions from central California, Geophys. Res. Lett., 39(16), n/a–n/a, doi:10.1029/2012GL052307, 2012b.

Karl, T., Misztal, P. K., Jonsson, H. H., Shertz, S., Goldstein, A. H., and Guenther, A. B.: Airborne Flux Measurements of BVOCs above Californian Oak Forests: Experimental Investigation of Surface and Entrainment Fluxes, OH Densities, and Damkohler Numbers, J Atmos Sci, 70, 3277-3287, Doi 10.1175/Jas-D-13-054.1, 2013.

Karion, A., Sweeney, C., Pétron, G., Frost, G., Michael Hardesty, R., Kofler, J., Miller, B. R., Newberger, T., Wolter, S., Banta, R., Brewer, A., Dlugokencky, E., Lang, P., Montzka, S. a., Schnell, R., Tans, P., Trainer, M., Zamora, R. and Conley, S.: Methane emissions estimate from airborne measurements over a western United States natural gas field, Geophys. Res. Lett., 40(16), 4393–4397, doi:10.1002/grl.50811, 2013.

Knox, S. H., Sturtevant, C., Matthes, J. H., Koteen, L., Verfaillie, J. and Baldocchi, D.: Agricultural peatland restoration: effects of land-use change on greenhouse gas (CO2 and CH4 ) fluxes in the Sacramento-San Joaquin Delta., Glob. Chang. Biol., 1–16, doi:10.1111/gcb.12745, 2014.

Leytem, A. B., Dungan, R. S., Bjorneberg, D. L. and Koehn, A. C.: Greenhouse Gas and Ammonia Emissions from an Open-Freestall Dairy in Southern Idaho, J. Environ. Qual., 42(1), 10–20 [online] Available from: http://www.ncbi.nlm.nih.gov/pubmed/23673734, 2011.

Mays, K. L., Shepson, P. B., Stirm, B. H., Karion, A., Sweeney, C. and Gurney, K. R.: Aircraft-based measurements of the carbon footprint of Indianapolis., Environ. Sci. Technol., 43(20), 7816–23, doi:10.1021/es901326b, 2009.

McGinn, S. M., Flesch, T. K., Harper, L. A. and Beauchemin, K. A.: An Approach for Measuring Methane Emissions from Whole Farms, , 14–20 [online] Available from: https://www.agronomy.org/publications/jeq/abstracts/35/1/14, 2006.

Misztal, P. K., Karl, T., Weber, R., Jonsson, H. H., Guenther, A. B., and Goldstein, A. H.: Airborne flux measurements of biogenic isoprene over California, Atmos Chem Phys, 14, 10631-10647, DOI 10.5194/acp-14-10631-2014, 2014.

Park, J.-H., Goldstein, A. H., Timkovsky, J., Fares, S., Weber, R., Karlik, J., and Holzinger, R.: Active Atmosphere-Ecosystem Exchange of the Vast Majority of Detected Volatile Organic Compounds, Science, 341, 643-647, 10.1126/science.1235053, 2013.

Peischl, J., Ryerson, T. B., Brioude, J., Aikin, K. C., Andrews, a. E., Atlas, E., Blake, D., Daube, B. C., de Gouw, J. a., Dlugokencky, E., Frost, G. J., Gentner, D. R., Gilman, J. B., Goldstein, a. H., Harley, R. a., Holloway, J. S., Kofler, J., Kuster, W. C., Lang, P. M., Novelli, P. C., Santoni, G. W., Trainer, M., Wofsy, S. C. and Parrish, D. D.: Quantifying sources of methane using light alkanes in the Los Angeles basin, California, J. Geophys. Res. Atmos., 118(10), 4974–4990, doi:10.1002/jgrd.50413, 2013.

Ro, K. S., Johnson, M. H., Stone, K. C., Hunt, P. G., Flesch, T. and Todd, R. W.: Measuring gas emissions from animal waste lagoons with an inverse-dispersion technique, Atmos. Environ., 66, 101–106, 2013.

Ryerson, T. B., Trainer, M., Holloway, J. S., Parrish, D. D., Huey, L. G., Sueper, D. T., Frost, G. J., Donnelly, S. G., Schauffler, S., Atlas, E. L., Kuster, W. C., Goldan, P. D., Hu, G., Meagher, J. F. and Fehsenfeld, F. C.: Observations of Ozone Formation in Power Plant Plumes and Implications for Ozone Control Strategies, , 292(x), 719–724, 2001.

Tang, X., Misztal, P. K., Nazaroff, W. W., and Goldstein, A. H.: Siloxanes Are the Most Abundant Volatile Organic Compound Emitted from Engineering Students in a

Classroom, Environmental Science & Technology Letters, 10.1021/acs.estlett.5b00256, 2015.

Teh, Y. A., Silver, W. L., Sonnentag, O., Detto, M., Kelly, M. and Baldocchi, D. D.: Large Greenhouse Gas Emissions from a Temperate Peatland Pasture, Ecosystems, 14(2), 311–325, doi:10.1007/s10021-011-9411-4, 2011.

Turnbull, J. C., Karion, a., Fischer, M. L., Faloona, I., Guilderson, T., Lehman, S. J., Miller, B. R., Miller, J. B., Montzka, S., Sherwood, T., Saripalli, S., Sweeney, C. and Tans, P. P.: Assessment of fossil fuel carbon dioxide and other anthropogenic trace gas emissions from airborne measurements over Sacramento, California in spring 2009, Atmos. Chem. Phys., 11(2), 705–721, doi:10.5194/acp-11-705-2011, 2011.

Turner, D. A., Edis, R. B., Chen, D., Freney, J. R., Denmead, O. T. and Christie, R.: Determination and mitigation of ammonia loss from urea applied to winter wheat with N-(n-butyl) thiophosphorictriamide, Agric. Ecosyst. Environ., 137(3-4), 261–266, 2010.

VanderZaag, A. C., Flesch, T. K., Desjardins, R. L., Baldé, H. and Wright, T.: Measuring methane emissions from two dairy farms: Seasonal and manure-management effects, Agric. For. Meteorol., 194, 259–267, 2014.

Zhang, Y. et al., Nitrous oxide emissions from maize–wheat field during 4 successive years in the North China Plain, Biogeosciences, 11, 1717–1726, 2014. doi:10.5194/bg-11-1717-2014

## GLOSSARY OF SYMBOLS AND ACRONYMS

| | |
|---|---|
| AGAGE | Advanced Global Atmospheric Gases Experiment |
| AGS | agricultural soils sector for $N_2O$ |
| ARB | California Air Resources Board |
| AWB | agricultural waste burning sector for $N_2O$ |
| CALGEM | California Greenhouse Gas Emission Measurements |
| CalNex | California research study at the nexus of air quality and climate change |
| $CH_4$ | methane |
| CO | carbon monoxide |
| $CO_2$ | carbon dioxide |
| $CO_2$eq | carbon dioxide equivalent |
| CP | crop agriculture sector for $CH_4$ |
| DLS | dairy livestock sector for $CH_4$ |
| DOE | Department of Energy |
| EDGAR | Emission Database for Global Atmospheric Research |
| EMT | energy manufacturing transformation sector for $N_2O$ |
| GEIA | Global Emissions InitiAtive |
| GHG | greenhouse gas |
| GWP | global warming potential relative to $CO_2$ on mass-basis for different averaging times (g $CO_2$-eq/g other gas) |
| IDE | indirect emissions from NOx & $NH_3$ sector for $N_2O$ |
| IPU | industrial processes and product use sector for $N_2O$ |
| LBNL | Lawrence Berkeley National Laboratory |
| LF | landfill sector for $CH_4$ |
| LGR | Los Gatos Research Inc. |
| LSM | land surface model |
| *m/z* | mass to charge ratio |
| MeOH | methanol |
| MNM | manure management sector for $N_2O$ |
| MODIS | Moderate Resolution Imaging Spectroradiometer |

| | |
|---|---|
| MW | molecular weight |
| MYJ | Mellor-Yanada-Janjic scheme for PBL simulations in WRF |
| NDLS | nondairy livestock sector for $CH_4$ |
| NG | natural gas sector (including oil production) for $CH_4$ |
| $NH_3$ | ammonia |
| NOx | generic term for the mono-nitrogen oxides |
| $N_2O$ | nitrous oxide |
| N2O | indirect $N_2O$ emissions from agriculture sector for $N_2O$ |
| NOAA | National Oceanic and Atmospheric Administration |
| O&G | oil and gas |
| OPR | oil production & refineries sector for $N_2O$ |
| PBL | planetary boundary layer |
| PL | petroleum sector (refinery and on-road mobile source) for $CH_4$ |
| PMF | Positive Matrix Factorization |
| ppb | parts per billion |
| PST | Pacific Standard Time |
| PTR-MS | Proton Transfer Reaction Mass Spectrometer |
| RCO | buildings (residential & others) sector for $N_2O$ |
| RH | relative humidity |
| RMS | root mean square |
| RMSerr | root-mean-square error |
| SFBI | scaling factor Bayesian inversion |
| STILT | Stochastic Time-Inverted Lagrangian Transport |
| Tg | tera gram, $10^{12}$ g |
| TEC | Thermo Electron Corporation |
| THD | Trinidad Head station |
| TNR | non-road transportation sector for $N_2O$ |
| TRO | road transportation sector for $N_2O$ |
| UC | University of California |
| USEPA | United States Environmental Protection Agency |
| VOC | volatile organic compound |

| | |
|---|---|
| WGC | Walnut Grove, California |
| WL | wetland sector for $CH_4$ |
| WRF | Weather Research and Forecasting |
| WST | waste (solid & wastewater) sector for $N_2O$ |
| WW | wastewater sector for $CH_4$ |